Tuberculosis: platforms for addressing diagnostic challenges using aptasensing

A Thesis

submitted in partial fulfilment of the requirements for the degree of

Doctor of Philosophy

by

Satakshi Hazra

166106004

Under the supervision of

Prof. Sanjukta Patra

Department of Biosciences and Bioengineering

Indian Institute of Technology Guwahati

Guwahati-781039, Assam, India

April 2024

Dedicated
to
My Family

INDIAN INSTITUTE OF TECHNOLOGY GUWAHATI

Department of Biosciences and Bioengineering

Assam, Guwahati-781039

DECLARATION

I do hereby declare that the research findings in this thesis is the result of research work carried out by me in the Department of Biosciences and Bioengineering, Indian Institute of Technology Guwahati, India, under the supervision of **Prof. Sanjukta Patra.**

I also declare that the contents of this thesis have not been the basis for award of any other degree, diploma, fellowship or any other similar title of any other University or Institution.

As per general norms of reporting research findings, due acknowledgments have been made, whenever findings of other researchers have been cited in this thesis.

Satakshi Hazra

Satakshi Hazra

Date: 21-04-2024

Place: IIT Guwahati

INDIAN INSTITUTE OF TECHNOLOGY GUWAHATI

Department of Biosciences and Bioengineering

Assam, Guwahati-781039

CERTIFICATE

This is to certify that the work described in the thesis entitled **"Tuberculosis: platforms for addressing diagnostic challenges using aptasensing**" is an authentic record of the results obtained from the research work carried out by **Satakshi Hazra** in the Department of Biosciences and Bioengineering, Indian Institute of Technology Guwahati, Guwahati-781039, Assam, India, under my supervision and this work in part or as a whole has not been submitted elsewhere for the award of any other degree.

Date: 21-04-2024

Place: IIT Guwahati

Prof. Sanjukta Patra

(Supervisor)

ACKNOWLEDGMENTS

A PhD program can be an enlightening and life-changing experience full of never-ending obstacles, countless chances for personal development and the thrilling possibility of learning something new. It demands constant commitment, tenacity, and an unrelenting pursuit of intellectual growth. It would not have been possible for me to complete this amazing chapter of my life at IIT Guwahati without the help and support of numerous people who have played significant roles along the way. I want to express my gratitude to everyone who made this incredible journey memorable and helped me to improve it in every possible way.

I would like to begin by conveying my sincere gratitude to my PhD supervisor, ***Prof. Sanjukta Patra****. She has been a guiding light throughout my PhD journey, providing me with guidance, feedback and continuous support. She has consistently inspired me to strive for excellence as an independent researcher. Furthermore, I am indebted to her for the necessary resources she has provided, which has contributed to the successful implementation of my research ideas. I consider myself fortunate to work under a supervisor who exhibited genuine concern for my well-being at different phases of this journey.*

I am deeply indebted to my doctoral committee members ***Prof. Pranab Goswami, Prof. Bithiah Grace Jaganathan, Prof. Debapratim Das and Prof. Manish Kumar*** *for their positive feedback and critical suggestions throughout the progress of my work. It has not only enriched my thesis but also strengthened my overall understanding of the subject. Moreover, their generosity in dedicating their time to provide constructive direction on my work at difficult times has been immensely beneficial.*

I am grateful to ***Dr. Rajkumar P. Thummer, Dr. Shirisha Nagotu, Prof. B. Anand, and Prof. Manish Kumar*** *for allowing me to work and learn in their laboratories at various times during this journey. I would like to thank* ***Prof. R. Swaminathan,*** *the founder and former head of Department of Biosciences and Bioengineering for his invaluable suggestions during*

my journey.

I express my heartfelt gratitude to ***Prof. Rakesh Bhatnagar*** *for allowing me to learn about the functioning of a BSL-3 laboratory and carry out a part of my work at his state-of-the-art research laboratory amidst the beautiful campus of Jawaharlal Nehru University. I am immensely thankful to* ***Dr. Manish Gupta****, for his invaluable guidance and cheerful company during my stay and consistent support throughout the entire tenure of my PhD. Sir, you continue to inspire me and you have been a guiding star through all the ups and downs of this journey.*

I would like to express my sincere gratitude to the former and current heads of the Department of Biosciences and Bioengineering, ***Prof. V. Venkata Dasu, Prof. Kannan Pakshirajan, Prof. Latha Rangan, and Prof. Rakhi Chaturvedi*** *for providing all necessary departmental facilities during their respective tenures. I am deeply indebted to the* ***Department of Biosciences and Bioengineering, IIT Guwahati*** *and the institute as a whole for providing the essential infrastructural facilities, conducive work environments and a wonderful campus life that enabled me to focus on my research. Furthermore, I extend my gratitude to the dedicated* ***office staff members, cleaners and gardeners*** *associated with the Department of Biosciences and Bioengineering, IIT Guwahati for their cooperation.*

I would like to extend my gratitude to the ***Ministry of Human Resource Development (MHRD), India*** *and the* ***Indian Institute of Technology Guwahati*** *for providing me with the financial support during PhD.*

I would like to acknowledge the talented group of officials and teaching assistants at ***Central Instrumental Facility, IIT Guwahati*** *for proving prompt analysis of nanomaterials and motivating me to learn more about various high-end instruments housed at the facility.*

I want to express my gratitude to all of the members, past and present of the ***Enzyme and Microbial Technology Laboratory (EMTL)*** *for their indispensable role in the progress*

of my research. I am deeply grateful to all of you for teaching me so much in so many domains of personal and professional growth. I would like to thank ***Dr. Mohd Faheem Khan*** *who helped me take baby steps into the world of molecular biology and shared valuable insights on effective planning of experiments. I wish to express my appreciation to my colleagues* ***Bhaskar, Satyam, Mukesh, Prithwi, Mayur, Risha, Ghadir, Tarun, Senthamizh and Srinidhi and Sourav*** *for their support, encouragement and assistance throughout this journey.*

I extend my heartfelt gratitude to my esteemed seniors ***Dr. Gundappa Saha, Dr. Anurag Priyadarshi, Dr. Dileep Ahari, Dr. H. K. Krishna, Dr. Aman Prakash, Dr. Naveen Kumar Singh, Dr. Vinay Bachu and Dr. John Jyoti Kalita;*** *all of whom have now transitioned into roles as professors, postdocs, or professionals in various institutions, for their invaluable contributions to my PhD journey. I am profoundly grateful for the research discussions exchanged over numerous cups of coffee, which have not only fuelled my academic curiosity but have also broadened my research perspective.*

I would like express gratitude to ***Mr. S. R. Vignesh****, whose mentorship and guidance have been instrumental through the journey. It has played a pivotal role in helping me conquer the intricacies of computational research. His constant encouragement, with phrases like "you can do it," served as a beacon of motivation during challenging times, instilling in me the confidence to push forward.*

I want to extend my deepest gratitude to my wonderful juniors ***Poulomi, Suchetana, Sushovan, Subhobroto, Surabhi, Alka, Priyanka, Pratik and Sonia*** *who have been an integral part of my PhD journey. Your support, whether it was enjoying a hearty meal together, taking a walk in the rain, indulging in delightful gossips, or embarking on fun trips, has been immensely cherished.*

Throughout my tenure at IIT Guwahati, I was fortunate to develop wonderful

friendships that offered priceless memories in every circumstance. My heartfelt appreciation go to my friends ***Rajib, Chandrima, Gloria, Saddam, Darshana, Yashwant, Gaurav, Uttariya, Manish, Manasa, Jibon, Nitin, Anjali, Sinchini, Anusuya and Shivani*** *who helped me in various ways throughout this remarkable journey. Your presence provided much-needed breaks, offering an escape from the confines of the lab. Beyond the academic rigors, it's these moments of camaraderie that have truly enriched my experience.*

I would also like to thank ***Dr. Vikas Rana*** *and* ***Dr. Manashjit Gogoi*** *for their conscious efforts and help during my journey.*

I owe a lot of gratitude to ***Riddhi*** *and* ***his family*** *for their persistent support and encouragement throughout my PhD journey. He has been a constant pillar of strength and a source of inspiration, and I am truly grateful to have him by my side.*

I also want to express my deep appreciation for my feline friend ***Luchui****, who taught me the importance of unconditional love, sound sleep, and playfulness during the tough times of this journey.*

Last but not least, I am honoured to be able to learn so much and get endless blessings from my wonderful grandparents ***Didan, Gia, Dadai and Mommom.*** *It is for their faith in my dreams that I could push forward in this journey. Their love and continuous encouragement has been the bedrock upon which I've been able to build this journey.*

It's hard to find words that adequately express the depth of gratitude I feel towards my parents for their boundless love throughout my PhD journey. From the earliest stages of my academic pursuit to this very day, their love, encouragement, and sacrifices have been my guiding light. Their belief in my abilities, even during moments of self-doubt, has been a source of strength that propelled me forward. ***Meme and Babai****, your endless sacrifices, whether they were emotional, or otherwise, coupled with your continuous support has been the wind beneath my wings, enabling me to surf through difficult and challenging times. This*

accomplishment would not have been possible without their selfless dedication and belief in my aspirations. I am forever grateful for their presence in my life and their invaluable contributions to every aspect of it.

Finally, I thank the infinite beauty of nature for inspiring my scientific journey.

Date: 21-04-2024
Place: IIT Guwahati

Satakshi Hazra

Satakshi Hazra

TABLE OF CONTENTS

ABSTRACT

Tuberculosis (TB) remains a global health concern, impacting millions worldwide. According to the World Tuberculosis Report 2023, approximately 9 million people were diagnosed with TB in 2022, with 1.5 million succumbing to the disease. Despite advancements, TB persists as one of the top infectious killers globally. Early diagnosis is paramount in combating TB spread and reducing mortality rates. In India, where TB is particularly prevalent, timely detection is crucial due to its high burden of cases. Thus, emphasizing the significance of early diagnosis is pivotal; both globally and in high-burden countries like India in the fight against TB.

Several detection technologies and tests approved by the World Health Organization (WHO) aid in diagnosing TB; including sputum smear microscopy, Xpert MTB/RIF assay and TB culture. Sputum smear microscopy, though widely available and inexpensive, has limitations in sensitivity, especially in detecting paucibacillary and extrapulmonary TB cases. Xpert MTB/RIF, offering rapid detection and simultaneous rifampicin resistance assessment, faces challenges in cost and infrastructure requirements. TB culture, considered as the gold standard, provides accurate diagnosis but demands specialized laboratory facilities and prolonged turnaround times. Additionally, these methods may not be suitable for resource-limited settings or for diagnosing latent TB infection, highlighting the need for more accessible and sensitive diagnostic tools.

Addressing the existing drawbacks of TB detection with new age biosensing platforms is crucial to enhance diagnostic accuracy and efficiency. Biosensors offer advantages such as rapid detection of TB biomarkers, reducing turnaround time for diagnosis and enabling point-of-care testing; which can expedite treatment initiation and curb disease transmission. Moreover, biosensors can facilitate the detection of low concentrations of biomarkers, improving sensitivity and aiding in the diagnosis of early-stage TB cases.

The biorecognition element of any biosensor is designed to act as the capture agent to bind to any target biomarker from a sample. A novel class of these biorecognition molecules harbouring several advantages over antibodies; called aptamers, are short, single-stranded nucleic acid molecules that can bind specifically to target with high affinity. They act as excellent biorecognition elements in biosensing due to their versatility, stability, and ease of modification. Thus, designing an aptasensing platform to detect several biomarkers of TB can be a promising avenue for rapid and accurate diagnosis of TB. However, the current methods in development of aptamers encounter several drawbacks, including the need for multiple partitioning processes, which can be time-consuming and resource-intensive. There is a lack of streamlined and standardized processes for developing aptamers. Existing protocols for aptamer selection typically involve complex and labor-intensive systematic evolution of ligands by exponential enrichment (SELEX) procedures, which require specialized equipment and expertise. Addressing this challenge is crucial to expedite the translation of aptamer-based diagnostics as a screening tool from bench to bedside, facilitating their broader utilization in TB healthcare settings.

To achieve this, one modified SELEX approach for development of an aptasensing technique and one systematic SMART workflow scheme to design high-affinity aptamer screening tool is described in the current study. We then checked the validity of the same to check the presence of secretory biomarkers bearing diagnostic relevance to TB. To achieve this, recombinant expression clones of three significant TB secretory biomarkers Ag85B, ESAT6 and MPT64 were constructed. These secretory biomarkers have been found to be abundantly secreted by the causative agent, *Mycobacterium tuberculosis* (MTB) in TB patients' blood, cerebrospinal fluids, urine etc. These biomarkers are selected from a larger repertoire of TB secretory biomarkers due to their ability to distinguish BCG vaccinated, non-tuberculous mycobacteria (NTM) and *mycobacterium tuberculosis* complex (MTBC) in TB

diagnosis.

Ag85B is a powerful biomarker as it is abundantly secreted and there is no clinically approved testing platform for the same. So, Ag85B was considered as target biomarker for development of a new SELEX methodology. The structural and functional properties of Ag85B protein were investigated using molecular, biochemical, and biophysical techniques to confirm the biological intactness. It was ensured that the Ag85B is purified in its native conformation. We identified and validated the purified Ag85B using mass spectrometry analysis. Additionally, circular dichroism spectroscopy confirmed that the purified protein retained its characteristic secondary structural elements. Ag85B was also checked for its enzymatic functionality to obtain K_M values, not reported in earlier literature. A DNA library (69 mer) was used to obtain specific aptamers with a novel "COFA" SELEX methodology. COFA stands for "Cut-off filtration based assembly" wherein a molecular sieve (filter) is used to partition target-bound aptamers in 12 rounds of iterative binding, partitioning, PCR amplification and enrichment steps. In this process, the other two biomarkers were used as controls to ensure the development of aptamers or binders that would only be specific to the detection of Ag85B.

Secondary structure predictions and CD spectra were evaluated for the characterization of putative G quadruplexes in the screened aptamers. The ΔG value for thermodynamic stability indicated that the aptamer was stable and formed characteristic hairpins with one big and two small loops indicating its strong ability to interact with the clefts of the biomarker useful for recognition. One aptamer was selected and thereafter taken for further studies. The aptamer showed a dissociation constant of ~939 nM when probed with CD spectroscopy measuring the spectral shifts it undergoes upon target-induced conformational changes. Electrophoretic mobility shift assay (EMSA), isothermal calorimetry (ITC) and CD spectroscopy also showed strong binding affinities between the target and best

DNA aptamer. A two site binding with increased affinity for the first side could also be predicted from the isothermal calorimetry data. Further investigation might highlight the stoichiometry of association between the developed aptamer and Ag85B. Moreover, the aptamer was found to be serum stable, suitable for clinical applications. To probe the binding interactions, *in silico* molecular docking analysis with Ag85B was also carried out. More than one site on the surface exposed regions of Ag85B interacted well with the chosen aptamer. Moreover, the nature and significance of these docked structures were validated to ensure that strong H-bonds and other non-covalent interactions were responsible for the stability of the aptamer-target complex during binding.

Further, to validate the binding affinity, we checked the ability of the developed aptamer to specifically distinguish between MPT64 and ESAT6 on an aptamer linked immobilized sorbent assay (ALISA) using surface coated biomarkers. The developed ALISA platform showed a concentration dependent increase in the absorbance values indicating correct performance of the aptamers. Furthermore, the K_D value of the aptamer was determined to be within the range of 800-900 nM in spiked serum samples. The aptamer was more specific towards detection of Ag85B as compared to either MPT64 or ESAT6. To investigate the ability of aptamers to detect Ag85B, we developed a fluorescence-based aptasensor. In the sensing platform, fluorescently labelled aptamer acted as a donor and graphene oxide as the energy acceptor. The aptasensor showed LOD values within the range of 68-74 nM in spiked serum samples. We tested the aptasensor reproducibility with spiked Ag85B in serum. Our results cumulatively suggest the successful development of a sensitive aptasensor capable of detecting Ag85B from clinical samples. For further assessing the practical applicability and diagnostic potential of the developed aptasensor, we verified cross-reactivity, analytical precision and recovery range of spiked antigen. The highest recovery of ~103% could be reported from our study. This validated that at lower concentrations of

Ag85B, the developed aptasensor was more sensitive. This in turn could reinforce that this aptasensor is fit to detect miniscule amounts of Ag85B biomarker from patient serum even at very early stages of TB infection.

Then we also extended our investigation to the study of aptamers and their interaction pattern with the aptatopes (regions on a target molecule recognized by an aptamer) for designing better aptamers for the biomarker immunogenic protein, MPT64. MPT64 is secreted by actively replicating MTB into the blood of infected patients. A detailed investigation of the structure and interacting pattern of existing DNA aptamers for MPT64 has improved our understanding of aptatopes and crucial aspects of epitopic regions instrumental for development of both diagnostic and therapeutic aptamers. In this study, we aimed to investigate specific residues of MPT64 that are less likely to undergo mutations and thus will be instrumental for designing aptamers that recognize them. We tailored our approach to finding mimotopes (peptide mimics of epitope on a target molecule) of MPT64 that would aid in the development of such aptamers. Our findings suggest that computational approaches like multiple sequence alignment, *in silico* docking, linear epitope prediction, motif filtering followed by secondary structure prediction can aid in the design of pre-structured libraries for aptamer development. We coined the methodology as Systematic Mimotope-guided Aptamer Refinement Technique, i.e. “SMART” approach for repurposing old aptamers for new diagnostic and therapeutic uses. Additionally, we designed a methodology of using these MPT64 mimotopes as target molecules for SELEX and develop futuristic high-affinity aptamers. The SELEX methodology is still in its developmental stages and currently being carried out. Furthermore, we synthesized and characterized gold nanoclusters as a sensitive nanoprobe to incorporate with our MPT64 aptamer and build a futuristic aptasensing nanoplatform. Gold nanoclusters synthesized in our study was characterized by UV-visible and fluorescence spectroscopy, FETEM, HRTEM, EDX, XPS

and FTIR. The synthesized gold nanoclusters had defined shape and an average diameter of 2.75 nm.

In conclusion, our study offers new insights into the intricacies of designing high-affinity aptamers via the combination of computational tools as well as experimental novel SELEX methodologies. This will help us understand the mechanistic details of aptamer-target interactions and help us utilize the same to develop sensitive aptasensing detection platforms for TB; in a quest to address the existing diagnostic challenges.

LIST OF ABBREVIATIONS

aa	Amino acid
Ag85A/B/C	Antigen 85A/B/C
ALISA	Aptamer linked immobilized sorbent assay
Amp	Ampicillin
ANOVA	Analysis of variance
APTES	(3-Aminopropyl) triethoxysilane
AuNC	Gold nanocluster
BSA	Bovine serum albumin
$CaCl_2$	Calcium chloride
CD	Circular dichroism
CFP10	Culture filtrate protein 10
COFA	Cut-off filtration assembly
DNA	Deoxyribonucleic acid
dsDNA	Double stranded DNA
DST	Drug susceptibility testing
ELISA	Enzyme linked immunosorbent assay
EM	Electron microscope
ESAT6	Early secretory antigenic target 10
FAM	Fluorescein amidite
GO	Graphene oxide
HIV	Guman immunodeficiency virus
HPLC	High pressure liquid chromatography
Kan	Kanamycin
kDa	Kilodalton
LAMP	Loop mediated isothermal amplification
LB	Luria Bertani
LOD	Limit of detection
LPA	Line probe assay
MALDI	Matrix assisted laser desorption ionization

$MgCl_2$	Magnesium chloride
MOTT	Mycobacteria other than tuberculosis
MPT64	Immunogenic protein 64
MS	Mass spectrometry
MTB	*Mycobacterium tuberculosis*
MTBC	*Mycobacterium tuberculosis* complex
MWCO	Molecular weight cut-off
NAAT	Nucleic acid amplification test
NTM	Non-tuberculous mycobacteria
OD	Optical density
ORF	Open reading frame
PBS	Phosphate buffered saline
PCR	Polymerase chain reaction
PLIP	Protein ligand interaction profiler
POC	Point of care
RNA	Ribonucleic acid
rpm	Rotations per minute
RT	Room temperature
SD	Standard deviation
SDS-PAGE	Sodium dodecyl sulphate - polyacrylamide gel electrophoresis
SEC	Size exclusion chromatography
SELEX	Selective evolution of ligands by exponential enrichment
ssDNA	Single sranded DNA
TAE	Tris-acetate EDTA
TB	Tuberculosis
TBE	Tris-borate EDTA
TEOS	Tetraethyl orthosillicate
UV	Ultra violet
X-ray	X radiation (Röntgen radiation)

LIST OF FIGURES

LIST OF TABLES

1

Introduction & Review of Literature

Abstract

TB remains a leading global health threat, necessitating robust diagnostic efforts to curb its spread and prevent further morbidity and mortality. Early diagnosis is crucial not only for effective treatment but also for screening populations, that helps prevent outbreaks and reduces the burden on healthcare systems worldwide. This chapter provides an overview of the drawbacks of the traditional TB testing methods and the challenges associated with the same. Following this, the chapter covers a brief outline of the WHO endorsed and emerging technologies for the diagnosis of TB. Especially, several studies show the use of immunodominant diagnostic biomarkers of TB throughout the life cycle of the bacterium inside the host. Therefore, this chapter reviews the advantages of functional nucleic acids in addressing the diagnostic loopholes through biosensing of such biomarkers. A special class of such functional nucleic acids, known as aptamers; are new-age recognition molecules generated by a process known as SELEX. The significance of aptamer designing for capture and detection of secretory antigens of MTB from patient samples through aptasensing are provided. Further, the integration of nanomaterials to improve the performance of aptamers in sensing are also discussed. This chapter concludes by explaining the purpose of the thesis, which is to develop a systematic approach for curating DNA aptamers against Ag85B and MPT64 biomarkers intended towards early and confirmatory TB diagnosis.

1.1 Introduction

Since the dawn of humanity, diseases have been an ever-present force shaping the course of civilization. As human civilizations developed and expanded, infectious diseases found new opportunities for transmission. TB is a highly contagious infectious disease, spread by MTB that has plagued mankind ever since. Every year, 10 million people continue to fall ill with TB. The advent of modern diagnostics brought new hope in the fight against TB. In 2022, despite being a preventable and curable disease, TB remained the second leading cause of death after the COVID-19 pandemic [1]. About a quarter of the global population is estimated to have been infected with TB [2]. In 2022, there were 7.5 million newly diagnosed cases of TB worldwide (Fig. 1.1). This figure, which is above the pre-COVID baseline (and previous historical peak) of 7.1 million in 2019, is the highest since WHO started tracking TB globally in 1995. It was 5.8 million in 2020 and 6.4 million in 2021. Generally, although progress has been made in reducing the TB burden worldwide, this has been insufficient to reach the first milestone of the End TB Strategy [1]. The estimated global difference between the number of TB cases (incident cases) and the reported number of newly diagnosed cases (notified cases) decreased to 3.1 million in 2022, down from approximately 4 million in 2020 and 2021. Another danger to the worldwide control of TB is drug-resistant strains of MTB. In certain parts of the world, the prevalence of extensively drug-resistant TB (XDR-TB) and multi-drug-resistant TB (MDR-TB) have showed a considerable increase. In 2022, there were estimated 410000 cases of multidrug-resistant or rifampicin-resistant TB (MDR/RR-TB) worldwide. Only 175650 people were successfully diagnosed to start treatment in 2022, which is still less than the pre-pandemic level of 181533 people in 2019 and represents roughly two in five of those in need of clinical care [1].

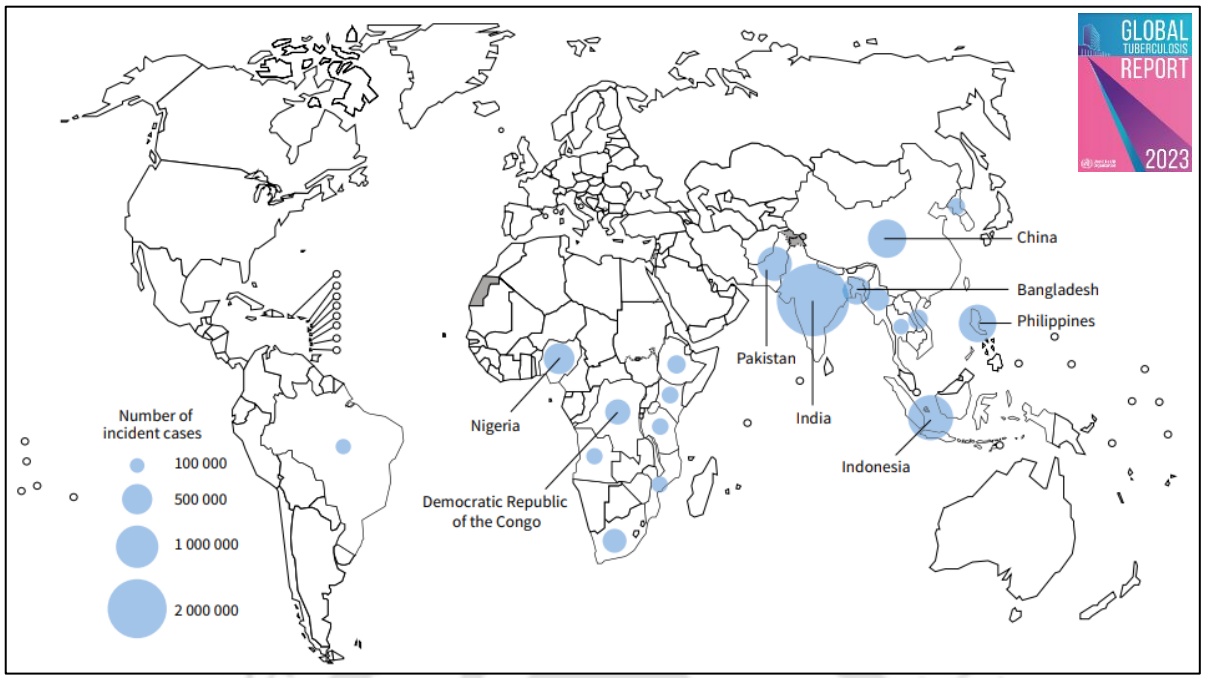

Fig. 1.1 Global TB map showing eight countries that accounted for about two thirds of global cases in 2022. (Ranked in order from first to last in terms of numbers of cases: India, Indonesia, China, the Philippines, Pakistan, Nigeria, Bangladesh and the Democratic Republic of the Congo) Source: Global Tuberculosis Report, 2023.

1.2 History of Tuberculosis

It has been hypothesized that the genus Mycobacterium originated more than 150 million years ago, in the Jurassic period [3]. Present-day TB is caused by six or seven clades, strains with common ancestors of MTB, which have separate geographic origins [4]. The earliest archaeological evidence of human TB came from the Egyptian mummies and there is enough evidence to conclude that TB was widespread in Africa which later travelled across the globe [5]. In the medieval Europe, scrofula, a disease affecting cervical lymph nodes, was described as a new clinical form of TB also known as "king's evil" [6]. In 1720, for the first time, the infectious origin of TB was conjectured by the English physician Benjamin Marten. However, the great pioneer of bacteriology, Robert Koch in 1882 demonstrated conclusively that *Bacillus tuberculosis*, now known as MTB, was the etiological agent of TB. Following this, the microbiological diagnosis of TB was practiced through staining and culturing techniques until paediatrician Clemens Freiherr von Pirquet developed the intracutaneous tuberculin test [6]. It was since 1900 that Albert Calmette and Camille Guérin researched on developing a TB

vaccine from attenuated tubercle bacillus which failed to produce progressive TB when injected into animals and named it the Bacille Calmette-Guerin or BCG [7]. Thus, began the era of oral BCG vaccinations in infants until the Lubeck disaster which raised questionable debate on the efficacy of BCG. Following emergence of various strains that considerably differed from the original strain of the 1920s, due to variable passage conditions in different laboratories, several disparities arose with respect to the immunogenicity of BCG [8].

1.3 Taxonomy of *Mycobacterium tuberculosis*

MTB belongs to the phylum Actinobacteria. Within this phylum, it resides in the class Actinobacteria, order Actinomycetales, and family Mycobacteriaceae. MTB belongs to a larger group of mycobacteria containing several other members known as the MTBC. All members have a 99.9% similarity at the nucleotide level and identical 16S rRNA sequences but differ remarkably in terms of their host tropisms, phenotypes, and pathogenicity (Fig. 1.2). To create phylogenetic relationships, sequence data from a variety of genes, including as 16S rRNA, rpoB, and hsp65 genes, have been utilized [9]. The MTBC consists of two independent clades, one composed exclusively of MTB lineages from humans and the other composed of both animal and human isolates. Scientists have assumed that all are derived from a common ancestor, but share different host spectrums. For example, except for *Mycobacterium bovis*, *Mycobacterium africanum*, *Mycobacterium canettii* or rodent pathogens *Mycobacterium microti* have limited host spectrums. Although MTB is the main human TB pathogen, other members of the MTBC have distinct host preferences. *M. bovis*, for instance, mainly infects cattle, but it can also cause zoonotic TB in people. Towards this end, it is intriguing to know that the speciation events that shaped the spatiotemporal evolution of the bacterium had an immense effect on the pathogenicity and the global epidemiology of TB. Different strains of MTB are tracked using genetic variation analysis, or genotyping, to gather data on patterns of transmission, infectivity, and pathogenicity.

There are variable genomic regions in the members of the MTBC that led to the classification of “ancestral” and “modern” strains. Strains can be classified as "ancestral" or "modern" based on the existence or lack of an MTB-specific deletion (TbD1), such as the Beijing and Haarlem MTB clusters. Nonetheless, MTB typically low degree of genetic variety suggests that the population as a whole emerged from clonal proliferation after an evolutionary bottleneck that is thought to have happened between 15,000 and 35,000 years ago [10]. Research supports the theory that India is an ancient endemic focus of TB as indicated by the ancestral MTB genotypes that are predominant in the Indian subcontinent [11].

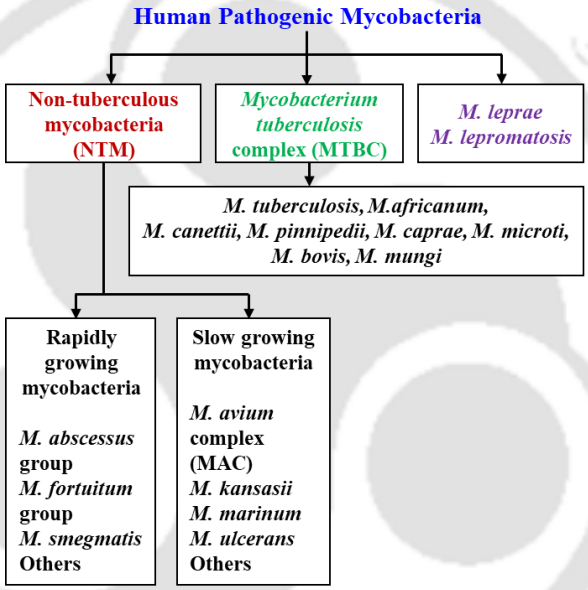

Fig. 1.2 Classsification of Mycobacteria species.

1.4 Infection Cycle of *Mycobacterium tuberculosis*

MTB infection is spread by aerosolized droplets from infected patients. An uninfected person inhales these droplets, primarly transmitted by coughs, sneezes, spits or or any other forceful expiratory maneuver that shears respiratory secretions. Sometimes these airborne particles, called droplet nuclei (lesser than 5 μm in diameter) have the ability to remain in the air for extended periods of time, enabling them to be transmitted over distances greater than one meter [12]. Poorly ventilated airspaces are prome to carry transmission to individuals. The inhaled bacilli settle in the lung's terminal air spaces, where they infiltrate alveolar macrophages

and begin to replicate. There are certain other "unusual" transmission routes also reported for MTB transmission. Due to their thick mycolic acid rich cell walls, MTB can persist in environment for extended periods of time in soil, river water, wastewater, fomites, dust and cadavers [13].

Stage 1: When the droplet nuclei enters the airways, the infection is only likely to develop if the bacilli travels to the small airsacs of the lungs called the alveoli [14]. In this early microenvironment, the phagocytic cells in the lungs, including macrophages, neutrophils, monocytes and dendritic cells (DCs) are recruited to actively fight the incoming bacteria. Establishment of early granulomas are a characteristic feature of this stage. Once the granulomas begin to develop, the mycobcateria is benefitted by further recruitment of phacocytic cells that provide a conducive niche for their survival and expansion. Thus, these early granulomas (primary granulomas) actually make the infection worse by encouraging the phagocytosis of apoptotic infected macrophages by numerous incoming macrophages [15]. Phagocytosis of infected cells by newly incoming macrophages induces the formation of secondary granulomas. Bacterial population expansion continues with further involvement of ESX1 type VII secretion system (or several other virulence pathways of the mycobacteria) which inhibit apoptotic or necrotic cell deaths and allow accumulation of larger number of cells within favourable phagocyctic cellular environments [16]. In these stages of innate immune responses, involvement of several pattern recognition receptors (PRRs) are vital for local and systemic induction of proinflammatory cytokines, chemokines and cell-adhesion olecules that eventually lay the foundation for induction of adaptive immune responses. Multiplication within the alveolar sacs allow the bacilli to spread to other areas of the body like bones, brain or kidneys etc through the bloodstream or lymph nodes. If the body's immune system is able to thwart further multiplication of the bacilli, the person develops latent TB where the bacilli remains quiescent and evades the body's immune system.

This can also be attributed by the delayed onset of adaptive immunity which is a result of delayed migration of bacilli from the lungs to the draining lymph nodes aided by DCs. In this condition, the patient harbours a small number of tubercle bacilli within the body in the "arrest" phase of immunological equilibrium, that are alive in nature but fails to spread to others. There are several key contributors of this clinically quiescent stage in the infection cycle. For example, the bacterial dormancy regulons (DosR-DosS two component signal transduction module), resuscitation-promoting factor (Rpf), and the toxin-antitoxin (TA) gene pairs regulate the metabolic status of the latent bacilli [17–19]. In the diagnostic perview, tuberculin skin tests (TSTs) or interferon-gamma release assays (IGRAs) yield positive results but culture-based tests or sputum smear microscopic analyses are usually negative.

Stage 2: TB disease develops when the bacilli starts to spread and the body's immune system fails to keep the bacteria under control. The bacilli escapes the The disease pathogenesis begins months to years later from the time the individual first contacted the bacterium. Although the underlying mechanisms are not fully understood, CD4+ T cells and TNF are two of the major elements that mediate protective immunity in TB and that prevent reactivation, as demonstrated by the increased frequency of TB in individuals treated with TNF-blocking agents or coinfected with HIV respectively. The persistence of bacteria is also dependent on the marked reduction in the ESAT6 and Ag85B specific CD4+ T cells. ESAT6 and Ag85B are key immunodominant secreted antigens found in the circulating blood which finds importance as biomarkers for diagnosis and serve as important vaccine candidates. The progression of latent TB to active disease can be trigerred by multiple factors like coinfection (often with HIV), compromised or weakened immunity, organ transplantations, cancer, age, diabetes, liver complications, malnutrition etc.

However, transmission by expectoration routes in cases of cavitary TB is particularly severe considering their highly infectious bacterial load [20]. Human T cell responses may play

a role in the transmission of TB from host to host by contributing to the destruction of lung tissue that in noted in cavitary TB.

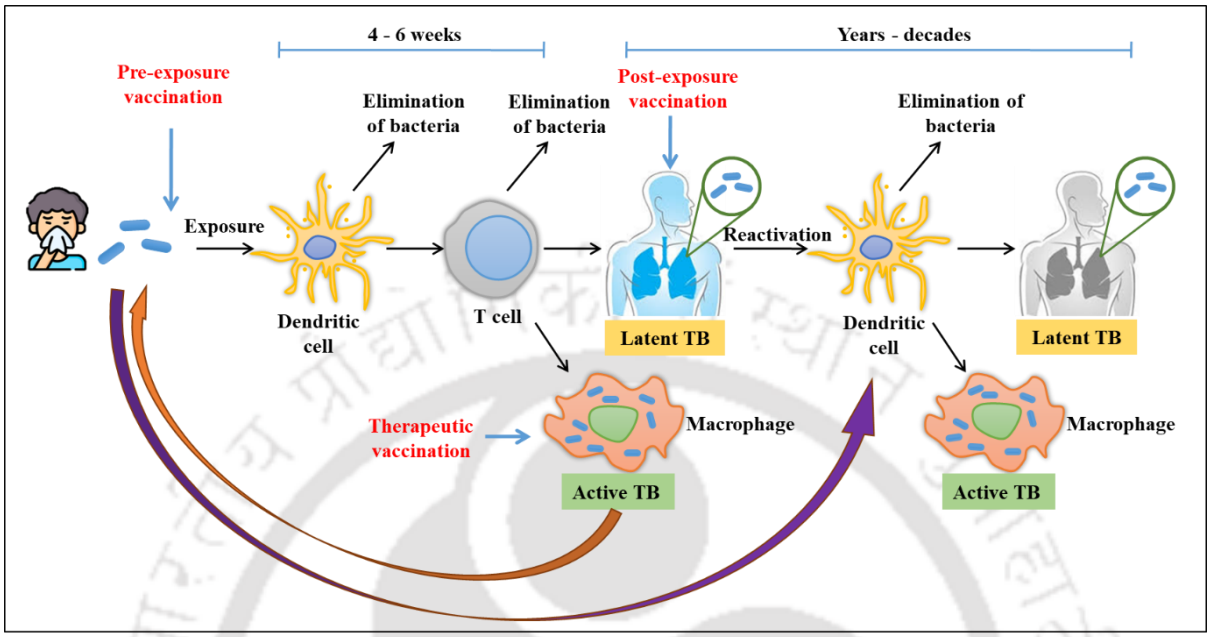

Fig. 1.3 *M. tuberculosis* infection cycle and stages in human host.

1.5 Present status of diagnostics in TB

The COVID-19 pandemic significantly reduced the number of active case finding for TB, highlighting the urgent need for new diagnostic instruments [1] During the COVID-19 pandemic, POC diagnostic tools were developed to highlight the shortcomings of ineffective testing, which can result in unacceptable delays in diagnosis and treatment, as well as an increased risk of transmission. COVID-19 related disruption in the laboratory based diagnosis of TB; particularly in highly endemic areas led to a significant decrease in diagnosing active disease [21,22].

Despite the importance of identifying and diagnosing active TB disease in infected individuals, there are obstacles. For many years, the confirmatory detection of TB in laboratory settings were microbiological and microscopic analyses of the causative agent MTB which takes 2-6 weeks. Moreover, in the case of pulmonary TB, all of these diagnostic tests necessitate MTB positive sputum; however, a large number of active TB patients- including those with

HIV, diabetes, and children, frequently do not exhibit a MTB positive sputum and, consequently, are unable to provide microbiologically positive specimens [23,24]. Furthermore, sputum-based diagnostics are insignificant in extra-pulmonary diseases, where samples- such as biological or tissue fluids like pleural, cerebral, or synovial fluids are frequently obtained through invasive procedures. For all these reasons, it is necessary to have sensitive and specific TB diagnostic tests in order to quickly determine the existence of active disease, or rule it out [25].

In order to reduce the detection time from several weeks (taken in conventional detection methods) to one hour, the current clinical diagnoses focuses on other alternatives such as detecting the presence of nucleic acids or biomolecules specific to MTB. Currently, the WHO relies on automated polymerase chain reaction (PCR) test to detect total DNA of the bacilli from sputum and a urine based biomarker for patients unable to produce sputum [1]. Also, sputum may contain other microbes albeit not as contaminants, but indicators of other concomitant diseases which challenge the gold standards in present-day diagnostics. The above require expensive instruments, sample pretreatments, processing, and skilled technicians and moreover cannot distinguish live or dead bacilli in the patient's body. These molecular confirmatory techniques are unaffordable for low-income countries. Other approaches to detect TB specific biomarkers include immunological antibody-based assays. Primarily, all types of antibodies are costly to produce and have limited shelf-lives due to their reduced thermal stabilities. Amongst the existing technologies, the following methods are still being used in lower to middle income countries, in spite of their disadvantages:

- Chest X-ray: Chest X-rays are not sensitive enough to detect TB in early stages or in individuals with mild or asymptomatic forms of the disease. So, relying solely on chest X-rays may lead to false-negative results. Also, the patient's extrapulmonary TB negative status cannot be confirmed by a negative chest X-ray result. Therefore, additional TB diagnostic tests

are always used to confirm the results of chest X-rays. In contrast to other TB tests, the results of a chest X-ray test can be obtained quickly; however, the test necessitates specialized equipment and personnel with the necessary training [26]. Moreover, in the radiographic findings, other respiratory conditions, such as pneumonia or lung cancer, can present with similar abnormalities.

- Liquid culturing systems: Liquid cultures take extended incubation times for growth of the mycobacterium bacilli and therefore are more susceptible to contamination. There is a high set up cost of laboratory for automated liquid culture systems and related infrastructure.

- Mantoux Test or Tuberculin skin test (TST): This test follows the injection of a purified protein derivative (PPD) to assess the delayed type hypersensitive reaction in individuals indicating the chances of previous exposure to the causative agent. Following injection, the PPD exploits the delayed-type hypersensitivity reaction, within 24 to 72 hours, that results in tissue swelling [27]. Although it is widely used, it is not a true indicator of an active TB disease. Thus, TST is unable to distinguish between the latent TB and active TB. The TST will also produce a positive result for individuals who have been vaccinated against TB with the BCG vaccine.

- Sputum Smear Microscopy: It provides false positive results in patients having HIV/AIDS. It indicates lack of specificity due to the fact that it identifies acid-fast bacilli (AFB), which include MTB as well as NTM. Variability in staining techniques and interpretation may lead to inconsistent results. Challenges to collect multiple samples and repeated testing of the same patient for better chances of finding tubercule bacilli in sputum also poses a significant challenge to the healthcare provider. Conventional fluorescence microscopy has also shown promise as an alternative wherein less manpower and improved sensitivities are noted [28]. False positive outcomes are a plausible reason for the failure of

fluorescence microscopy, however, in comparison to intense light sources, light-emitting diodes (LEDs) are more robust, sustainable, and have a longer lasting battery life expectancy. Thus, these qualities make LED microscopy feasible for use in resource-limited settings. Accordingly, the WHO recommends that conventional fluorescence microscopy can be replaced by LED microscopy [1,29].

- GeneXpert MTB/RIF: The GeneXpert MTB/RIF assay is an expensive tool, especially in resource-poor healthcare settings. The GeneXpert system requires uninterrupted power supplies and state of the art laboratory infrastructure which can be challenging for lower income countries. Moreover, the chances of false-negative results in smear-negative or extrapulmonary TB cases are high. Since this technique detects the entire MTBC, it fails to differentiate between different species that are clinically relevant to humans. Also, obtaining reliable results are a significant challenge due to the requirement of regular calibration and maintenance of the instrument.

- Interferon-Gamma Release Assays (IGRA): Tests like the QuantiFERON-TB Gold and T-SPOT.TB measures the release of interferon-gamma by T cells which is a direct indicator of body's response to TB-specific antigens. Although IGRAs are unaffected by BCG vaccination, there is a likelihood of discrepancies due to variations in immune status, technical flaws, lack of appropriate cutoffs and difficulty in interpreting borderline zones in serial testing of patients [30]. These IGRAs can only be performed under strict guidelines and with specialized laboratory equipments. Little et al. evaluated the effectiveness and cost of IGRA tests versus GeneXpert and sputum smear tests in India and came to the conclusion that it is not advisable to use IGRA tests to diagnose TB in developing nations like India because of the higher costs of these tests may not always be beneficial to the health care systems in developing nations [31].

- Serological tests: These tests help in detecting the overall load of IgG/IgM

immune response indicators produced against MTB in the patient's body. But the immune status of the patient can lead to variable test results. These tests have limitations of variability through diverse genetic populations and are not recommended for primary diagnosis due to issues related to sensitivity as not all individuals will produce detectable levels of antibodies in mild to early cases of TB infection. Despite the overall affordability of serological tests, WHO cautioned against their use in the diagnosis of active TB due to inconsistencies in the results [32].

- Nucleic Acid Amplification Tests (NAATs): These tests amplify and detect the genomic load in the form of DNA or RNA of MTB, thereby providing rapid and sensitive results. Examples include Truenat TB and CBNAAT (Cartridge-Based Nucleic Acid Amplification Test). But, these have operational challenges due to the requirement of high throughput laboratory settings. Very low bacillary load in smear-negative patients, chances of contamination in handling patient samples, cost considerations and the inability to differentiate between live and dead bacilli are crucial parameters that limit the practical applicability of NAATs.
- Line Probe assays (LPAs): Line probe assays, like the GeneXpert test, yield fast results but necessitate a biosafety level 3 laboratory and highly skilled personnel. Since line probe assays use open-tube formats, there is a greater chance of sample contamination because the test samples are exposed to outside environments [33].
- LAM tests: This test is specific for lipoarabinomannan antigen from urine but has higher sensitivity only in cases of HIV-TB coinfections. These lateral flow LAM tests are reasonably priced and don't call for expensive lab equipment or highly skilled workers. The generated test can be used as self-screening tests because it is typically simple to interpret. Because of this, POC diagnostic procedures like lateral flow assays (LFAs) are perfect for environments with limited resources. It produces more false-negative and false-positive results

in patients with unknown HIV status and multiple bacterial infections respectively. It has variable performance with respect to the stage of TB infection within the body and is not a true indicator of different forms of TB [34]. The antibodies used in LFAs are the limiting factor. This is due to the low stability of antibodies, posing a major challenge in the development of LFAs.

A schematc diagam explaining the advantages and disadvantages of common TB tests in practice is shown in Fig. 1.4.

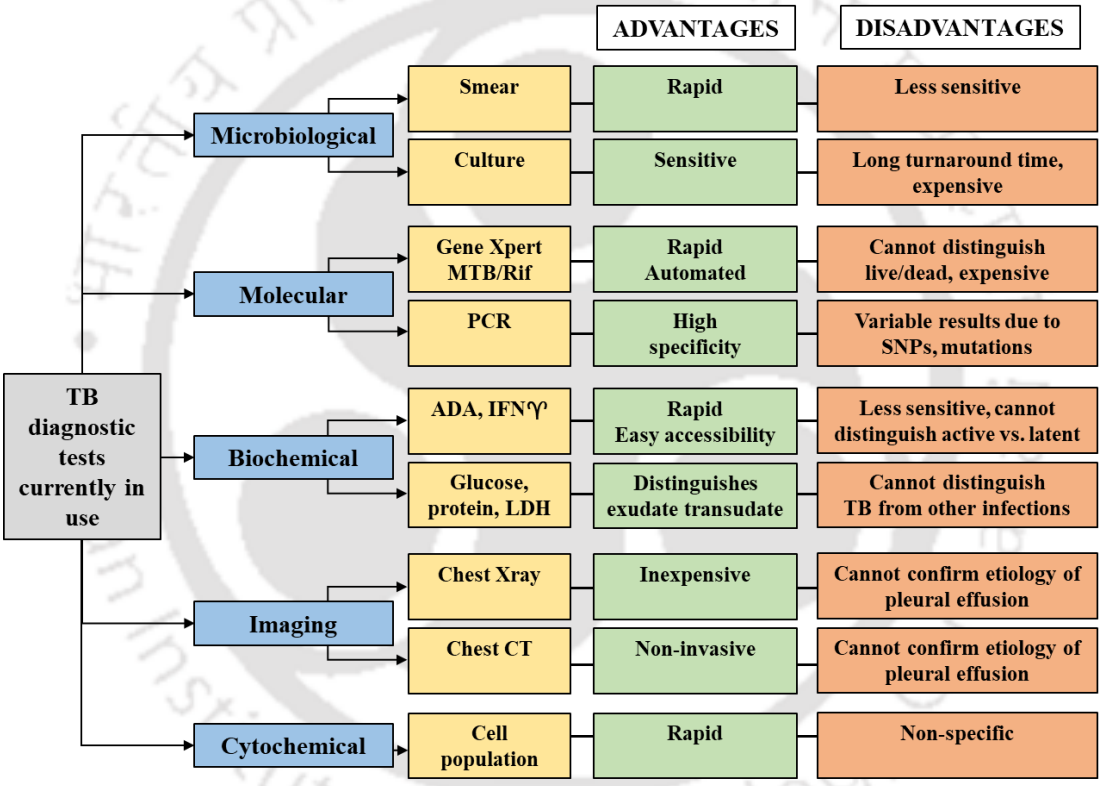

Fig. 1.4 Schematic chart showing different types of TB diagnostics.

1.6 Diagnostic biomarkers of *Mycobacterium tuberculosis:* challenges and knowledge gap

New approaches to enhance diagnosis and treatment are desperately needed to meet the WHO End TB strategy to bring in 50% reduction in TB incidence rate by 2025, given the shortcomings and difficulties of the TB diagnostics currently in use. The application of biomarkers represents one strategy that could bring in paradigm shifts in the diagnostic

landscape of TB. A biomarker is “a defined characteristic that is measured as an indicator of normal biological processes, pathogenic processes or responses to an exposure or intervention” [35]. The use of these biomarkers can be divided into three categories: prognostic markers for the likelihood of developing active TB, POC testing, in patients with latent tuberculosis infection, to indicate reactivation risk and treatment response markers that may forecast the results of TB treatment [36]. Here, the relevance of any biomarker can be measured by its "validation" which refers to assay performance characteristics (e.g., measurement accuracy), while "quantification" refers to the assay's connection to biological processes (e.g., the assay’s ability to predict the infection stage or progression of disease).

Both pathogen and host biomarkers have been thoroughly studied in the field of TB. Antigen detection and presence or absence of DNA are two types of pathogen-based biomarkers [37]. On the other hand, hematologic markers, antibodies, cytokines and chemokines, RNA, immunodominant proteins, metabolites and multiple biomarkers elucidated by the “omics” approaches form the repertoire of host-derived biomarkers. Ideally, a biomarker or a “biosignature” would be readily available for detection from an accessible body sample, such as blood or urine, and the equipment used to analyze the presence or absence of the biomarker would be easy to use. Additionally, the biomarkers could serve as practical endpoints for clinical trials by acting as indicators of cure after TB treatment or provide cues regarding protective efficacy after TB vaccination [38].

Several reports hypothesize that the diagnosis of active TB can be monitored by the relative amounts of T-cells at the site of disease rather than in blood [39,40]. However, invasive procedures like these have limited applicability in diagnostics. Thus, the relevance of antibody-based assays in confirmatory diagnosis to distinguish three special groups: in patients with active disease, in latent TB patients to indicate reactivation risk and predict treatment success; and in people other than those with active disease, to indicate protection from TB by new

vaccines is met with several clinical challenges [37].

There are still many clinical difficulties in diagnosing smear-negative TB in children and adults with HIV. Due to inadequate health care delivery systems and limited access to care, including ineffective coordination between national HIV/AIDS and TB programs, current diagnostic toolkits are not being utilized to their full potential both in areas with high HIV coinfection rates.

One of the major barriers to the development of novel TB diagnostics is the inaccuracy and market failure. In 2016, Albert and his colleagues have reported that the TB diagnostics pipeline included more than 50 companies developing new TB diagnostics but the roll out seemed ineffective and slow due to the existing biasness in industries to avoid developing diagnostics specially suitable for resource-limited settings [41]. In the global context of the 'big three' diseases viz. TB, malaria and HIV/AIDS, a colossal majority of people are unaware of their HIV infection status or fails to get tested early. Often, in underdeveloped countries, diagnostic focus is driven only towards neglected tropical diseases and early TB fails to get checked [42]. For instance, several models of rapid tests for malaria are synonymous to the ones that are widely in need for TB diagnostics, yet only a minor fraction of patients undergoing malaria treatment undergo testing [43–45]. These findings cumulatively suggest that even the existing diagnostic strategies are poorly implemented in many resource-limited settings.

A glimpse of the WHO-endorsed products (for example, LPA, LAMP and others) for rapid TB testing is shown in Fig. 1.5. Sequencing facilities and centralized drug susceptibility testing (DST) are the two major emerging technologies that have led to a paradigm shift in TB diagnostics over the last decade. On the other hand, the Global TB report 2023 has also highlighted the severe lack of implementation of the WHO recommended rapid tests, especially in India (Fig. 1.6). Finally, the knowledge gap to effectively understand the biology of MTB

and its interactions with the human host, particularly in HIV-infected adults and children has thwarted the development of newer diagnostics.

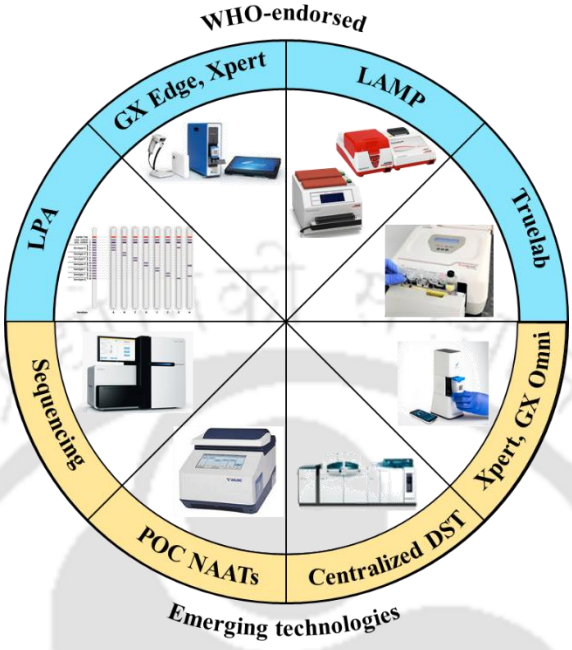

Fig. 1.5 WHO-endorsed and emerging molecular tests for TB and drug resistance.

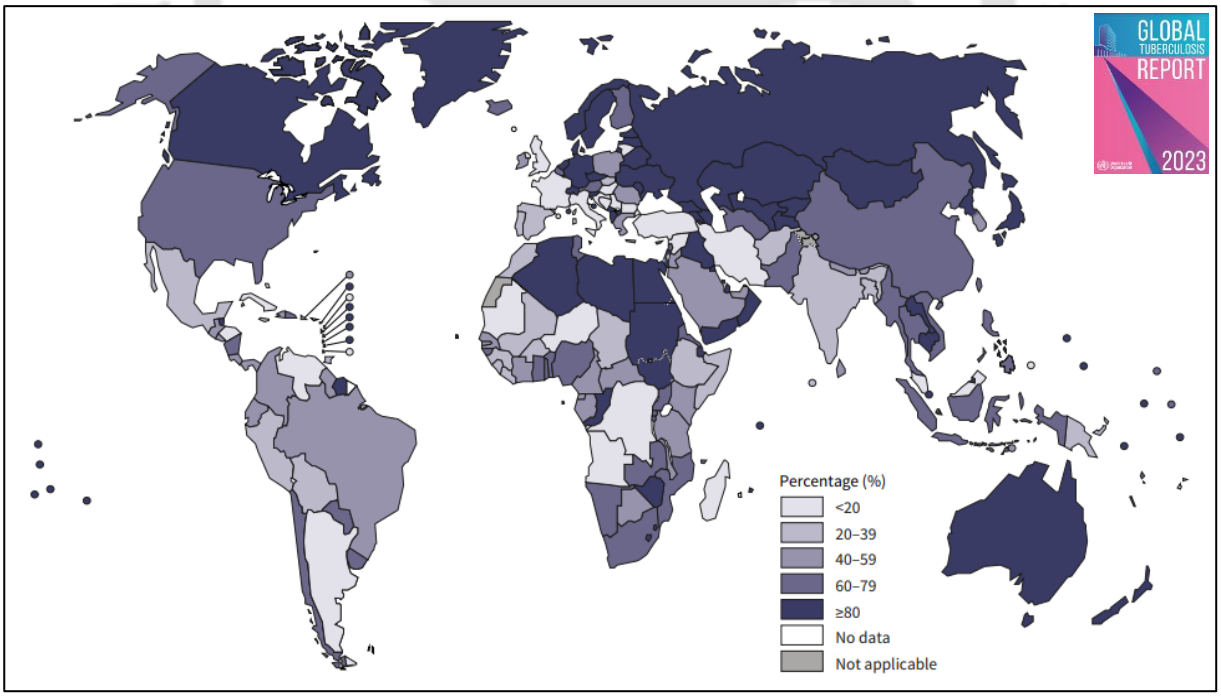

Fig. 1.6 Percentage of people newly diagnosed with TB who were initially tested with a WHO-recommended rapid diagnostic test, 2022. Sorce: Global tuberculosis report, 2023.

1.7 Secretion systems in *Mycobacterium tuberculosis*

Broadly, genes belonging to the following classes encode the proteins performing

multiple roles: (i) proteins of virulence and adaptation in active and dormant phases of TB, (ii) proteins of cell wall and membrane processes, (iii) proteins of housekeeping, intermediary metabolism and synthesis pathways, (iv) proteins of secretory pathways, (v) other conserved and regulatory proteins [46].

For proteins which are secreted into the actively growing culture filtrates of MTB, the general secretory pathway proteins (Sec), twin-arginine translocation proteins (Tat) and secretion system Esx (Esx-1 to Esx-5) proteins are inevitable in pathogenesis. The secretory proteins contain an N-terminal signal sequence. These secretory apparatus proteins secrete multiple PE-PGRS (characterised by presence of polymorphic domains rich in glycine), PE (Pro-Glu near their N-terminus) and PPE (Pro-Pro-Glu near their N-terminus) family proteins which are antigenic determinants coded in the MTB genome [47].

Studies have demonstrated that proteins released by the these secretion systems influences the pathogenicity of the bacilli within the host and are immunodominant in nature that substantiates their use as important antigenic biomarker (targets).

1.7.1 Role of secretory proteins in TB diagnostics

One major drawback of using only antibodies for clinical diagnostics is that antibodies and the delayed type hypersensitivity response last long after the subclinical or clinical disease has subsided, making immunological diagnosis frequently unresolvable. Under these circumstances, antigen-based serological tests have the potential to offer reliable and affordable tools for the diagnosis of TB. Thus, the diagnosis of excretory/secretory proteins is of paramount importance in diagnosis of TB (Fig. 1.7) [48].

MTB uses various strategies to survive within the cells; the most important of these tools are secreted proteins, such as immunogenic protein (MPT64), the 6-kDa early secreted antigenic target (ESAT6), the 10-kDa culture filtrate protein (CFP10), and the antigen 85 (Ag85) complex which has a significant role in the virulence of MTB.

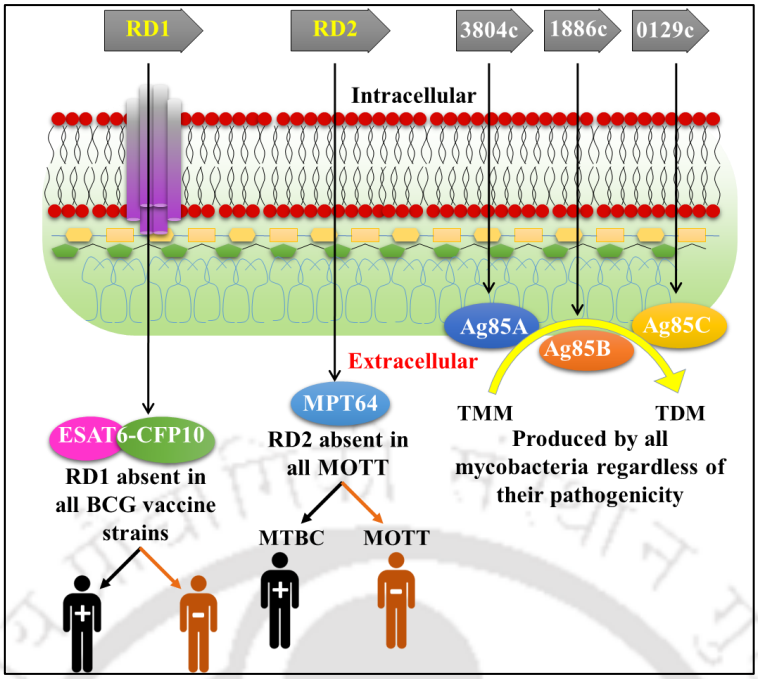

Fig. 1.7 Major secretory biomarkers (Ag85 complex, ESAT6, CFP10 and MPT64) of *M. tuberculosis*.

1.7.2 Role of Ag85 complex in TB diagnostics

The Ag85 complex comprising of three distinct proteins is one of the major contituents in the cell wall and is most predominantly found in the culture filtrates of MTB. The CMN (*Corynebacterium*, *Mycobacterium*, and *Norcardia*) genera include these proteins. The cell walls of organisms belonging to the CMN genera are made up of interconnected polysaccharide-mycolate complexes and peptidoglycans. The surface of these cell walls is characterized by the presence of mycolic acid. Long chain fatty acids called mycolic acids are found in the cell wall envelope and are essential for the organism's survival during pathogenesis in a host cell. The mycolic acid found in the mycobacterium cell envelope is made up of roughly 60-90 carbons [49]. The Ag85 complex is the main secretory antigen, and it has an important role in the pathogenicity of the bacilli. As a part of the complex, three dominant exported fibronectin-binding proteins, consisting of Ag85A (*fbpA*), Ag85B (*fbpB*) and Ag85C (*fbpC*), Ag85B, 30 kDa; Ag85A, 31 kDa; Ag85C, 31.5 kDa play various pathophysiological functions. Research on MTB H37Rv has demonstrated that approximately 60% of the total proteins in the culture fluid are made up of the main Ag85 complex components, Ag85A and Ag85B.

Compared to Ag85A, the Ag85B component has a little bit more. All three Ag85 members have a high homology in sequence and structure. Regardless of pathogenicity, all mycobacterial species typically express Ag85A, Ag85B, and Ag85C, the three distinct proteins of the Ag85 complex, in a 2:3:1 ratio. Moreover, Harth et al. found that Ag85B, the main extracellular protein of MTB, is present in the culture from day three onwards [50].

The Ag85 complex allows the macrophages to efficiently uptake the bacilli and thereby providing it with a favourable niche for survival. It interacts with the gelatin binding site of human fibronectin. This results in the enhancement of complement-mediated phagocytosis by host macrophages [51]. Ag85 attaches itself to fibronectin, a surface eukaryotic protein. Moreover, it binds to the precursor of elastin. This suggests that Ag85 plays a part in macrophage cell adhesion and invasion [49].

Belisle and his colleagues demonstrated that all three Ag85 antigens catalyse the transfer of mycolates via a mycolyltransferase exchange process, leading to the formation of trehalose monomycolate (TMM) and trehalose dimycolate (TDM) also known as cord factor [52]. Ag85 complex can be reliably detected in sera from TB patients through indirect ELISA using monoclonal antibodies against purified Ag85 complex, as demonstrated by some recent studies [53].

Role of Ag85 complex in skin tests: Presence of Ag85 proteins in a PPD may also contribute to the varying results. Activated T cells secrete a lymphokine called T-cell fibronectin (FN) which has selective binding to Ag85 proteins. This lymphokine plays a significant part in the onset of a delayed hypersensitivity reaction as an inflammatory mediator. Every Ag85 complex member has the ability to attach to the T-cell fibronectin lymphokine and impede its function thereby producing variable results [54].

Role of Ag85 complex in ELISA: Using the ELISA technique, Kumar et al. found that Ag85C had the highest sensitivity (89.77%) and specificity (92%) among all the antigens used

($p < 0.0001$). In patients with negative smear and culture, the antigen positivity rate was 95%. The study was proven to be valid for all types of age groups [55]. In a different investigation, Dayal et al. created an ELISA test to find IgG antibodies against the Ag85 complex. The outcomes were comparable to the Ziehl-Neelson (ZN) staining, and culture on Lowenstein Jensen (LJ) medium for identifying MTB [56]. Using synthetic peptides of Ag85 complex, an ELISA based early diagnosis of pulmonary and extrapulmonary TB towards a sensitive, specific, rapid and cost effective immunoassay was proposed by Kashyap and colleagues. The use of synthetic peptides (7-10 amino acid long) of the Ag85 complex proved to be effective in comparison to the whole antigen for developing the assay [57].

Role of Ag85 complex in amplification reactions: PCR is a highly effective means of detecting the presence or absence of genetic elements of the bacilli from patient samples. Following such observations, PCR using the fbpB gene (encoding Ag85B protein contributing to 41% of the total mycobacterial proteins in log-phase culture supernatants) was successful. Thus, the mRNA coding for this gene has been utilized as a target for reverse transcriptase-PCR [58,59]. Moreover, Wilkinson et al. showed that during the first 24 hours of infection, Ag85B mRNA levels increase 54-fold and 14.6 times compared to 16S rRNA of MTB. Thus, during the initial phases of MTB intracellular infection, there is a rise in mRNA levels linked to both Ag85B and 16S, signifying the pathogen's intracellular proliferation [60]. In another report, successful PCR amplification of the Ag85 genes via 162 bp length amplicon and found in all mycobacterial species established the diagnostic accuracy of Ag85 genes as a biomarker. The authors also used a Southern blot technique for differentiation of TB from non-TB mycobacterial species using a specific probe in the presence of T4 polynucleotide kinase. The results were reproducible as it showed 94.6% sensitivity and 93.9% specificity with the culture-based methods. Therefore, a combination of PCR and Southern blot method is significant for rapid diagnosis of TB in patients with active and latent TB infection [61]. Xu and his colleagues

designed a novel real-time recombinase polymerase amplification (RPA) based technology for identifying MTB within 20 minutes which could specifically target Ag85B. Particularly, the combination of fluorescent probes/primers could provide a detection limit of 4 copies per microliter of sample. The Ag85B-based RPA could determine the genomic DNA extracted from MTB with high reliability [62].

Role of Ag85 complex in LC-MS/MS technique: Using the LC-MS/MS technique, Kashyap et al. showed that CSF from patients with tuberculous meningitis (TBM) contained the 30-kDa protein antigen, the hallmark of Ag85 complex. Using this method, they were able to identify the Ag85 complex in CSF from 89% (71 out of 80) of the suspected TBM patients [63].

Role of Ag85 complex in biosensing technique: Use of Ag85 complex proteins in biosensing formats have shown promise. Mukundan et al. developed a sandwich immunoassay for the direct detection of Ag85 complex using waveguide-based optical biosensor. The proposed sensor has a detection limit of 100 pM for Ag85. However, poor antibody stability precludes the use of this assay on clinical samples at present. [64]. Using a capture antibody, another indirect ELISA Ag85B assay was designed by and Murphy and colleagues for a biosensing platform. After the assay was developed, the bioreceptor anti-Ag85B was crosslinked onto carbon electrodes modified with gold nanoparticles (AuNP) and Ag85B binding was successfully assessed electrochemically using cyclic voltammetry [65]. Ma and his team designed a promising powerful platform using a silicon nanowire field-effect transistor (SiNW-FET) biosensor where Ag85B antibody was used as a bioreceptor too. Compared with other methods, the SiNW-FET biosensor can detect MTB with a remarkably broad dynamic linear range in a shorter time. The biosensor had a low limit of detection (LOD) of 0.01 fg/mL (0.33 aM) for Ag85B, good stability and specificity, and a 30-second response time. This sensor's wide dynamic range, which extends 12 orders of magnitude from 1 fg/mL

to 100 ng/mL or higher, makes it possible to identify a wide range of target Ag85B antigen concentrations in real clinical samples [66].

Singh and his colleagues developed a novel indirect sandwich immune-PCR assay for the detection of Ag85B for pulmonary and extrapulmonary TB patients. In this technique a amino-modified reporter DNA was covalently crosslinked with the antidetection antibody. The detection limit of Ag85B by this immuno-PCR was found to be 1 fg/mL, which was 106-fold lower than an analogous enzyme-linked immunosorbent assay (ELISA) [67]. Similarly, Khan and colleagues developed an immune-PCR technique to detect Ag85B in osteoarticular TB patients. Sensitivities of 87·5 and 70·5% were observed in bodily fluids of confirmed patients. Markedly, the sensitivities obtained by immune-PCR or reverse transcriptase-immuno-PCR were significantly higher than ELISA and GeneXpert assay [68]. In another study, use of monoclonal antibody against Ag85B protein based on sandwich-type biosensor using bio-layer interferometry was employed for detecting the antigen. It is a rapid method to discriminate MTBC and NTM with immobilized antibodies on sensor chips [69].

While antibody-based detection platforms for Ag85B offer a valuable tool for diagnosing TB, their limitations in terms of cost, extended production times (including mice immunizations, testing and large scale up processes) along with operational challenges can restrict their effectiveness and utility, particularly in diverse or resource-limited settings. Conventional antibody-based ELISA or immunoassays require multiple steps, including sample preparation, washing, incubation, and detection, making them time-consuming and labor-intensive. Moreover, there are issues of limited specificity or sensitivities [70].

1.7.3 Role of MPT64 in TB diagnostics

The MPT64 biomarker, is highly immunogenic and is secreted in the early culture filtrates. According to one study, the mycobacterium carefully regulates the amount of MPT64 expression. An increase in the amounts of MPT64 is found to be detrimental as it could prevent

macrophage apoptosis in the host, thereby leading to an increase bacterial motility.

Role of MPT64 in skin tests: Results of studies on the MPT64 antigen have been controversial with respect to skin tests [71]. Numerous investigations have demonstrated that this antigen only slightly increases lymphocyte responses in a small proportion of TB patients. For example, merely 6% of PPD-reactive TB patients exhibited a positive intradermal response of hypersensitivity to MPT64 [72,73]. In contrast with these results, a higher injection dose of MPT64 applied as a patch test, could discrimate between patients and healthy donors with a specificity of 100%. However, the use of this antigen in diagnosis through patch-test is complicated because it is present in several of the current BCG strains.

Role of MPT64 in ELISA: Several studies have reported the use of MPT64 in determining the IgG and IgA levels by direct and indirect ELISA [74]. Serological diagnosis with MPT64 has been shown in various reports by direct, sandwich as well as aptamer-antody dual recognition ELISAs [74–76]. Moreover, prokaryotic expression of early secretory protein MPT64 from MTB and its application in serological diagnosis of TB by ELISA to evaluate its sputum viability was also shown by researchers. [77,78].

Role of MPT64 in amplification reactions: Currently, there are four major MTB DNA-specific sequences identifiable by PCR. Meanwhile, MPT64 is the gene sequence specific for MTBC and exists at only one site on the MTB genome rendering it the most specific sequence for PCR assays as depicted in many studies [79–82]. Many reported that MPT64 was the most specific and sensitive sequence for the amplification of DNA by PCR, nested PCR and real-time immunoPCR (RT-I-PCR), as well as immunoPCR variants (modified with magnetic beads or gold nanoparticles) tested on patient samples [80,83]. Since MPT64 is secreted by actively dividing cells, it is universally acceptable that a single copy of MPT64 gene represents one bacterial cell [80,83].

Role of MPT64 in biosensing technique: Voltammetric immunoassays for MPT64

based on a unique syngergestic amplification strategy using rolling circle amplification on a gold electrode was shown by Gou and colleagues [84]**.** Ultrasensitive biosensing platform based on functionalized graphene devices and SPR phase difference for MPT64 detection was put forward by Seo and Nzuzza with their team in separate studies [85,86].

1.8 Nucleic acids used in biosensor applications

Nucleic acids are versatile molecules used in detection of analytes (bacteria, fungi, proteins, small molecules drugs, pollutants etc.) on sensing platforms. The ease, convenience, and accuracy of detection through nucleic acids have led to the fast development of nucleic acid biosensors (NABs) in the healthcare industry. Aspects like infrastructure and labor, the primary obstacles in the TB healthcare industry; can be solved by implementation of simple NABs. NABs can also minimize the chances of false-positives that may arise through antibody-based or enzyme-linked immunoassays. A representation of the annual number of publications in the last 15 years for NABs in TB is shown in Fig. 1.8.

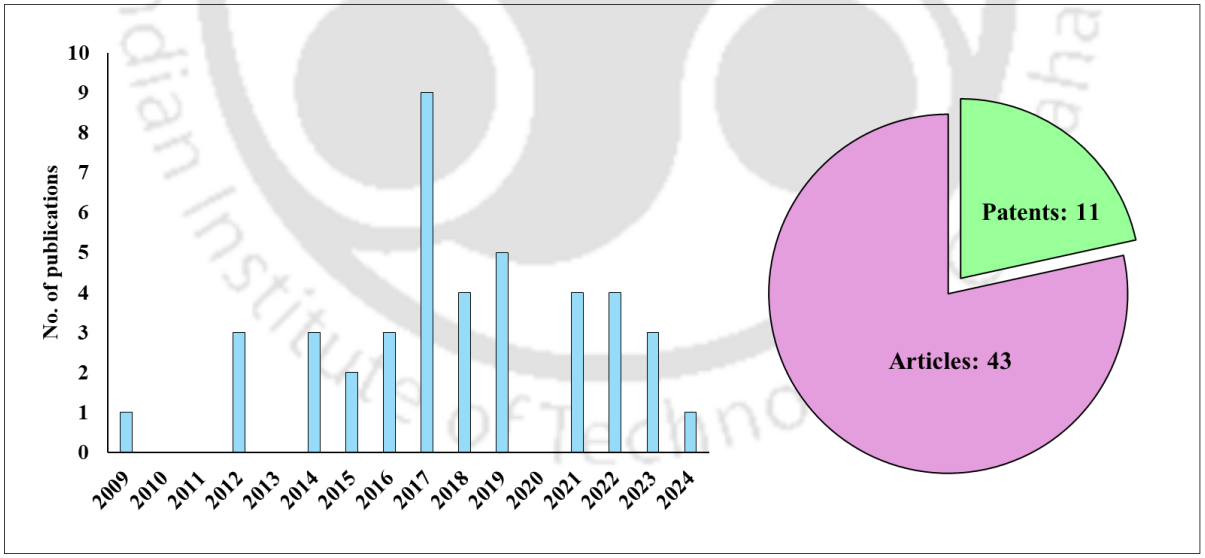

Fig. 1.8 Annual number of research articles and patents published in the last 15 years. PubMed search keywords: nucleic acid biosensor + tuberculosis + clinical. www.pubmed.ncbi.nlm.nih.gov, accessed on 19th April 2024. A representative pie chart regarding the number of patents and articles is also shown.

1.8.1 Types of NABs for infectious disease diagnostics

Nucleic acids can easily be coupled to a variety of transducers such as electrochemical,

optical, or mass based platforms to deliver a quantifiable output. Traditional NABs work on complementary hybridization or antigenic protein capture process during a biorecognition event. DNA, RNA, peptide nucleic acid (PNA), and aptamers are the four different types of nucleic acid molecules employed in NABs [87]. DNA aptamers may have more promising applications in *in vivo* diagnostics, while RNA aptamers may have promising applications in therapy. Thus, the mode of operation in NABs can be categorized into two major classes as illustrated in Fig. 1.9. For the hybridisation strategy, each of the single stranded capture nucleic acid probes are designed complementary to the sequences to be detected and the recognition event is dependent on appropriate Watson-Crick base-pairing across the two single-stranded molecules [88]. The binding event is also dependent on various factors like pH, temperature and ionic conditions. On the other hand, in the target-capture based strategy, the capture nucleic acid probes undergo a receptor-ligand interaction leading to a conformational change upon binding to the target. This in turn brings the nucleic acid label (electroactive redox indicators) closer to the transducer surface thereby facilitating electron transfer. Variations in electrical signals (such as voltage, current, or conductance) brought on by electroactive indicators can serve as a reflection of the change. It is based on the selectivity of the capture probes towards the target of interest [89].

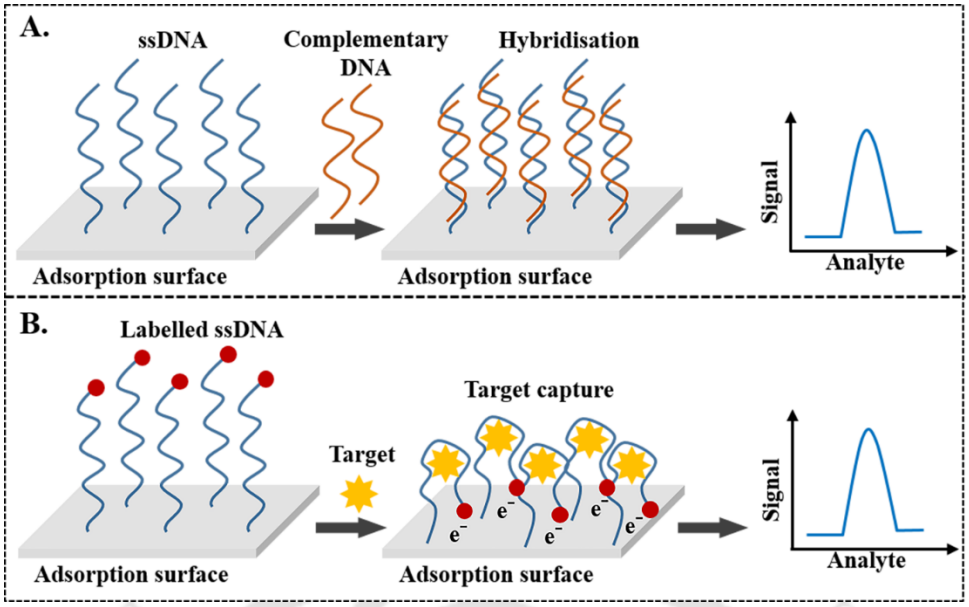

Fig. 1.9 Detection schemes of NABs on transducer platforms. A. Hybridization with complementary DNA, B. Target capture induced conformational change.

Traditional NABs use only NAs for detection. Nevertheless, with the advent of functional NAs (FNAs), the diversity and applicability of NABs is now extended to various walks of life. FNAs are defined as nucleic acids that can carry out not only complementary nucleic acid detection, but can be tailored to exhibit catalytic activity, monitor gene regulation or elicit specific binding interactions to small molecules, proteins, metal ions and bacteria [90]. In order to obtain a detectable signal, these FNAs are coupled to enzymatic amplification steps like nucleic acid sequence-based amplification, rolling-circle amplification, loop-mediated isothermal amplification, strand-displacement amplification, recombinase-polymerase amplification, hairpin amplification and hybridization-based chain reaction for making them suitable for real time and/or POC testing devices [91]. To improve the rate of reaction even more, nowadays many FNA-based amplification strategies are coupled with nanomaterials [92].

Different examples of three major groups of NABs and their working principles (with schematic illustrations are depicted below (Fig. 1.10-Fig. 1.12).

1.8.1.1 Electrochemical NABs

In electrochemical NABs (ENABs), the proximity of the detection label increases upon

the binding induced conformational change of the nucleic acid on the electrode surface. After binding to the target, the nucleic acid containing redox-active substances like methylene blue or ferrocene (or labels) comes closer to the electrode. A "signal-off" ENAB relays out the signal after binding, whereas a "signal-on" ENAB creates it. Depending on the configuration, the electrical signal might be due to potential, current, or impedance changes [93,94]. ENABs comprise of a working electrode, a capture probe, and an electroactive redox indicator. The size of the capture probe and surface characteristics of the electrodes have a significant impact on how well these biosensors operate. The small size of the functionalized nucleic acids (typically falling in the range of ~15 kDa) is crucial for efficient electron transfer in ENABs.

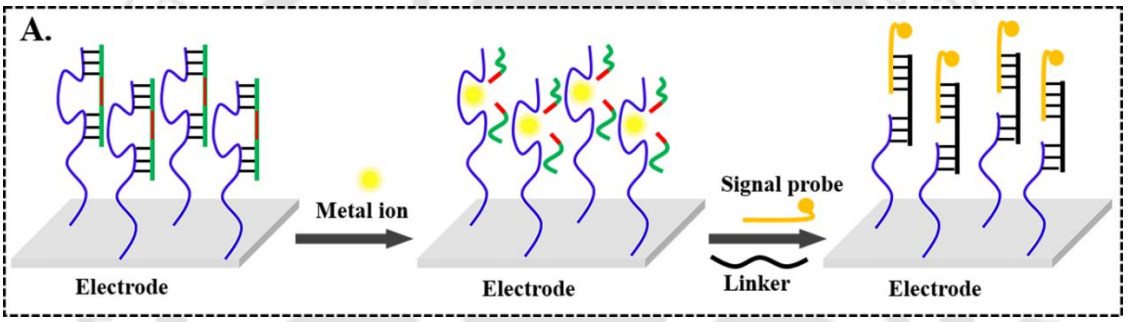

Fig. 1.10 FNAs for ENABs. The DNAzyme is immobilized on the electrode followed by the binding of the metal ion that leads to the concomitant cleavage of the substrate strand. Signal amplification takes place when the connection is established between the linker and the signal probe.

1.8.1.2 Fluorescence NABs

Fluorescence NABs (FNABs) are highly efficient tools that have replaced many traditional antibody-based fluorescence assays, utilising only a pair of fluorophore and quencher. In a typical "signal-on" mode, the fluorophore and quencher are held apart from one another by the aptamer. Consequently, when the nucleic acid recognition molecule undergoes favourable interactions with its target and undergoes conformational change, it brings the fluorophore and quencher close together, blocking the signal in a "signal-off mode". Small molecules and protein biomarkers are routinely studied by this mechanism of aptamer fluorescence resonance energy transfer (FRET) in diagnostic biosensors [95,96].

Fluorescent FNAs can be made to exist in two different forms: (i) by modifying with a

fluorescent chemical group and by (ii) conventional dyeing using a fluorescent dye. Low-fluorescence molecules can be made fluorescent by simple methods. The flexibility of engineering composite fluorescence nanoscale materials in amalgamation with nucleic acids make fluorescence-based platforms diverse for biosensor applications.

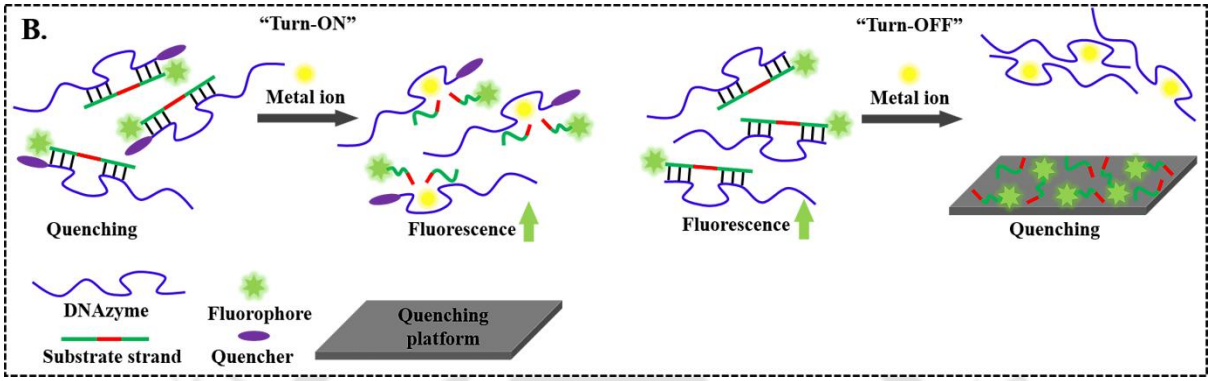

Fig. 1.11 FNAs for FNABs. Both "turn-ON" (shift from low to high fluorescence) and "turn-OFF" (shift from high to low fluorescence) patterns for FNABs upon target metal ion binding to the DNAzyme.

1.8.1.3 Colorimetric NABs

Colorimetric NABs (CNABs) are designed to sense changes in colour for signal detection [97]. The recent developments in CNABs show that several lateral flow assays (LFA), which are known for fast antigen testing as now being integrated with nanoscale detection labels for novel colour-change based naked eye interpretation in diagnostics. FNAs for CNABs are particularly interesting for its use in resource-poor settings that do not require high-end instruments.

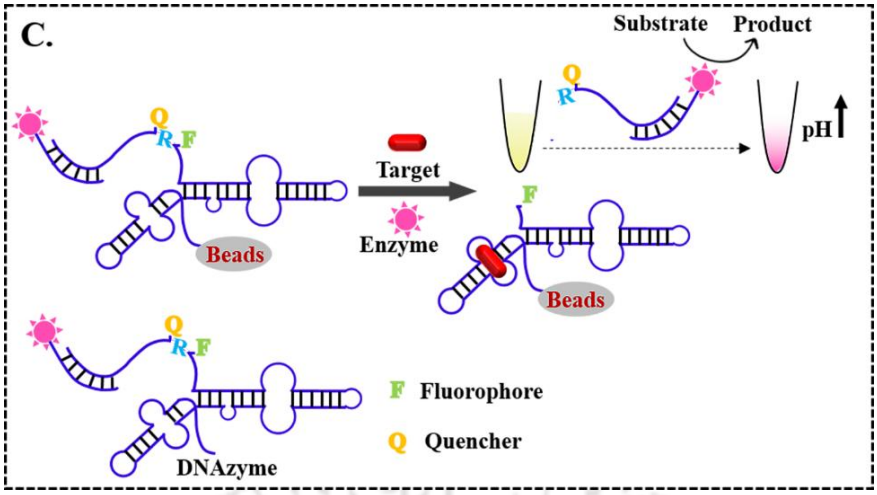

Fig. 1.12 FNAs for CNABs. Enzyme conjugated to one end of the DNAzyme can convert the substrate to the product; thereby producing colour change that is visible to the naked eye.

1.8.2 Aptamers and SELEX

A special class of FNAs, called aptamers have been designed to meet the existing challenges of traditional biorecognition elements for sensing puposes. They are short sequences of artificial DNA, RNA, XNA, or peptide that bind to a specific target molecule or family of target molecules, offering unique advantages in biosensing, bioimaging, and drug-related applications. These aptamers function as molecular recognition beacons that fold into three-dimensional conformations and bind to a variety of targets, including proteins, peptides, small molecules, and metal ions. The term "aptamers" (derived from the Greek word aptus; "to fit") was coined by Andy Ellington and Jack Szostak in independent works that followed a similar general strategy [95,98] (Fig. 1.13).

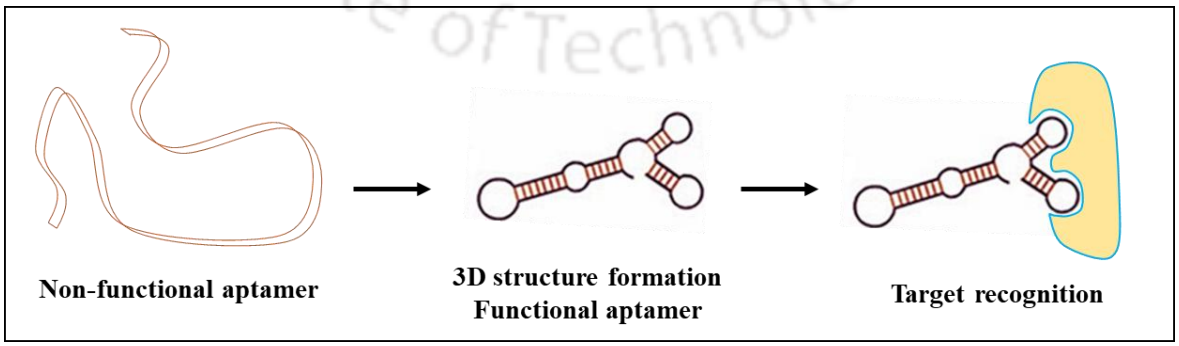

Fig. 1.13 Use of aptamers as biorecognition molecules.

The majority of aptamers are generated synthetically using a rapid and iterative selection technique called systematic evolution of ligands by exponential enrichment (SELEX), which searches among several random sequences for binders using a chosen target as an enrichment factor. In SELEX, chosen molecular targets are incubated with a random pool of oligonucleotides as a starting library. In order to establish a fresh pool of aptamer sequences for carrying over to the following round of selection, bound sequences from each selection round are recovered and PCR-amplified. The number of rounds required to locate target-binding aptamers is typically between five and twenty [99]. An aptamer's single-stranded chain is often folded into a distinctive binding architectural form, which may include a secondary structure and a three-dimensional structure. They exhibit the capability to not only interact with their target protein through their tertiary structure but also interact with complementary nucleic acids to create multiple double-stranded or "stem and loop" formations [100]. Moreover, aptamers can be integrated with direct DNA sequencing of clinical samples in the near future. Targeted next-generation sequencing (NGS) approaches (directed towards identification of resistance loci) or whole genome sequencing (WGS) approaches (for sequencing of whole genomes) for MTB genomes are currently in use, but have several limitations [101]. We hypothesize that aptamers can be made to act as capture agents to bind to MTB genomic sequences, which could improve the accuracy and efficiency of sequencing; particularly in complex or low-abundance samples. In other words, aptamers could facilitate the targeted sequencing to delineate population-wide trends in resistance patterns through targeted sequencing of specific regions of the genome, allowing for a more focused analysis, as opposed to sequencing entire genomes or transcriptomes. This combination of aptamer-mediated capture and next-generation sequencing could lead to faster diagnostics.

In a particular microenvironment, aptamers fold into distinct three-dimensional conformations through shape complementarity, electrostatic interactions, π–π stacking

interactions, and hydrogen bonding.

Use of such aptamers in miniaturized biosensor formats have led to the development of "aptasensors" that have revolutionized the approaches of clinical diagnostics. Aptasensors are essential requirements for TB diagnostics in the future due to their advantages, which include high specificity and strong affinity, the ability to bind to a wider range of targets, increased stability, lower synthesis and storage costs etc. [102–104]. Nowadays, aptamers are primarily designed to meet the WHO's ASSURED (affordable, sensitive, specific, user-friendly, rapid and robust, equipment-free, and deliverable to end users) criteria for diagnostics [105]. Aptamers have various advantages over antibodies. A comparative discussion of the use of aptamers and its advantages over antibodies is represented in Table 1.1.

Table 1.1: Advantages of aptamers over antibodies.

Parameter	Aptamer	Antibody
Molecular weight	Relatively smaller (15-50 kDa)	Large (150-700 kDa)
Structural uniqueness	Various 3D structures, stem-loops, internal loops, purine-rich bulges, hairpin structures, pseudo-knots, kissing complexes, and G-quadruplex structures	β sheets (unless designed separately)
Shelf life	Long	Short
Production	Easy (few hours to months)	Laborious, multi-step process (few months to a year depending on success rate)
Screening process	Iterative rounds against known target minimize time taken	Laborious and expensive
Animal immunization	Not required	Required (except for engineered antibodies)
Quality control	Minimal to no batch-to-batch variation	High chances of batch-to-batch variation

Ease of modification	High	Low
Targets	Wide array of targets including cells, viruses, polysaccharides, small metaboloites, nucleic acids, small inorganic molecules, ions, amino acids (aa),	Immunogenic molecules like protein antigens, but can recognize cells, virus, polysaccharides, nucleic acids
Immunogenicity (allergic propensity)	None	High (unless humanized)
Stability	Improved thermal and chemical stability	Poor stability at different temeratures and pH
Specificity to target	High	High
Reannealing capability	Can reanneal if denatured	Fails to retain structure if denatured
Cost	Low	High
Binding affinity	Nanomolar, picomolar, femtomolar, attomolar	Nanomolar, picomolar, femtomolar
Forces of interaction with target	Electrostatic, hydrophobic, Van-der waals, hydrogen	Electrostatic, hydrophobic, Van-der waals, hydrogen
Ease of binding studies for *in vitro* diagnostics	High, can be made to select for ligands under a wide range of chemical conditions	Low, restricted to binding under physiological conditions

1.8.2.1 Advanced aptasensors for TB

The primary components of an ideal TB aptasensor include the following: (i) the TB biomarker (proteins, nucleic cid, whole bacterium, small molecules, metabolites, etc); (ii) the biorecognition element (DNA/RNA/PNA aptamer) for specific biomarker capture along with labels for signal amplification, (iii) transducers (piezoelectric, optical, electrochemical, microfluidic etc.) and (iv) the signal output domain. Fig. 1.14 shows the different components of a TB aptasensor.

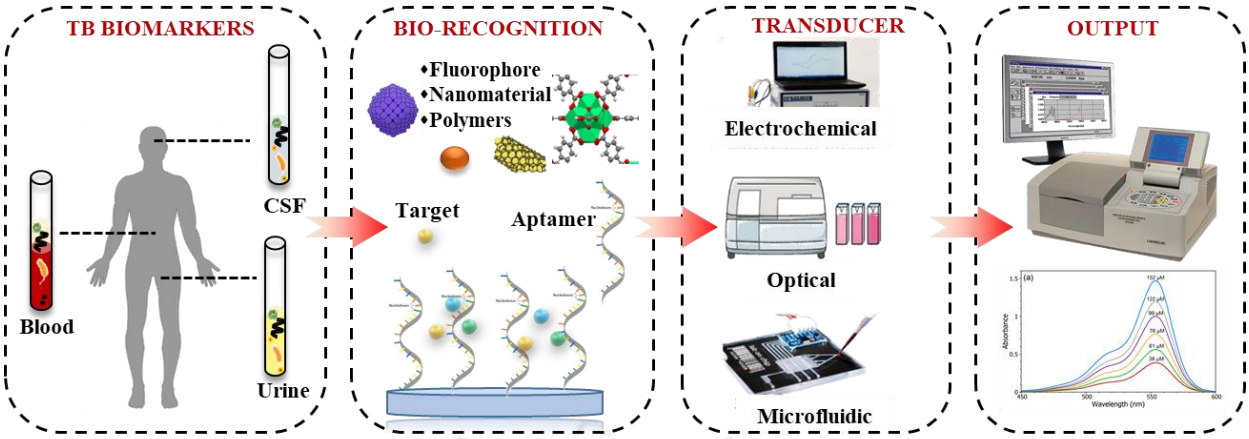

Fig. 1.14 Essential components of a TB aptasensor.

Aptamers against immunodominant antigens of the MTB, such as CFP-10, ESAT-6, and CFP-10-ESAT-6 heterodimer have been identified and investigated for their detection of active TB in clinical sputum samples [106–108]. Some of them are discussed below and in Table 1.2.

Mozioglu and colleagues selected CFP-10, ESAT-6, and the H37Rv aptamers using two different SELEX selection protocols and showed higher binding affinity of the aptamers to MTB H37Ra [109]. Thus, advancements in aptamer development suggests use of multiple aptamers for multipronged detection of more than one target for TB detection [110].

HspX TB biomarker has been detected by DNA aptamers in sputum samples of TB infected individuals. Lavania et al. reported specificities of 94.1% and 91.2% through the ALISA method, which was better than the conventional antibody based assay, and had a specificity of 68.2% [111]. Another aptamer-based biosensor assay for MPT64 with aptamers on gold electrodes reported a LOD of 81 pMoles for MPT64 and reduced reaction time to only 30 minutes [112]. Recently, another HspX ALISA was developed to detect pleural TB (pTB) and its performance was compared with qPCR, GeneXpert and ELISA in pleural fluid samples. The technique detects pTB with ~93% sensitivity and ~98% specificity [113].

Detection of CFP10 antigen by chronoamperometry for early diagnosis was reported by Yunus et al. using anti-CFP10 aminated aptamer covalently immobilized onto the

disposable screen-printed carbon electrode via carbodiimide chemistry with diazonium modified electrode [114]. Detection of CFP10 in sputum by another research group depicted use of CFP10 aptamers with dual amplification via DNA crosslinking click reaction and target release cycle. Gold nanoparticles, each loaded with a number of quadruplex aptamer motifs, bound on the electrode surface remarkably enhance the signal [115]. Das and his colleagues combined the electrochemical property of methylene blue (MB) and the recognition property of aptamers to develop aptasensor against HspX which succesfuly detected 10 pg of the target analyte in CSF samples of tuberculous meningitides [116]. Another novel aptasensor for detection of MPT64 antigen using fullerene nanoparticles, nitrogen-doped carbon nanotubes and graphene oxide (C_{60}NPs-N-CNTs/GO) was designed by Chen and colleagues. Additionally, conductive polyethyleneimine (PEI)-functionalized Fe-based metal-organic framework (P-MOF) was used as a sensing platform to absorb bimetallic core-shell Au-Pt nanoparticles (Au@Pt), which could accelerate electron transfer and increase the immobilization of MPT64 antigen aptamer I (MAA I). In this technique, tetraoctylammonium bromide (TOAB) triggered the intrinsic electroactivity of the tracer label following the standard sandwich-type protein-aptamer recognition, resulting in a distinct current response. With a limit of detection (LOD) as low as 0.33 fg/mL, the suggested aptasensor demonstrated a broad linear range for MPT64 detection under ideal conditions, ranging from 1 fg/mL to 1 ng/mL. Most importantly, it demonstrated a promising potential for TB diagnosis in clinical practice by successfully detecting MPT64 antigen in human serum [117].

In another work, a rapid, sensitive and highly selective electrochemical aptasensor was developed for the detection of MPT64 using prussian blue nanoparticles (PBNPs) and poly-diallyl dimethyl ammonium chloride (PDDA) modified electrode surface. Au nanoparticles (AuNPs) were linked on the PBNPs by electrostatic adsorption, after that, the aptamer and detection enzyme horseradish peroxidase were applied on the Au@ PBNPs that worked as the

signal enhancer. The aptasensors showed a linear range of 1 to 10,000 $pgmL^{-1}$, and the LOD was reported to be 21 $fgmL^{-1}$ [118,119]. Li and his colleagues had also reported a dual-aptamer-based voltammetric biosensor for MPT64 using a gold electrode modified with a peroxidase loaded composite consisting of gold nanoparticles and a Zr(IV)/terephthalate metal-organic framework [118]. Sypabekova and colleagues also used a long linker aptamer in the form of thiol modified PEGylated HS-$(CH_2)_6$-$OP(O)_2O$-$(CH_2CH_2O)_6$-TTTTT-aptamer in the presence of co-adsorbents for label-free MPT64 aptasensor fabrication. This electrochemical impedance spectroscopic platform yielded a 80 pM LOD in an overall assay time of thirty minutes [112]. Furthermore, an electrochemical aptaelectrode based on nanocomposite consisting of chitosan, iron-oxide nanoparticles and functionalized graphene has been fabricated to detect MPT64 with an LOD of 0.9 $fgmL^{-1}$ within 20 minutes was developed by Thakur et al. [120].

Jeon and colleagues created an aptamer beacon responsive to antigen TB7.7, in a hairpin-like structure labeled with 5′-FAM and 3′-BHQ1 dyes that undergoes conformational change upon binding and generates a fluorescence signal when TB7.7 is present. Furthermore, GO was added to raise the signal-to-background ratio and thereby increase the aptasensor's sensitivity. Following the optimization procedure, the developed aptasensor detected TB7.7 in buffer and serum with a low detection limit of 0.8779 nM and 0.7089 nM, respectively, demonstrating high sensitivity and specificity [96].

Kumari and her colleagues recently demonstrated the utility of two aptamers designed against two novel biomarkers like GlcB (malate synthase G, expressed independently of HIV coinfection) and HspX (alpha-crystallin, a dormancy responsive antigen) proteins for detection of abdominal TB [121]. Their study showed that the aptamers performed better than polyclonal antibodies raised against the two biomarkers for detecting TB from ascitic fluid samples via simple ALISA based methods.

Li et al. described a dual amplification strategy-based electrochemical aptasensor to

detect MTB antigen MPT64. They employed urchin-like Ce-metal organic frameworks (MOFs) as a support matrix to accelerate electron transfer. Moreoer, a novel redox nanoprobe anthraquinone-2-carboxylic acid (AQCA) conjugated ordered mesoporous carbon material (of CMK-3) was employed for signal amplification [122]. The desgned aptasensor showed a good linear relationship in the range from 100 fg/mL to 10 ng/mL with a low detection limit of 67.6 fg/mL.

Huang and his team developed a sensitive aptasensing platform for ESAT6 detection using MXene/C_{60}NPs/Au@Pt nanocomposite as signal amplification unit. (bimetallic core-shell Au@Pt nanoparticles, fullerene nanoparticles, MXene, a novel type of metal carbides and nitrides material,) [123] Their work was comparable to commercial ELISA assays and even exhibited better specificity of 96.7% vs 83.3% of ELISA in clinical serum sample diagnosis.

Recently, a novel aptasensor encompassing a surface-activated titanium carbide $Ti_3C_2T_x$ mediated adsorption of acetylene black coupled with polyaniline as a signal tag for the detection of the ESAT-6 antigen was proposed by Zuo et al. [124]. This sensor showcased a triple-signal amplification strategy with an additional NiMn layered double hydride (NiMn LDH) and nitrogen-doped carbon nanotubes (N-CNTs). The authors used biotinylated aptamer specific for ESAT6 immobilized onto a streptavidin-coated sensing interface, forming an amplification platform for further signal enhancement of the sensor.

Table 1.2 Selected examples of TB-aptasensors against secretory biomarkers as targets.

- **Target**: MPT64

Aptasensor	Label/ electrode/ immobilization/ sensing surface	Sequence (5′ - 3′)	Assay format	Detection strategy	Amplification strategy	Analytical parameter	Reference
Electrochemical and Piezoelectric	PEI-Fe-MOF/Au@Pt GCE/5′ thiol; SAM	$SH–(CH2)_6$ – TGGGAGCTGAT GTCGCATGGGT TTTGATCACATG A	DPV turn on	Sandwich assay	Au-C60NPs-NCNTs/ GO label PEI-Fe-MOF TOAB	In PBS pH 7.0: 0.33 fg/mL LOD; 1 fg/mL-1 ng/mL LR. In 2% clinical healthy human serum: 94.8%-102.0% recovery, Recovery not reported in TB infected serum.	[117]
	GDE/5′ thiol; SAM	$SH–(CH2)_6$ – TGGGAGCTGAT GTCGCATGGGT TTTGATCACATG A	DPV turn on	Sandwich assay	-GNPs-C60-PAn label	In PBS pH 7.0: 20 fg/mL LOD; 0.02-1000 pg/mL LR. In healthy human serum: 97.28%-107.3% recovery.	[125]
	GDE/5′ thiol; SAM	$SH–(CH2)_6$– TTCGGGAATGA TTATCAAATTTA TGCCCTCTGAT	DPV turn on	Sandwich assay	Au@PB-HRP label	In PBS pH 7.0 + HQ + H_2O_2: 21 fg/mL LOD; 1-10,000 pg/mL LR. In human serum: 97.4%-110% recovery.	[119]
	GDE/5′ thiol; SAM	$SH–(CH2)_6$– TTCGGGAATGA TTATCAAATTTA TGCCCTCTGAT	DPV turn on	Sandwich assay	AuNPs/MOF label HRP	In PBS pH 7.0 + HQ + H_2O_2: 10 fg/mL LOD; 0.02-1000 pg/mL LR. In healthy human serum: 95.9%-111.6% recovery.	[119]

GDE/5′ thiol; SAM	HS–(CH_6)6–OP(O)2O–(CH_2CH_2O)6-5′ -TTTTT-aptamer	EIS turn on	Change in impedance	-	In SELEX buffer/1% human serum: 3.7 ng/mL (81 pM) LOD; 2.26 ng/mL-2300 ng/mL (49 pM-50 nM) LR.	[112]
Au-IDE/5′ thiol; SAM		EIS turn on		-	LOD: 188.6 fg/mL (4.1 fM); LR: 4.6 fg/mL-230 ng/mL (0.1 fM-5 nM). In sputum/$[Fe(CN)_6]^{3-/4-}$: 76.47% sensitivity; 100% specificity. In serum/$[Fe(CN)6]^{3-/4-}$: 82.24% sensitivity 100% specificity (relative to AFB).	[126]
Streptavidin-PEDOTCNT-FTO/5′ biotin aptamer	[Btn]–GTACAAACGACGGCCAGTCCTTGGGATGATTCAAGCAAAGCCTCACGCCTACGGCTAAGTCATAGCTGTCTCTCCTG	DPV turn on	Change in impedance	PEDOT-CNTs sensing platform	In PBS pH 7.0 + $[Fe(CN)_6]^{3-/4-}$: 0.5 ± 0.2 fg/mL LOD; 1 pg/mL 1-10 ng/mL LR. Sensitivity of 176 µA fg/mL cm^{-2}. In human serum: 88%-95% recovery (matrix effect).	[127]
Streptavidin-CHITIOGR-FTO/5′ biotin Aptamer	[Btn]–GTACAAACGACGGCCAGTCCTTGGGATGATTCAAGCAAA–GCCTCACGCCTACGGCTAAGTCATAGCTGTCTCTCCTG	DPV turn on	Change in impedance	CHIT-IOGR nanocomposite film sensing platform	In PBS pH 7.0 + $[Fe(CN)_6]^{3-/4-}$: 0.9 fg/mL LOD; 1 fg/mL -10 ng/mL LR. Sensitivity of 100 µA fg/mL cm^{-2}. In human serum: 83-95% recovery (matrix effect).	[120]

- **Target**: ESAT6

Aptasensor	Label/ electrode/ immobilization/ method/ sensing surface	Sequence (5′ - 3′)	Assay format	Detection strategy	Amplification strategy	Analytical parameter	Reference
Electrochemical and Piezoelectric	Pt@AuNPs-GCE/5′ thiol; SAM	$SH–(CH_2)_6–$ GGGAGCTCAGA ATAAACGCTCA ACCTCCCTGGG TCAC– CATAGACTCCA TCTAAGATGCTT CGACATGAGGC CCGGATC	CV turn off	Change in impedance	Pt@AuNPs platform PDDA-MOF-rGO Toluidine blue reporter	In PBS pH 7.0 + KCl + $MgCl_2$: 0.33 fg/mL, LOD; 10 pg/mL-200 ng/mL LR. In clinical healthy human serum: 99-102% recovery.	[84]
	NG@Zr-MOF-on-Ce-MOF@Tb-GCE/5′ -PO_4^{3-}	$PO_4^{3–}$- GGGAGCTCAGA ATAAACGCTCA ACCTCCCTGGG TCACA– TAGACTCCATCT AAGATGCTTCG ACATGAGGCCC GGATC	CV turn off	Change in impedance	NG@Zr-MOF-on-Ce-MOF platform Toluidine blue reporter	In PB pH 7.0: 12 fg/mL LOD; 100 fg/mL-10 ng/mL LR. In 50% diluted healthy human serum: 90-94.3% recovery.	[128]

GP/PANI-SPGE/5′ –NH_2; Glutaraldehyde crosslinker	NH_2–GCCTGTTGTGAGCCTCCTAACCCCATCTTATACGTATATGG–ACTCATCTCGACCCCCCGATAGGCTTGGTACATGCTTATTCTTGTCTCCCC	DPV turn on	Aptamer-Antibody sandwich assay	GP/PANI platform Fe_3O_4/Au MNPs reporter	In PBS pH 7.4 + H_2SO_4: 1.5 ng/mL LOD; 5-500 ng/mL LR. In healthy and infected sputum samples: 100% sensitivity and specificity relative to culture and smear microscopy methods.	[129]
Au-IDE/3′ thiol CPAuNPs; Hybridization	GGGAGCTCAGAATAAACGCTCAAACGTATTCCATAGTGCTTTATTACTCGCACTTGTGTTCGACATGAGGCCCGGATC–C6	MSPQC turn on	AuNPs-capture probe	Dissociation of aptamer/CP dsDNA Duplex	In $[Fe(CN)_6]^{3-/4-}$: LOD and LR not reported. In M7H9 culture medium/clinical pathogenic MTB sample: 103 CFU/mL LOD.	[130]

- **Target**: Ag85A

Aptasensor	Label/ electrode/ immobilization/ sensing surface	Sequence (5′ - 3′)	Assay format	Detection strategy	Amplification strategy	Analytical parameter	Reference
Optical	ATTO647 N	GCTGTGTGACTC CTGCAAGCGGG AAGAGGGTAAG GGGAGGGAGGG TAACGCGGA GAAGGCAAGCA GCTGTATCTTGT CTCC (Apt 22) GCTGTGTGACTC CTGCAATCAGG AAAGAACTTAG GGGTGGGAGGA GGGTATAAATA CGGAATG–CAGCTGTATCTT GTCTCC (Apt 8)	FL turn on	Change in aptamer hairpin	GO quencher	In PBS: 51.2 ng/mL (1.5 nM) LOD; 170.5-6820 ng/mL (5-200 nM) LR. In 2% healthy human serum: 91.8-97% recovery; 2.1 nM LOD.	[131]

- **Other TB aptasensors**

Aptasensor	Target	Label/ electrode/ immobilization/ sensing surface	Sequence (5′ - 3′)	Assay format	Detection strategy	Amplification strategy	Analytical parameter	Reference
Electrochemical and Piezoelectric	CFP10	GP/PANI-SPGE/5′ –NH_2; Glutaraldehyde crosslinker	NH_2–GCCTGTTGTGA GCCTCCTAACC CCATCTTATACG TATATGG–ACTCATCTCGA CCCCCGATAGG CTTGGTACATG CTTATTCTTGTC TCCC	DPV turn on	Aptamer-Antibody sandwich assay	GP/PANI platform Fe_3O_4/Au MNPs reporter	In PBS pH 7.4 + H_2SO_4: 1.5 ng/mL LOD; 5-500 ng/mL LR. In healthy and infected sputum samples: 100% sensitivity and specificity relative to culture and smear microscopy methods.	[129]
	CFP10	Au-IDE/3′ thiol CPAuNPs; Hybridization	GGGAGCTCAGA ATAAACGCTCA AACGTATTCCA TAGTGCTTTATT ACTCGCACTTGT GTTCGACATGA GGCCCGGATC–C6	MSPQC turn on	AuNPs-capture probe	Dissociation of aptamer/CP dsDNA Duplex	In $[Fe(CN)_6]^{3-/4-}$ LOD and LR not reported. In M7H9 culture medium/clinical pathogenic MTB sample: 103 CFU/mL LOD.	[130]
	CFP10	GDE/5′ (DBCO)-DNA thiol; Hybridization	CCTGAAAGGGG CCTGCCCCACT ATCTCACATGG GGTTCAGTTGG TTGTACG	DPV turn on	AuNPs-DNA - Hybridization - DNAzyme and HRP	Dissociation of aptamer/CP dsDNA	In PBS pH 7.4 + HQ + H_2O_2: 10 pg/mL LOD; 0.01-100 ng/mL LR. In clinical healthy and TB infected sputum samples parameters not reported.	[119]

	HspX	AuNPs-SPCE/3′ thiol; SAM	AGGGCTTTTTTT TTTTTTAGTTCG TTTG-C6–SH	DPV turn off	5′ MB -AuNPs sensing platform	Switching of aptamer hairpin	In Tris buffer pH 7.5: 10 pg/mL LOD; 0.01-500 ng/mL LR. In 10% CSF samples/Tris buffer pH 7.5: Sensitivity (~95%), specificity (~97.5%), LOD of 10 pg/mL	[116]
	IS6110	AgNPs sensing platform	/5ThioMC6–D/TCCTGGGCTG GCGGGTCGCTT CC	EC-SERS turn on	AgNPs	Change in Raman scattering intensity	In 0.1 M NaF: 280 µg/mL LOD; LR in NaF and parameters in synthetic urine not reported	[132]
	H37Rv	Au-IDE/5′ thiol; SAM	SH–GGGAGCTCAGA ATAAACGCTCA ACCCTGCGGGG CTGCCCGA–TATGT–GTCCAAGTGGT GTTCGACATGA GGCCCGGATC	MSPQC turn on	SWCNTs	Dissociation of aptamer/SWCNTs composite	In detection medium: 100 CFU/mL LOD; LR not reported. In detection medium/20% clinical sputum samples: 86% sensitivity; 90% specificity relative to culture method, and 100% sensitivity; 91% specificity relative to BACTEC MGIT 960 automated system.	[130]
Optical	TB7.7	FAM label	CACCTAATACG ACTCACTATAG CGGATCCGA	FL turn on	GO quencher	Change in FRET	In buffer: 6.76 ng/mL (0.8779 nM) LOD; 7.7-2310 ng/mL (1 nM-300 nM) LR. In 10% human serum: 5.46 ng/mL1 (0.7089 nM) LOD; 7.7-	[96]

						2310 ng/mL (1 nM-300 nM) LR. In clinical active TB serum samples: 41.67% sensitivity; 92.86% specificity relative to AFB (matrix effect)	
LAM	-	GGCGCCATAGC GACGGGGCCAT TCCAAGAA-biotin (direct dot-blot) GCGGAATTCTA ATACGACTCAC TATAGGGAACA GTCCGAGCCGG CGCCATAGCGA CGGGGCCATTC CAAGAAGGGTC AATGCGTCATA (indirect dot-blot assay)	Col turn on	HRP reporter Smartphone device	Direct and Indirect dot-blot assay	In PBS: 104 CFU/mL (direct), 105 CFU/mL (indirect dotblot assay) limit of quantification (LOQ); 104-107 CFU/mL LR In infected and healthy sputum samples parameters not reported	[133]

1.8.2.1.1 Library selection for SELEX

Oligonucleotide libraries represent the random pool of DNA or RNA from where the aptamers are selected through a series of selection steps. There are four parameters that are important for consideration while optimization of initial library selection: pre-structured libraries, the length of the constant and the random regions, and the nature of the nucleic acid. A random region and two constant (flanking) sections make up the library sequences. The constant regions allow PCR amplification using complementary primers binding to them. Each sequence in the library has a random area that is distinct. Moreover, the longer the random region, the better chances of obtaining potential candidate sequences. Typically, selection libraries comprise of 10^{14}-10^{15} distinct sequences. It has been shown that designing a library with more GC-richness can cumulatively improve the structural and functional uniqueness of a library. Thus, the final selection outcome of selected aptamers is greatly dependent on the diversity of the initial library sequences and the length of the random and flanking regions [134]. A study has shown that the target-binding motif was most prevalent in the 50 and 70 nucleotide choices amongst the six distinct random area lengths (16, 22, 26, 50, 70, and 90) that were examined [135]. Nucleic acids having modified 5^{th} carbon position in pyrimidines and 7^{th} nitrogen or 8^{th} carbon positions in purines can attribute to additional functionality too. These modified nucleic acids are made up of altered nucleotides or sugar and backbone changes that often enhance the chemical and biological stability. Pre-structured libraries that readily form stem-like double stranded structure within the constant regions can be pre-incorporated to increase predictability of final aptamer structure [136]. On the other hand, G-quadruplexes are stacked polymorphic DNA structures with intermediate loop regions that interact with ligands in different ways and can be pre-incorporated in the initial DNA libraries to necessitate unique structural and functional binding motifs [137]. Synthetic and modified nucleic acids are also found in DNA libraries as seen in a recently published work where aptamers show increased stabilities [138]. Another class of

functionally enhanced libraries produce "threomers", which are aptamers harbouring the α-L-threofuranosyl nucleic acid (TNA) backbone, which interact with improved affinities [139,140]. Modified libraries containing alkyne-modified uridine (5-ethynyl-deoxyuridine (EdU)) instead of thymidine was put forward by Pfeiffer and coworkers in a novel "click-chemistry" method where libraries can be modified and generated according to desired application for any target of interest [141].

Another special class of nuclease-resistant aptamers, called spiegelmers have found the interest of many, for both diagnostic and therapeutic applications. For example, for cardiac troponin detection in a modified sandwich assay, these spiegelmers have shown increased detection sensitivities in the study reported by Tolnai et al. [142]. Spiegelmers were also shown to be effective in electrochemical detection of various targets as showed by Rana and her group towards detection of hepcidin, an important biomarker of liver for iron-related disorders [143]. The chiral form of the target and D-form oligonucleotides are used in the SELEX procedure to create spiegelmers, and the L-form target is then prepared chemically. Compared to other anologous compounds, these are less expensive and does not require plenty resources to produce.

1.8.2.1.2 Separating binders and non-binders during SELEX

SELEX based selection strategies suffer various challenges of isolating the correct nucleic acid sequences that bind to the target of interest. Aptamers often bind to selection platforms, solid supports, protein-tags and unwanted molecules during selection, which can lead to enrichment of non-target aptamers. To avoid such discrepancies, introduction of counter and negative SELEX steps are useful to eliminate non-target aptamers. For cell-based SELEX, portioning bound and unbound aptamer candidates are performed by centrifugation. Two major separation techniques exist for protein-based SELEX are: (i) magnetic separation and (ii) capillary separation. Magnetic separation necessitates the use of magnetic microspheres coated with streptavidin loaded onto selection columns for isolating biotin-labelled nucleic acids or

nickel nitrile-acetic acid (Ni-NTA) or cobalt coated magnetic beads for isolating aptamers specific to any His-tagged target protein. Due to the use of easy availability of magnetic racks and spheres, magnetic separation is a very easy process for any protein-based SELEX platform [144].

Based on different electrophoretic mobility constants, capillary electrophoresis can separate free aptamers, proteins, and aptamer-protein complexes from one another. Chao and Zhu elaborated the use of capillary electrophoresis for selection of aptamers for various applications [145]. Morihiro and his team developed DNA aptamers containing azobenzene by capillary electrophoresis (CE)-SELEX process, a unique strategy that detects human thrombin in a photo-responsive detection approach [146]. Overall, CE-SELEX provides tuneable, quantifiable partitioning but has limitations of pooling limited library size and diversity of aptamers due to the small volume it can process.

Other novel separation techniques have come up in the recent past to improve aptamer selection. For example, centrifugal separation, fluorescence-activated cell sorting (FACS), gold nanoparticle assisted separation of ssDNA or sequential partitioning methods have shown potential to reduce the overall time of SELEX, bypass multiple enrichment steps, easy visualization through fluorescence intensity during the selecting process in order to improvise the traditional SELEX procedures [147–150].

1.8.2.1.3 Amplification of binders by PCR

Theoretically, strong or unspecific aptamers are less likely to be selected during the screening stage than aptamers with high affinity for the target. In order to selectively enrich the pool of specific aptamers or binders, PCR is routinely performed in between intermediate SELEX steps for amplifying them. Ideally, multiple PCR cycles also introduces a bias, which can be detrimental for successful selection of aptamers due to the formation of multiple non-desired products [151] Thus, careful optimization of PCR cycles is also crucial for successful

SELEX.

Due to exponential enrichment, the incorporation of errors are maximum during the PCR step. Asymmetric PCR can also be used to improve the selection of sense-strands in PCR cycles with unequal ratios of forward and reverse primers [152]. Also, a real-time PCR step after each enrichment cycle of SELEX also maximizes the chances of obtaining the correct number of SELEX cycles beyond which there is build-up of spurious products in PCR of varying lengths. After PCR, the common methods for separating the desired strand from the double strand is often achieved by selectively end-labelling primers (for example, biotinylated reverse primers) or using lambda exonuclease to digest one strand with 5′ phosphorylation after PCR. Failure of SELEX can also occur when PCR by-products dominate the aptamer pool, potentially masking and outcompeting genuine binders.

1.8.2.1.4 Improving final aptamers

For improving the quality of the aptamers, it is necessary to introduce selective selection pressure. For example, increasing the stringency of binding conditions is one way to generate aptamers with higher specificities. Several factors that need careful optimization for improving aptamer affinities are decreasing the target-nucleic acid incubation times, increasing the amount of competitors found in real samples as well as incorporating multiple washing steps with surfactants during the final rounds of SELEX. Monitoring techniques like flow cytometry, dot blot assays, fluorescence spectrophptometry, and ELISAs can help to study the aptamers generated after each cycle. For kinetic parameters of the generated aptamers, circular dichroism, surface plasmon resonance and biolayer interferometry are useful [99].

Recently, site-directed mutagenesis and truncation techniques have also led to the development of aptamers with improved affinities. *In silico* models of aptamer-target docking studies also guide rational truncation approaches. Moreover, the effect of spacers and modifiers on the equilibrium binding affinity of aptamer sequences are verified via multiple analytical

techniques that can help improve equilibrium binding constants for any target.

1.8.3 Nanomaterials and aptamer development

The integration of nanotechnology with biosensors have proved to be immensely beneficial for improving the functionality and sensing capacity of conventional biosensors. Nanoscale materials have been used for the design and development of nano-biosensors that possess excellent target detection sensitivities for infectious diseases [153].

Nanomaterials can be defined as, "a natural, incidental or manufactured material containing particles, in an unbound state or as an aggregate or as an agglomerate and where, for 50% or more of the particles in the number size distribution, one or more external dimensions is in the size range 1 nm-100 nm" according to the European commission [154]. For sensing applications, these nanomaterials can be broadly grouped into four classes: (i) carbon-based nanomaterials, (ii) inorganic-based nanomaterials, (iii) organic-based nanomaterials and (iv) composite-based nanomaterials.

Metal nanoclusters belonging to the second class, typically composed of several to hundreds of metal atoms, have attracted great interest in recent years. On the basis of novel these metal nanclusters, rapid colorimetric tetal echniques have enabled the detection of ions, cancer, and other biomarkers. Fluorescent metal nanoclusters (FMCs) have garnered a lot of attention due to their unique optical, chemical, and physical properties. These characteristics are useful for many applications, such as sensitive and fast detection and cellular imaging [155]. However, because of very small color variations, their colorimetric applications for rapid tests based on the naked eye or simple UV-vis absorption spectrophotometry are getting established. There is a lot of potential for using peroxidase-like FMNCs for various applications, especially in POC diagnostics.

In a recent work, Q. Chen et al. created aptamers-BSA-AuNCs, which use the TMB/H_2O_2 system, dual thiolated aptamers, and BSA-AuNCs to selectively detect *Salmonella typhimurium*.

The bacteria captured the aptamer-BSA-AuNCs and TMB to bring them together, allowing for a local increase in their concentration, thereby aiding in the formation of Au−S bonds between BSA-AuNCs and both aptamers. This is a novel example of the use of DNA-linked FMC based biosensor for clinical applications [156].

Taken together, several advancements in the domain of nanotechnology has fueled the development of sensitive labels for attachment to aptamers for construction and fabrication of TB aptasensors (Fig. 1.15).

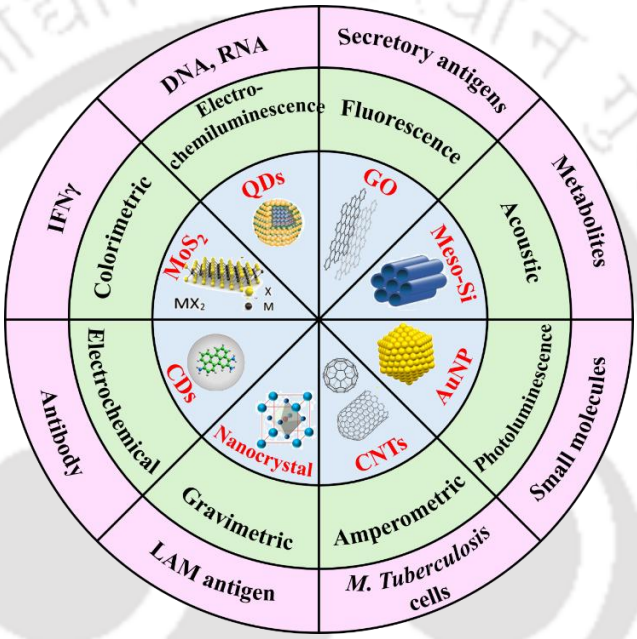

Fig. 1.15 Use of nanomaterials for development of biosensors in TB. TB-specific biomarkers include antibodies, LAM antigen, bacterial cells, small molecules, metabolites, secretory antigens, DNA/RNA and IFNγ among others that can be detected by aptasensors. Aptamers integrated with nanomaterials like nanocrystals, carbon nanotubes (CNTs), gold nanoparticles (AuNP), mesoporous silica (Meso-Si), graphene oxide (GO), quantum dots (QDs), molybdenum disulphide (MoS_2), or carbon dots (CDs) are used in sensing.

1.9 Real sample analysis for aptasensors

Aptamers are operational under optimum pH ranges, out of which their affinities fall sharply. Therefore, after preparing the final aptamers, specific buffer solutions ensuring good compatibilities are required for aptamer immobilization onto surfaces for real sample detection. There are a number of crucial parameters that are significant to ensure practical applicability of aptasensors for TB detection in real samples. The LOD of any designed aptamer is reported to

show higher values in real or spiked human samples when compared to buffers for *in vitro* diagnostics [131]. Thus, real specimens have significant challenges that affect the reproducibility of an aptasensor. These include diluted standard serum samples, and wide range of clinical samples such as human blood, red blood cell depleted whole blood, serum, urine, sputum etc for various POC testings. It is necessary to perform analysis on TB-infected samples in a class II biological safety cabinet in order to prevent exposure to contagious bacteria and to safeguard products, workers, and the environment. It is common practice to obtain clinical serum samples as the supernatant of centrifuged blood. To lessen background interference in the actual sample matrix, the serum samples are either used with or without salmon sperm DNA, which is stored in aliquots at -80 °C [128,157]. The majority of TB aptasensors have been shown to recover above 90% of spiked concentrations of TB biomarkers in diluted standard serum. Many aptasensors suffer from reduced sensitivity in real samples which is ascribed to the matrix effect, which arises from background interference caused by non-specific serum binding or interaction with other biological components of the real sample. Use of various background controls for proper interpretation of results when working with aptasensors is thus mandatory. In summary, TB aptasensors have shown better performance with real sample analysis than TB immunosensors and are more suitable to be developed into POCs for TB diagnostics due to their enhanced stabilities and no requirement for sample pre-treatment steps [120].

1.10 Motivation of the research work

There is an urgent need to develop rapid, more accessible, cost-effective, and TB-specific diagnostic screening assays due to the rise in TB infections and related deaths. Furthermore, specific recognition molecules that could detect the presence or absence of TB biomarkers on improved sensing platforms can lead to the development of robust diagnostic devices. Thus, a possible solution could be the use of aptamers as sensitive biorecognition elements for the detection of secretory TB biomarkers that can in the future deliver POC TB diagnostic devices.

Countries with limited resources that cannot afford expensive diagnostic laboratories would benefit from the development of such diagnostic tools. These tests would also enable quick diagnosis turnaround times and possibly speed up the onset of treatment.

In this study, we aimed to study these two important aspects using Ag85B and MPT64 antigens and designing aptamers to detect them. The existing lacunae of these two biomarkers in diagnostics is that there is no reported aptasensor platform against Ag85B biomarker and there is no reported aptasensor designed using the epitopic regions of the MPT64 biomarker for TB diagnostics. Our study will shed light, contribute to the development of sensitive screening methodologies for TB aptamers.

1.11 Objectives of the thesis

Based on the available literature and the potential for future research in understanding the role of aptamers in addressing the challenegs in TB diagnostics, the following objectives were formulated.

- Cloning, expression, purification and characterization of tuberculosis biomarkers.
- Screening and characterization of DNA aptamers against tuberculosis biomarker Ag85B.
- Development of aptasensor for detection of tuberculosis biomarker Ag85B.
- Screening of DNA aptamers for tuberculosis biomarker MPT64 through mimotope-based prediction.

1.12 Organization of the thesis

Chapter 1: Introduction and review of literature

This chapter provides an overview of challenges associated with the diagnosis of TB and the role of aptamers in addressing the diagnostic loopholes. A brief outline of the biomarkers of TB throughout the life cycle of the bacterium inside the host is shown. The role of aptamers in

detection of secretory antigens of MTB discussed in detail and the methods to characterize the aptamers are also highlighted. Use of nanomaterials for the development of TB aptasensors is also highlighted. This chapter concludes by explaining the purpose of the thesis, which aims to develop one DNA aptamer using a modified SELEX mechanism and depict its binding functions to its cognate ligand Ag85B in human serum for active TB diagnosis.

Chapter 2: Cloning, expression, purification and characterization of tuberculosis biomarkers

This chapter shows the cloning, expression and purification of the target protein diacylglycerol acyltransferase/mycolyltransferase Ag85B (gene: fbpB) and counter proteins that were considered for the study. Protein overexpression and purification studies of the histidine tagged antigenic biomarkers were met with a number of challenges: (i) the concentration of the proteins was too low to proceed for aptamer studies, (ii) there was considerable degradation of proteins during isolation from inclusion bodies, (iii) persistent presence of background proteins in the isolates and (iv) difficulty in bringing the proteins in soluble fractions during isolation. However, CD spectra analysis of Ag85B, MPT64 and ESAT6 proteins in phosphate buffer gave secondary structural elements in accordance with the reported literature. Enzymatic assay of Ag85B target antigen was assessed.

Chapter 3: Screening and characterization of DNA aptamers against tuberculosis biomarker Ag85B

A modified SELEX approach was used to screen aptamers against Ag85B. A new method "COFA-SELEX" (cut-off filtration assembly based SELEX) was used for the study. This chapter depicts the screening of recombinant clones of aptamer inserts into the cloning vector. Confirmation of clones is done by restriction digestion and PCR. Secondary structure predictions and CD spectroscopy is evaluated for characterization of putative G quadruplexes in the aptamers. One aptamer was selected and thereafter taken for further studies. EMSA and ITC is

carried out to show binding affinity between the target antigen and best DNA aptamer. Binding was also shown by docking analysis.

Chapter 4: Development of aptasensor for detection of tuberculosis biomarker Ag85B

The characterization of dissociation equilibrium constant through ALISA is done in this chapter. This chapter proposes the method to prove the efficiency of DNA aptamer based detection of Ag85B antigen. In this study, for the first time aptamers for Ag85B were developed and used for the establishment of a highly sensitive and selective GO-based aptasensor for detection of Ag85B. The generated aptamer (Ag85B-18C-20) was labeled with the fluorophore named fluorescein (FAM), having an absorbance maximum at 495 nm and emission maximum at 520 nm. FAM is the energy donor and GO acted as the energy acceptor. LOD is also calculated.

Chapter 5: Screening of DNA aptamers for tuberculosis biomarker MPT64 through mimotope-based prediction

This chapter proposes to develop a two level screening procedure for repurposing existing MPT64 aptamers: i) epitope based screening of of MPT64 to develop peptide mimotopes and ii) using the selected peptide mimotopes in designing a library for screening aptamers against MPT64.

Chapter 6: Discussion and future perspectives

This chapter gives a brief conclusion and future perspective that summarizes and highlights the critical findings from the work carried out. This chapter also emphasises the future direction of research aimed at elucidating the application of developed aptamers for multiple antigen based aptasensing platform for diagnosis of TB.

2

Cloning, expression, purification and characterization of tuberculosis biomarkers

Abstract

This chapter exploits the purification of three important secretory biomarkers of TB for use and application in designing aptasensing platforms for TB. Towards this, we cloned, expressed, purified and characterized recombinant Ag85B, MPT64 and ESAT6 proteins. The genes were amplified from H37Rv genomic DNA followed by their incorporation into suitable vectors (pET28a and pQE30) followed by its expression and purification through N-terminal His-tag using Ni-affinity from an *E. coli* host. All the recombinant proteins were purified in good quantity for use as a biomarker for detection studies using aptasensing. Each of the recombinant proteins were characterized for their size and biological intactness by SDS-PAGE, western blot as well as CD spectroscopic studies. The application of recombinant Ag85B protein as a target with two non-targets (MPT64 and ESAT6proteins used as controls) were to design a sensitive fluorescence based aptasensing platform. Additionally, several diagnostic aspects of MPT64 as a unique secretory biomarker is also explored and the findings have been summarized in the penultimate chapter of this thesis.

2.1 Overview

The genomic DNA of MTB H37Rv was fully sequenced by 1998. It is 4.4 million base pairs long and encodes for approximately 4,000 genes accounting for ~90% of the genome [46]. It also has a very high guanine + cytosine content that is albeit reflected in the biased nature of aa constituting the proteins of MTB. The genome sequence provides useful information about the majorly secreted antigens of MTB like Ag85B, ESAT6 and MPT64 among others. Earlier reports had identified their presence in culture filtrates of MTB [158]. Interestingly, these antigens are secreted at different times during the growth of the bacterium signifying their role in disease progression.

ESAT6 protein was reported to be present in the early and exponential phase of multiplication of the bacilli along with it molecular partner-chaperone CFP10. Only the pathogenic strains of the genus mycobacterium secrete ESAT6. Rv3875 open reading frame (ORF) codes for ESAT6, and the gene size is 288 bp and expressed as a 10 kDa protein. It can therefore be used as a potential biomarker for MTB, enabling quick, precise, and accurate detection of the infection at an early stage [159].

The Ag85 complex comprising of three individual proteins is a part of the outer cell wall and is gradually released during growth fom day 3 onwards [50]. Ag85B of Ag85 complex is the most abundant of the three proteins (Ag85A, Ag85B, Ag85C) and is synthesized from Rv1886c ORF on the genome to form a 30 kDa protein [65,160].

MPT64 protein encoded by Rv1980c ORF is found to be excreted by the bacterium from as early as 2 days which accumulates in the growth medium. It is reported to be used a apid differentiation biomarker of MTB from NTM. Thus, one or more of these proteins can serve as important biomarkers of TB disease [161].

Recombinant Ag85B, ESAT6 and MPT64 proteins have been well characterized in earlier reports [162]. Herein, we report the cloning, expression, purification and characterization

of N-terminally 6xHis-tagged proteins (Ag85B, ESAT6 and MPT64) for studying their applications as diagnostic biomarkers Table 2.1.

Table 2.1 Three major TB secretory biomarkers considered for the present study.

Name of biomarker	Gene name	locus name	Gene length	Amino acids	Mass (kDa)	Cloned in vector
Diacylglycerol acyltransferase/mycolyl-transferase Ag85B	fbpB	Rv1886c	978 bp	325	34.581	pQE30
Immunogenic protein MPT64	mpt64	Rv1980c	687 bp	228	24.855	pET28a
6 kDa early secretory antigenic target ESAT6	esxA	Rv3875	288 bp	95	9.904	pET28a

2.2 Materials

The MTB H37Rv genomic DNA was obtained from BSL3 facility, School of Biotechnology, Jawaharlal Nehru University, New Delhi. The primers were synthesized from Integrated DNA Technologies. The primer sequences, buffer compositions and reaction components used for the work are listed in Appendix section. All other chemicals used were of molecular biology grade. All solutions were prepared using water obtained from a Millipore water purification system. All the buffer solutions were filtered using the 0.22 µM syringe filters and sterilized for storage not more than 5 days.

2.3 Experimental methods

2.3.1 Primer Synthesis

The Ag85B (https://www.genome.jp/dbget-bin/www_bget?mtu:Rv1886c), ESAT6 (https://www.genome.jp/dbget-bin/www_bget?mtu:Rv3875) and MPT64 (https://www.genome.jp/dbget-bin/www_bget?mtu:Rv1980c) were amplified from H37Rv genomic DNA using specially designed primers along with prefabricated enzyme restriction sites. The FASTA sequences were downloaded for the protein and used for primer designing. Preference for restriction enzyme sites were checked using the NEBcutter tool

(https://nc3.neb.com/NEBcutter/) and Tm and GC percentages were calculated using the NEB Tm calculator (https://tmcalculator.neb.com/#!/main). The reverse complement tool (https://www.bioinformatics.org/sms/rev_comp.html) was used to check for the correctness of the as designed reverese primer. Compatible adapter sites were also added to the primers for the ease of restriction digestion for each restriction site. The forward and reverse primers for Ag85B gene were constructed with *Kpn*I and *Bam*HI respectively. The forward and reverse primers for ESAT6 gene were constructed with *Nde*I and *Xho*I restriction enzyme sites, respectively. The forward and reverse primers for MPT64 gene were constructed with *Bam*HI and *Xho*I, respectively.

2.3.2 Bacterial cell culture

The *E. coli* strains DH5α, BL21(DE3) and M15 were cultured and propagated in LB broth and agar respectively. The bacterial cultures were subjected to growth at 37 °C, 180 rpm (in shaker incubator) in the presence of suitable standard antibiotic (kanamycin and/or ampicillin) concentrations. The detailed information related to *E. coli* strain and selective media compositions used in this work have been incorporated in the Appendix section.

2.3.3 Nucleic acid quantification

The concentrations were assessed by UV-visible spectrophotometer (Multiskan Skyhigh plate reader, Thermo). Before measurement, the blank was set with nuclease free water. Readings were taken for dsDNA or ssDNA as per instrument specifications. The ratiometric significance of $\lambda_{260\ nm}/\ \lambda_{280\ nm}$ optical density values indicated purity within the range of 1.8-2.0. A ratio of ~1.8 is generally accepted as “pure” for DNA.

2.3.4 Protein quantification

Bradford Reagent has been used to determine protein concentration. The reagent contains coomassie brilliant blue G-250 that interacts with the basic and aromatic aa in the protein solution. Calibration curves prepared in suitable buffers and used for individual protein

estimations using BSA as standard.

2.3.5 Plasmid isolation

Plasmid DNA was isolated from cells using the MN Nucleospin® plasmid isolation kit. The cells were first revived from glycerol stocks by streaking them on a fresh LB-agar plate containing suitable antibiotics. A single colony from the agar plate was then inoculated in 5 mL of LB-antibiotic liquid medium and allowed to grow overnight at 37 °C and 180 rpm. The overnight culture was then centrifuged at 11,000 x g for 30 seconds, and the plasmid DNA was isolated according to the manufacturer's protocol. (https://www.mn-net.com/media/pdf/45/51/02/Instruction-NucleoSpin-Plasmid.pdf).

2.3.6 PCR amplification

The The DNA amplification was carried out through PCR using Quick load Taq 2X master mix in a thermocycler (SureCycler 8800, Agilent). A total 50- 100 ng genomic DNA was used as template for all kind of PCR reactions. The PCR reaction mixture conditions and compositions are mentioned in Appendix.

2.3.7 Restriction digestion and ligation

The cloning process involved digesting both the amplified PCR product and the vector using the same set of two different restriction enzymes (for performing sticky end ligation). Subsequently, the digested products were purified either through a PCR purification kit or by extracting them from excised agarose gel fragments using a gel extraction kit after visualization on a UV transilluminator. Following purification, the digested PCR product (insert) and the plasmids (vector) were ligated together using quick ligation kit. The ratio of vector to insert was determined using NEBioCalculator online tool (https://nebiocalculator.neb.com/#!/ligation). The ligation mixture consisting of vector, insert, DNA ligase and reaction buffer was incubated at 4 °C overnight and then transformed into *E. coli* DH5α cells.

2.3.8 Competent cell preparation and transformation

E. coli DH5α and BL21(DE3) cells were grown overnight in 5 mL LB medium at 37 °C and 180 rpm. The overnight culture was then diluted to 50 mL of fresh LB medium (OD_{600} = 0.1) and allowed to grow until the OD_{600} reached 0.3-0.5 at 37 °C and 180 rpm. The cultures were kept on ice to stop further growth for 30 minutes. The cells were harvested by centrifugation at 3000 rpm for 2 minutes. The resulting cell pellet was resuspended in 30 mL of ice-cold 0.02 M $MgCl_2$ and 0.08 M $CaCl_2$ and incubated on ice for 45 minutes. Subsequently, another round of centrifugation was performed, and the cell pellet was gently resuspended in 2 mL of ice-cold 0.1 M $CaCl_2$. For storing at -80 °C, glycerol was added at a final concentration of 20% as a cryoprotectant. To introduce the plasmid DNA into the cells, the cells were mixed with the plasmid DNA and the mixture was incubated on ice for 30 minutes, followed by a brief heat shock at 42 °C for 120 seconds. The cells were then immediately transferred back to ice for 1 minutes. Subsequently, 1 mL of LB medium was added to the cells and incubated at 37 °C and 180 rpm for 1 hour. After incubation, the transformed cells were pelleted by centrifugation at 2000 x *g* for 3 minutes. The cells were then plated on selective plates containing antibiotic(s). Transformed recombinant colonies were visible after incubation for 16-24 hours at 37 °C. Colonies were screened for correct inserts by restriction digestion and sequencing of positive clones. All the positive recombinant clones were stored at -80 °C for long-term storage.

2.3.9 Cloning, expression and purification of Ag85B

The Ag85B ORF was amplified from the H37Rv genomic DNA. It was cloned under the T5 promoter in pQE30 vector at *Bam*H1/*Kpn*I restriction enzyme sites. After digestion, the ligation mixture was transformed in *E. coli* DH5α cells and positive recombinants were first selected by colony PCR followed by physical mapping by restriction digestion. Recombinant plasmids were then transformed into *E. coli* M15 cells (containing pREP4 plasmid) and selected on antibiotic containing agar plates for protein expression. For protein purification, using 0.1%

inoculum from overnight cultures, secondary cultures were grown to OD_{600} ~ 0.6 and thereafter induced with 1 mM IPTG at 37 ºC for 4 hours. Bacterial cells were pelleted down and sonicated in lysis buffer followed by centrifugation at 11000 x g. For higher yield of the recombinant protein, purified inclusion bodies were used for the extraction of the protein. Briefly, the cell pellets were sequentially washed in three wash buffers with brief incubation for 20 minutes each time followed by a centrifugation step at 11000 x g at 4 ºC. The washed inclusion bodies were solubilized in solubilization buffer overnight, followed by dialysis to remove the detergent. The supernatant was analyzed on SDS-PAGE and thereafter taken for Ni-affinity chromatography. The supernatant was kept on binding with Ni-NTA resin and the flow through was collected. The resin was washed with 10 column volumes of wash buffer. The bound His-tagged Ag85B from column were eluted with elution buffer containing 250 mM imidazole. Presence of contaminating bands were removed by size-exclusion chromatography. Purified Ag85B protein was visualized on SDS-PAGE, and then electroblotted over nitrocellulose membrane to proceed with western blotting. The transfer of protein from gel to nitrocellulose membrane was confirmed by staining with Ponceau reagent and electrochemiluminescent substrate was used for developing the blot. For downstream applications, purified protein was stored in aliquots containing 10 % glycerol at -80 ºC.

2.3.10 Cloning, expression and purification of MPT64

The MPT64 ORF was amplified from the H37Rv genomic DNA. It was cloned under the T7 promoter in pET28a vector at *Bam*H1/*Xho*I restriction enzyme sites. After digestion, the ligation mixture was transformed in *E. coli* DH5α cells and positive recombinants were first selected by colony PCR followed by physical mapping by restriction digestion. Recombinant plasmids were then transformed into *E. coli* BL21(DE3) cells and selected on Luria Bertani, antibiotic containing agar plates for protein expression. For protein purification, using 0.1% inoculum from overnight cultures, secondary cultures were grown to OD_{600} ~ 0.8 and thereafter

induced with 1 mM IPTG at 20 ºC for 20 hours. Bacterial cells were pelleted down and sonicated in lysis buffer followed by centrifugation at 11000 x g for 30 minutes. The supernatant was filtered through a .45 µm sterile filter disc and thereafter taken for Ni-affinity chromatography. The remaining of the steps were followed as mentioned in section 2.3.9.

2.3.11 Cloning, expression and purification of ESAT6

The ESAT6 ORF was amplified from the H37Rv genomic DNA. It was cloned under the T7 promoter in pET28a vector at *Nde*1/*Xho*I restriction enzyme sites. After digestion, the ligation mixture was transformed in *E. coli* DH5α cells and positive recombinants were first selected by colony PCR followed by physical mapping by restriction digestion. Recombinant plasmids were then transformed into *E. coli* BL21(DE3) cells and selected on antibiotic containing agar plates for protein expression. For protein purification, using 0.1% inoculum from overnight cultures, secondary cultures were grown to OD600 ~ 0.6 and thereafter induced with 1 mM IPTG at 37 ºC for 5 hours. Bacterial cells were pelleted down and sonicated in lysis buffer followed by centrifugation at 11000 x g. For higher yield of the recombinant protein, purified inclusion bodies were used for the extraction of the protein. Briefly, the cell pellets were sequentially washed in three wash buffers (wash buffer 1, wash buffer 2 and wash buffer 3) with brief incubation for 20 to 30 minutes followed by centrifugation to obtain pellets at 11000 x g at 4 ºC. The washed inclusion bodies were solubilized in solubilization buffer for 3 hours at 37 ºC, followed by dialysis overnight to remove the detergent. The supernatant was analyzed on SDS-PAGE and thereafter taken for Ni-affinity chromatography. The remaining of the steps were followed as mentioned in the previous sections.

2.3.12 CD spectroscopic analysis

After every purification experiment, purified eluates were pooled together and desalted in 20 mM phosphate buffer using PD10 columns (GE Healthcare) according to the manufacturer's protocol prior to Far-UV CD spectroscopy. Far-UV CD of purified Ag85B,

ESAT6 and MPT64 was recorded under continuous nitrogen purging on a J-1500 spectropolarimeter (Jasco, Japan) at 25 °C. The far-UV CD spectra were acquired from 250 to 190 nm. A continuous scan rate of 100 nm/min with 5.0 nm bandwidth and 1 second data integration time was used. The acquired spectra are the average of five scans, and the buffer signal was subtracted from the final signal of each sample to remove the background signal of the buffer components. Measurements of 0.15 mg/mL protein were recorded using a quartz cuvette with a path length of 0.2 cm.

2.3.13 MALDI analysis

Intact mass of the recombinant His-tagged Ag85B protein was confirmed by MALDI (MALDI/TOF analyzer, make: Bruker, model : Autoflex Speed) analysis (10 shots, linear positive mode). Purified Ag85B was concentrated using a Amicon Ultra centrifugal filter (10,000 MWCO) and was mixed with the MALDI matrix sinapinic acid before use.

Also, in a separate experiment, the trypic digestion of the Ag85B peptides were analysed by MALDI-TOF-TOF and searched using Mascot (Matrix Science, London, UK) by an MS/MS ion search. Variable modifications were selected as deamidated (NQ),oxidation (M). The mass values were set as monoisotopic with a peptide Mass Tolerance of ± 0.5 Da. Maximum number of missed cleavages allowed was set at 2. The spectral match hits were screened with standard MudPIT scoring with significance threshold $p < 0.05$.

2.3.14 Enzyme activity assay for Ag85B

Enzyme kinetic study for the recombinant Ag85B was performed following the change in fluorescence of resorufin butyrate ($\varepsilon = 6220\ M^{-1}\ cm^{-1}$) at $\lambda_{excitation}$ at 500 nm and $\lambda_{emission}$ at 593 nm. The assay was performed according to the protocol by Favrot and colleagues with slight modifications [163]. Resorufin butyrate concentrations were varied from 0 µM-150 µM and 1µM of purified Ag85B (dialyzed previously in 100 mM phosphate buffer) (pH 8.0) was used for the reaction. Reactions were performed in triplicates in a microplate reader (Varioskan LUX,

Thermo Fisher Scientific). Origin Pro 2019b software was used to analyze kinetic data using non-linear regression.

2.4 Results and Discussion

2.4.1 Cloning, expression and purification of Ag85B

The Ag85B gene amplification resulted in an amplified band ~850 bases (Fig. 2.1A). The digested insert were eluted from the gel and ligated with pre-digested vector followed by transformation into *E. coli* DH5α cells. The positive Ag85B clones from colony PCR (colonies 1, 3 and 6) (Fig. 2.1B) was checked by restriction digestion with the pair of restriction enzymes *Kpn*I/*Bam*HI. The restriction digestion result after gel electrophoresis indicated release of desired length Ag85B gene insert along with ~3400 bases size of pQE30 vector backbone (Fig. 2.1C). After confirmation through sequencing, the Ag85B recombinant plasmids were then transformed into *E coli* M15 cells for expression. Due to the inherent complex nature and high instability index (computationally calculated to be 46.85 using ProtParam tool), the Ag85B protein expression was majorly found in the inclusion bodies (Fig. 2.1D). Purified inclusion bodies were solubilized in presence of zwitterionic surfactant *N*-lauryl sarcosine to allow solubilization. The eluted fraction after Ni-affinity chromatography was successively purified using size-exclusion chromatography to eliminate contaminating proteins (Fig. 2.1E). Three predominant fractions as visualized on SDS-PAGE from size-exclusion chromatography were pooled down and concentrated (Fig. 2.1F). Western blot was carried out to determine biological intactness of the purified Ag85B protein (Fig. 2.1G). The plasmid construct prepared in clone manager software is also shown in Fig. 2.1H.

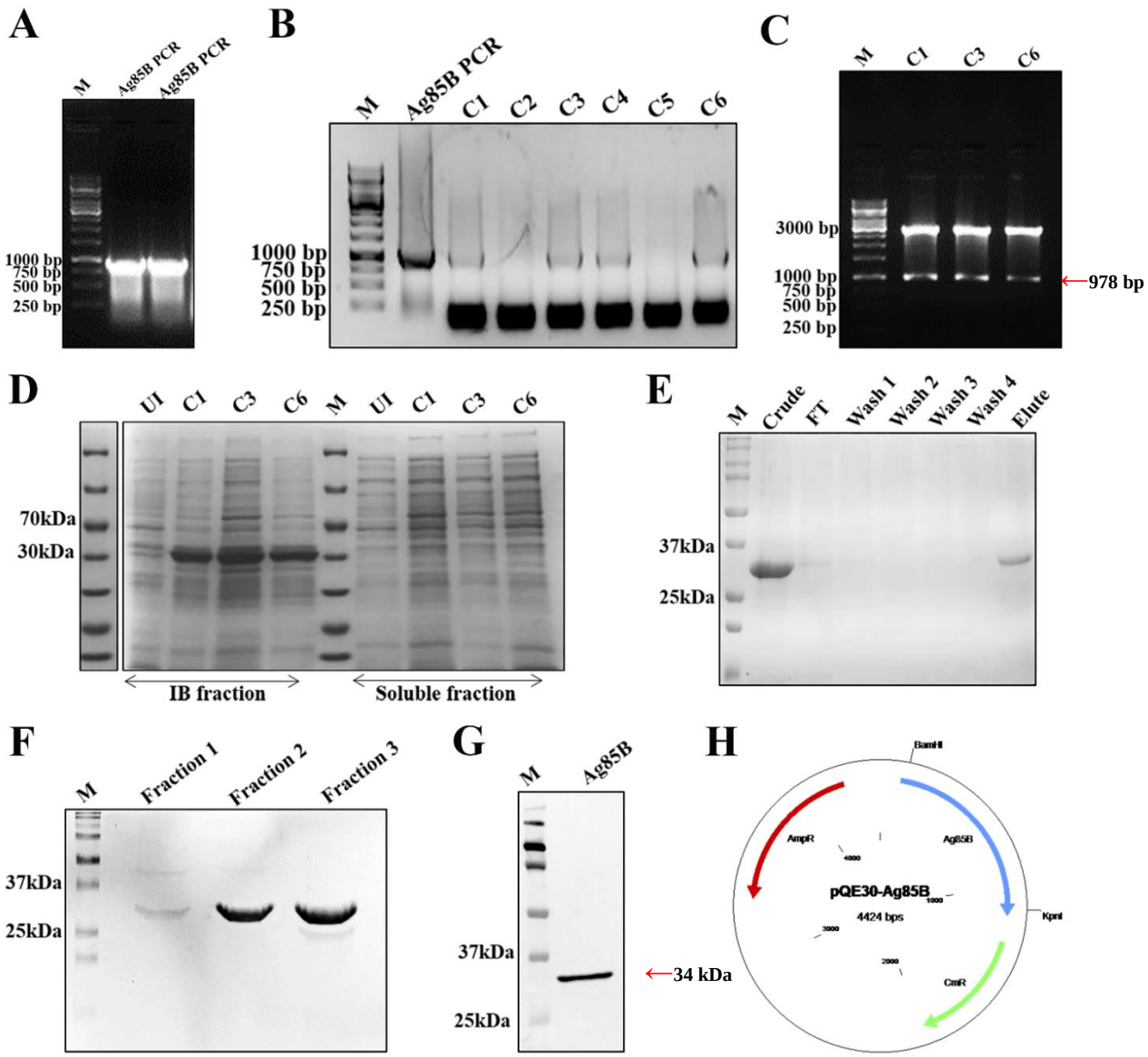

Fig. 2.1 Cloning, expression and purification of Ag85B. (A) PCR amplification. (B) Screening of colonies by colony PCR, C1 to C6 colonies screened. C1, C3, C4, C6 were positive. Control Ag85B PCR run on Lane 2. (C) Digestion of plasmids from clones C1, C3 and C6 with two enzymes KpnI and BamH1 is represented with a fall out band corresponding to the insert size of Ag85B, ≈ 978 bp. (D) Coomassie stained SDS-PAGE showing expression by IPTG induction of clones C1, C3 and C6. Overexpression of Ag85B noted in inclusion bodies (IB) fraction. UI represents uninduced control. (E) Ni-affinity chromatography for purification of His-tagged Ag85B. (F) Purified and concentrated fractions of Ag85B after size-exclusion chromatography. (G) Western blot of Ag85B, M.W. of Ag85B is ≈ 34 kDa. (H) Plasmid map represents the construct pQE30-Ag85B containing Ag85B gene. M represents the molecular weight marker.

2.4.2 Cloning, expression and purification of MPT64

The MPT64 gene amplification resulted in an amplified band ~700 bases (Fig. 2.2A). The digested insert were eluted from the gel and ligated with pre-digested vector followed by transformation into *E. coli* DH5α cells. The positive MPT64 clones from colony PCR (colonies

1, 4, 6 and 7) was checked by restriction digestion with the pair of restriction enzymes *Xho*I/*Bam*H1 (Fig. 2.2B). The restriction digestion result after gel electrophoresis indicated release of desired length MPT64 gene insert along with ~5300 bases size of pET28a vector backbone (Fig. 2.2C). After confirmation through sequencing, the MPT64 recombinant plasmids were then transformed into *E coli* BL21(DE3) cells for expression (Fig. 2.2D). The low temperature based induction with IPTG was done for soluble expression. The protein expression was continued for another 20 hours to accumulate sufficient quantity of protein. Briefly, the harvested cell pellets were lysed in presence of 0.01 M PMSF in lysis buffer. The supernatant after centrifugation containing the MPT64 protein was allowed to bind to Ni-affinity resin and the eluted fractions were visualized on SDS-PAGE (Fig. 2.2E). The recombinant MPT64 protein was mainly expressed in the form of inclusion bodies and partly in soluble form, and the protein concentration was about 2.0 mg/mL after purification by Ni^{2+}-NTA chromatography. All the eluted fractions containing 300 mM imidazole was pooled down and successively purified using size-exclusion chromatography to eliminate contaminating proteins. The elution of His-tagged purified MPT64 protein is monitored by an increase in the UV absorbance of the purification system (Fig. 2.2F). The collected fraction was concentrated, buffer exchanged and visualized by western blot to determine biological intactness of the purified protein (Fig. 2.2G). The plasmid construct prepared in clone manager software is also shown in Fig. 2.2H.

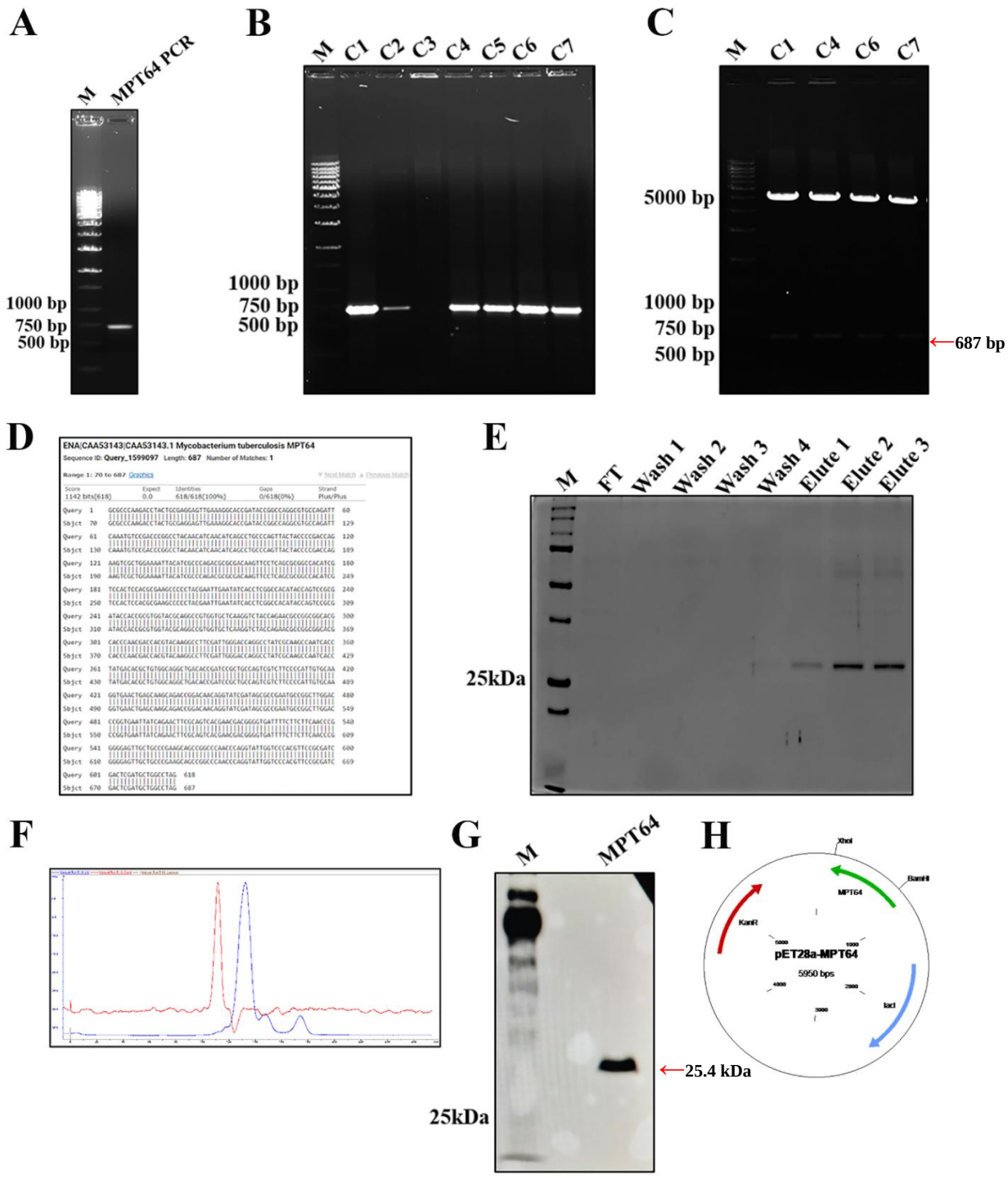

Fig. 2.2 Cloning, expression and purification of MPT64. (A) PCR amplification of MPT64 from *M. tuberculosis* H37Rv genome. (B) Screening of colonies by colony PCR, C1 to C7 colonies screened. C1, C4, C6, C7 were positive. (C) Digestion of plasmids from clones C1, C4, C6 and C7 with two enzymes XhoI and BamH1 is represented with a fall out band corresponding to the insert size of MPT64, ≈ 687 bp. (D) Sequencing result confirming the MPT64 gene with 100% sequence similarity in BLAST. (E) Coomassie stained SDS-PAGE showing expression and Ni-affinity chromatography for purification of His-tagged MPT64 protein from soluble fraction of clone C6. (F) UV (blue line) and conductivity (red line) following the elution pattern of MPT64 in size-exclusion chromatography. (G) Western blot of MPT64, M.W. of MPT65 is ≈ 25.4 kDa. (H) Plasmid map represents the construct pET28a-MPT64 containing MPT64 gene. M represents the molecular weight marker.

2.4.3 Cloning, expression and purification of ESAT6

The ESAT6 gene amplification resulted in an amplified band ~300 bases (Fig. 2.3A). The digested insert were eluted from the gel and ligated with pre-digested vector followed by transformation into *E. coli* DH5α cells. The positive ESAT6 clone was checked by restriction digestion with the pair of restriction enzymes *Nde*1/*Xho*I. The restriction digestion result after gel electrophoresis indicated release of desired length ESAT6 gene insert along with ~5300 bases size of pET28a vector backbone (Fig. 2.3B). After confirmation through sequencing, the ESAT6 recombinant plasmids were then transformed into *E coli* BL21(DE3) cells for expression (Fig. 2.3C). The expression was induced by IPTG at different concentrations (0.5 mM, 1 mM and 5 mM) and checked for ESAT6 protein for 4-5 hours with the induced bands appearing around 11 kDa (Fig. 2.3D). In the uinduced sample, there was no expression. Briefly, the harvested cell pellets were lysed in presence of 0.01 M PMSF in lysis buffer. The supernatant after centrifugation containing the ESAT6 protein was allowed to bind to Ni-affinity resin and the eluted fractions were purified using size-exclusion chromatography to eliminate contaminating proteins. The collected fraction was concentrated, buffer exchanged and visualized by western blot to determine biological intactness of the purified protein (Fig. 2.3E). The plasmid construct prepared in clone manager software is also shown in Fig. 2.3F.

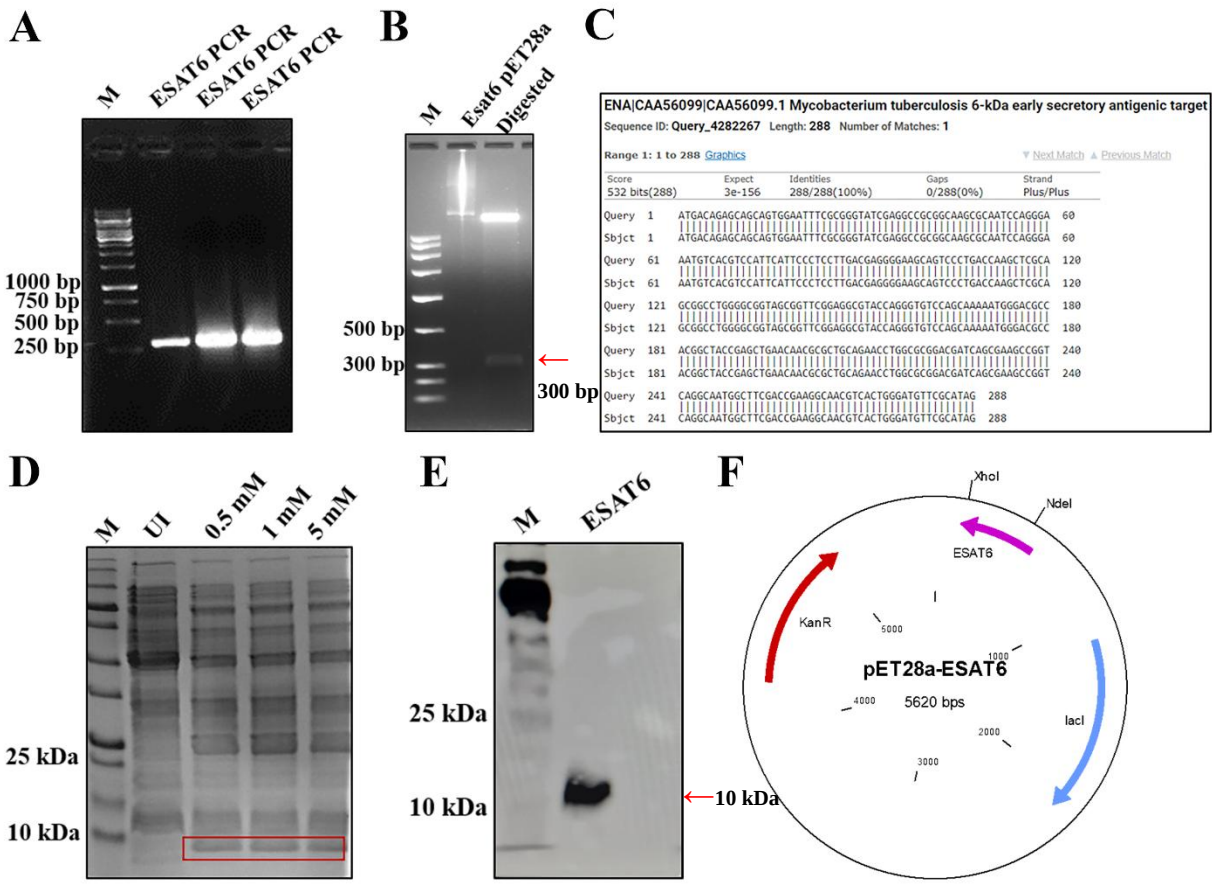

Fig. 2.3 Cloning, expression and purification of ESAT6. (A) PCR was used to amplify ESAT6 gene at annealing temperatures ranging from 52 °C to 62 °C, resulting in a ~300 bp product. (B). Recombinant ESAT6-pET28a plasmid digested with (C) BLAST results of sequencing confirmation of ESAT6 gene. (D) Coomassie stained SDS-PAGE showing expression of ESAT6 checked under different concentrations of IPTG inducer (0.5 mM, 1 mM, 5 mM) where the ESAT6 expression is confirmed around band corresponding to to ~10 kDa; compared with uninduced (UI) control where there is no induced protein band corresponding to ~10 kDa. (E) Western blot of purified His-ESAT6 detected with the help of anti-His antibody on nitrocellulose membrane confirming size and intactness of the protein. (F) Plasmid map represents the construct pET28a-ESAT6 containing ESAT6 gene. M represents the molecular weight marker.

2.4.4 Characterization of Ag85B, ESAT6, MPT64 proteins

CD spectroscopy has been extensively used to determine the structure and folding of proteins. It provides valuable information regarding the structural alterations and folding that the recombinant proteins may show. Hence, the integrity of the intact form of Ag85B, MPT64 and ESAT6 was confirmed by far-UV CD analysis. The analysis showed that Ag85B constitutes ~ 14 % α-helix, ~ 24.7 % anti-parallel β-sheets, ~ 6.4 % parallel β-sheets, ~18.1 % turns, 36.8 % random coils (determined in Spectra Manager software, Jasco Inc.) which correlated well with previous reports (Fig. 2.4A) [164]. To prevent degradation of the purified protein, aliquots of

Ag85B was flash freezed in liquid nitrogen and stored at either -80 °C for further use. Likewise, the CD spectroscopic analysis of the MPT64 and ESAT6 showed that the two proteins maintained similar secondary structural elements as reported earlier. For MPT64, a strong CD spectrum intensity was observed at ~190 nm along with two negative peaks at ~208 and ~222 nm [165]. For ESAT6, the CD spectrum showed a predominance of alpha helical contents. It had a strong positive peak ~195 nm along with two negative peaks at ~211 nm and ~218 nm [166].

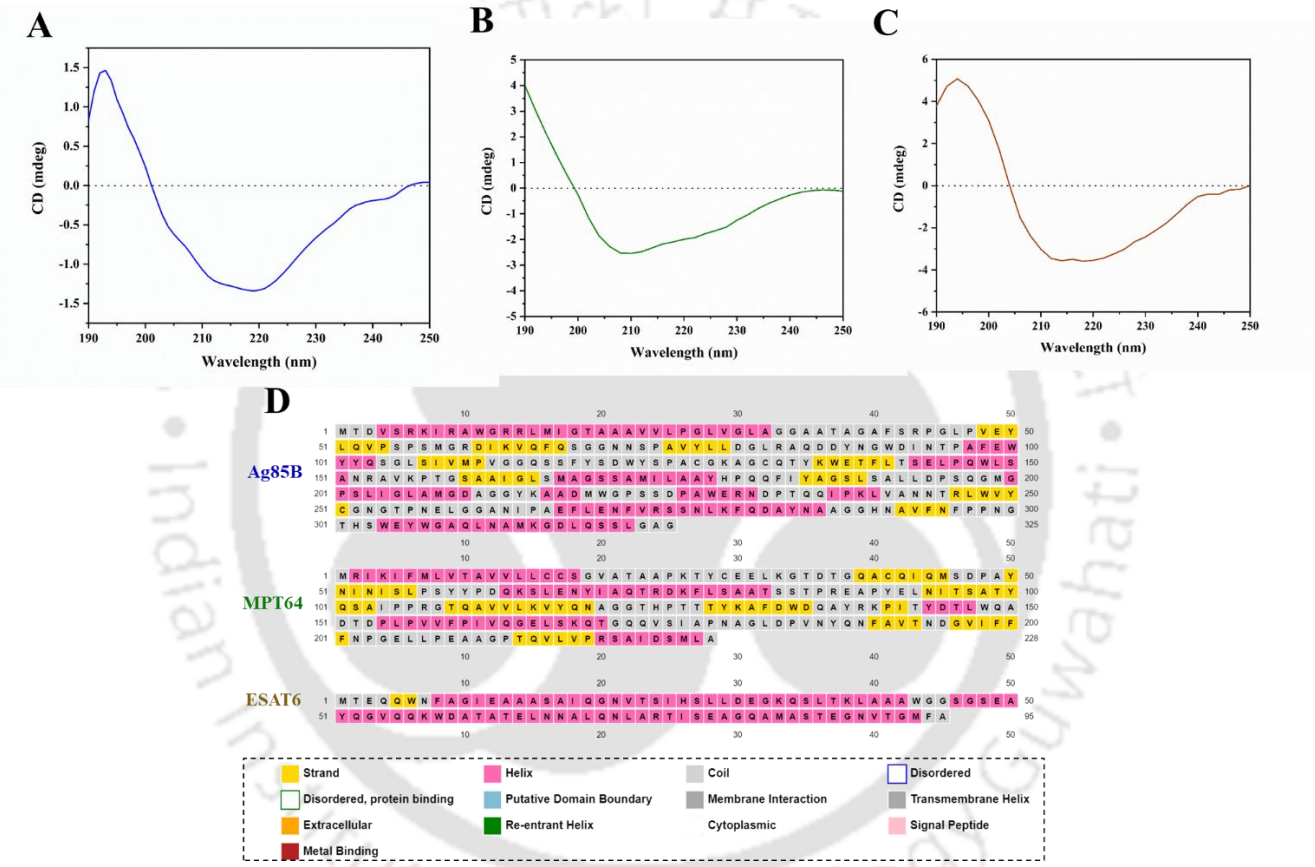

Fig. 2.4 Far-UV CD spectra of protein biomarkers. (A) Ag85B protein was subjected to a desalting column pre-calibrated with 50 mM phosphate buffer. The desalted protein eluted (0.25 mg/mL) in phosphate buffer was then analysed via far-UV CD spectroscopy. (B) MPT64 protein was subjected to a desalting column pre-calibrated with 20 mM phosphate buffer. The desalted protein eluted (0.28 mg/mL) in phosphate buffer was then analysed via far-UV CD spectroscopy. (C) ESAT6 protein was subjected to a desalting column pre-calibrated with 20 mM phosphate buffer. The desalted protein eluted (0.3 mg/mL) in phosphate buffer was then analysed via far-UV CD spectroscopy. For (A), (B) and (C) the data obtained are represented as CD (millidegrees) vs wavelength (nm). (D) The PSIPRED algorithm was employed to predict the secondary structure elements of Ag85B, MPT64 and ESAT6 for a visual representation of their secondary structural elements.

2.4.5 MALDI analysis for Ag85B

Intact mass of Ag85B was found to be ~ 33kDa by MALDI-TOF mass spectrometry. It also indicated that there were no other contaminating peaks, and the Ag85B was purified without any background proteins from *E. coli* (Fig. 2.5).

For the identification of individual peptides, a sequence coverage of 16% was obtained for Ag85B by an MS/MS ion search from the petide fragments obtained in MALDI-TOF-TOF (refer to Appendix).

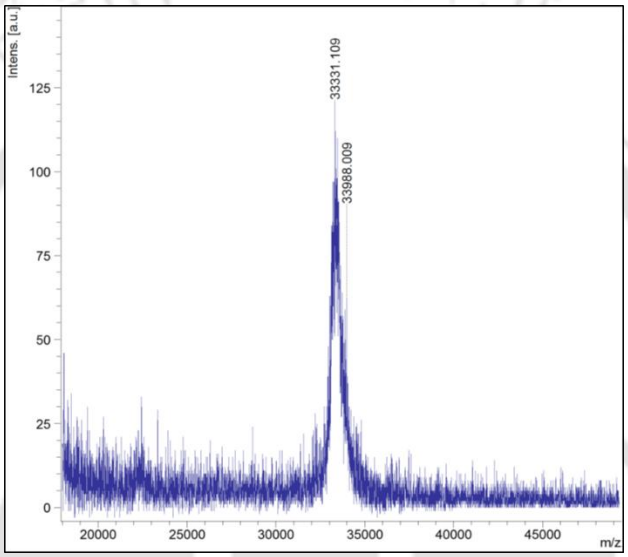

Fig. 2.5 MS analysis of Ag85B. Intact mass as obtained from MALDI-TOF MS is shown by the molecular weight corresponding to the peak (33331.109) showing highest intensity. *N.B. The additional marking to the peak (33988.0) is for representation purposes only.*

2.4.6 Enzyme activity assay for Ag85B

Ag85 class of enzymes (Ag85A, Ag85B and Ag85C) employ mycolic acids as their substrates. All three enzymes are members of the α/β-hydrolase superfamily and are capable of catalyzing the production of mycolyl arabinogalactan (mAG) or trehalose dimycolate (TDM) from trehalose monomycolate (TMM) and respective mycolic acid acceptors. This is due to their previously reported conservancy in active site residues and ability to accept various substrates containing the acyl moiety [167,168]. Interestingly, Ag85 proteins utilize a ping-pong reaction mechanism with a catalytic triad core group of a nucleophilic serine (Ser 124), histidine base (His 260), and glutamic acid (Glu 228) [169]. Resorufin butyrate, a fluorogenic substrate was

earlier used as an acyl donor for Ag85C for testing the enzymatic activity by Favrot et al. [163]. Keeping in mind the similarities in sequence and active site residues, herein we checked the ability of Ag85B to enzymatically accept resorufin butyrate as a substrate and assesss its enzymatic activity. The enzymatic hydrolysis of resorufin butyrate was monitored by the production of resorufin at the excitation wavelength (visible to the naked eye as a pink coloured product) (Fig. 2.6).

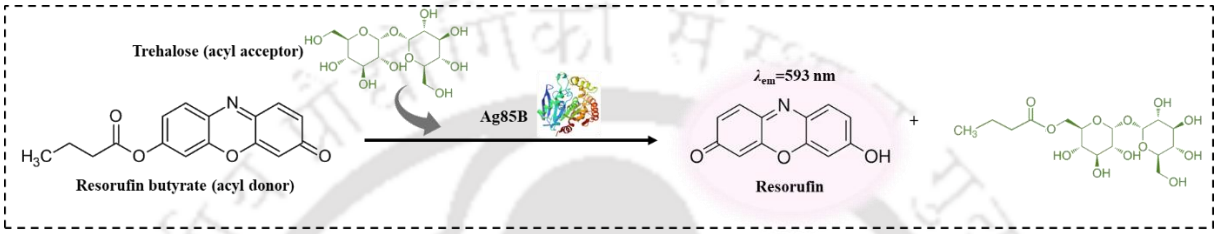

Fig. 2.6 Proposed reaction mechanism for Ag85B enzyme assay.

After optimization of assay conditions, relative fluorescence values were recorded in absence (no enzyme) and presence (with enzyme) of Ag85B with 25 µM to 150 µM of resorufin butyrate (Fig. 2.7A). The results indicate that the response was linear for the duration of the 60-min read, and a linear regression line was fit with an R^2 = 0.968 was obtained (Fig. 2.7B). Further, we assessed the K_M of resorufin butyrate in the assay. The K_M was estimated at ~154.43 ± 26.21 µM by fitting the non linear Michaelis-Menten's equation using Origin Pro 2019b (Fig. 2.7C). The results confirmed that the expressed Ag85B protein was well folded and enzymatically active [163]. The enzyme assay was pivotal to confirm the integrity of the recombinant Ag85B to confirm that the purified recombinant protein mimics the exact conformation of the protein *in vivo*.

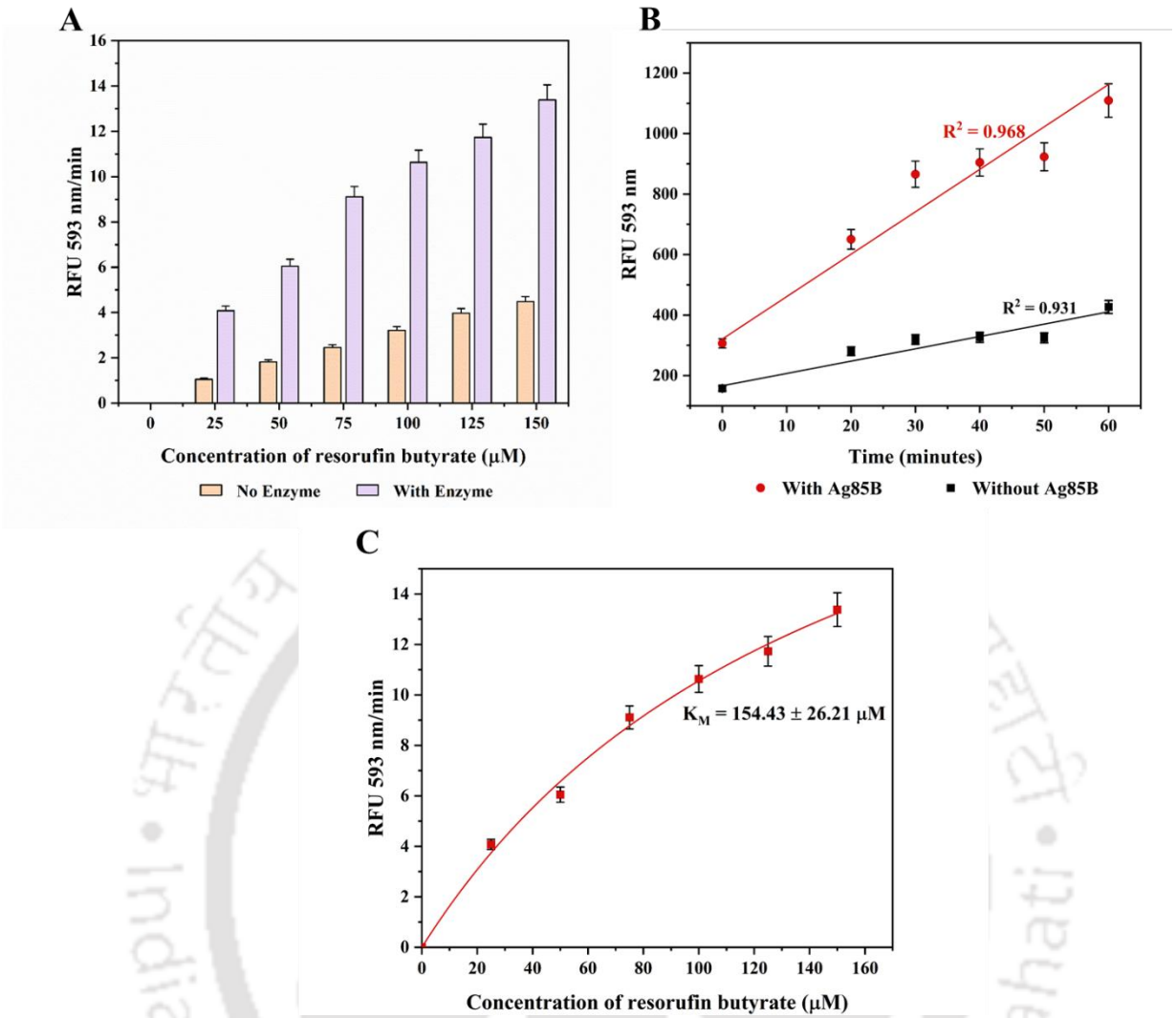

Fig. 2.7 Reaction kinetics for Ag85B enzyme assay. (A) Relative fluorescence intensities measured upon formation of product resorufin showing linear relationship to the concentration of resorufin butyrate added as substrate in presence and absence of Ag85B. (B) Assay kinetics in reaction buffer with and without Ag85B. (C) Michaelis Menton plot for Ag85B enzymatic reaction used for calculation of K_M.

2.4.7 Challenges faced in cloning, expression and purification of GC-rich DNA sequences of *M. tuberculosis*

Several challenges during the cloning, expression and purification of MTB biomarkers were incountered in our study. MTB H37Rv genome harbours a GC content of an average of 65.6%. In particular, designing of primers for molecular cloning poses a serious challenge due to the higher Tm values because of an extra H-bond in a G:::C pair [170]. Consequently, the higher probabibilty of the primer pairs forming primer dimers (heterodimers upon annealing to the other primer or homodimers upon self annealing), secondary structures and hairpins hamper

the proper annealing of the primers to the genomic DNA template. On the other hand, such structures might also block the DNA polymerase to initiate the synthesis of any new strand. Interestingly, for gene sequences >1000 bases, reports show that enhancers like DMSO or betaine aid in PCR amplification with longer stretches of primers [171]. But we did not employ any enhancer keeping in mind that our sequences were all within the aforementioned range. Earlier, researchers have also reported the use of codon optimization approach to change the nucleotide composition of primers at the Wobble base or improving codon bias by altering the nucleotide sequence of the entire gene keeping the amino acid composition same [172]. On the contrary, another parallel hypothesis suggests that increased amounts of G and C bases in a sequence positively correlates with increased levels of transcription [173]. Believing in the latter theory, we did not consider codon optimization as a prerequisite for our PCR optimizations.

In the same way, we optimized the primer and template amounts for each PCR step. We noticed that more than 50 ng template per reaction of PCR was detrimental and led to the formation of non-specific bands. This observation was also balanced with a maximum annealing time of 30 seconds to ensure specific annealing of primers to the desired locations of the genome and avoid formation of spurious bands in a time-restricted fashion. We also did not consider alterations to the choice of polymerases (other than Taq polymerase) and Mg^{2+} ion concentrations for improving the fidelity of amplification.

Thus, our systematic approach to generate maximum amplification was bifurcated into a two step process for PCR: (i) synthesis of primer pairs with optimum lengths and choice of restriction sites and compatible cushioning sites in order to keep the GC content such that the predicted annealing temperatures do not cross the extension temperature, (ii) careful optimization of annealing temperature.

Another important aspect of using *E.coli* as an overexpression host for MTB genes was to optimize the culture conditions carefully during protein expression. MTB proteins are rich in

glycines, alanines, prolines and arginines and for *E. coli* it is rather challenging to produce them from the point of view of codon bias and with limited cellular machinery. Reports suggest that truncation and fusion constructs help in addressing such challenges but, in our application of MTB proteins as biomarkers, truncation was not a viable option [174].

Interestingly, we could not overexpress Ag85B biomarker from its pET28a recombinant clone in *E. coli* BL21(DE3). The failure suggested that the protein could be toxic in nature to the cell due to its pathogenic origin from MTB. On the other hand, we also hypothesized that the recombinant plasmid might be undergoing basal level leaky expression that could not be detected by us in *E. coli* BL21(DE3). Hence, we resorted to the cloning of the gene in a different vector (pQE30) and checked its expression in *E. coli* M15 cells that harbours an additional low-copy plasmid called pREP4. The desirable feature of using this expression system is that there is improved cis-repression of the *E. coli* T5 promoter (found on the pQE30 vector) by the lac repressor encoded on the pREP4 plasmid. This ensured minimal basal-level expression before induction by IPTG and gave better results. There was no such problem encountered for the recombinant expression of the two other biomarkers, MPT64 and ESAT6. All our expression systems gave high protein yields, but did not show any secretion of recombinant proteins into the extracellular medium. This continues to be a major challenge in overexpression of pathogenic proteins in *E. coli* [175]. We also kept all induction temperatures below 30 °C throughout the expression studies to prevent maximum protein from ending up in inclusion bodies. Moreover, since the molecular weight of our biomarkers were all within the range of <35 kDa, we could purify them successfully without the addition of any additives (like glycerol) into the culture medium that improves the expression conditions and solubility for higher molecular weight recombinant proteins [176].

During purification of recombinant Ag85B, due to its inherent nature of high instability index as theoretically computed by ProtParam and also supporting evidences from CD

spectroscopic studies by Wahid and his colleagues, we also faced significant challenges in keeping the purified protein stable during storage as well as during use with other assay components (like DNA aptamers) in the application studies [164]. There was no such problem in purification of MPT64 and ESAT6 proteins.

Intriguingly, research supports the use multiple chaperones and complex constructs with costly vectors to aid in soluble protein overexpression from GC rich nucleotide sequences. However, in our study we made use of only one simple vector with His-tag fusion and optimized culture conditions to give maximum recombinant protein yields.

Our thoughts align with an important finding by Shilling and colleagues where specific alterations in the design of promoter and translation initiation regions of pET28a contributed to improved yields of protein expression in *E. coli* [177]. Thus, cloning, expression and purification issues in *E. coli* could be addressed by a combined approach of bioinformatics analysis, design engineering and careful optimizations of culture conditions.

2.5 Conclusion

The aim of this tudy was to successfully clone, express, purify and characterize the protein biomarkers that will be used to generate aptamers. The biomarkers were chosen based on their roles in diagnosis of TB. The coding DNA sequence for each individual biomarker from the MTB H37Rv genome was used to design primers and incorporate the sequences into suitable cloning and expression vectors. During this, optimization of PCR conditions was crucial due to the GC-rich nature of the genes. Recombinant protein expression in *E. coli* for pathogenic proteins has been a topic of intense research. Following the existing literature, the overexpression of all three proteins Ag85B, MPT64 and ESAT6 were checked under various concentrations of IPTG, time and duration of induction as well as temperature for the cultures. Also consistent with previous observations, the pH of buffers and handling temperature, especially for Ag85B during protein purification greatly influenced the structural integrity over time [164].

A large number of overexpressed proteins become inclusion bodies, where they mostly exist in their unfolded form and lose their structural integrity. But, in this study, the purification conditions for Ag85B were carefully optimized to give a good yield of the protein (1 mg/mL) from purified inclusion bodies under native conditions. By examining the mass-to-charge ratio of the peptides produced as a part of MS, along with the peak in MALDI we were able to precisely determine the integrity of Ag85B. Far-UV CD spectroscopy validated the secondary structural elements of the purified proteins which correlated well with previous reports.

Sometimes, tagging a protein can cause its native function to be compromised. This highlights how crucial it is to evaluate the His-tagged protein's functional characteristics. To avoid any negative effects on the protein's intended biological activity, this evaluation was done through an enzymatic assay for Ag85B.

This study proves that all three recombinant protein biomarkers were successfully cloned, expressed, purified and characterized to confirm their native structure and biological intactness for use in generation of aptamers.

3

Screening and characterization of DNA aptamers against tuberculosis biomarker Ag85B

Abstract

One of the most important methodologies in the development of aptamers is the SELEX process. Herein, we developed a novel, simple and timesaving "cut-off filtration assembly based" (COFA) SELEX methodology that shows several advantages over traditional SELEX. Optimizations with respect to target incubation times, target concentration, template concentration were evaluated for the process of selection. We streamlined the process of final selection of aptamers from sequencing data by use of multiple sequence alignment and motif clustering to select the aptamers. We report for the first time the use of a COFA aptamer (coined as Ag85B-18C-20) for recognition of TB biomarker Ag85B and studied their secondary structure, CD spectroscopic properties. We also evaluated its potential to undergo target-induced conformational change. The 69 nucleotide long aptamer bear the properties of a putative G-quadruplex embedded inside hairpin flanking regions capable of binding to target Ag85B with good affinity. Computational docking revealed important amino acid residues that form non-covalent bonds with the nucleotide bases of the DNA aptamer that are crucial for stabilization of the target:aptamer complex. Furthermore, the binding interactions of the developed aptamer were also checked by EMSA and ITC. The success of this developing this DNA aptamer against Ag85B protein will facilitate the development of a sensitive aptasensor platform for TB.

3.1 Overview

Various commercial antibody-based recognition systems or immunosensors have been reported against the immunodominant secretory TB biomarkers [48]. But, nucleic acids have special properties that make them new-age "smart" bio-elements for various diagnostic applications. In the last two decades, a special class of small nucleic acid molecules called "aptamers" have revolutionized the domain of clinical diagnostics [102]. The term aptamer has its origin from Latin word "aptus" meaning "to fit" and Greek "meros" meaning "location". Interestingly, these aptamers (varying from 20 to 200 nucleotides in length) can fold and adopt various structural forms like hairpins, stems, loops, triplex and quadruplexes. It is these unique conformational forms that are key to the sensor's performance where an aptamer is used as a biorecognition element.

G-quadruplexes are interesting conformations in aptamers, especially because of a higher negative charge density; double that of dsDNA; which may improve interactions with protein targets. These structures constitute stacks of Hoogsteen hydrogen-bonded guanines stabilized by cations such as K+ or Na+ connected by loops, bends etc. There are various other topological variants of DNA apart from G-quadruplexes; for example duplex, triplex, i-motifs etc. that are known to have unique interaction patterns with proteins. Aptamers harbouring a stretch of nucleotides showing a higher propensity to form G-quadruplexes are known to interact more strongly with its target protein [178,179].

Aptamers are generated by an iterative process known as SELEX. Various SELEX methodologies have been reported in literature. But, there are certain disadvantages of traditional SELEX used for generating aptamers against protein biomarkers. Existing SELEX methods to develop single stranded DNA aptamers against secretory biomarkers of TB reports the use of immobilized proteins. The complex nature of such SELEX methods due to labourious and time-consuming steps and the inability to isolate the aptamer sequences that may interact with the

epitopic regions which are otherwise prevented from interacting due to the immobilization of targets on solid supports limits the application of same. The current methodology of our study addresses the challenge and allows interaction between the free protein target and the DNA pool in solution. The current strategy ensures that all the amino acid sidechains available on the exposed regions of the protein target are able to interact freely with the DNA which in turn leads to the isolation of highly specific aptamer sequences that recognize multiple regions of the folded form of the target (here Ag85B). Moreover, it saves time and complex portioning processes that use additional PCR steps. This novel strategy uses a molecular weight "cut-off" filtration assembly (COFA) for interaction and isolation of DNA aptamers binding to the Ag85B biomarker. Molecular weight cutoff filters have been widely used for filtration and centrifugal separation of biomolecules in solution. With the help of COFA SELEX approach, a 69 nucleotide long DNA aptamer against target Ag85B was developed and the structural characteristics were determined. A schematic presentation of COFA SELEX approach is depicted in Fig. 3.1.

Moreover, till date, Ag85B detection is reported only through immunoassay techniques [67,180–183]. These methods that use antibodies as a recognition molecule against recombinant Ag85B protein for detection which are very costly to produce and cannot be stored at room temperature for extended periods of time, thereby limiting their application in portable detection devices. Thus, the current process addresses this challenge and proposes the use of a rather stable recognition molecule like DNA aptamer; which is cost-effective in terms of its production for large scale applications and has excellent thermal stabilities through a wide range of temperatures.

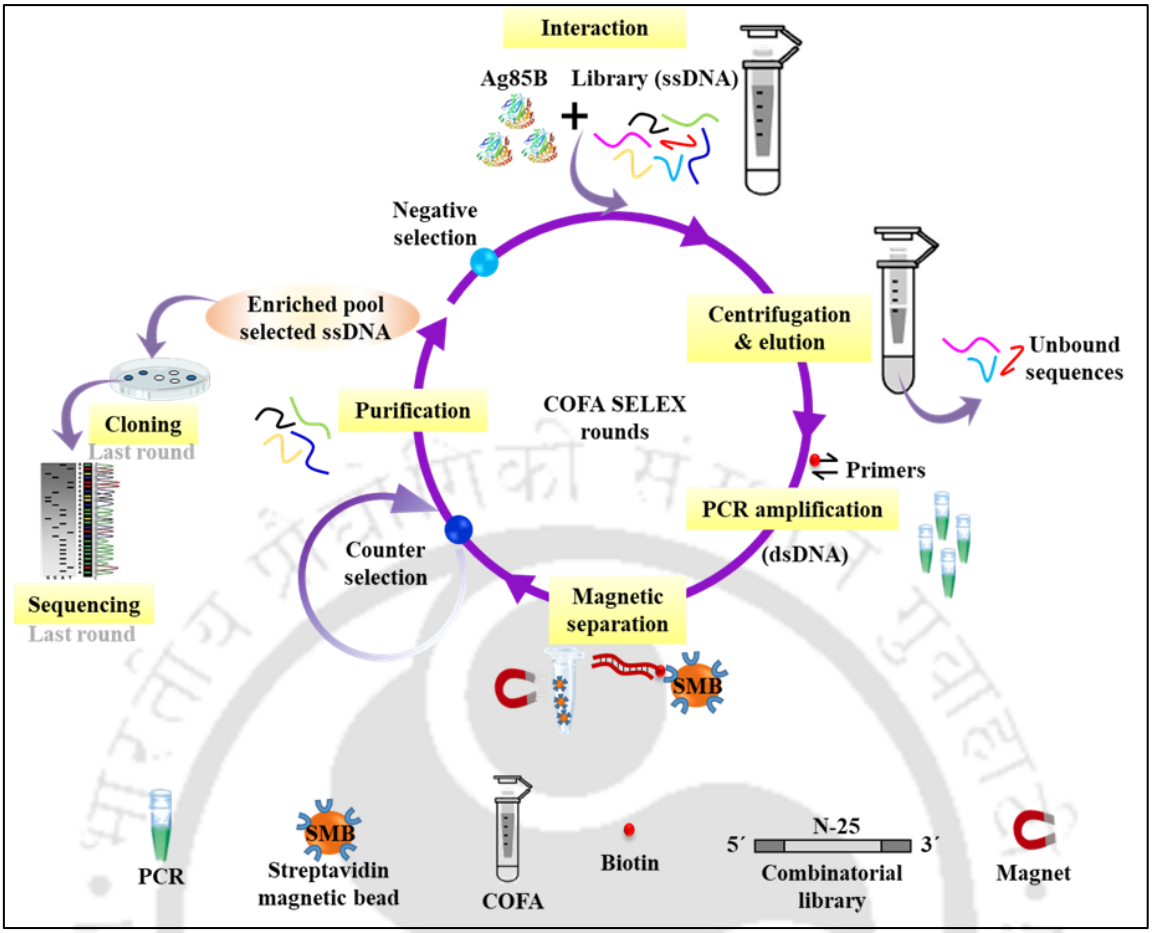

Fig. 3.1 Schematic representation of COFA SELEX strategy.

The specificity and binding affinity of the developed aptamers were analyzed through various methods like CD spectroscopy, ITC and EMSA. The dissociation constants of aptamer for Ag85B were calculated and the findings is incorporated in this chapter.

3.2 Materials

A single stranded DNA library (10^{14}-10^{15}) was procured from Integrated DNA Technologies (IDT, USA). The library was constructed with a central random region of 25 nucleotides (N_{25}) flanked by two conserved primer binding sites for PCR amplification. The primer sequences used for the amplification are listed in Appendix. The primers, library and aptamers were synthesized by Integrated DNA Technologies. Streptavidin coated magnetic particles were purchased from Roche, molecular weight cut-off filters were purchased from Merck and SYBR Gold (10000X) nucleic acid stain was obtained from Invitrogen. All other

chemicals used were of molecular biology grade. All solutions were prepared using water obtained from a Millipore water purification system. All the buffer solutions were filtered using the 0.22 µM syringe filters and sterilized for storage not more than 5 days.

3.3 Experimental methods

3.3.1 Optimization of PCR conditions for amplification

Several parameters were optimized in order to obtain maximum amplification during each cycle of SELEX. A schematic workflow is presented in Fig. 3.2.

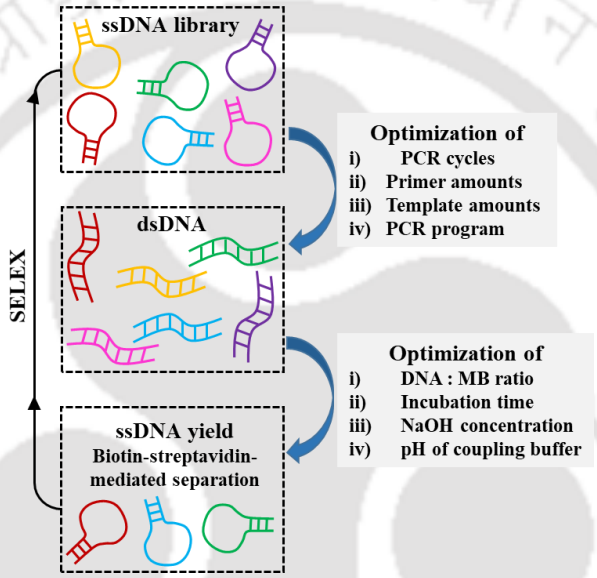

Fig. 3.2 Schematic workflow of optimizations to obtain maximum yield of ssDNA during SELEX.

3.3.2 COFA SELEX approach for *in vitro* selection of aptamers

Amicon® Ultra (Merck) centrifugal filter of appropriate molecular weight cut off were washed with nuclease-free water followed by binding buffer (10 mM KCl, 5 mM $MgCl_2$, 50 mM phosphate buffer (pH 8.0). Initially, 10 nmoles of the starting library in 500 µL binding buffer was treated at 95 °C for 5 minutes, on ice (or 4 °C) for 5 minutes, followed by RT for 5 minutes, and placed in ice. Before starting SELEX, in order to eliminate the sequences that bind to the regenerated cellulose centrifugal filter, DNA library diluted in binding buffer was passed through them. The flow through from the assembly was taken for the consecutive rounds. Before use, 8 nmol of DNA library was suspended in 1 mL of the binding buffer and heated for 10 minutes at

90 °C and then cooled to RT. In each successive rounds of SELEX, the amount of the target protein Ag85B and incubation time was decreased in order to improve stringency of binding as tabulated in Table 3.1. The mixture of the ssDNA and the target protein was loaded onto the centrifugal filter and centrifuged at 2000 rpm for 5 to 15 minutes depending on the total volume. The flow through contained the unbound DNA and protein. After resuspension in nuclease-free water, concentration was checked using a μDrop Duo plates microplate spectrophotometer and taken further for PCR. Amplification conditions were: initial denaturation at 95 °C for 5 minutes and final extension at 68 °C for 10 minutes; and 30 cycles of denaturation at 94 °C for 60 seconds; annealing at 55 °C for 30 seconds and extension at 68 °C for 30 seconds. For the first few cycles (1^{st} to 3^{rd}), the number of PCR cyles to get smear-free bands were separately optimized. Once the number of suitable PCR cycles was determined, the bulk PCR reaction was run to generate a good quantity (~ 1 mL) of PCR mixture. An aliquot of the amplified products were analyzed on 3.5 % agarose gel to verify the length of the dsDNA products for each cycle. A total of 900 μl of pooled PCR product from each round was subjected to binding with 100 μl of streptavidin coated magnetic particles (Strepmag-RO, Roche) diluted in coupling buffer (50 mM phosphate buffer, pH 7.5, 0.5 M NaCl, 1 mM EDTA) for 1 hour at RT. The magnetic particles bound to the biotinylated DNA strand was separated from the suspension using a magnetic stand. Then the DNA bound magnetic particles were washed two times with 400 μL of the coupling buffer. The sense strand was separated from the magnetic particles by denaturing with 100 μL of 150 mM NaOH olution for 2 min; and the solution was immediately neutralized by a sufficient volume of 1M NaH_2PO_4. Then the beads were again eluted by 100 μL of coupling buffer, combined with the previous solution and kept on ice. The concentration and yield of ssDNA was checked and taken for the next round of SELEX. A total of 16 SELEX cycles were performed out of which 2 were against cellulose membrane as counter SELEX (after 4^{th} and 8^{th}) and 2 against ESAT6 and MPT64 as negative SELEX (after 5^{th} and 11^{th}). The concentration and yield of ssDNA was

checked and taken for the next round of SELEX. It is to be noted that elution of the bound libraries from the filter-bound retentate portion of the COFA was done using 100 µL of hot water (~95 °C); each time for positive rounds of SELEX. An enrichment assay to calculate the percentage of DNA selected after each round was also done [184].

Table 3.1 Reaction conditions for target binding during COFA-SELEX.

Cycle number	Negative/counter selection step	Ag85B (µg/mL)	Incubation time (min)
1	-	250	90
2	-	225	90
3	-	200	90
4	Yes	175	90
5	Yes	150	45
6	-	125	45
7	-	100	45
8	Yes	75	45
9	-	50	30
10	-	50	30
11	Yes	~40.25	30
12	-	~33.33	30
13	-	~29.8	15
14	-	25	15
15	-	25	15
16	-	~12.5	15

3.3.3 Cloning and sequencing analysis

At the end of the final round of SELEX, the amplified product was cloned into pGEMT vector and transformed into *E. coli* Top10 competent cells. Following blue-white screening on XGal plates, and all the white colonies were chosen and plasmids were isolated. The recombinant plasmids were verified for the aptamer insert using colony PCR. The positive colonies were selected and sequenced (1st BASE, Malaysia). The sequences of the obtained aptamers were

clustered into groups and multiple sequence analysis was done by Clustal Omega (https://www.ebi.ac.uk/Tools/msa/clustalo/). Secondary structure prediction and QGRS mapping to find G quadruplexes were done. The default parameters used for computing were set with maximum 30 sequences of QGRS length, minimum G-group of 2 and loop size between 0-36 nucleotides. Mfold (UNAfold) (http://www.unafold.org/mfold/applications/dna-folding-form.php) predicted ΔG values for the two selected aptamer candidates.

3.3.4 Characterization of selected aptamers

The effect of ionic strength and pH on aptamer structure was studied. Presence of salt ions is a crucial factor that maintains the suitable structure of DNA aptamers. The binding buffer contained 10 mM KCl, 5 mM $MgCl_2$, 50 mM sodium phosphate buffer (pH 8.0). For the experiments, the K^+ and Mg^{2+} ion contents spiked in water were separately checked in respective experiments. For pH experiments, sodium acetate buffer (pH 4), trisodium citrate buffer (pH 6), sodium phosphate buffer (pH 7 and pH 8), sodium carbonate-sodium bicarbonate buffer (pH 10) was used. For the investigation, tris based buffers were not considered. For probing the effect of ionic content, the following media were used: ultrapure water, KCl spiked in ultrapure water, $MgCl_2$ spiked in ultrapure water and binding buffer. K^+ and Mg^{2+} were spiked at the concentration of the binding buffer. The effect of 50 mM sodium phosphate buffer was not examined separately.

3.3.5 CD spectroscopic analysis of selected aptamers

The CD study was performed to measure the binding affinity of both the aptamers to the target protein Ag85B. The CD spectra were recorded on J-1500 CD spectrometer (JASCO, Japan) at RT. For all the measurements, 5-7.5 μM of aptamers were heated at 95 °C for 5 minutes and then cooled to RT followed by incubating the aptamer solution with various concentrations of target Ag85B in binding buffer for 90 minutes. The spectra were recorded in continuous mode between 220 to 320 nm at a scan rate of 100 nm min^{-1} for an average of 5 scans. The spectra

were recorded for the aptamers without Ag85B and with Ag85B protein at concentrations ranging from 100 nM to 1000 nM. The binding buffer influence was removed from the recorded spectra as baseline correction and plotted after smoothening by OriginPro 2019b software.

3.3.6 Docking analysis of selected aptamers

To explore Ag85B protein and aptamer interactions, *in silico* molecular docking study was performed. The dot bracket notation of the two aptamers from Mfold (http://www.unafold.org/mfold/applications/dna-folding-form.php) were used further. The 3D structure of the aptamer was generated using the RNA Composer web server (http://rnacomposer.cs.put.poznan.pl/), and 3D RNA structures were converted to 3D DNA. With the results of 3D DNA generation, GROMACS package was used to perform 3D structure optimization using steep descent algorithm (energy minimization). The final optimized structure were utilized for antigen-aptamer docking. Meanwhile, the reported structure of Ag85B (PDB ID: 1F0N; resolution 1.80 Å, no missing residues) was retrieved from RCSB PDB database and hydrogens were added using PyMol software and used as a receptor for docking. The HDOCK server (http://hdock.phys.hust.edu.cn/) was used to computationally construct the three-dimensional (3D) complex of Ag85B and aptamers. An outline scheme of the molecular docking workflow adopted for the study is highlighted Fig. 3.3 [185].

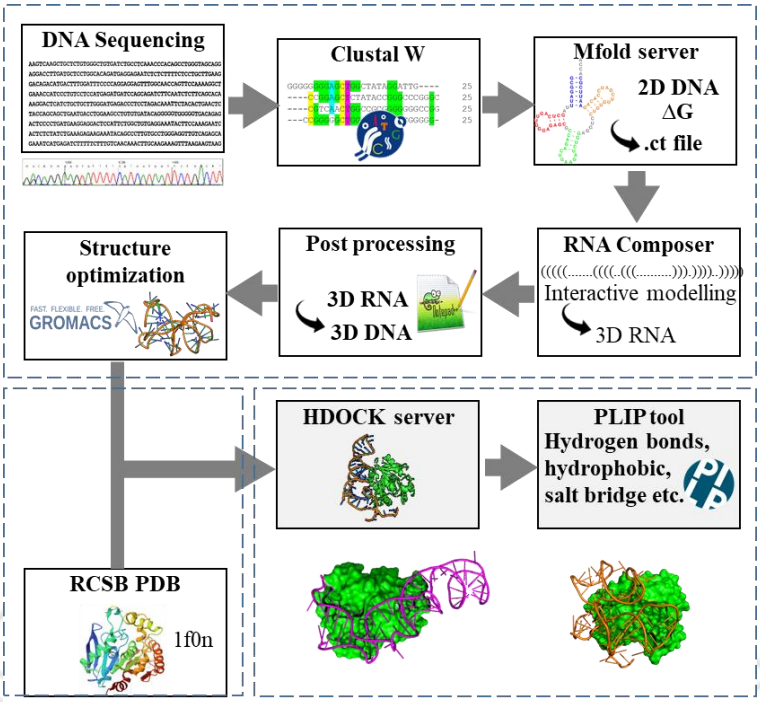

Fig. 3.3 Schematic workflow of computational docking used for the current study.

3.3.7 EMSA of aptamer Ag85B-18C-20 with target Ag85B

EMSA represents a very simple method to visualize the binding between an aptamer and its protein target. Ag85B at various concentrations (0 µM to 10 µM) and 25 nM of the aptamer Ag85B-18C-20 were mixed in the binding buffer (24 µL) and incubated at RT for 90 minutes. 7 µL of the reaction mixture containing the protein-aptamer complexes were loaded onto a 10% PAGE tris-borate-EDTA (TBE) gel and separated at 70 V for 4 hours at 4 °C. After electrophoresis, the gel was stained with SYBR gold nucleic acid stain for 10 minutes and visualized using GelDoc EZ Go (Biorad).

3.3.8 ITC study of aptamer Ag85B-18C-20 with target Ag85B

All ITC experiments were performed using a MicroCal ITC200 instrument (GE Healthcare, USA) at 25°C and corrected for heat of dilution of the titrant. All buffers were degassed prior to each experiment. All titrations were performed with the Ag85B-18C-20 aptamer in the syringe and purified Ag85B protein in the cell. Binding experiments consisted of 25 successive injections spaced every 120 seconds, where the first injection was of 1.5 µL that

accounted for diffusion from the syringe into the cell during equilibration. For each ITC experiment, 50 μM of aptamer and 1 μM of Ag85B protein was used. Based on the best curve fit, the data was fitted into two independent sites binding model using manufacturer-provided data-fitting package within Origin 7 software (OriginLab) [186]. Dissociation constant (K_D) was calculated using the formula $K_D = 1/K_A$, where K_A is association constant of the tested aptamer candidate.

3.4 Results and Discussion

3.4.1 Optimization of PCR conditions

An efficient amplification by the symmetric PCR is instrumental to prepare the optimum amounts of dsDNA as the starting template for generation of ssDNA. PCR program that gave the best results were an initial denaturation of 95 °C for 5 minutes and final extension at 68 °C for 10 minutes; with 30 cycles of denaturation at 94 °C for 60 seconds; annealing at 55 °C for 30 seconds and extension at 68 °C for 30 seconds followed by an infinite hold at 4 °C. Moreover, it is imperative to note that the template DNA for each PCR was ensured to be of "high purity" in order to avoid the appearance of spurious products in the following cycles. All the dsDNA was carefully gel extracted and purified in order to maximize yield. We have also observed the appearance of spurious products of higher molecular weights appearing as aberrant "smeary bands" forming as a result of PCR over-amplification. Millions of ssDNA folding upon itself to form secondary structures that can act as templates can give rise to such unwanted PCR products. Several concatenated sequences harboring multiple reverse and forward primer binding regions can lead to the development of undesired smeary bands (Fig. 3. 4).

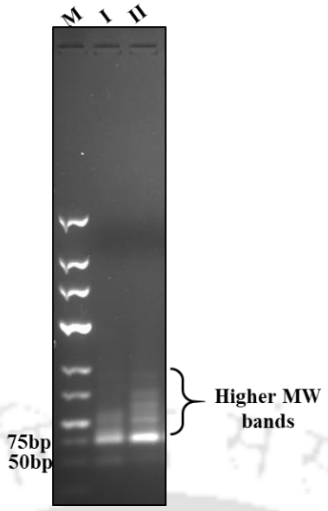

Fig. 3.4 Optimization of PCR overamplification. dsDNA bands showing smears above that appear as smears.

Thus, if correct template amounts are not provided, this becomes a major issue that affects the SELEX cycles negatively. Therefore, the correct amounts of ssDNA template that should ideally be "feeded" to the PCR was optimized for each positive, negative or counter selection cycles during SELEX (Fig. 3.5).

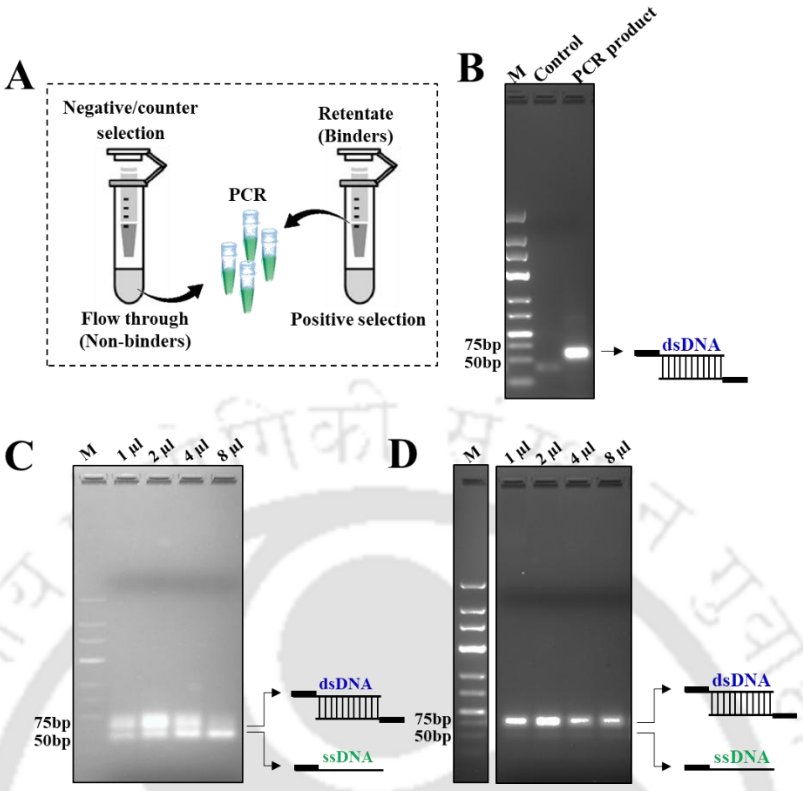

Fig. 3.5 Optimization of DNA template amounts for PCR. (A) Pictorial representation of selection of DNA from a COFA assembly where the flow-through fraction (containing sequences that do not bind Ag85B) is chosen in a negative/counter selection step and the retentate fraction (containing sequences that does bind to Ag85B) is chosen in a positive selection step. (B) Estimation of size of dsDNA product with amplification using the DNA library (69 bases). dsDNA bands are visualized ~75 bp on 3.5% agarose gel. Control: ssDNA library. (C) Represents dsDNA bands resulting after PCR with 2 µL → 8 µL of template DNA from the negative selection step in 5th cycle, optimum was found to be 2 µL. (D) Represents dsDNA bands resulting after PCR with 2 µL → 8 µL of template DNA from the negative selection step in 11th cycle, optimum was found to be 2 µL. ssDNA is representation of residual DNA template in PCR. dsDNA bands were gel purified for next round. M represents the molecular weight marker.

3.4.2 *In vitro* selection of aptamers by COFA SELEX

The COFA SELEX approach was designed to address the existing challenges for development of aptamers. This method allowed the ssDNA sequences to interact freely with the protein, thus allowing all the "aptatopes" on Ag85B to come in contact with the ssDNA during SELEX. Interaction with a wide array of aptatopes allowed specific aptamers to get eluted in the retentate fraction of the filtration assembly. Moreover, this technique bypasses an additional step to characterize immobilized proteins on a solid support.

During SELEX, each PCR round (with biotinylated reverse primers) was followed by a biotin-streptavidin separation step. It is one of the easiest ways to get a good amount of ssDNA

yield. Only desired biotinylated strands bind with high affinity to the streptavidin coated magnetic beads for easy separation. Selective isolation of the binders is crucial for the generation of correct aptamers from the pool of amplified dsDNA. In terms of time, the biotin-streptavidin step was instrumental to reduce the overall time of each SELEX cycle. [187]

After each cycle the concentration of the DNA binders were noted and a gradual enrichment of the aptamer candidates were seen. A total 16 rounds of SELEX cycle was performed, but after 12 rounds of screening, no further increase in affinity between ssDNA pool and Ag85B occurred as seen by the reduced band intensites as shown in Fig. 3.6. Following each negative or counter selection cycle, the band intensities on the agarose gel showed a decrease in the enrichment of aptamer candidates. This specifically reinstated the idea that much of the binders in the initial cycles had affinity to both Ag85B and other non-target proteins (MPT64 or ESAT6). One particular observation as opposed to existing literature is the increased amount of bound DNA in the first cycle as depicted by the bar graph (Fig. 3.6). It can be explained by the fact that not all unbound ssDNA was successfully partitioned after the first cycle of SELEX. This was attributed to the presence of high amounts of DNA library in the first binding event with Ag85B. In particular, due to the high purity of DNA library (template) used in the first round, PCR conditions were separately optimized as compared to the other PCR rounds [188]. This was not particularly detrimental to the selection because the ssDNA that showed affinity towards the empty molecular weight cut-off filter was also selectively eliminated by passing the initial DNA library through it prior to starting SELEX. The percentage of bound DNA decreased beyond cycle 12 because there was no further enrichment of those aptamer candidates; thereby indicating that more stringent conditions did not improve their affinity. The enrichment of binders is shown Fig. 3.7. A similar observation was also noted by Lorenzo-Gómez and his team [184].

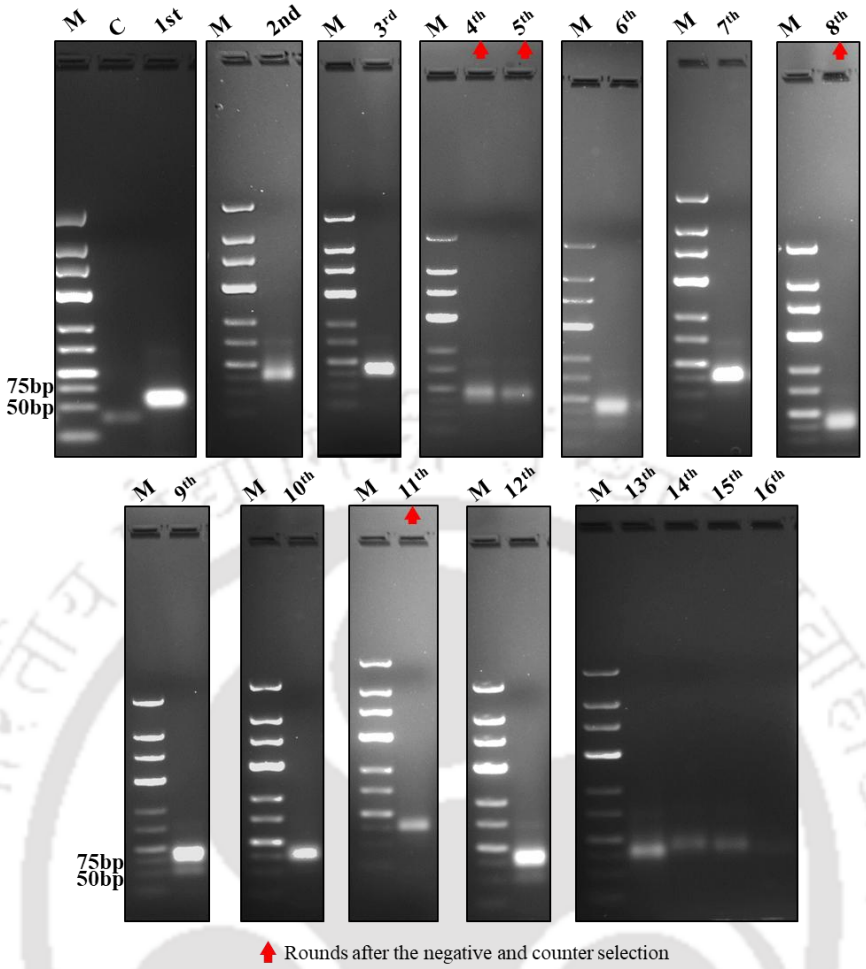

Fig. 3.6 PCR products at the end of each cycle in COFA SELEX (1st to 16th cycles). dsDNA bands are visualized corresponding to ~75 bp on 3.5% agarose gel. C represents control initial ssDNA template (69-mer library) used for SELEX corresponding to ~50 bp on 3.5% agarose gel. Lanes marked 1st to 16th represent the corresponding SELEX cycle number. M represents low-range DNA ladder.

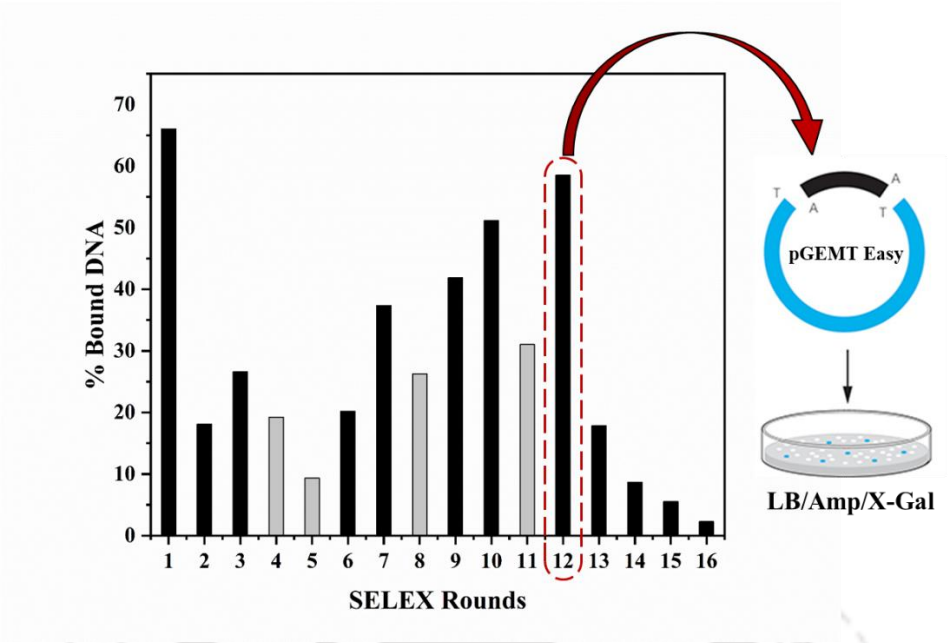

Fig. 3.7 Enrichment assay during SELEX. The fraction bound DNA corresponds to the eluted DNA in the retentate of the filtration assembly. With increase in cycle number, there is gradual increase in the % bound DNA. The final sequences corresponding to the 12th round were cloned into pGEMT vector.

The sequences at the end of 12th cycle were cloned into pGEMT vector and recombinant colonies were screened. Colony PCR of the positive aptamer clones revealed the presence of correct aptamer insert on agarose gel (Fig. 3.8A). Plasmids from a selected number of both white and blue colonies were also digested with *Eco*R1 restriction enzyme to check the presence and absence of aptamer inserts respectively (Fig. 3.8B and 3.8C).

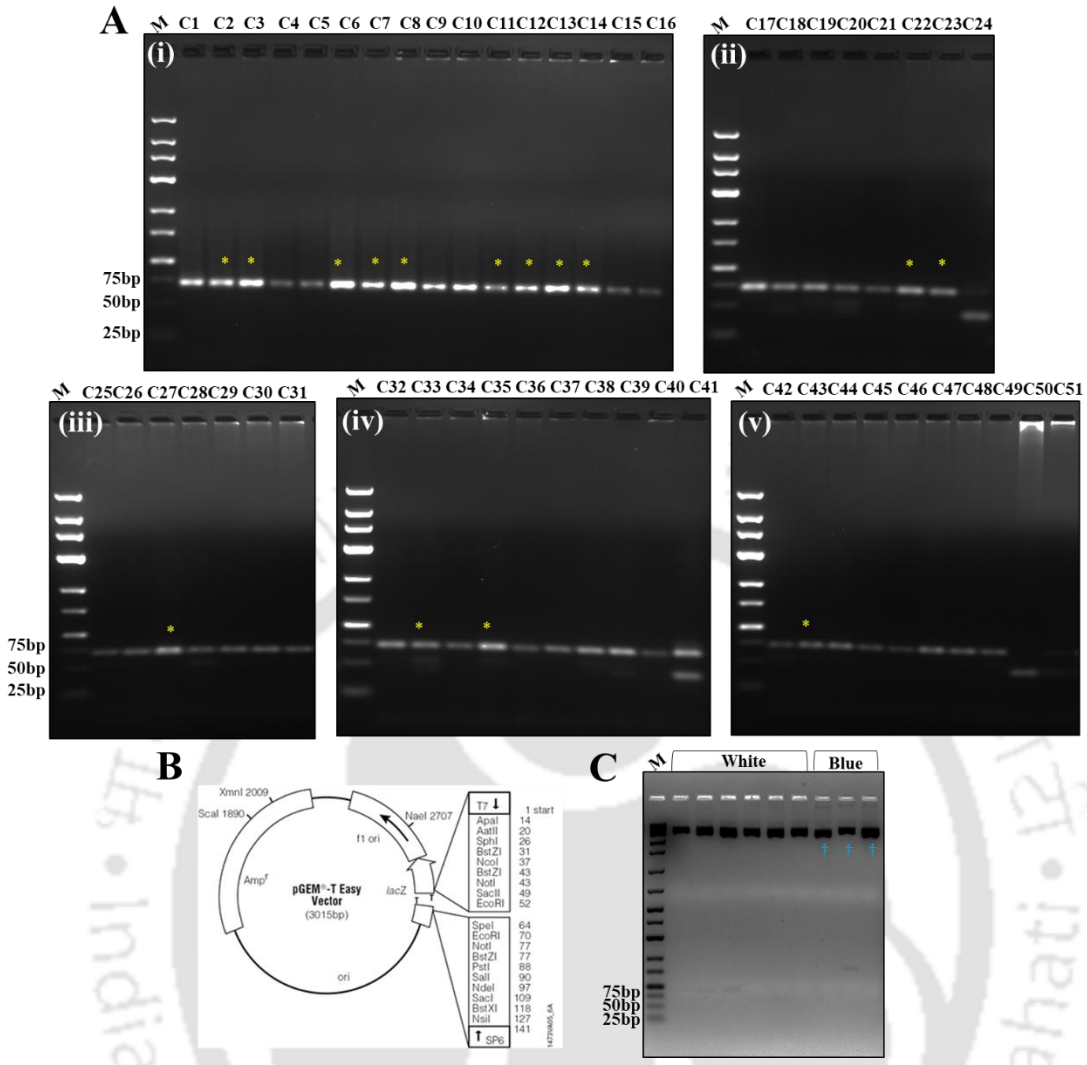

Fig. 3.8 Confirmation of putative aptamer clones. (A) (i)→(v) Colony PCR of 51 screened white colonies (represented as C1 to C51) showing positive inserts corresponding to ~69 bases that were sent for sequencing. (B) pGEMT vector map showing *Eco*RI digestion site. (C) EcoRI digestion of plasmids isolated from 6 white and 3 blue colonies to confirm presence and absence of the correct length of inserts (~69 bases). * indicates the colonies that carried the correct length and intact primer binding sequences of aptamer inserts, confirmed after sequencing. † indicates blue colonies.

3.4.3 Cloning and sequencing analysis

The sequencing results showed that the correct aptamer insert came in around 15 colonies out of the 51 colonies screened. Other orphan sequences bearing deletions in the central random region or improper inserts without the presence of conserved primer binding sites were not considered further. These 15 unique sequences were analysed using online ClustalW (https://www.genome.jp/tools-bin/clustalw) multiple sequence alignment tool. The flanking primer-binding sites of the aptamers were restricted from the multiple sequence alignment due

to its common occurrence in all the DNA sequences. The unique sequences were categorized into two preponderant groups after nucleotide composition analysis through MSA. Random region sequences were G rich in group 1 but did not display any conservation. 2 sequences from Group-I (named Ag85B-18C-20 and Ag85B-4C-12) had multiple repetitive consensus motifs, and thus were considered further (Fig. 3.9).

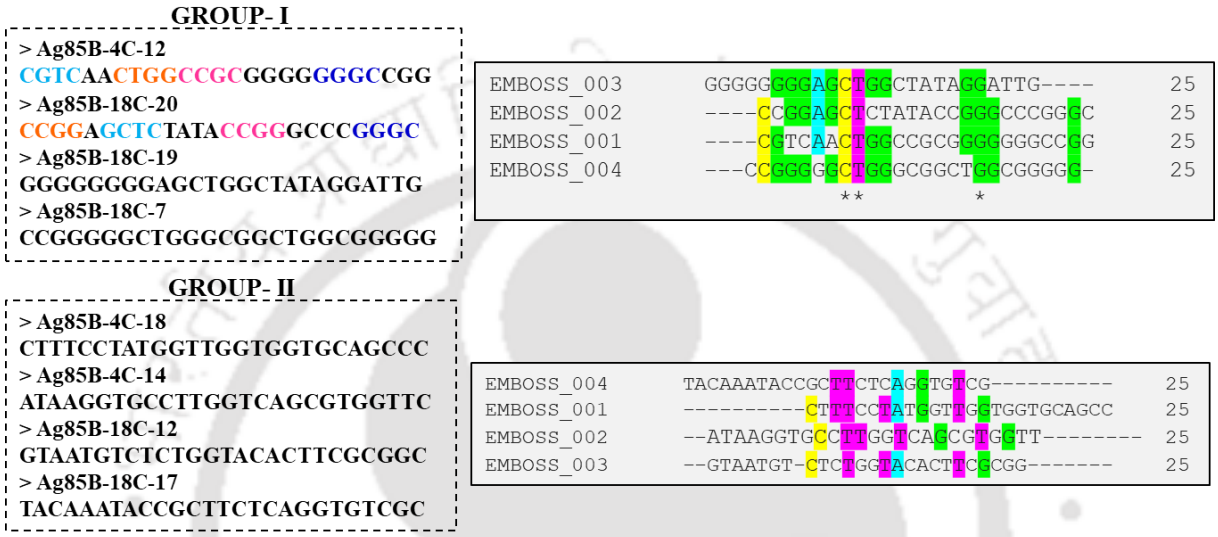

Fig. 3.9 Clustering of aptamer sequences based on sequencing results. Group I and Group II aptamer sequences analysed by MSA. The conserved and consensus motifs are highlighted in colours to denote their repetitive occurences in both Ag85B-18C-20 and Ag85B-4C-12 aptamer.

3.4.4 Secondary structure prediction and QGRS analysis

The secondary structures of Ag85B-4C-12 and Ag85B-18C-20 were predicted by using Mfold. The ΔG values for Ag85B-18C-20 and Ag85B-4C-12 were deduced as ΔG = -9.45 kcal/mol and -8.66 kcal/mol kcal/mol respectively. The ionic conditions was selected for measurement at 25 °C. Ag85B-18C-20 has one big loop with three small stem loop structures, connected through one long arm; whereas Ag85B-4C-12 is comprised of one big loop and three smaller loops connected by three stem structures (Fig. 3.10). Further, the propensity of these two aptamers to form G quadruplexes due to the presence of G-rich repeats were checked by the QGRS mapper tool (https://bioinformatics.ramapo.edu/QGRS/index.php). The QGRS mapping analysis revealed the presence of G quadruplexes with scores as depicted in Table 3.2.

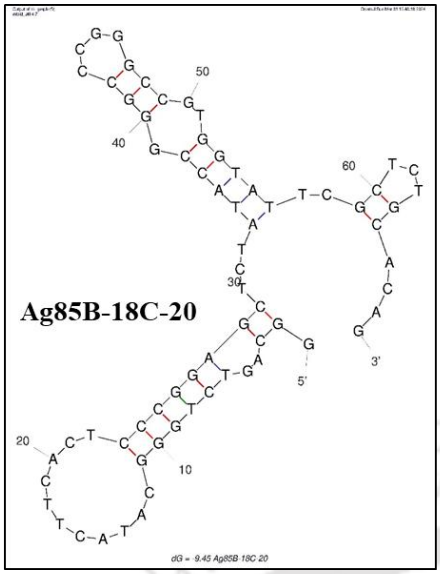

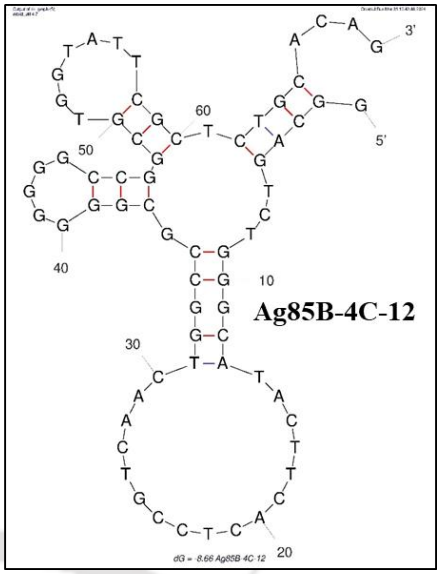

Aptamer	N-25 Sequence (5' to 3')	ΔG value
Ag85B-18C-20	CCGGAGCTCTATACCGGGCCCGGGC	-9.45 kcal/mol
Ag85B-4C-12	CGTCAACTGGCCGCGGGGGGGCCGG	-8.66 kcal/mol

Fig. 3.10 Secondary structure prediction by Mfold.

Table 3.2 QGRS mapping of Ag85B-18C-20 aptamer.

Aptamer	Position	Length	QGRS	G-score
Ag85B-18C-20	26	28	GGAGCTCTATACCGGGCCCGGGCCGTGG	14

3.4.5 Analysis of aptamers by CD spectroscopy

CD spectroscopy can highlight several unique aspects in the topological characterization of aptamers [189]. Intriguingly, both the aptamers in binding buffer displayed a unique ellipticity curve depicting the maximum (positive) and minimum (negative) peaks centred around ~275 nm and ~245 nm respectively (Fig. 3.11). This was consistent with the formation a probable G quadruplex structure flanked by double-stranded regions of hairpin duplexes. Characterestic domain of the duplex DNA appears at 270-280 nm [190]. So, our observation can be correlated to the presence of a G quadruplex (as shown by the QGRS prediction tool) embedded within the flanking regions forming stem-loop secondary structures [190,191]. On the other hand, our observations are in line with the study reported by Olejko and his co-workers, where presence of $MgCl_2$ influenced the appearance of CD spectroscopic peaks in DNA. The presence of 5 mM

$MgCl_2$ in our binding buffer did contribute to the formation of "G4" higher order structures. Literature reports suggest that orientations of the G quadruplexes are strongly dependent upon ionic concentrations and solvents that influence the polarities of DNA strands and loop orientations in DNA [192,193].

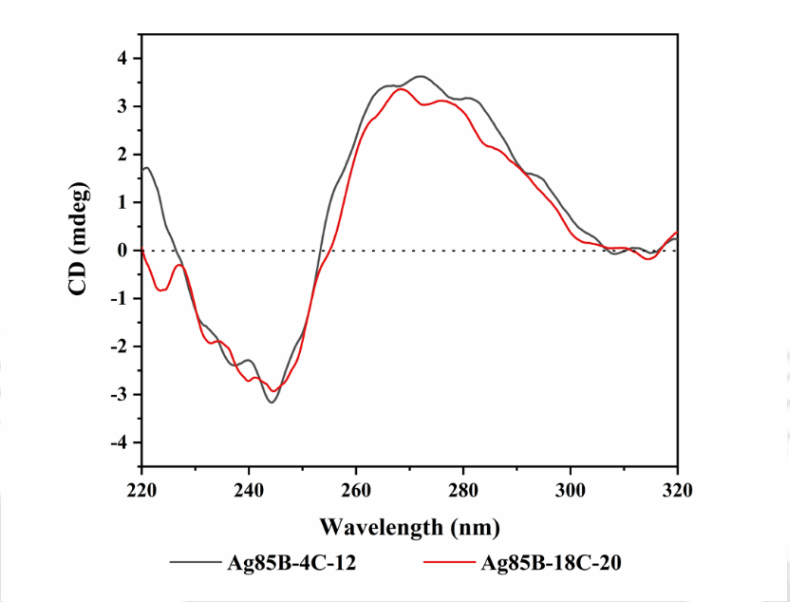

Fig. 3.11 CD spectroscopic analysis of aptamers screened against target Ag85B.

Under specific physico-chemical conditions (pH, ionic strength), linear aptamers preserve a typical three-dimensional conformation with respect to a particular binding site. This is especially important for design and development of sensors [194]. Therefore, the effects of monovalent and divalent cations (KCl and $MgCl_2$ salts) on the native confirmation of the developed aptamers were examined. In case of Ag85B-18C-20 aptamer, presence of KCl and $MgCl_2$ salts spiked in milli-Q water led to a bathochromic shift in the positive peak wavelength from λ_{269} nm with KCl to approximately λ_{278} nm.

In case of Ag85B-4C-12 aptamer, two positive peaks at wavelengths near 264 nm and 275 nm were noted in KCl spiked in milli-Q water. A dip in wavelength was observed around wavelength 270 nm. For $MgCl_2$, two positive peaks at 270 nm and 280 nm was seen with a small dip around 275 nm wavelength (Fig. 3.12A). For, Ag85B-18C-20 aptamer, only one individual peak was observed for both KCl and $MgCl_2$. These indicate that the structure of Ag85B-18C-20

aptamer was well maintained in the presence of salts in water and suitable for studying binding interactions of target-induced conformational changes around the positive peak regions of aptamers (Fig. 3.12B).

With respect to the large negative peaks of the aptamer molecules, aptamer Ag85B-18C-20 showed two negative peaks around 240 nm in presence of KCl spiked in milli-Q. In $MgCl_2$, three negative peaks were noted at wavelengths 230 nm and 250 nm. For Ag85B-4C-12 aptamer, the negative peak was observed at 242 nm and for $MgCl_2$, it was observed approximately around 246 nm (Fig. 3.12).

It was also observed that there was a major hyperchromic shift when solvent changed from water to divalent cationic salt $MgCl_2$ for both the aptamers. The result validate the effect of ionic interaction on the structure of aptamer (Fig. 3.12).

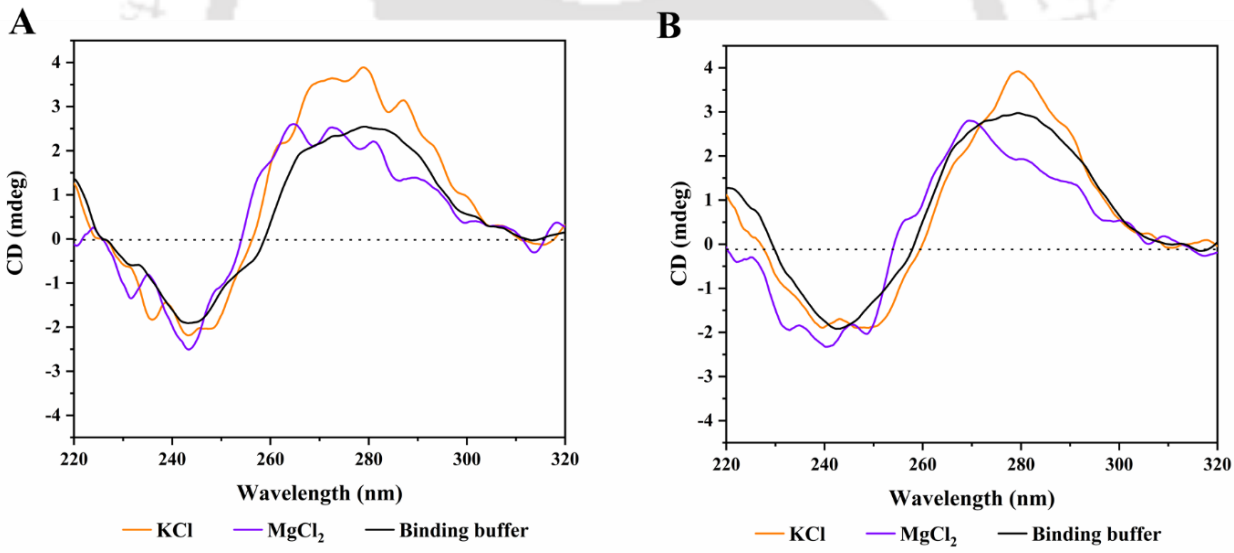

Fig. 3.12 CD spectroscopic analysis of aptamers in different ionic conditions. (A) Ag85B-4C-12 (B) Ag85B-18C-20

A similar study was done to find out the effect of different pH conditions on the structural folding of the aptamer. The CD peak intensities of the aptamers did not change in either acidic or basic conditions. The Ag85B-4C-12 aptamer showed a bathochromic shift at pH 10. Moreover, it was observed that the peak shape at negative CD spectral region was disordered at pH 4 (Fig. 3.13).

An interesting observation was that except for pH 4, the Ag85B-18C-20 aptamer was able to retain its structural ability at neutral to basic pH [195]. Ag85B-18C-20 aptamer had peak intensities at ~278 nm and 250 nm which were similar for pH 6, pH 7 and pH 8 and pH 10.

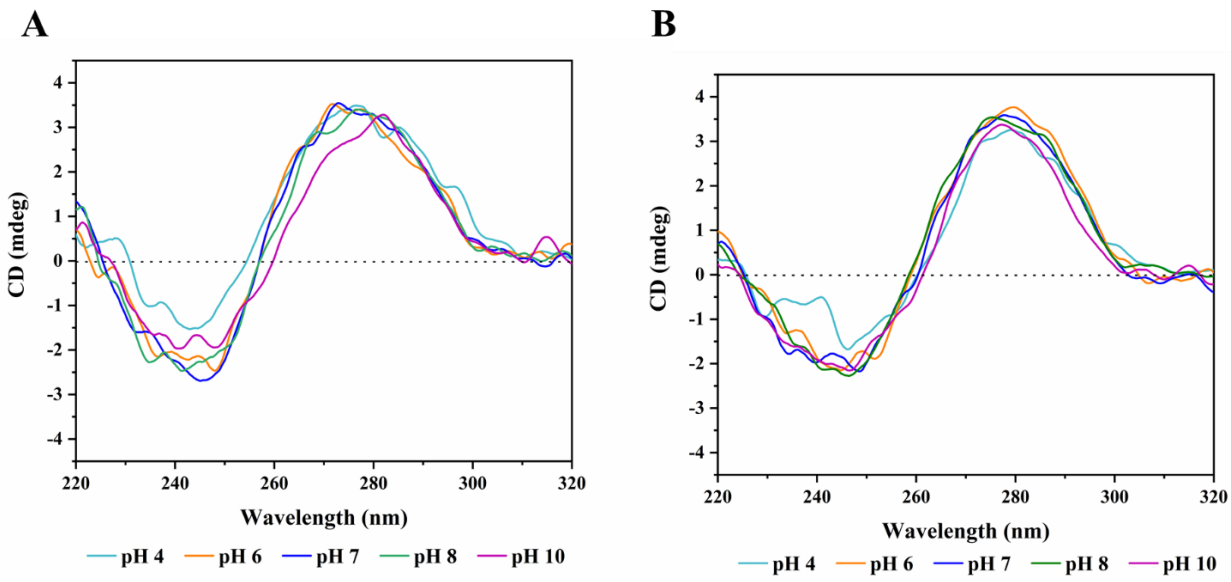

Fig. 3.13 CD spectroscopic analysis of aptamers in different pH conditions. (A) Ag85B-4C-12 aptamer (B) Ag85B-18C-20 aptamer.

3.4.6 Computational docking analysis

HDOCK provided docking results, including 10 top models based on its scoring function. Among these top 10 docking models, the top 3 models with the lowest docking score (threshold below −200; the most possible binding model) and confidence score above 0.7 (threshold greater than 0.7; very likely to bind), for Ag85B-4C-12 and Ag85B-18C-20 aptamers were reported. Pymol was used for 3D structure visualization of Ag85B:Ag85B-4C-12 and Ag85B:Ag85B-18C-20 protein aptamer docked complexes (Fig. 3.14). PLIP tool was used to compute the type of interactions between the aptamers and Ag85B for the best aptamer-protein binding model out of the top 3 models. Interestingly, the PLIP analysis revealed that hydrogen bonds, salt bridges and hydrophobic interactions were involved in the interaction between the aptamers and Ag85B leading to a strong binding between Ag85B and the aptamers [144]. The details of the interacting residues (interacting amino acid: nucleotide base) is tabulated in Table 3.3.

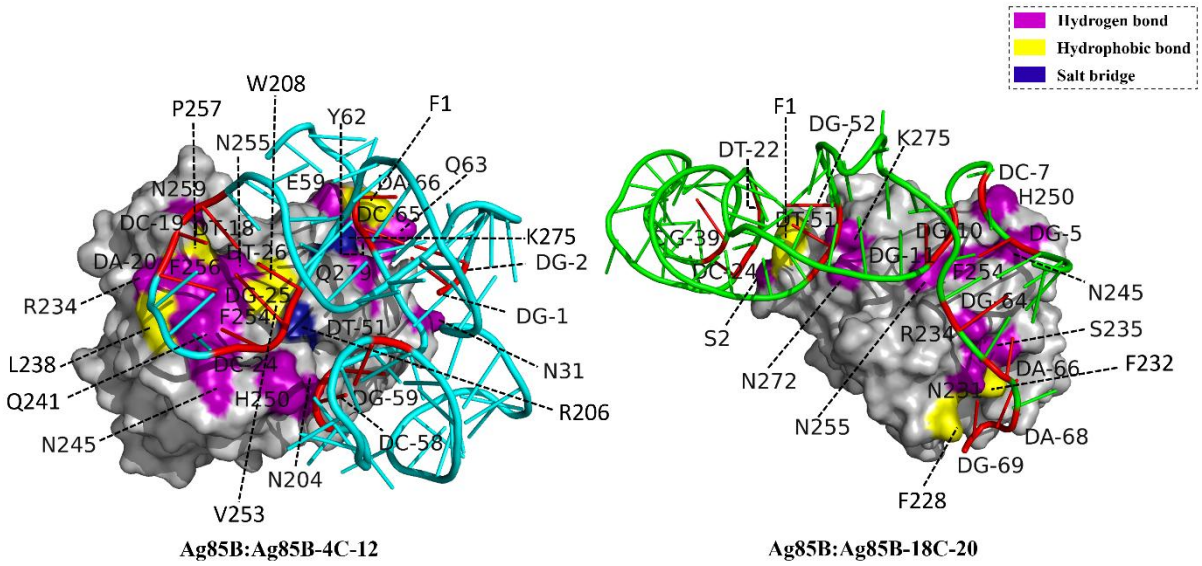

Fig. 3.14 Docked model of Ag85B-4C-12 and Ag85B-18C-20 aptamers with Ag85B. Ag85B protein represented in grey. The two screened aptamers are shown in two separate colours. All the interacting residues are labelled using either aa abbreviation codes (in the protein) or DA, DT, DG and DC (in the aptamers) with corresponding residue numbers.

Additionally, we also tried to locate key residues of Ag85B that were recognized by both the aptamers in order to locate a probable binding groove or pocket. Polar and positively charged residues like 234ARG, 245ASN, 250HIS, 254PHE, 255ASN on Ag85B are found to interact well with the negatively charged DNA backbone suggesting a potential binding site. Based on the parameters of better stability (as depicted by the ΔG value) and higher docking score; aptamer Ag85B-18C-20 was considered further. The results were then braced with the CD spectroscopic analysis.

Table 3.3 Identification of aptamer-Ag85B contact residues and type of non-covalent interactions involved in stabilization of the complexes during *in silico* docking.

Aptamer	Hydrogen bonds	Hydrophobic interactions	pi-Stacking	Salt Bridge	pi-Cation Interactions
Ag85B-18C-20	2SER:24C 231ASN:39G 231ASN:69G 231ASN:66A 234ARG:64G 235SER:68A 245ASN:5G 250HIS:7C 254PHE:10G 255ASN:11G 272ASN:51T 275LYS:51T	1PHE:22T 228PHE:69G 232PHE:68A	232PHE:68A	275LYS:52G	228PHE:69G
Ag85B-4C-12	31ASN:51G 59GLU:66A 62TYR:1G 63GLN:2G 204ASN:59G 234ARG:20A 241GLN:24C 245ASN:24C 250HIS:25G 254PHE:25G 255ASN:26T 256PHE:20A 259ASN:19C 279GLN:65C	1PHE:65C 208TRP:26T 238LEU:20A 253VAL:25G 257PRO:18T	None	206ARG:26T 250HIS:59G 250HIS:58C 275LYS:66A 275LYS:65C	None

We also expanded our docking studies with the Ag85B-18C-20 aptamer to investigate its binding affinity to the other two biomarkers (Ag85A and Ag85C) of the Ag85 family of proteins. This exploration stemmed from the possibility that all three proteins could be present in the blood of an individual infected with TB as secretory biomarkers. The specific binding of our Ag85B-

18C-20 aptamer solely to Ag85B, excluding Ag85A and Ag85C, would demonstrate its target specificity. The docked structures of Ag85B-18C-20 with Ag85A or Ag85C are depicted in Figure 3.15. Our docking results indicate that the aptamer formed significantly fewer hydrogen bonds with Ag85A or Ag85C compared to Ag85B. (Table 3.4, 3.5).

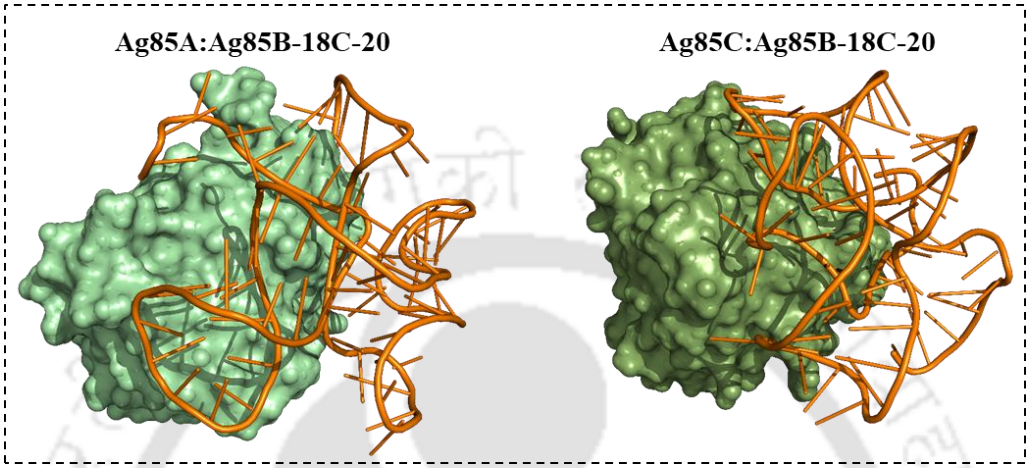

Fig. 3.15 Docked model of Ag85B-18C-20 aptamer with Ag85A and Ag85C. Ag85A and Ag85C are shown in separate colours.

Table 3.4 Interacting residues of Ag85B-18C-20 aptamer with Ag85A.

Aptamer	Hydrogen bonds	Hydrophobic interactions	pi-Stacking	Salt Bridge	pi-Cation Interactions
Ag85B-18C-20	63GLN:2G 141GLN:44G 234ARG:20A 241GLN:24DC 254PHE:25G 279GLN:64G 285THR:62C	238ILE:20A 253VAL:25G 256PHE:20A 257PRO:18T	None	206ARG:260T 234ARG:20A 275LYS:65C 280ARG:27C	None

Table 3.5 Interacting residues of Ag85B-18C-20 aptamer with Ag85C.

Aptamer	Hydrogen bonds	Hydrophobic interactions	pi-Stacking	Salt Bridge	pi-Cation Interactions
Ag85B-18C-20	82GLN:66A 137THR:25G 175ASN:66A 182SER:63T 183ASP:64G 188ARG:26T 240ASP:44G	97THR:18T 101ARG:19C 180PRO:65C	None	188ARG:26T 197ARG:25G	None

3.4.7 Analysis of binding of aptamer with Ag85B by CD spectroscopy

Till this point, we have understood that both the screened aptamers Ag85B-4C-12 and Ag85B-18C-20 exhibited good stability in buffer solutions and displayed affinity for Ag85B. It is also well known that upon binding to targets, structural alterations in aptamers can be probed using CD spectroscopy [196]. In the presence of increasing amounts of Ag85B, (100-5000 nM), a concentration-dependent change in the CD spectra was observed, suggesting some Ag85B-dependent structural reorientations in the aptamers as a function of aptamer-protein interactions (Fig. 3.16) [197]. Interestingly, for Ag85B-18C-20, the small yet significant changes around the ~275 nm and ~245 nm peaks were more pronounced as compared to Ag85B4C-12. It is

imperative to note that changes in aptamer structure around the ~275 nm peak cannot be attributed to a sequential increase in peak intensity with gradual increase in concentration of the Ag85B protein (Fig. 3.16 B). Rather, we hypothesize that, the Ag85B protein induces a change in the overall ellipticity of the aptamer suggesting a possible role of the G-quadruplex orientations and the dynamic structure-switching functionalities that the aptamer can adopt in solution during the interactions [186,198,199]. Interestingly, the differential affinity of such unique structure-switching motifs could also be reflected by the presence of K^+ ions in our binding buffer which has also been shown in earlier reports by other researchers [200].

Intriguingly, it is often noted that the CD spectral wavelength values for G-quadruplexes reported in literature is not absolute for the type of structure it adopts (i.e. parallel, hybrid, mixed or antiparallel). In a critical review, the authors have claimed that the wavelengths are represented as averages of values published in the literature; that may vary with the type of G-quartet stacking, strand segment orientation, and loop arrangements affecting the precise values at which peaks may form [195,201]. This leads to the ambiguity in interpretation of G-quadruplex structures. Thus, further studies are required to interpret the results our Ag85B-18C-20 aptamer and Ag85B interaction pattern.

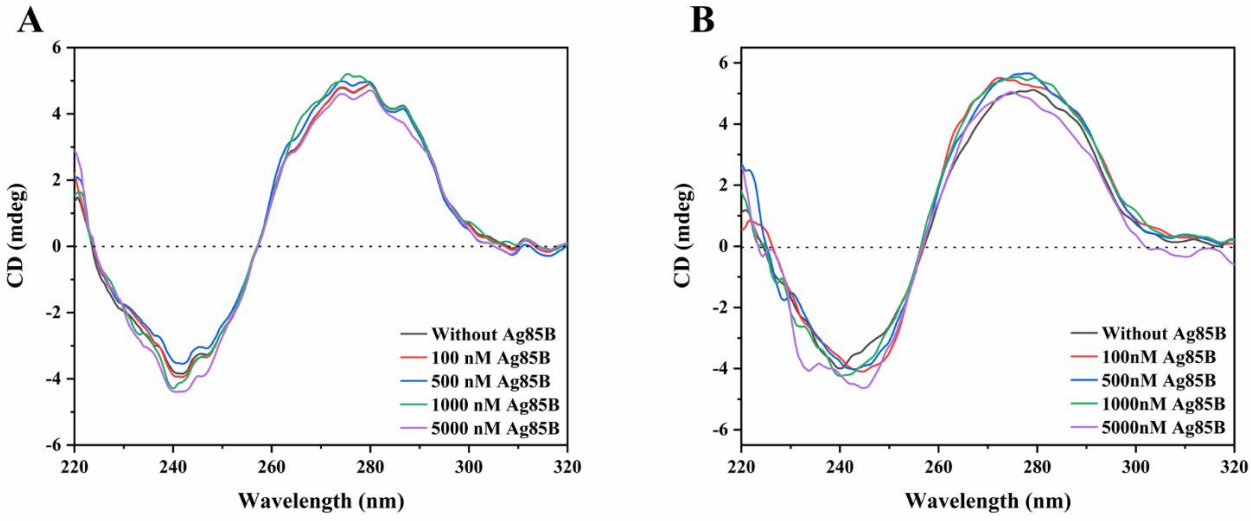

Fig. 3.16 CD spectroscopic analysis of aptamer binding with Ag85B at different concentrations. (A) Aptamer Ag85B-4C-12 (B) Aptamer Ag85B-18C-20.

So far, based on the parameters of better thermodynamic stability (as depicted by the ΔG value), higher docking score and greater tendency to undergo target-induced conformational changes; we concluded that the Ag85B-18C-20 aptamer was a better candidate for developing an aptasensor. This DNA sequence of Ag85B-18C-20 aptamer is deposited at the Indian Patent office, under patent application no. 202431029861.

For determination of the binding affinity; we calculated the K_D value of the Ag85B-18C-20 aptamer by obtaining the best fit non-linear plot of difference in peak intensity versus protein concentration via Origin Pro 2019b software. K_D value was obtained as 938.46 ± 432.38 nM for Ag85B-18C-20 aptamer (Fig. 3.17).

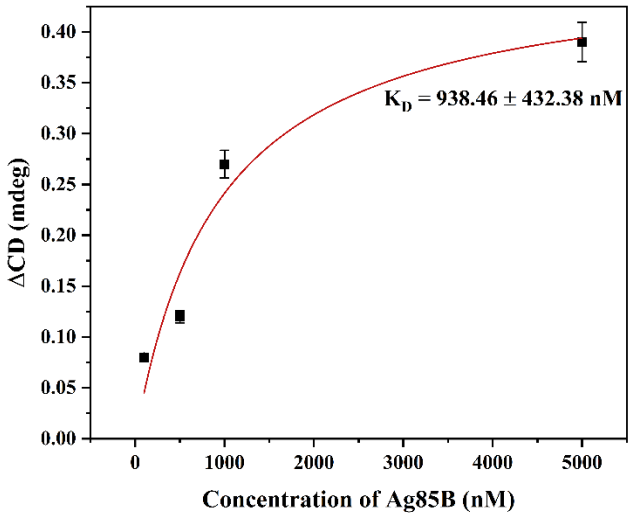

Fig. 3.17 K_D calculation from CD spectroscopy. Non linear plot showing K_D for Ag85B-18C-20 aptamer fitted to a one site binding model.

3.4.8 EMSA of aptamer Ag85B-18C-20 with target Ag85B

In order to assess the binding behaviour of Ag85B-18C-20, the EMSA study yielded useful information. [202]. With increasing concentrations of the Ag85B protein, the free Ag85B-18C-20 aptamer readily engaged in interactions, forming aptamer-protein complexes. The escalating intensity of the bands with rising protein concentrations directly signifies a positive interaction between the aptamer and the protein. Due to reduced electrophoretic mobilities, the aptamer-protein complexes appear as bands with higher molecular weights compared to the aptamer alone. These aptamer-protein complexes displayed a slower migration rate in native

polyacrylamide gel electrophoresis compared to unbound aptamers.

Earlier in this study, we also predicted the probability of Ag85B-18C-20 aptamer to form spontaneous G-quadruplexes by QGRS mapping. On the other hand, it is well established that aptamer assays involving human serum are strongly influenced by the stability of the aptamers in serum [186]. Thus, before using Ag85B-18C-20 aptamer for the upcoming serum-based detections, we also checked its stability in serum and the pattern of monomeric or multimeric forms it adopts in solution. It is usually interpreted that aptamers having a G-quadruplex embedded in its structure show multimeric bands (one as a monomer at the desired length accompanied by multiple higher molecular weight bands above the monomer) during migration on a native polyacrylamide gel (Fig. 3.18A). Commercially purchased Ag85B-18C-20 aptamer was found to be serum stable for 3 hours (Fig. 3.18B).

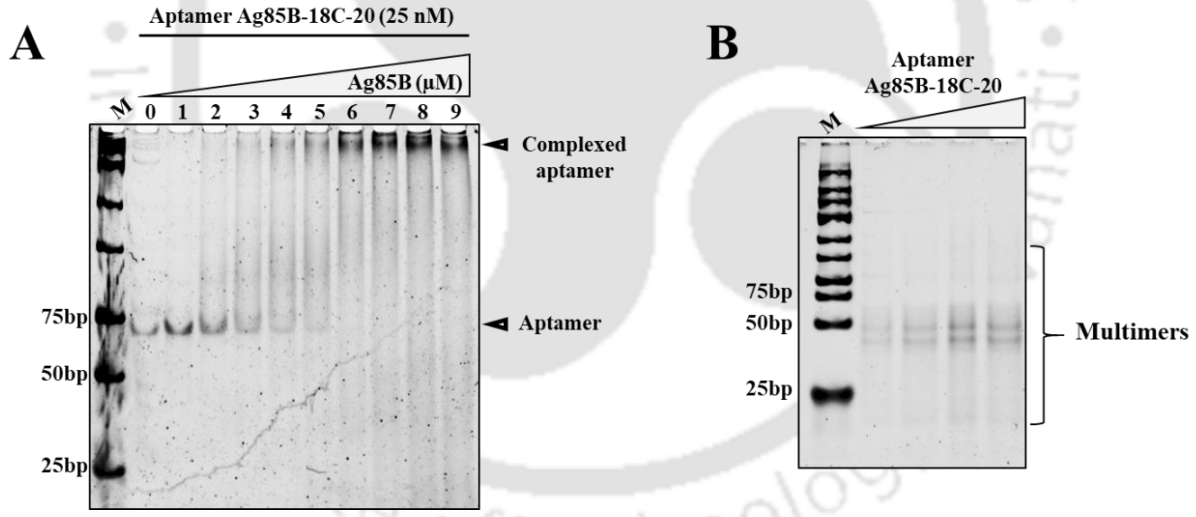

Fig. 3.18 Native PAGE analysis of aptamer Ag85B-18C-20 interactions with Ag85B probed by EMSA. (A) Interaction studies of Ag85B-18C-20 aptamer with increasing concentrations of Ag85B visualized by SYBR gold staining of (B) Native PAGE analysis of Ag85B-18C-20 aptamer following incubation in 50 fold dilted human serum for upto 3 hours at 37°C. The aptamer was serum stable.

3.4.9 ITC study of aptamer Ag85B-18C-20 with target Ag85B

In order to know the binding mechanism and interaction pattern of Ag85B to Ag85B-18C-20 aptamer, we employed ITC. ITC is a powerful tool to know the number of binding sites (single or multiple) on Ag85B where the aptamer would presumably interact. Our results of the ITC experiment are similar to the binding studies of HupB aptamers studied by Kalra et al. in

2018 wherein they report a two site binding mechanism between the developed aptamer and target [186]. Our titration data showing heat resulting from injection of Ag85B into the Ag85B-18C-20 aptamer solution is in close resemblance with their findings (Fig. 3.19). Our ITC data was fitted in a two site binding model and data analysis revealed that among the two independent binding sites in Ag85B (arbitrarily denoted as site 1 and site 2 for Ag85B-18C-20 aptamer), the aptamers exhibited higher affinity for one site (assigned as site 1 with a K_D value of 14.9 nM) over the other (assigned as site 2 with a K_D value of 16500 nM). However, the thermodynamic parameters of ΔH and ΔS obtained after the curve fitting did not provide conclusive results to term the Ag85B-18C-20 aptamer binding to Ag85B as a spontaneous reaction. Hence, we feel that the proportions of Ag85B and Ag85B-18C-20 aptamer that was used for the ITC titrations need further optimization to obtain a better interpretation of binding stoichiometry between the target and aptamer in the binding buffer.

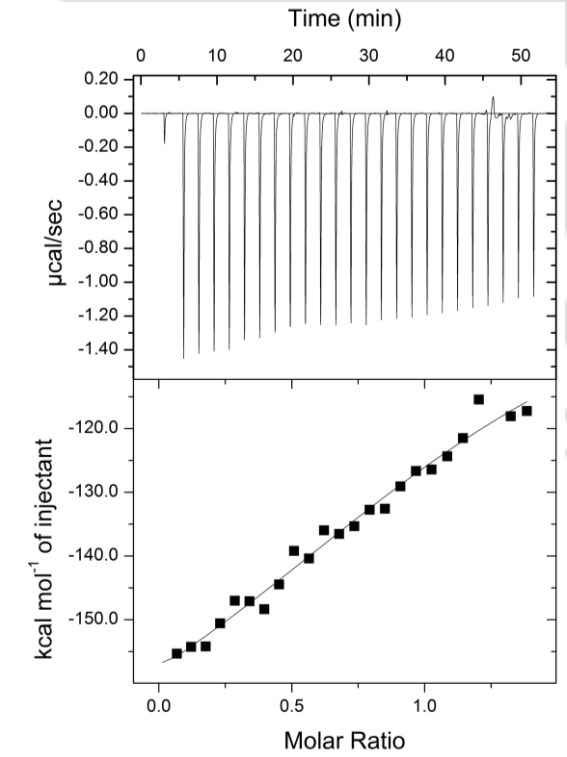

	Site 1	Site 2
K_a	$6.68x10^7\ M^{-1}$	$6.05x10^4\ M^{-1}$
K_D	14.9 nM	16500 nM
ΔH	-1.90×10^5	-9.11×10^5
ΔS	-603 cal/mol/deg	-284 cal/mol/deg

Fig. 3.19 ITC analysis of binding between Ag85B and Ag85B-18C-20 aptamer. Two site binding of Ag85B-18C-20 aptamer to Ag85B using ITC. Shown are the titrations of Ag85B into a solution of the Ag85B-18C-20 aptamer. Top, titration data showing the heat resulting from each injection of Ag85B into the aptamer solution; bottom, integrated heats after correcting for the heat of dilution. Binding experiments were performed at room temperature in binding buffer.

3.5 Conclusion

This study is the first report of screening aptamers with high affinity and specificity for Ag85B protein of MTB. A specific 69 nucleotide long ssDNA aptamer Ag85B-18C-20 against Ag85B was developed following the COFA SELEX process. Our process circumvented the bottlenecks of traditional SELEX by saving time, using minimal quantities of target as well as allowing dynamic interactions between the target and aptamer pool freely in solution. To reduce non-specific binding interactions, aptamers were screened in presence of two non-target TB proteins, namely MPT64 and ESAT6. Two aptamers were characterized before selecting the best aptamer for further studies. The conformational changes of the screened aptamers exposed to various pH and ionic compositions have been monitored using CD spectroscopy.

The binding of the developed aptamer towards Ag85B was confirmed by computational docking, CD spectroscopy, EMSA and ITC studies. The binding constants were determined independently following these studies (CD spectroscopy and ITC), but were not found to be similar. Additional studies would add to our analysis in future. The aptamer Ag85B-18C-20 developed by us against Ag85B is significantly different from the other reports on Ag85B sensing methods.

4

Development of aptasensor for detection of tuberculosis biomarker Ag85B

Abstract

Optical biosensors serve as valuable tools for detecting disease biomarkers. Numerous fluorescence-based optical detection systems have demonstrated the ability to detect TB biomarkers with high specificity and sensitivity. In this study, we conducted a systematic analysis of the interactions between the Ag85B-18C-20 aptamer and its target Ag85B using a fluorescence-based graphene oxide quenching platform. Intriguingly, we observed strong interaction between the developed aptamer and the target, even in the presence of other interfering substances in human serum. The aptasesnsing system exhibited a wide linear response across the range of Ag85B concentrations tested. Moreover, the developed aptasensor exhibited specificity towards the target Ag85B and could detect nanomolar concentrations of the biomarker with high sensitivity from human serum. To the best of our knowledge, we present, for the first time, an optical aptasensor designed for the rapid screening and detection of TB using the Ag85B biomarker.

4.1 Overview

Search for efficient aptasensor platform for clinical diagnosis of TB is one of the on-going research activities aggressively being pursued globally to design and develop flawless detection system for deployment in resource limiting TB endemic zones of the world.

Before the design and development of a clinically relevant aptasensor, we tried to focus on enumerating the special features of the developed aptamer in terms of its binding affinity. The equilibrium dissociation constant (K_D) is the basic parameter to evaluate the binding property of the aptamer-target. Dissociation constants of aptamer-target complexes typically range from the low micromolar to high picomolar levels. We have detrmined the K_D using a simple UV-visible spectrophotometer and biotin-labelled aptamer in an aptamer-linked immobilized sorbent assay (ALISA) or enzyme-linked apta-sorbent assay (ELASA) analogous to the same format as ELISA [203,204]. We have used direct ALISA in our studies, where the target Ag85B protein is immobilised onto the surface of 96-well plates, followed by blocking with BSA and the addition of the biotinylated aptamer and streptavidin-conjugated horseradish peroxidase (HRP). Upon addition of the substrate for signal production, the product is measured for the generated absorbance at 450 nm (OD_{450}). The absorbance corresponds to the binding affinity of the aptamer; till saturation point is reached. This assay has shown considerable reproducibility in terms of K_D evaluations and estimation of the aptamer's binding affinity [205–208]. A pictorial representation of the ALISA method is shown in Fig. 4.1.

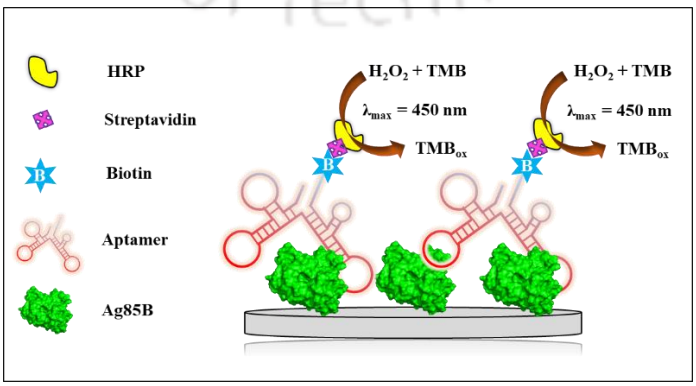

Fig. 4.1 Schematic representation of ALISA method used in the current study.

One of the most critical requirements in developing rapid detection tests is the generation of noise free decipherable signal and lower detection limits from the specific interaction of the biorecognition element with the target of interest. Various biosensors have been developed for the rapid detection of TB [209]. The domain of biosensing using aptamers have gained momentum in the last decade giving rise to various optical, electrochemical, piezoelectric and lateral-flow based tools for TB biomarkers. The ease of interpretation of optical sensing platforms have allowed researchers to develop aptasensors with either direct or labelled detection schemes [210]. When compared to other techniques, fluorescence spectroscopy offers the following advantages. First, because of its high sensitivity, single receptor molecules can now be studied in this manner. Furthermore, selective research of intermolecular interactions under diverse circumstances is possible through the transfer of fluorescence energy from donor to acceptor. The availability of a wide range of fluorescent probes in the commercial market is an additional benefit. The research approach can be greatly expanded by using the fluorescent probes to label molecules that lack fluorescence properties. Donor-acceptor fluorescence pairs are a great tool to study receptor-ligand interactions by using fluorescence spectroscopy because of their high spatial resolution [211,212]. Since the fluorescent probe is another important component that affects how well fluorescent aptasensors work, choosing one requires taking into account a number of factors: i) it should be able to produce a clear and detectable signal (high quantum yield at convenient wavelength); ii) it should be easily excitable (high absorptivity at convenient wavelength); iii) it should not be affected by other components in the matrix; iv) it should have good stability and water solubility; and v) it should be modifiable with specific functional groups.

Till date, the majority of optical based platforms reported for TB are for estimation of IFN-γ which is a soluble cytokine produced by T-cells significant for TB diagnosis as a host-derived biomarker. Among these, the labelled aptasensing platforms for IFN-γ have shown the

use of FAM, TPE, BODIPY, TAMRA, Alexa Fluor, Chol, ROX, graphene quantum dots etc. as sensitive labels for detection [213–219]. Only surface plasmon resonance (SPR) and fluorescence based detections have been reported for these aptasensors. Moreover, direct or unlabeled optical aptasensors reported for IFN-γ include chemiluminescence, colorimetric and liquid crystal based polarized light microscopy aptasensors so far.

On the contrary, only three published reports exist for optical aptasensing platforms for pathogen-derived biomarkers in TB [220]. Use of ATTO647N label for sensitive detection of Ag85A biomarker was reported by Ansari and his colleagues with a K_D of 62.95 nM for the reported aptasensors on a fluorescence platform [131]. An aptasensors based on FAM and BHQ1 conjuagted label was fabricated by Jeon et al. for sensitive fluorescence based detection of TB7.7 antigen with a K_D of 5.3 nM [96]. Lastly, unlabeled or direct colorimetric detection for glycolipid biomarker LAM through direct and indirect dot-blot aptamer assays [133].

Thus, from these published reports it can be deciphered that the fluorescence based optical signal systems that employ aptamers as recognition elements can effectively tailor multiple aspects of both worlds that contribute towards building of a successful aptasensor. The fluorescence labels are capable of showing high sensitivity, quantitative analysis and real-time detection; whereas aptamers are capable of contributing to the versatility, flexibility, multiplexing capabilities and requirement of small sample volumes. Because of their high sensitivity and specificity, fluorescence-quenching “signal OFF” and “signal ON” platforms designed with a donor and acceptor pair are proven to be promising methods for detection [214]. Additionally, the fluorescence based method are reaching new heights with the invention of various highly efficient fluorophores tailored for various applications [221].

Fluorescein amidites, abbreviated as FAM are single isomer derivatives of fluorescein having unique luminescent properties. It is the most popular fluorescent dye attachment for oligonucleotides and works with the majority of fluorescence detection devices. It is usually used

in the pH range of 7.5-8.5, making it highly water soluble and showing good absorption and emission properties. Because of its high molar extinction coefficient, high quantum yield of fluorescence, and good stability when conjugated to DNA during synthesis, less toxicity, and resistance against photo bleaching it could be utilized for simple optical applications [222].

Because of its exceptional electrical conductivity, graphene oxide (GO) can be utilized as an extremely effective nanomaterial via charge-transfer processes in fluorescence. GO offers a number of benefits as a quencher: i) There are many bonding sites provided by the 2D planar surface area; ii) Additional bioconjugation is made possible by the oxygen-containing functional groups; and iii) It is affordable, non-toxic, water soluble, and biocompatible [223]. GO readily interacts with the negatively charged phosphate backbone of DNA through hydrophobic interactions and π–π stacking. Numerous studies on GO have reported the successful interaction with DNA, which consequently quenched the fluorophores attached with the DNA. Reports suggest that temperature, ion concentration, electrostatic repulsion, buffer pH, and several other factors have a significant impact on DNA-GO interactions [224].

Herein, we report the application of a novel G-quadruplex bearing aptamer specific to Ag85B selected through the novel COFA SELEX methodology as described in the previous chapter to develop a fluorescence-based detection platform of the biomarker. After investigating the aptamer-protein interactions and verifying the proper functionality of Ag85B-18C-20 aptamer, we incorporated the aptamer into a sensing assay. Following a simple quenching phenomenon between the FAM modified “donor” aptamer and the GO “acceptor”, a fluorescence based two step aptasensor platform for quantitative detection of Ag85B protein in spiked human serum samples was studied. A schematic representation is depicted in Fig. 4.2. Also, the fluorescence intensity is directly proportional to the protein concentrations in the reaction mixture which in turn produces reproducible results over a wide Ag85B concentration range. A detailed account on the findings is incorporated in this chapter.

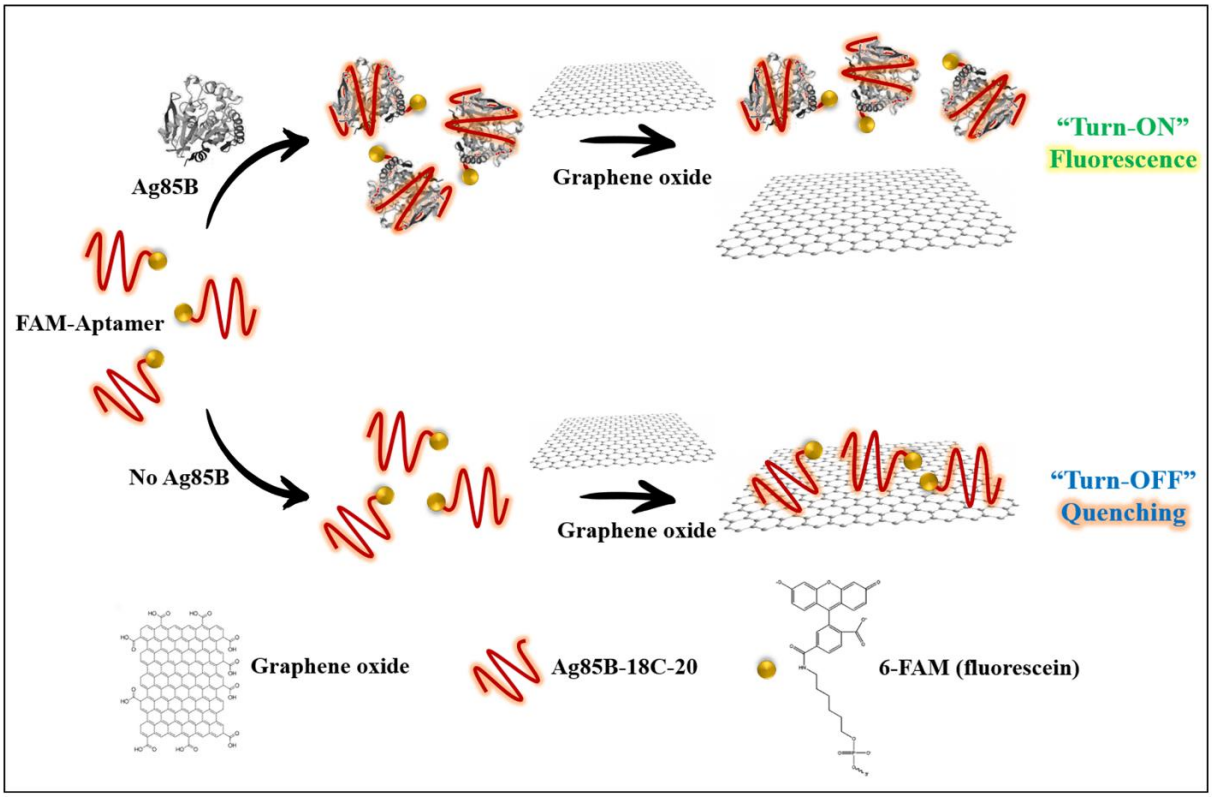

Fig. 4.2 Schematic representation of GO-based fluorometric aptasensing designed for this study towards sensitive detection of Ag85B biomarker.

4.2 Materials

The aptamer Ag85B-18C-20 was synthesized by IDT, USA with a fluorescein (6-FAM) and biotin modifications at the 5′ end. GO was obtained from Sigma. 96 well plates (black, with lid and clear bottom) for fluorescence were purchased from ThermoFisher Scientific. HRP-Conjugated Streptavidin (catalog. no. N100) was also obtained from ThermoFisher Scientific. 3,3′,5,5′-Tetramethylbenzidine (TMB) Liquid Substrate System was from Sigma Aldrich. 2 M stop solution was purchased from Himedia Laboratories Pvt. Ltd. All other chemicals used were of molecular biology grade. All solutions were prepared using water obtained from a Millipore water purification system. All the buffer solutions were filtered using the 0.22 µM syringe filters and sterilized for storage not more than 5 days. Serum samples (n=3) were collected from Indian Institute of Technology Guwahati Hospital from healthy adults (age 32-55 years, with no known history of TB disease).

4.3 Experimental methods

4.3.1 Determination of dissociation constant by ALISA

This technique was adopted from an earlier report by Sypabekova and his colleagues with slight modifications [225]. In brief, 1600 ng/mL of purified Ag85B protein was coated overnight in 96 well plates using 50 mM carbonate-bicarbonate buffer, pH 9.6 overnight at 4 °C. After washing with binding buffer and blocking with 1 % BSA for 3 hours at 4 °C, commercially obtained 5′-biotin labelled Ag85B-18C-20 aptamer was added to wells for 90 minutes at 37 °C in binding buffer supplemented with 15 mM NaCl. After washing with binding buffer, streptavidin-horseradish peroxidase (HRP) was added at 1:10,000 dilution and incubated for 30 minutes at RT. Recommended amounts of TMB substrate was added to the wells and the reaction was quenched using 1 M H_2SO_4. Thereafter, the OD_{450} was measured in a microplate reader. In the negative control, the wells were coated without Ag85B protein and aptamer. Before analysis, the OD of the background (nuclease free water) was subtracted from the OD of the experimental samples. The experimental conditions were tested both in binding buffer and 50-fold diluted serum samples in triplicates. Initially, the efficacy of the method was checked using binding buffer and was subsequently validated in 3 serum samples (named Serum 1, Serum 2, Serum 3).

The reproducibility of the aptasensors was tested with three independent measurements for each serum sample and presented separately in the chapter.

4.3.2 Determination of aptamer specificity using ALISA

The binding specificity of Ag85B-18C-20 aptamer was checked by comparing the OD_{450} values with target Ag85B and non-target proteins ESAT6 and MPT64. ALISA method as discussed above was carried out by coating 1600 ng/mL of ESAT6 and MPT64 proteins overnight in 96 well plates. To assess binding specificity, the OD_{450} of non-target proteins were compared to that of Ag85B at saturating concentration of 4000 nM for the Ag85B-18C-20 aptamer. The statistical significance of the change in absorbance between the target and non-

target proteins was analysed using ANOVA.

4.3.3 Characterisation of GO for fluorometric aptasensor

Characterization of GO was done by prior to performing the experiments using FETEM (Make: JEOL, Model: 2100F), FESEM (Make: Zeiss, Gemini 300), EDX (in TEM), UV-vis and fluorescence spectroscopy. An aliquot of 10 µL of GO suspension in water (1 mg/mL) was briefly sonicated in an ultrasonicator water-bath for 2 minutes prior to dilution and experimental analysis. For FETEM analysis, the drop cast method was used on Cu-coated carbon grid (Electron Microscopy Sciences).

4.3.4 Optimization of GO concentration for fluorometric aptasensor

GO based quenching was performed in triplicates using the microplate reader (Varioskan LUX, Thermo). Briefly, the concentration of GO was varied from 0 to 60 µg/mL and the fluorescence intensity was measured by incubating with 100 nM of FAM-Ag85B-18C-20 aptamer for 15 minutes. Excitation and emission was set at 495 nm and 520 nm wavelength respectively.

4.3.5 Design and development of fluorometric aptasensor for detection of Ag85B

Working solutions of GO at 120 µg/mL and FAM-labelled Ag85B-18C-20 aptamer at 10 µM stock concentration was prepared and kept away from direct light. Briefly, fixed amounts of FAM-labelled Ag85B-18C-20 aptamer (100 nM) and varying concentrations of purified Ag85B (0 nM to 100 nM) was incubated for 1 hour at RT in 96 well plates. For the quenching to happen, GO was added at the optimized concentration of 30 µg/mL and kept for 10 minutes at RT with intermittent shaking. The change in fluorescence intensity was monitored at λ_{Ex} = 495 nm and λ_{Em} = 520 nm. The experimental conditions were optimized in binding buffer before performing the assay on serum samples in triplicates. The LOD of the prepared aptasensor was calculated by performing regression analysis of the intercept of calibration line obtained by plotting relative fluorescence versus concentration of Ag85B in Origin Pro 2019b.

4.3.6 Determination of reproducibility of the aptasensor

The FAM labelled Ag85B-18C-20 aptamer was tested for cross-reactivity by evaluating its ability to bind to non-target proteins ESAT6 and MPT64 proteins and the same was compared with that of target Ag85B protein. LOD was calculated by the formula 3.3σ/S, where σ = standard deviation (SD), S = slope of regression line. The coefficient of variation in spike and recovery assay at two levels of concentration were also calculated. The recovery assay was carried out at different concentrations of the spiked Ag85B to demonstrate the performance of the the proposed aptasensor. We also determined the analytical precision from a set of 20 independent experiments performed with two different levels of concentrations, i.e. 5 nM and 25 nM falling within the range of 0.05 nM to 100 nM (used to calculate LOD). The concentrations 5 nM and 25 nM was chosen based on earlier reports [180,206,208].

4.3.7 Statistical analysis

Statistical analysis was carried out by comparing the sets of data using one way ANOVA. The significance of the obtained results were checked by weighing the p-values as $p < 0.05$ (*), $p < 0.01$ (**), $p < 0.001$(***), $p < 0.0001$ (****) and $p < 0.00001$ (*****). All the statistical analysis were performed in Origin Pro 2019b. The experimental results were indicated as mean ± SD.

4.4 Results and Discussion

4.4.1 ALISA of aptamer Ag85B-18C-20 with target Ag85B

The equilibrium dissociation constant (K_D) measures how much the bound complex separates into free aptamer and free target, reflecting the aptamer's affinity for binding to its target molecule. High K_D values signify a weak aptamer-target complex binding, implying a low aptamer affinity for the target. ALISA was performed to determine the binding interaction between the selected aptamer Ag85B-18C-20 and the target Ag85B in spiked binding buffer and n=3 serum samples. This comparison was essential to investigate the binding potential and expected matrix-based differences that can affect the aptamer's binding potential in clinical

samples.

In binding buffer, concentration-dependent analysis of the binding affinity of Ag85B-18C-20 biotinylated aptamer to Ag85B showed linear correlation (Fig. 4.3A). Ag85B coated with no aptamer served as the negative control. OD_{450} was obtained by subtracting the background control (water) from all other wells. The R^2 value (Fig. 4.3A inset) showed that 90.6% of the absorbance values fitted the regression model. The regression equation for the difference in absorbance value and aptamer concentration (10-4000 nM) was y = 0.0303x + 0.0073, where x is the concentration of the aptamer in nM, and y is the absorbance value.

Using non-linear regression analysis, the K_D of Ag85B-18C-20 aptamer was found to be 310.83 ± 125.69 nM using one site binding kinetics (Fig. 4.3B) as shown below:

$$Y = \frac{B_{max}\, X}{K_D + X}$$

Where, X = Concentration of aptamer (nM)

K_D = Dissociation constant of aptamer (nM)

B_{max} = Maximum binding capacity (measured as OD_{450})

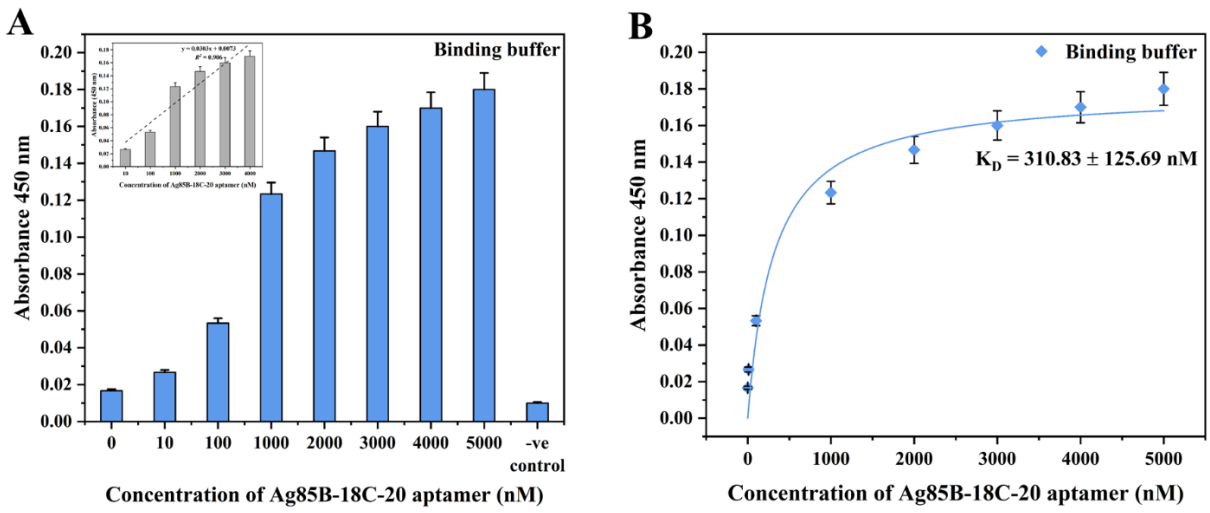

Fig. 4.3 Binding studies of Ag85B-18C-20 aptamer with Ag85B in binding buffer. (A) Concentration-dependent analysis of the binding affinity of Ag85B-18C-20 aptamer sequence to Ag85B using ALISA. The R^2 value (A INSET) showed that 90.6% of the absorbance values fitted the regression model. (B) K_D estimation of Ag85B-18C-20 aptamer using ALISA fitted to a one site binding model.

Whereas in Serum 1, concentration-dependent analysis of the binding affinity of Ag85B-18C-20 biotinylated aptamer sequence to Ag85B showed linear correlation and the R^2 value showed that 95.7% of the absorbance values fitted the regression model (Fig. 4.4A, Fig. 4.4A INSET). The regression equation for the difference in absorbance value and aptamer concentration (10-4000) was y = 0.0877x – 0.0198. Using one site binding kinetic model, the K_D of Ag85B-18C-20 aptamer was found to be 889.53 ± 356.04 nM (Fig. 4.4B).

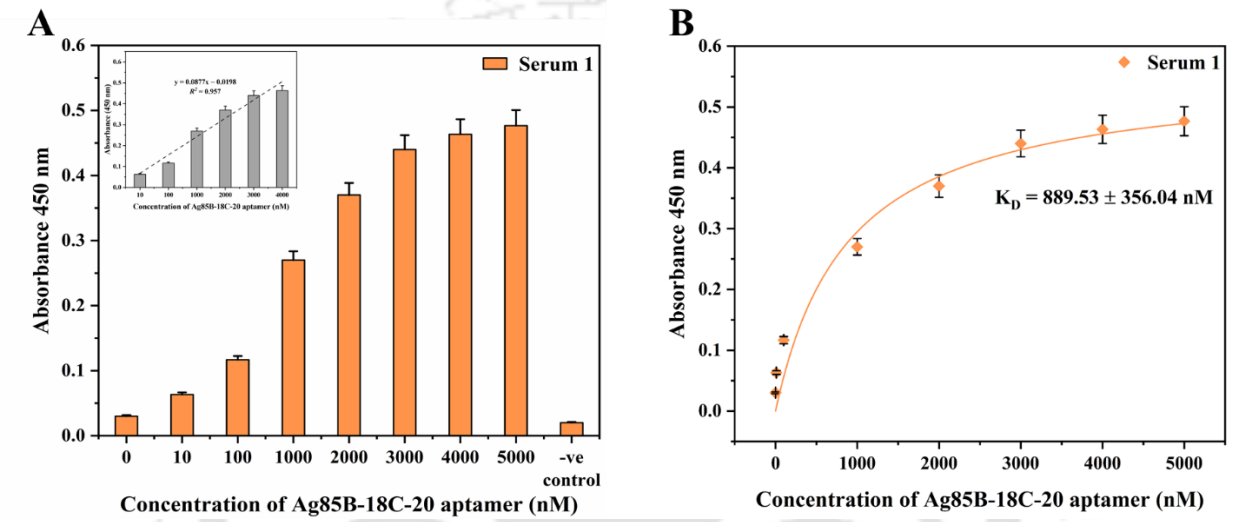

Fig. 4.4 Binding studies of Ag85B-18C-20 aptamer with Ag85B in Serum 1. (A) Concentration-dependent analysis of the binding affinity of Ag85B-18C-20 aptamer sequence to Ag85B using ALISA. The R^2 value (A INSET) showed that 95.7% of the absorbance values fitted the regression model. (B) K_D estimation of Ag85B-18C-20 aptamer using ALISA fitted to a one site binding model.

Similarly, in Serum 2, the regression equation for OD difference versus aptamer concentration was y = 0.0888x – 0.0038 with R^2 = 0.942, where x is the concentration of aptamer Ag85B-18C-20 in nM (Fig. 4.5A, Fig. 4.5A INSET). The calculated K_D was 846.5 ± 380.33 nM using one site binding model (Fig. 4.5B).

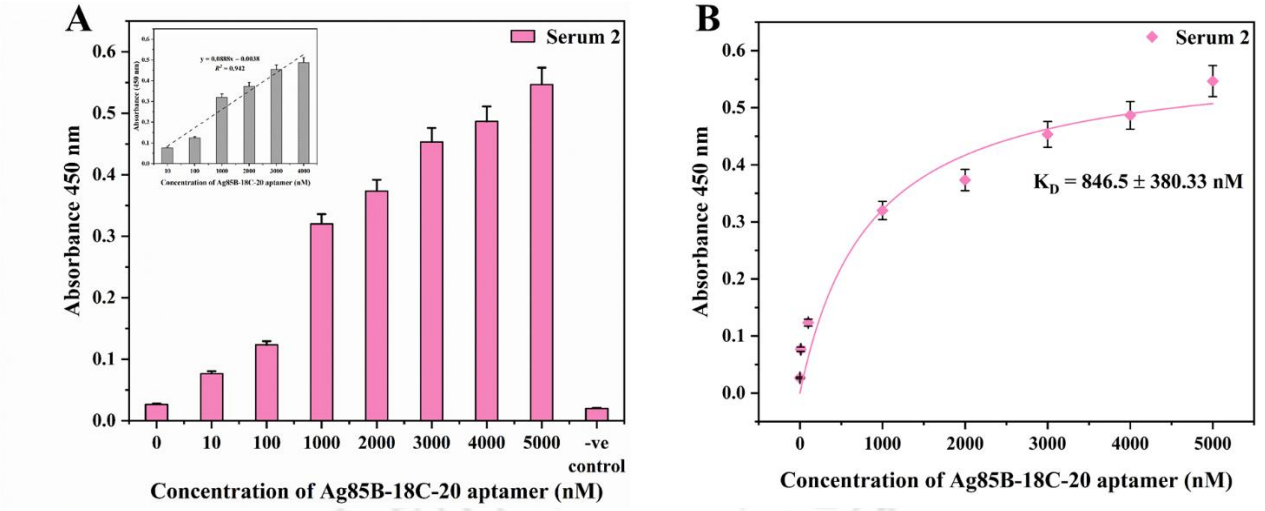

Fig. 4.5 Binding studies of Ag85B-18C-20 aptamer with Ag85B in Serum 2. (A) Concentration-dependent analysis of the binding affinity of Ag85B-18C-20 aptamer sequence to Ag85B using ALISA. The R^2 value (A INSET) showed that 94.2% of the absorbance values fitted the regression model. (B) K_D estimation of Ag85B-18C-20 aptamer using ALISA fitted to a one site binding model.

Likewise, in Serum 3, the regression equation for the difference in absorbance value and aptamer concentration (10-4000) was y = 0.0905x – 0.0078, with an R^2 = 0.948 (Fig. 4.6A). The K_D value was obtained as 821.73 ± 341.98 nM using one site binding model (Fig. 4.6B).

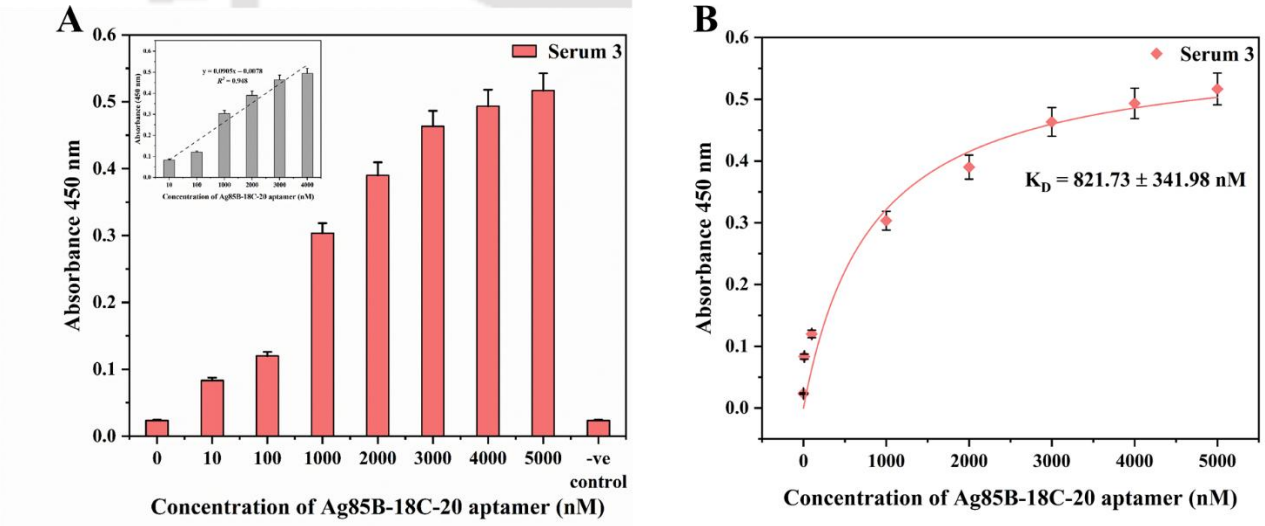

Fig. 4.6 Binding studies of Ag85B-18C-20 aptamer with Ag85B in Serum 3. (A) Concentration-dependent analysis of the binding affinity of Ag85B-18C-20 aptamer sequence to Ag85B using ALISA. The R^2 value (A INSET) showed that 94.8% of the absorbance values fitted the regression model. (B) K_D estimation of Ag85B-18C-20 aptamer using ALISA fitted to a one site binding model.

It can be argued that the K_D value of the Ag85B-18C-20 aptamer was more in all three serum samples than binding buffer. This is because of obvious differences in matrix, ability of a multitude of serum components to stick to the surface of wells as well as other crucial factors

that might influence the accurate measurement of K_D [226,227]. So far, our results showed that the Ag85B-18C-20 aptamer could be used as a biorecognition molecule to detect target Ag85B on sensor platforms.

Interestingly, it has also been reported that there are several advantages and disadvantages to each approach used for K_D calculation and it is recommended to perform data analysis using at least two methods to compare the obtained K_D values. [228]. In order to study the interaction pattern with an in-depth analysis, we also tried to analyse our OD_{450} values from the binding kinetics of the Ag85B-18C-20 aptamer with Ag85B with a two site binding model. Additionally, this was also done because, our docking data suggested that the aptamer in its 3D form interacted with the target Ag85B at more than one site, indicating the probability of interaction at multiple sites.

A comparative representation of the analysis using the one site as well as two site binding model for K_D calculation is represented in Table 4.1**.** The two site binding equation is shown below:

$$Y = \frac{B_{max1}X}{K_{D1} + X} + \frac{B_{max2}X}{K_{D2} + X}$$

Where, Where, X = Concentration of aptamer (nM)

K_{D1} = Dissociation constant of aptamer at site 1 (nM)

K_{D2} = Dissociation constant of aptamer at site 2 (nM)

B_{max1} = Maximum binding capacity at site 1 (measured as OD_{450})

B_{max2} = Maximum binding capacity at site 2 (measured as OD_{450})

In conclusion, the two site binding model ($R^2 \geq 0.99$) showed better fit than one site binding model ($R^2 \geq 0.95$) both for binding buffer and serum. However, at instances where K_D values were found to be lower in two site binding model, the high error percentages (>100) can be attributed to their lower reproducibility. Moreover, the corresponding K_D at the other site was

also higher than the values obtained via the one site binding model, indicating their lesser reliability. Hence, it can be inferred that the calculation of K_D in a software-simulated process for different models generate distinct errors; leading to the inconsistencies in confidence levels of the estimates. Therefore, we feel that the K_D values are not an absolute estimate (criteria) to determine the performance of an aptamer [228]. Vigorous research needs to be implemeneted to judge the correctness of each method.

Table 4.1 Comparative analysis of Ag85B-18C-20 apatmer binding using one site and two site binding models.

	One site binding model		Two site binding model		
	K_D	R^2	K_{D1}	K_{D2}	R^2
Binding buffer	310.83 ± 125.69 nM	0.961	7.13 ± 9.74	1086.59 ± 515.46	0.99
Serum 1	889.53 ± 356.04 nM	0.963	1910.72 ± 628.36	4.92 ± 6.95	0.995
Serum 2	846.5 ± 380.33 nM	0.954	2338.9 ± 1000.43	5.31 ± 7.73	0.992
Serum 3	821.73 ± 341.98 nM	0.961	1.29 ± 3.18	1758.67 ± 374.29	0.997

The pictorial representation of two site binding models of the Ag85B-18C-20 aptamer with Ag85B separately for binding buffer and serum are illustrated in Appendix for the reader's reference.

4.4.2 Specificity of detection

The specificity of our developed method using Ag85B-18C-20 aptamer at different concentrations was tested with the non-target proteins at similar concentrations. Since the change in absorbance with further change in concentration of aptamer did not show any significant increase beyond 4000 nM, we chose this concentration to statistically validate the ability of the aptamer to distinguish between target Ag85B and nontargets MPT64 and ESAT6.

In binding buffer (Fig 4.7A), the OD_{450} obtained by subtracting the background from sample wells was 0.17 ± 0.00 for Ag85B, 0.073 ± 0.01 for MPT64 and 0.09 ± 0.006 for ESAT6. It shows that at 4000 nM, the aptamer detects Ag85B more specifically than MPT64 and ESAT6. As compared to Ag85B, the OD_{450} values for MPT64 and ESAT6 depicted a reduction of 57%

and 47% respectively. Therefore, it can be inferred that the Ag85B-18C-20 aptamer showed more specificity towards binding with Ag85B. We found a statistically significant difference between the target Ag85B and the two non-target proteins tested with $p < 0.001$ for each of the comparisons.

As observed in Fig 4.7B, the K_D values are also in accordance to the specificities found in Fig 4.7A. In other words, the specificity of the Ag85B-18C-20 for Ag85B detection in binding buffer can be substantiated by the lower K_D value indicating better affinity for the target.

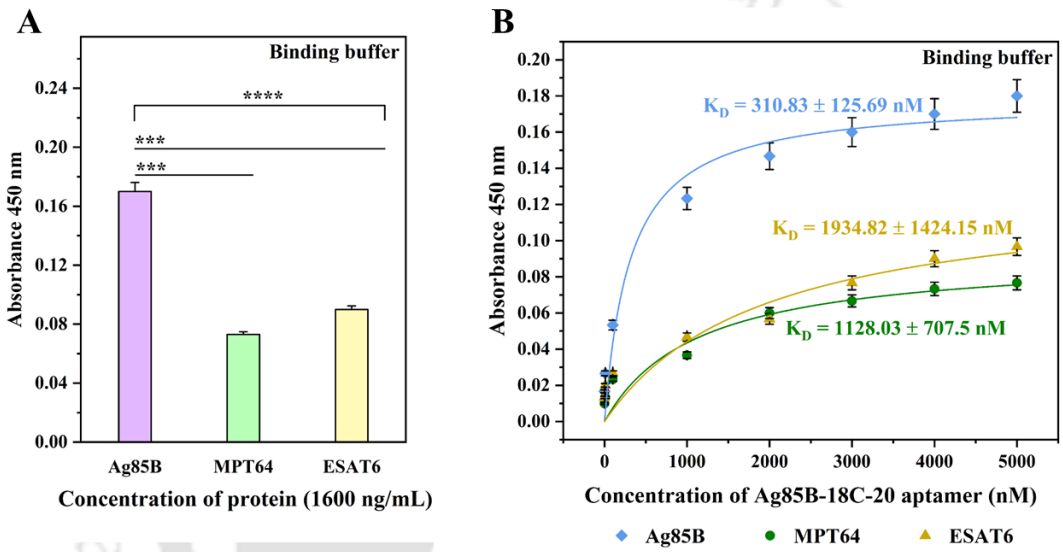

Fig. 4.7 Specificity of the direct ALISA to Ag85B in binding buffer. (A) Non-target proteins, MPT64, and ESAT6, at a concentration of 1600 ng/mL, coupled with the Ag85B-18C-20 aptamer (4000 nM) were employed in this study. (B) Comparative K_D estimation of target and non target proteins.

In case of Serum 1, we obtained the following OD_{450} for the samples tested; 0.463 ± 0.052 for Ag85B, 0.213 ± 0.002 for MPT64, and 0.157 ± 0.002 for ESAT6 (Fig 4.8A). As compared to Ag85B, the OD_{450} values for MPT64 and ESAT6 depicted a reduction of ~54% and ~64% respectively. We found a statistically significant difference between the target Ag85B and the two non-target proteins tested with $p < 0.05$ for each of the comparisons.

The K_D values are also in accordance to the specificities found in Fig 4.8A. In other words, the specificity of the FAM-Ag85B-18C-20 for Ag85B detection in binding buffer can be substantiated by the lower K_D value indicating better affinity for the target Fig 4.8B.

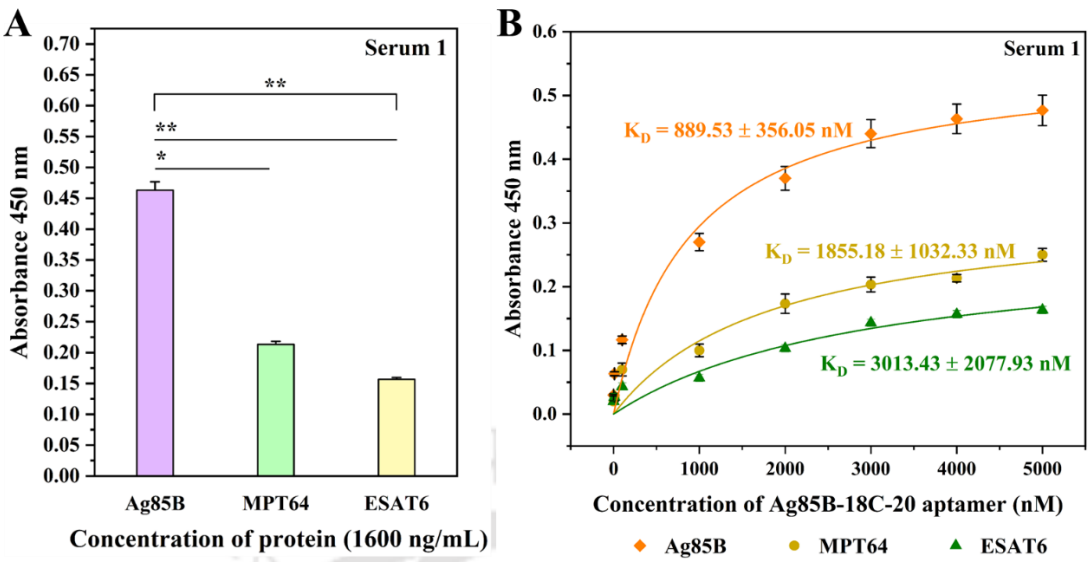

Fig. 4.8 Specificity of the direct ALISA to Ag85B in Serum 1. (A) Non-target proteins, MPT64, and ESAT6, at a concentration of 1600 ng/mL, coupled with the Ag85B-18C-20 aptamer (4000 nM) were employed in this study. (B) Comparative K_D estimation of target and non target proteins.

In Serum 2, we obtained the following OD_{450} for the samples tested; 0.487 ± 0.047 for Ag85B, 0.24 ± 0.006 for MPT64, and 0.15 ± 0.006 for ESAT6 (Fig 4.9A). As compared to Ag85B, the OD_{450} values for MPT64 and ESAT6 depicted a reduction of ~51% and ~70% respectively. We found a statistically significant difference between the target Ag85B and the two non-target proteins tested with $p < 0.01$ for each of the comparisons.

The K_D values are also in accordance to the specificities found in Fig 4.9A. In other words, the specificity of the FAM-Ag85B-18C-20 for Ag85B detection in binding buffer can be substantiated by the lower K_D value indicating better affinity for the target Fig 4.9B.

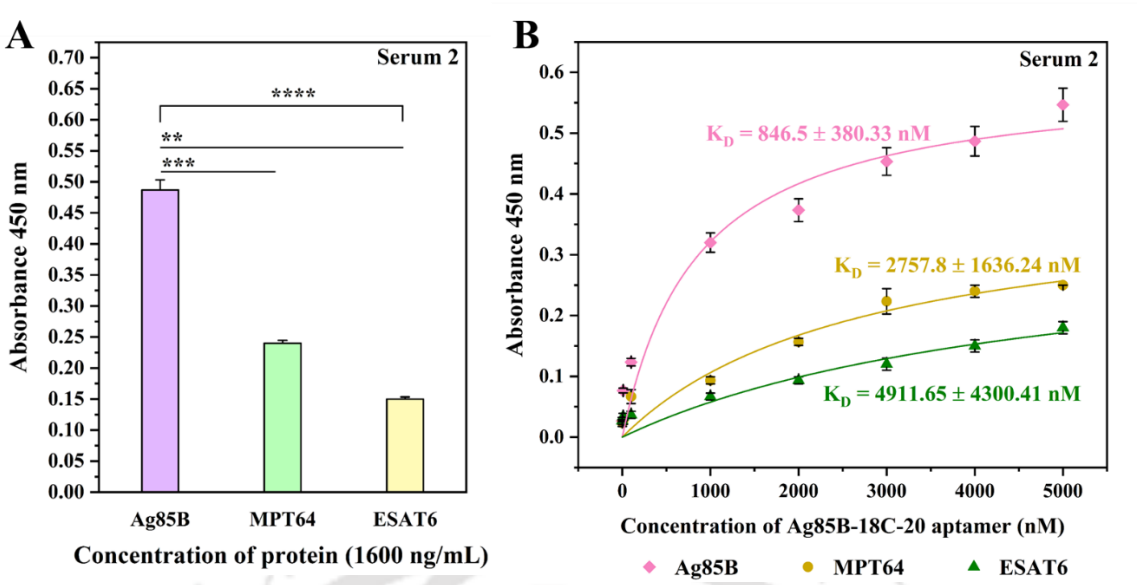

Fig. 4.9 Specificity of the direct ALISA to Ag85B in Serum 2. (A) Non-target proteins, MPT64, and ESAT6, at a concentration of 1600 ng/mL, coupled with the Ag85B-18C-20 aptamer (4000 nM) were employed in this study. (B) Comparative K_D estimation of target and non target proteins.

In Serum 3, we got the following OD_{450} values: 0.493 ± 0.05 for Ag85B, 0.243 ± 0.005 for MPT64, and 0.143 ± 0.005 for ESAT6 Fig 4.10A. As compared to Ag85B, the OD_{450} values for MPT64 and ESAT6 depicted a reduction of ~51% and ~71% respectively. We found a statistically significant difference between the target Ag85B and the two non-target proteins tested with $p < 0.01$ for each of the comparisons.

The K_D values are also in accordance to the specificities found in Fig 4.10A. In other words, the specificity of the FAM-Ag85B-18C-20 aptamer for Ag85B detection in binding buffer can be substantiated by the lower K_D value indicating better affinity for the target Fig 4.10B.

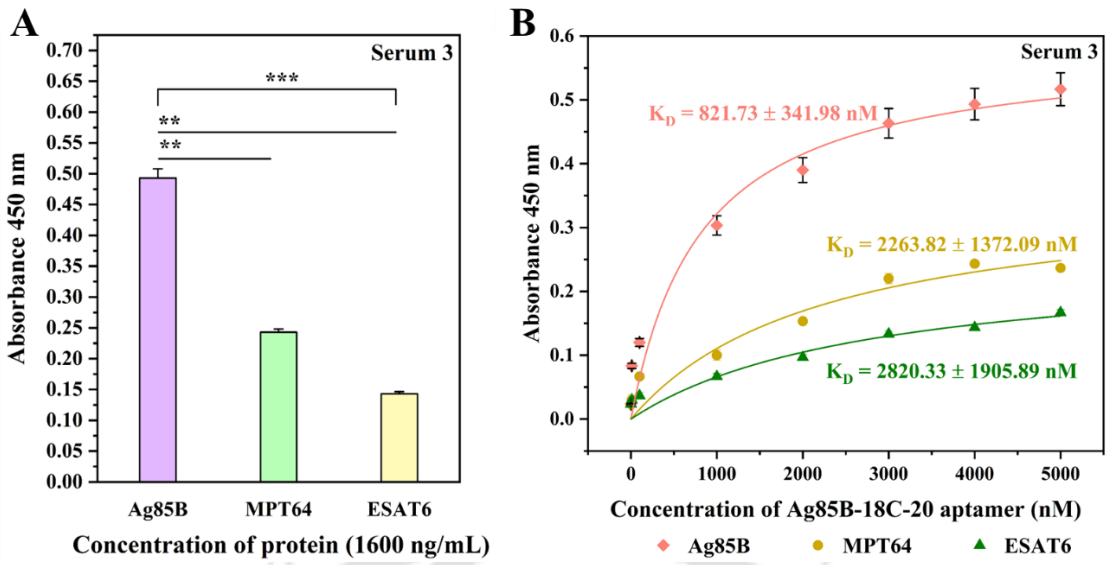

Fig. 4.10 Specificity of the direct ALISA to Ag85B in Serum 3. (A) Non-target proteins, MPT64, and ESAT6, at a concentration of 1600 ng/mL, coupled with the Ag85B-18C-20 aptamer (4000 nM) were employed in this study. (B) Comparative K_D estimation of target and non target proteins.

In conclusion, it can be inferred that the K_D values obtained for the target and non-target proteins gave us a fair idea about the specificity percentages in binding affinity of the developed aptamer. Encouragingly, although the experiments were carried out with samples from different age groups, sex and expected variabilities in serum, the K_D values of the Ag85B-18C-20 aptamer were almost identical (~820 nM to ~890 nM) for Ag85B and did not show much variation.

However, we hypothesize that testing our developed aptamer in more than just three serum samples would improve the process of analytical measurements. We report the results of K_D values and specificity separately for Serum 1, Serum 2 and Serum 3 (and not by averaging) because we wanted to know more about the minor variations seen in between clinical samples for real-world practical scenarios that would affect our aptasensor. The relative importance of these would help us modify the linear range of the methods used for calibration of the aptasensor and further optimization [229].

4.4.3 Characterization of GO

The morphology of GO in FETEM in Fig. 4.11A showed smooth folds of the overlapping 2D sheets represented by intense black regions. The observation rings in the SAED patterns of

GO in Fig. 4.11B confirmed their crystalline nature. Surface morphology of GO was observed by the FESEM as shown in Fig. 4.11C. GO shows a wrinkled sheet-like surface attributing to its large surface area [230]. The UV-visible spectroscopic analysis as shown in Fig. 4.12A revealed a shoulder peak at 300 nm and strong absorption at 232 nm. The π–π* transition of aromatic C–C bonds and the n–π * transition of C=O bonds, contribute to the low and high wavelength peaks respectively [231]. The EDX spectrum and their corresponding quantitative elemental mappings of GO is shown in Fig. 4.12B, showing the presence of carbon, oxygen and copper. The copper was present due to the Cu-grid holder used for FETEM sample preparation.

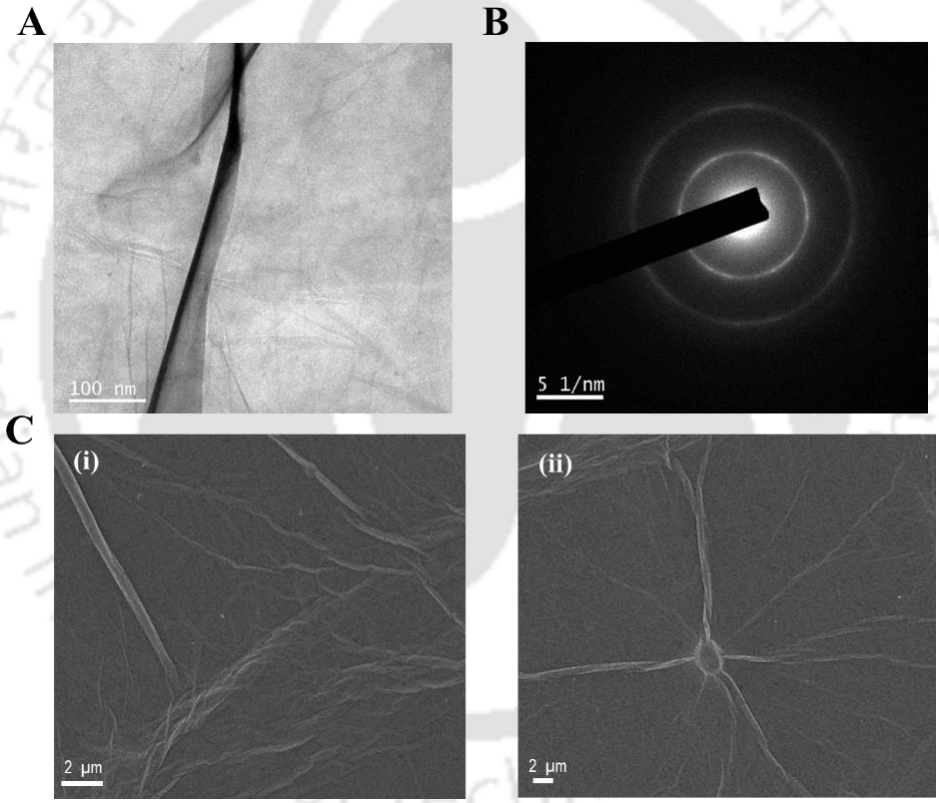

Fig. 4.11 Characterization of GO. (A) FETEM of GO (B) SAED pattern of GO. (C) (i) FESEM of GO at 10,000 x magnification, (ii) FESEM of GO at 5,000 x magnification

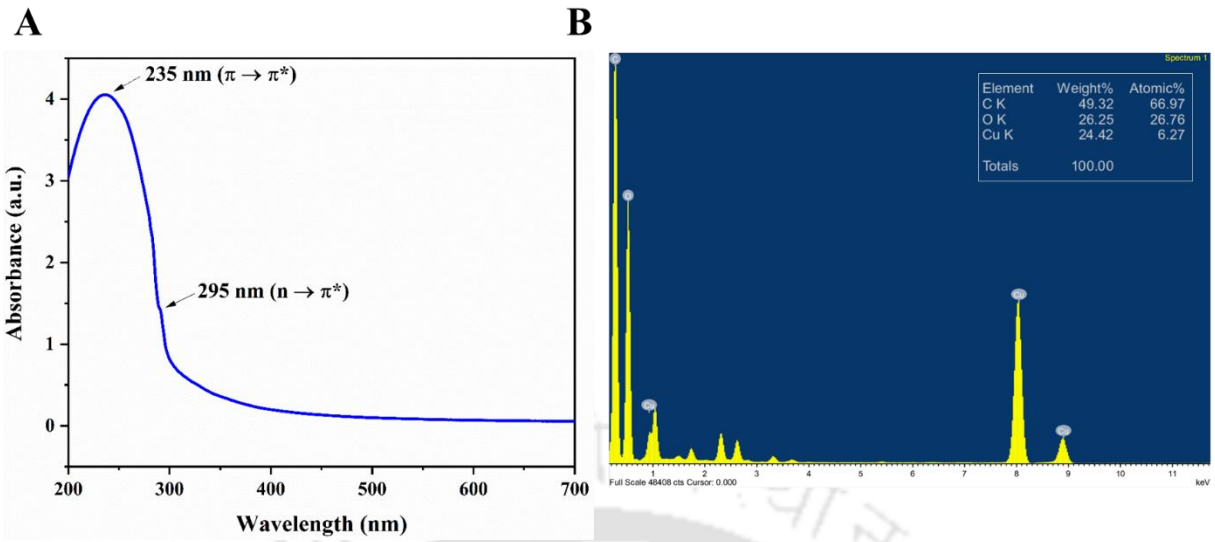

Fig. 4.12 Characterization of GO. (A) UV-Vis spectrum of GO. (B) EDX elemental analysis spectrum showing the composition (shown in inset) of GO.

4.4.4 Characterization of FAM labelled Ag85B-18C-20 aptamer

Spectral scan to determine the absorbance, excitation and emission patterns of FAM-Ag85B-18C-20 aptamer is depicted in Fig. 4.13. It corroborated well with previous reports [232].

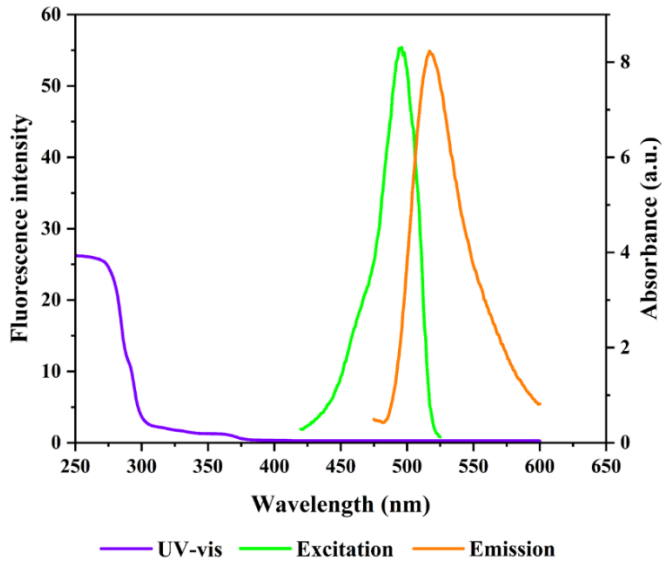

Fig. 4.13 Spectral scan of FAM-Ag85B-18C-20 by UV-Vis and fluorescence spectroscopy.

4.4.5 Optimization of GO concentration for aptasensor

The concentration of GO is crucial for the overall performance of the designed aptasensor. The aptamer concentration was fixed at 100 nM and the percentage of quenching at different concentrations of GO (0-60 μg/mL) was measured (Fig. 4.14A) [131]. When GO was introduced, the fluorescence intensity of the aptamer gradually reduced and reached the

minimum at ~30 µg/mL. At this concentration, fluorescence intensity reduced to almost 67% of the original value (0 µg/mL GO). Hence, 30 µg/mL GO was used as the optimized concentration of quencher in the next set of experiments. Fluorescence spectrum of FAM-Ag85B-18C-20 aptamer (100 nM) in binding buffer showed a typically high fluorescence attributed by the presence of FAM. In presence of GO, ~96% of the fluorescence from the FAM-labelled Ag85B-18C-20 aptamer was found to be quenched efficiently; thereby proving the successful quenching phenomenon of GO (Fig. 4.14B) [131].

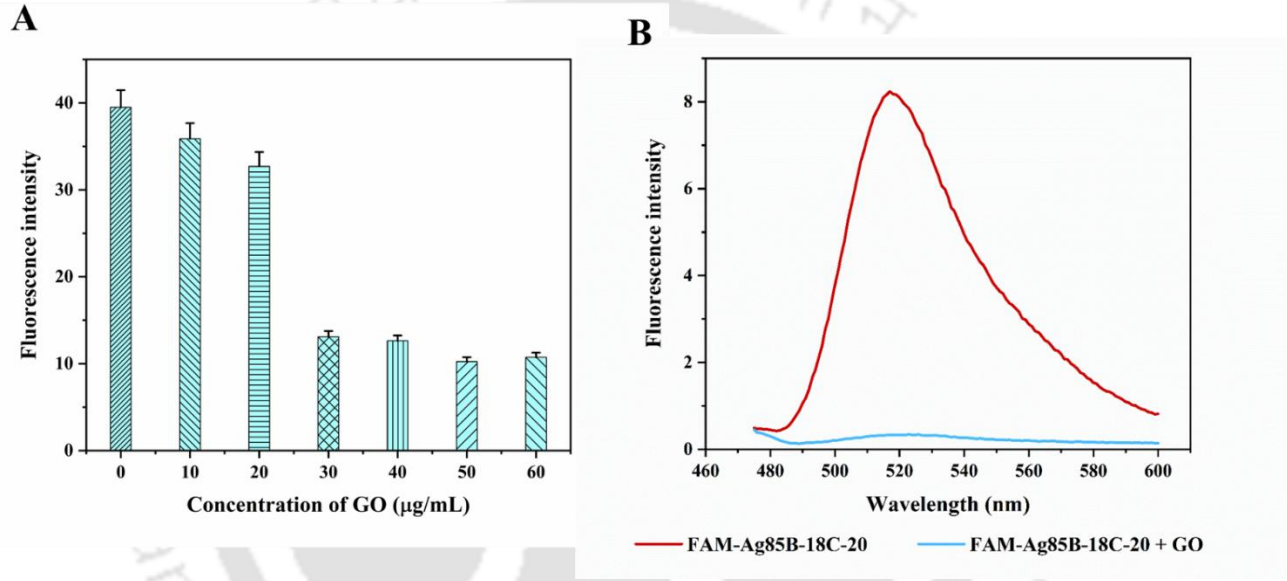

Fig. 4.14 Optimization of GO concentration for aptasensor. (A) Fluorescence intensity of the FAM-labelled Ag85B-18C-20 (100 nM) in the presence of different concentrations of GO (0-60 µg/mL). λ_{em} = 520 nm wavelength. (B) Fluorescence spectrum of FAM-aptamer (100 nM) in binding buffer in the presence and absence of GO quencher (30 µg/mL). ~96 % quenching was observed at 520 nm emission wavelength.

4.4.6 Diagnostic validation of the prepared aptasensor

The differential absorption of ssDNA on the GO surface in absence or presence of a target analyte is well reported [233]. In the absence of target molecule Ag85B, FAM-labelled Ag85B-18C-20 binds onto the GO via hydrophobic and π-interaction. So, the fluorescence of FAM is quenched by GO as a quencher. In the presence of target Ag85B, the aptamer interacts with it and forms Ag85B:Ag85B-18C-20 complex and does not bind onto the GO. It has been shown that GO hardly interacts with rigid double stranded DNA or aptamer-target complexes [131]. So,

in this condition, the fluorophore is far away from GO and the fluorescence intensity is high allowing the aptasensor to remain "ON". The aptasensor is turned "OFF" when FAM-Ag85B-18C-20 aptamer and GO are in close proximity allowing maximum quenching effect to occur through an effective energy transfer process. In accordance to this observation, the relative fluorescence intensity of the aptasensor evidently increased with the increasing concentrations of Ag85B over a wide linear range. It is interesting to note that the aptamer preferentially interacts with the target Ag85B more strongly than GO as an adsorbing surface, thereby allowing specific detection [232]. As a result, the noncovalent interactions between the aptamer-Ag85B is proven to be stronger than aptamer-GO. The LOD of an aptasensor depends on the properties of the aptamers (dissociation constants, aptamer configuration) as well as on the method of aptamer attachment to the detection surface and the properties of nanomaterials. The LOD was measured to be 45.44 nM in binding buffer based on 3.3 times SD of the blank signal (3.3σ)/slope (Fig. 4.15).

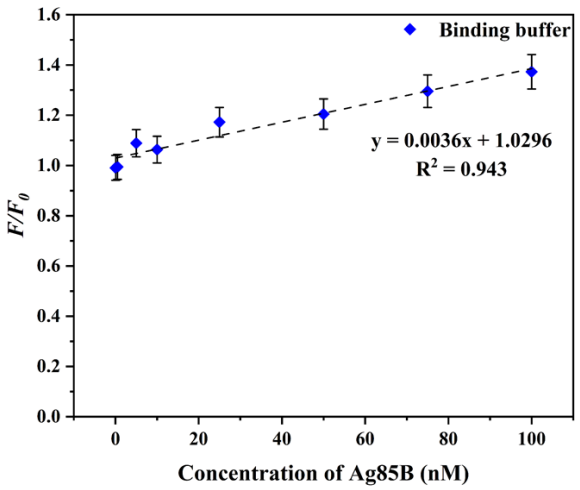

Fig. 4.15 Calibration plot of FAM-Ag85B-18C-20 aptamer in presence of GO in binding buffer. The linear relationship between the relative fluorescence intensity of the aptasensor and Ag85B concentration in binding buffer. F and F_0 are the fluorescence intensities of the aptasensor in the presence and absence of Ag85B at 520 nm wavelength.

As shown in Fig. 4.16, the sensor's diagnostic potential was tested in three different serum samples. Spiked concentrations of Ag85B in three different serum samples were evaluated and a LOD of 68.64 nM (Serum 1), 73.22 nM (Serum 2) and 73.34 nM (Serum 3) were

calculated.

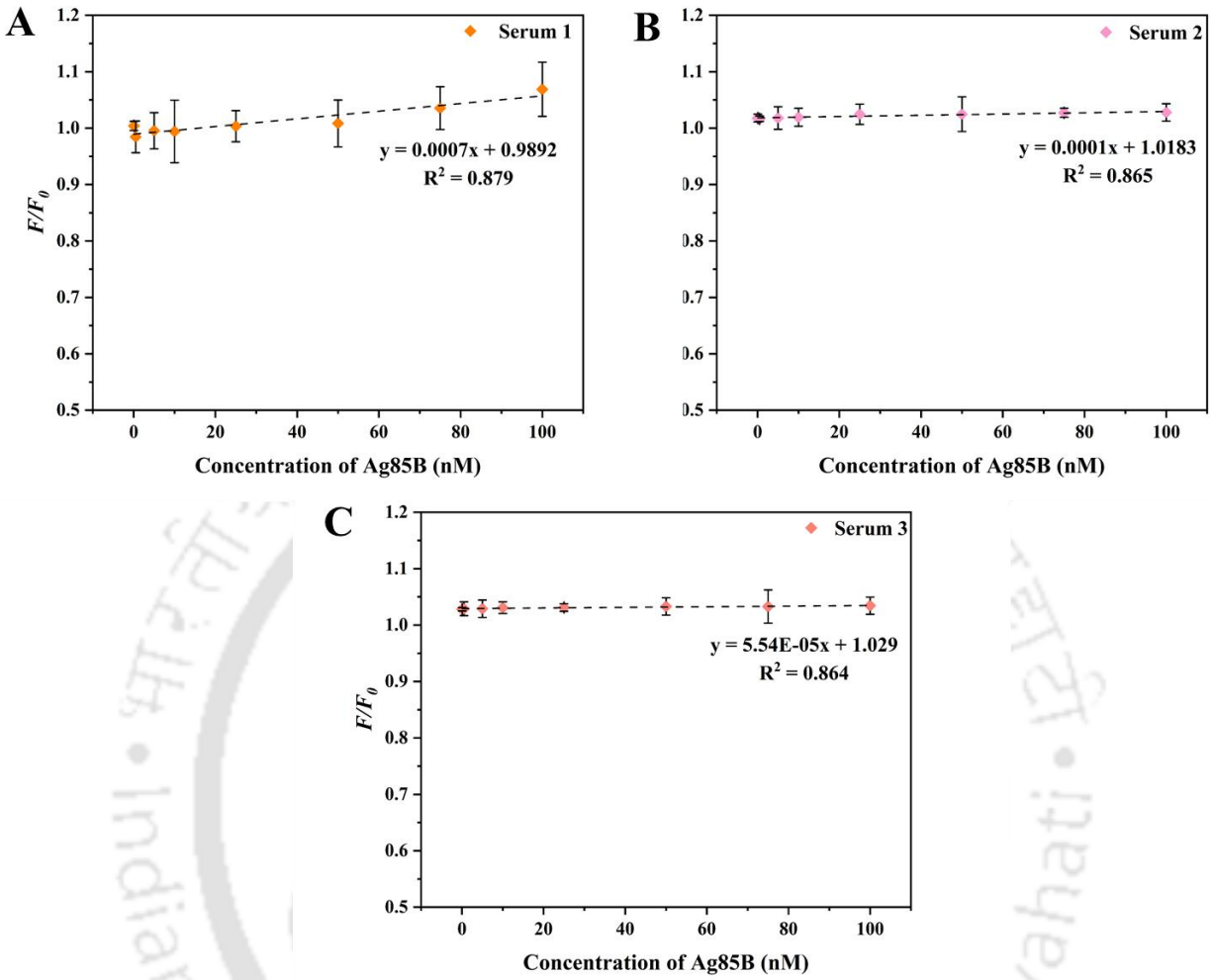

Fig. 4.16 Calibration plots of FAM-Ag85B-18C-20 aptamer in presence of GO in serum samples. The linear relationship between the relative fluorescence intensity of the aptasensor and Ag85B concentration in spiked samples (A) Serum 1 (B) Serum 2 (C) Serum 3.. *F* and F_0 are the fluorescence intensities of the aptasensor in the presence and absence of Ag85B at 520 nm wavelength.

We tried to analyze the performance of our sensor based on several key factors. As this is the first report on constructing an aptamer for Ag85B considering the variability in the clinical concentrations of Ag85B in serum samples of TB patients and the lack of studies correlating these concentrations with the exact timeline of an infection- a wider dynamic range (0.05-100 nM) was essential for sensor design. While the slope of the calibration curve is often considered as an indicator of sensitivity, it may not fully estimate sensor performance. Thus, it is important to highlight that our sensor maintained a consistent linear response across a broad concentration

range. It also demonstrates good precision and accuracy. Additionally, the high signal-to-noise ratio (S/N > 3) ranging from 44-246 in serum, implicates the ability of the sensor to distinguish small changes in concentrations [234]. However, there is scope to improve the performance of the sensor by further optimizing the experimental conditions. This result indicated that the developed aptamer holds potential for detection of Ag85B protein in clinical samples in future.

4.4.7 Cross-reactivity the FAM-labelled aptamer with non-target proteins

In order to validate the performance of the aptasensor, the relative fluorescence intensities was checked in presence of two non-target antigens like ESAT6 and MPT64 which can also be present in the circulating blood of patients along with Ag85B. As observed in Fig.4.17, in binding buffer, the fluorescence intensities of MPT64 and ESAT6 decreased to 1.023 ± 0.024 and 0.977 ± 0.014 respectively for 100 nM of spiked proteins. This cumulatively suggested the theory that the FAM-labelled Ag85B-18C-20 aptamer showed more affinity towards Ag85B as compared to the non-target proteins MPT64 and ESAT6 in the fluorescence sensing platform. To this end, it can also be reasonably argued that the FAM-labelled Ag85B-18C-20 aptamer albeit cross reacted with some amount of MPT64 or ESAT6 in the reaction. But statistical validation proved that the differences were significant p <0.01.

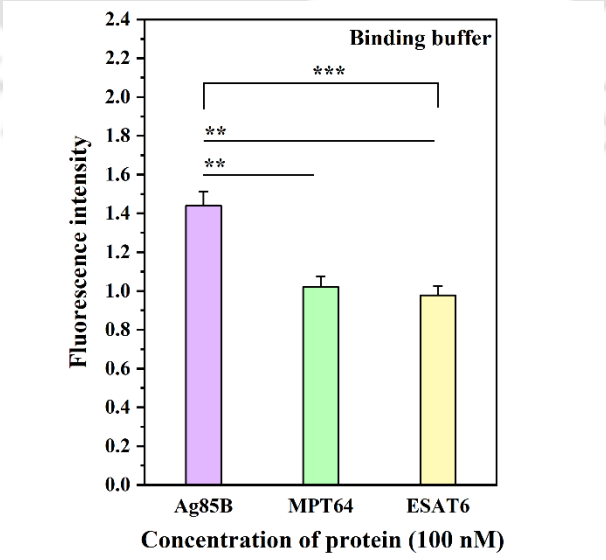

Fig. 4.17 Cross reactivity assay of FAM-labelled Ag85B-18C-20 aptamer in binding buffer.

After validation of specificity in binding buffer, we checked the performance of the aptasensor in three different serum samples.

For Serum 1, in presence of MPT64 and ESAT6, the fluorescence intensities of the system was found to be 37.6 ± 0.048 and 37.02 ± 0.7 respectively for 100 nM of spiked proteins. These values were lower than that obtained for target Ag85B (40.58 ± 0.78) at the same concentration of spiked protein. Similarly, for Serum 2 and Serum 3, the results indicate that the sensor showed higher affinities for Ag85B as compared to ESAT6 and MPT64. The results show that the aptamer Ag85B-18C-20 albeit cross reacted with some amount of MPT64 or ESAT6 in the reaction that contributed to the fluorescence (Fig 4.18). All the cross-reactivity studies were statistically analyzed. Comparison between target and non-target proteins both in binding buffer as well as serum samples were found to be statistically significant ($p < 0.05$) for all the experiments.

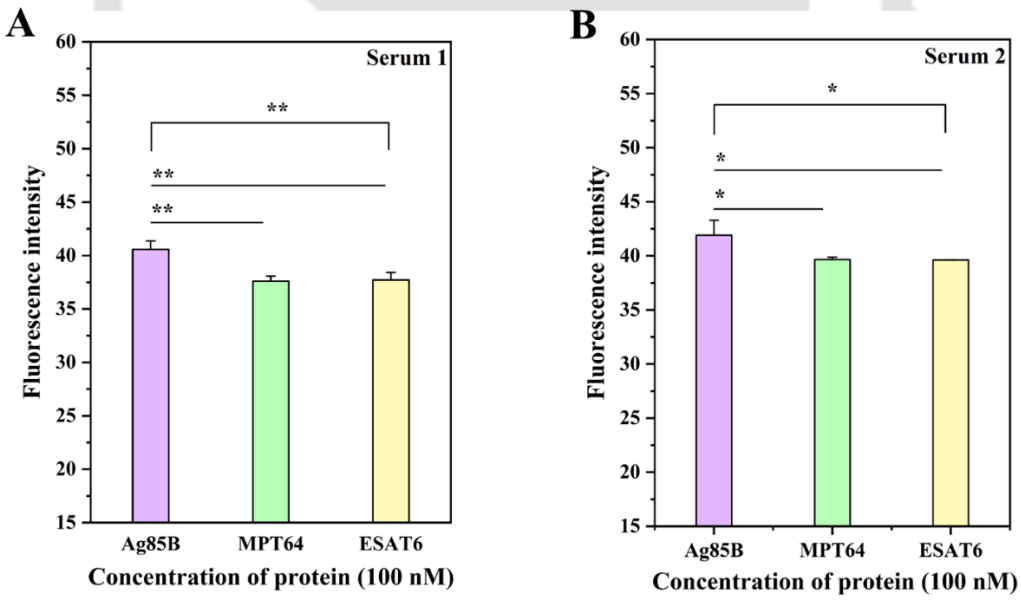

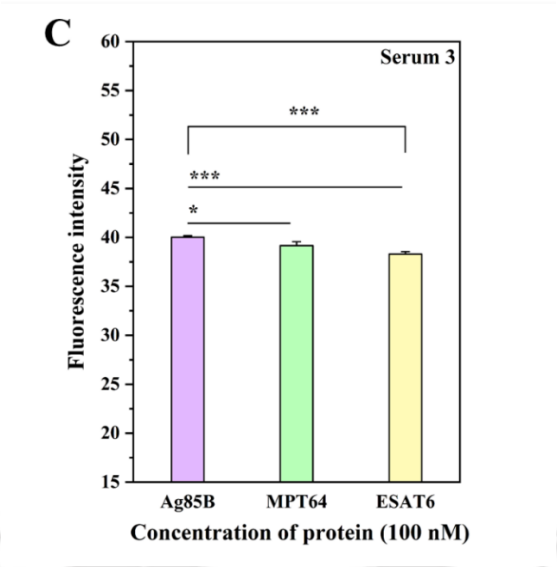

Fig. 4.18 Cross reactivity assay of FAM-labelled Ag85B-18C-20 aptamer in serum samples. (A) Serum 1 (B) Serum 2 (C) Serum 3.

4.4.8 Spike and recovery analysis of the Ag85B aptasensor

The spike and recovery method is an important technique for analyzing and accessing the accuracy of an analytical method [235]. In order to determine whether the reported sensing method was appropriate for real-world applications, a recovery assay to assess the sensitivity of the prepared sensor was also conducted. The recovery parameters from serum are essential for the fabrication of an aptasensor for clinical settings. The range of recoveries for the Ag85B spiked concentrations was from 76% to 104% (Table 4.2).

Table 4.2 Spike-recovery analysis for Ag85B detection.

Serum sample	Concentration of Ag85B spiked (nM)	Concentration of Ag85B recovered (nM)	Recovery ± SD (%)
1	.05	0.051 ± 0.001	101.37 ± 1.37
	.5	0.496 ± 0.028	99.12 ± 5.68
	5	4.59 ± 0.40	91.75 ± 7.80
	10	9.47 ± 1.49	94.65 ± 14.9
	25	21.67 ± 3.054	86.68 ± 12.22
	50	42.04 ± 4.43	84.09 ± 8.87
	75	60.70 ± 9.03	80.93 ± 12.04
	100	78.77 ± 11.31	76.89 ± 11.62
2	.05	0.051 ± 0.001	102.79 ± 2.09
	.5	0.511 ± 0.017	102.3 ± 3.46
	5	4.69 ± 0.38	93.81 ± 7.57
	10	9.66 ± 0.97	96.61 ± 9.69
	25	22.08 ± 2.58	88.32 ± 10.32
	50	42.60 ± 1.58	85.20 ± 3.16
	75	60.05 ± 6.96	80.07 ± 9.28
	100	75.59 ± 8.76	75.59 ± 8.76
3	.05	0.052 ± 0.001	103.8 ± 1.47
	.5	0.518 ± 0.016	103.53 ± 3.17
	5	4.74 ± 0.24	94.71 ± 4.81
	10	9.78 ± 1.06	97.78 ± 10.61
	25	22.23 ± 2.70	88.93± 10.80
	50	42.98 ± 2.27	85.95 ± 4.54
	75	60.34 ± 6.88	80.45 ± 9.17
	100	76.03 ± 8.32	76.03 ± 8.32

The fluorescence quenching measurements are known to be highly influenced by the cumulative effects of solvatochromism, risk of non-specific interactions of the target protein with the label on oligonucleotide probe and molecular crowding aspects altering protein/nucleic acid interactions in presence of serum contaminants [236–238]. Hence, it was imperative to test the

analytical performance of the prepared aptasensor for a better understanding of its reproducibility.

We determined the analytical precision of Ag85B detection from a set of 20 independent experiments performed with two different levels of concentrations. The serum samples were withdrawn randomly from either of the three to accomplish this experiment. To remove sample biasness, the samples were kept unmarked before initiating the experiment. Average recoveries were obtained as 4.627 ± 0.218 nM and 21.458 ± 2.41 nM which accounted for a coefficient of variation of 4.711% and 11.229% at 5 nM and 25 nM respectively (Table 4.3). This result suggests that the developed fluorescent aptasensor is suitable for detecting the Ag85B protein in spiked serum samples. However, further validation could be achieved by testing a larger number of serum samples.

Table 4.3 Analytical precision of the Ag85B aptasensor for spiked Ag85B protein detection.

Spiked	Recovered (nM)	Coefficient of Variation (%) (Intra-assay 20 experiments)
5 nM (~0.2 µg/mL)	4.627 ± 0.218	4.711
25 nM (~0.8 µg/mL)	21.458 ± 2.41	11.229

4.5 Conclusion

This study is the first report of establishing a fluorescence- based aptasensor for Ag85B protein of MTB. Initially, our findings suggest that the Ag85B-18C-20 aptamer showed good binding strength and affinity to Ag85B as exemplified by low K_D values of 310 ± 125.69 nM and within a range of 800-900 nM tested in both binding buffer and serum respectively via the ALISA method. We also validated the specificity and cross reactivity of our aptamer by obtaining the K_D values for non-target proteins MPT64 and ESAT6 which had higher K_D values (above ~1800 nM) that indicated lower affinity. Several optimizations in our ALISA method was done and we could successfully characterize the binding affinity and statistically correlate our specificity and cross reactivity studies in three serum samples.

To this end, we developed a sensor using a fluorescence based system with fluorescein labelled Ag85B-18C-20 as the aptamer probe and GO as the quencher molecule. The designed aptasensor was sensitive for detection of Ag85B in both binding buffer and serum sample as matrices. This aptasensor can detect Ag85B with low detection limits of 45.44 nM in binding buffer whereas 68-74 nM in serum. However, we speculate that there is scope to improve the performance of the sensor to detect even lower concentrations of spiked antigens in serum. Further validation of the sensor platform would require further testing of recovery percentages using femtomolar or attomolar concentrations of spiked antigens. However, for commercialization aspects; testing of the sensor using clinically infected TB serum samples would validate and justify our current findings. We had a relatively small serum sample size of n=3. Hence, a larger dataset can help produce better results depicting the true reproducibility of the sensing platform. Additionally, the selected aptamer could be used for multiplexed detection of TB along with other aptamers that have been previously selected against other TB antigens such as ESAT6 and MPT64. Based on its performance, the GO-based fluorescent aptasensor revealed a promising future for the detection of protein biomarkers of MTB.

5

Screening of DNA aptamers for tuberculosis biomarker MPT64 through mimotope-based prediction

Abstract

MPT64 is an important biomarker secreted specifically by all the organisms belonging to the MTBC. Several rapid and reliable sensors have shown the detection of MPT64. However, in terms of diagnostic accuracy, literature suggests that several mutations in the MPT64 gene influences the currently available immunochromatographic identification test kits available for MPT64 in the market. Thus, we resorted to the development of a practical approach with bioinformatics tools to predict the subtle amino acid differences on the surface-exposed epitopic regions or exosites on MPT64 that alters the ability of any biorecognition molecule to capture the said biomarker from clinical samples. Moreover, we translated our research to mimicking these epitopic regions to generate synthetic mimotopic peptides that would aid in the development of aptamers via a modified SELEX approach. We visualize aptamers as improved capture elements that would recognize the chemical equivalent of epitopes, i.e. aptatopes on MPT64 and help in diagnosing MPT64 from clinical samples. Herein, we also show the synthesis and characterization of gold nanoclusters as a nanomaterial that would be used as a label in signal amplification during optical sensing in the MPT64 biosensor (yet to be developed as a part of ongoing work). This chapter is thus summarized into two parts: i) aptatope based screening of binding sites for MPT64 for developing high-affinity aptamers and ii) synthesis and characterization of gold nanoclusters as a label for the developed aptamers.

5.1 Overview

One significant protein secreted by MTB is MPT64 (Rv1980c), a 24-kDa immunogenic antigen. MPT64 is only expressed and secreted from cells that are actively growing and is eliminated from almost all strains of *M. bovis* bacilli that are used to make the BCG vaccine. This highlights the importance of using MPT64 as a TB biomarker. Even in the case of a positive culture, differentiation of MTBC from mycobacteria other than tuberculosis (MOTT) is required. The MPT64 secretory biomarker is specific to MTBC and thus serve as the foundation for this quick immuno-chromatographic methods (ICT), which distinguishes between MTBC and MOTT. The Capilia TB-Neo assay (Tauns Laboratories, Numazu, Japan) and SD Bioline assay (Standard Diagnostic, Republic of Korea) can be used to identify MTBC from the positive culture with the help of these MPT64 secretory protein tests [239,240].

The Capilia TB-Neo assay is an improved version of Capilia TB but false-negative results due to mutations in the MPT64 gene have been reported. The differences between the results of ICT and other diagnostic methods may be shown by comparing the MPT64 gene sequences from the reported whole genome sequences of MTB clinical isolates belonging to any geographical region. Discordant results (where the samples are culture and smear positive while kit negative) are reported as negative for MTBC, leading to misleading false negative diagnoses. Previous studies indicated that the MPT64 antigen is highly conserved, but recent studies pointed out that a significant degree of variability in the diagnostic accuracy of MPT64 has been attributed to the type of the recombinant antigen used in assays [241].

This kind of analysis to find out key residues prone to mutation within the MPT64 is necessary to distinguish between MTBC and nontuberculous mycobacteria (NTM). There are only a few reports that report the polymorphism and deletions or substitutions of the MPT64 biomarker [242,243]. These amino acid changes in MPT64 due to strain diversity hold important clues for probing the structural differences and 3D folding of the protein. Recently, it was also

deciphered that there is a 63-bp deletion variant of MPT64 found in several isolates from the China and Vietnam region of MTB [244]. This necessitates the development of alternate biorecognition molecules (other than monoclonal antibodies raised against specific epitopes of MPT64) for improving diagnostic efficacy. The current literature lacks any database or cumulative findings for the mutational alterations and their corresponding structural discrepancies in MPT64 that can have significant implications for development of novel biorecognition molecules for POC diagnostics of TB.

Interestingly, aptamers have remarkable specificities in distinguishing proteins with respect to mutations in their sequence. Moreover, since epitopic regions are mostly located on the surface of protein exosites that predominantly interacts with an aptamer, it can be hypothesized that knowing the aa of MPT64 that are likely to undergo mutation or show variation across MTB strains can help us design better aptamers. Towards this end, it is also observed that there are multiple aptamers that are designed against biomarkers but none of them are actually reaching the translation stage into clinical diagnosis and commercialization for TB. Thus, we resorted to designing a rational approach to find better aptamers for MPT64 as per the SMART (Systematic Mimotope-guided Aptamer Refinement Technique) workflow shown in Fig. 5.1. Our approach highlights the amalgamation of both computational and experimental studies to provide useful insights for the design and development of DNA aptamers for MPT64 [245,246].

In this chapter, we compiled reported aptamers with known sequences targeting the MPT64 biomarker. Computational docking was performed to identify crucial moieties involved in binding interactions between these aptamers and MPT64. Additionally, we examined amino acid stretches less prone to mutations based on existing literature on MPT64 mutations. Through a comparative analysis of significant nucleotide motifs identified in computational docking and conserved amino acid stretches, we identified four peptide regions of MPT64 for our study. These regions included two aptatopes showing binding affinities with reported aptamers and two other

regions predicted as linear epitopes on the surface of the MPT64 protein to serve as mimotopes. We utilized epitopic prediction tools, focusing on regions exposed to the surrounding environment, which bear aa favorable for interaction with the negative backbone of a DNA aptamer. Furthermore, the identification of peptide epitope mimics (mimotopes) of TB secretory biomarkers has proven beneficial for various applications. [241,247]. The concept of mimotopes (peptides that mimic naturally occurring epitopes of a protein) have so far been applied for antibody-based recognition; but using the similar terminology for recognition by aptamers is a relatively new domain for research. Earlier reports of generating MPT64 peptide mimotopes through phage-display techniques or synthetic approaches have shown good potential for downstream applications [241]. This study by Yang et al. is also in accordance to our computational prediction that linear epitopes are located on surface of MPT64 and albeit can be used for developing recognition molecules like aptamers for clinical detection of MPT64.

Keeping this in mind, we tailored the idea of identifying the reported aptatopes on MPT64 protein with experimentally performing SELEX with synthetic mimotopes of MPT64 (selected on the basis of aa less likely to undergo mutations and located on surface) to obtain aptamers that would show increased binding affinities for MPT64. Moreover, peptides are well defined and easier to synthesize than recombinant full-length proteins. In other words, the developed aptamer would be a better candidate in detecting MPT64 from samples even if the biomarker harbors subtle differences in its amino acid sequence across patients infected with different clinical strains of MTB. The aptamer is likely to show improved binding affinities to at least four surface-exposed regions on MPT64 depicted in our study; making it a better diagnostic candidate for detecting the presence of MPT64 in clinical samples. Lastly, the additional advantage of synthesizing these peptides is that it can serve as surrogate diagnostic markers in serological tests for detecting MPT64.

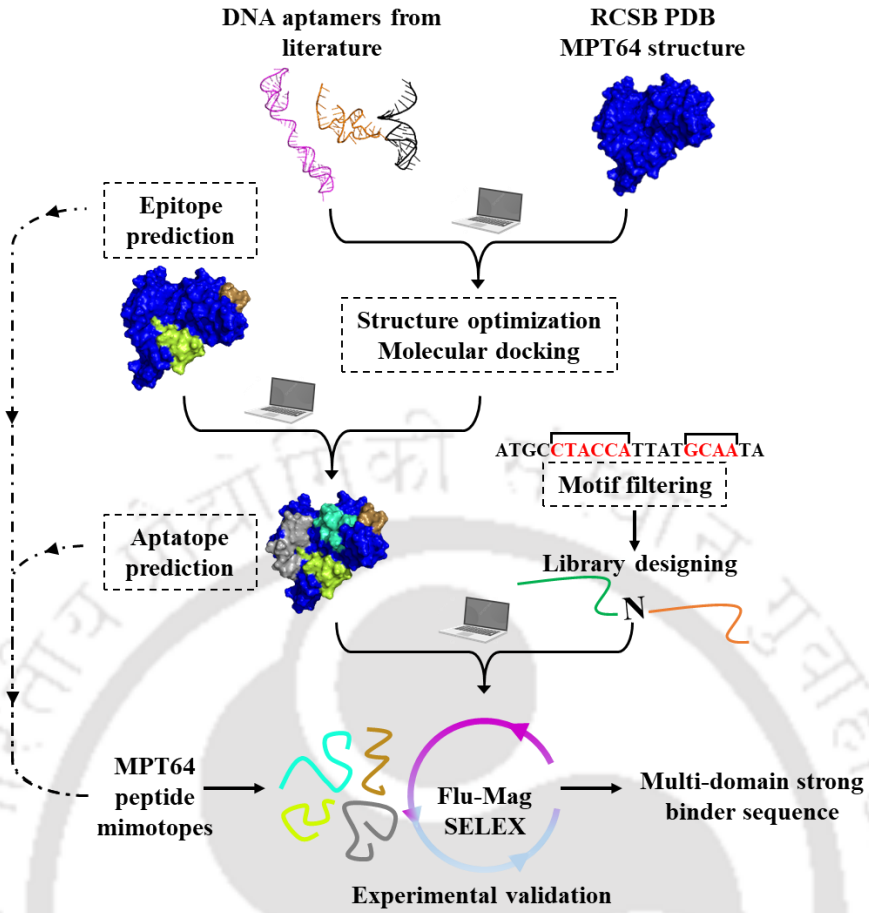

Fig. 5.1 "SMART" approach for development of novel DNA aptamers for MPT64.

Moreover, in the second part of the chapter we focus on the synthesis and characterization of gold nanoclusters as sensitive labels for the aptamers that will be generated in the first part. Gold nanoclusters (AuNCs) have garnered much attraction due to their novel structures, unique properties and extraordinary sensing capabilities [248,249]. Because of their stability, AuNCs can be synthesized and used more widely in the field of diagnosis because they can maintain their structure and characteristics in a variety of environmental circumstances. AuNCs demonstrate strong enzyme-like catalytic activities and fluorescence performance, as well as molecular-like electron energy-level changes from quasi-continuous to discrete energy-level fluorescence behaviour. Furthermore, because of their special physiochemical characteristics, which include high catalytic activities, low toxicity, a large Stokes shift, and a long fluorescence life, AuNCs show multiple benefits. As a result, the applications of AuNCs in fluorescence sensing appear

promising [250–253].

They are reported to be synthesized in the sub-nanomolar range (1.7 nm to 10 nm) by various methods. Interestingly, these AuNCs have remarkable surface functionalization properties that can be carefully tailored to endow them with variable luminescent properties. Existing literature over the period of last five years have highlighted the importance of tuning the properties of AuNCs for specific applications [249]. Especially, in biosensing for disease diagnostics, the incorporation of these AuNCs have helped to generate nanoprobes that showcase high-end modalities [254].

It should be noted that in our approach, thiol functional groups at the 5′ or 3′ends of DNA will be used to link the aptamers to the protein-stabilized AuNCs; however, they are not utilized as the NC stabilizer. Our approach will highlight the use of AuNCs as a functional label attached to one end of an aptamer and employing them on an aptasensing platform.

5.2 Methodology

5.2.1 Generation of a rational approach for aptamer library design

Step 1: Computational tools are an asset for developing and optimizing aptamers. Initially, we downloaded the sequences of 3 reported DNA aptamers of MPT64 and named them as MPT-A1, MPT-A2 and MPT-A3 for our study [120,255]. We analyzed the GC content of the aptamers. Then we followed the "SMART" approach schematic workflow outlined in Fig. 5.1.

Briefly, we (i) predicted the secondary structure from the nucleotide sequence using the Mfold web server, (ii) assembled the tertiary structure of the corresponding RNA model from the secondary structure on the RNA composer web server, (iii) transformed the tertiary RNA structure into a DNA structure, (iv) added hydrogen atoms using the PyMOL software since these atoms play major roles on the stabilization of aptamers tertiary structure and interaction with the target, (v) refined the final tertiary structure on GROMACS package, (vi) simulated the docking models through the HDOCK web server [256] and scores are calculated (Table 5.2) (vii)

identified the interaction residues using the Protein-Ligand Interaction Profiler (PLIP) web server. We tabulated the H-bonds, hydrophobic interactions and other salt or cation based interactions that were pivotal in the aptamer recognition. There were two potential binding pockets or exosites that were found crucial for establishing H-bonds with the aptamer backbone.

Step 2: In a parallel workflow, we used two prediction tools: ABCpred and Bcepred to predict epitopes of the MPT64. The purpose of the ABCpred server (https://webs.iiitd.edu.in/raghava/abcpred/) is to use artificial neural networks to predict epitope regions within an antigen sequence [257]. The ABCpred server helped in predicting linear epitope regions with a specified window length of aa. The Bcepred server allows the prediction of linear epitopes using one or more combination of physico-chemical properties (for example, hydrophilicity, flexibility/mobility, accessibility, polarity, exposed surface and turns) for epitope prediction [258]. The amino acid sequence of MPT64 protein was downloaded and divided into consecutive 20 mer regions starting from the N terminal side to the C terminal side. For example, if the first 20 mer sequence would comprise of the aa starting from the 1st to the 20th position of the protein sequence, the second 20 mer sequence would comprise of the aa from the 6th to the 25th position and so on. A window lag of 5 aa for each region was allowed. These were then uploaded to the servers for prediction. From a total of 43 sequences with scores $\geq$ 0.87 in ABCpred, 9 were shortlisted and matched with the scores of the physico-chemical properties (mentioned above) for each amino acid overlapping in that stretch. Depending upon the highest scores from both the servers, we filtered the epitopes with the following criteria: maximum length of 16 aa, one polar residue at N &/or C terminus, one charged residue per five residues, greater than 50% hydrophilic aa, less than 50% flexible aa and greater than or equal to 60% accessible residues. Moreover, peptide stretches having aa with side chain oxidation issues (for example tryptophan, methionine or cytosine) or beta sheet formers (-H*H*H*H*H*H*- rule i.e. alternate hydrophobic and hydrophilic aa) were avoided. With the aim of ease of synthesis of the peptides

by chemical means and choice of solvents to dissolve such peptides for aptamer selection, our search criteria was formulated as stated. Finally, the peptide stretches fulfilling all these criteria were listed and four unique non-overlapping peptide stretches named as MPT-E5, MPT-E9, MPT-E24 and MPT-E39 were selected and finalized.

Step 3: The MPT64 amino acid residues that showed positive H-bond formations in computational docking from Step 1 were braced with the epitopic prediction results of Step 2. Interestingly, it was observed that all three aptamers showed positive H-bond interactions with aa belonging to two of the final four peptides selected. These two potential epitopic exosites belong to the 41-56 (MPT-E9) as well as 120-135 (MPT-E24) amino acid stretch within the MPT64 protein. This reinforced our notion that the aptamers potentially bind to exosites that are also epitopic determinants of our secretory biomarker. These four peptides were then chemically synthesized and were characterized analytically by HPLC and mass spectrometry.

Step 4: After finding the nucleotide bases in the aptamer sequences that favored binding, we delved deeper into mapping the motifs (at least 4 nucleotide long without any gap) within the sequences of MPT-A1, MPT-A2 and MPT-A3 that formed H-bonds with MPT64 amino acid residues. Thereafter, we found three unique 4 nucleotide long stretches; namely GCAA (from MPT-A1), ATGA (from MPT-A2) and GGGA (from MPT-A3) that interacted strongly with their partner aa on MPT64 via H-bonds. Following this observation, we incorporated these consensus motifs from MPT-A1, MPT-A2 and MPT-A3 into our DNA combinatorial library design. In other words, the presence of these consensus motifs in the forward and reverse primer binding regions of the library will aid in establishing hydrogen bonds to enhance the affinity of the novel aptamer sequences, which will be the final product of our study. However, these pre-incorporated consensus motifs will introduce additional binding affinities, aside from the central random region of the combinatorial library, which is primarily responsible for interactions with the target in SELEX. This technique was envisioned in order to improve the final outcome of the number

of H-bonds that the DNA aptamer is likely to form while recognizing the epitopic exosites of MPT64 across diverse lineages of MTB harboring subtle amino acid changes in the sequence of MPT64. This is turn would help us develop robust detection platforms to confirm the presence of the secretory biomarker with reduced false-negative outcomes.

Step 5: To this end, a random ssDNA N_{24} combinational library, 60 mer with the sequence 5′-CTGAGGATTGATAATTCG-N_{24}-GAATATGAACTGCTTAAC-3′ bearing consensus motifs from the already existing aptamers in the forward and reverse primer binding sites are designed. The forward primer was designed with a 5′ fluorescein modification and the reverse primer carried a 5′ polydA_{20}-HEGL (hexa-ethylene glycol) spacer. This technique of SELEX using modified primers to generate specific aptamers was adopted from the method proposed by Stoltenberg and coworkers with minor modifications [259]. This technique named as FluMag SELEX has the following advantages: (i) use of fluorescent labels on primers for DNA quantification in each cycle, (ii) use of magnetic beads for easy target immobilization (herein, peptides of MPT64), (iii) requirement of minimal quantities of target for aptamer selection, (iv) rapid and efficient separation (partitioning) of bound and unbound DNA molecules.

Furthermore, as the emergence of higher molecular weight "smeary bands" post PCR amplification poses a recurrent issue encountered by several researchers during SELEX, and was also noted in our ssDNA enrichment studies (detailed in Chapter 3 of this thesis), we implemented an additional checkpoint to prevent such occurrences, employing the polydA20-HEGL spacer concept. The polydA_{20}-HEGL spacer at the 5′ end of the primer act as terminators of DNA polymerization thereby preventing unnecessary amplification. Under such conditions, since polymerization is stopped at the spacer, the complementary DNA strand does not contain the extra polynucleotide tail and thereby has a lower molecular weight. Therefore, the two DNA strands could be easily separated using size-based DNA purification (for example, denaturating

PAGE).This technique also saves time between two SELEX cycles. This experimental section for carrying out SELEX between the ssDNA library and the four unique peptides is currently being carried out and not a part of the current thesis.

5.2.2 Synthesis and characterization of MPT64 peptide mimotope

Our *in silico* predicted peptide mimotopes were generated synthetically and procured from GL Biochem (China). An initial solubility check was performed with solvents like DMSO, water and PBS. The analysis for mass and peptide purity was done by MS and HPLC data. Details of MS and HPLC instrumentation and critical parameters for analysis is depicted in the Appendix. Following characterization of peptides, it was taken for immobilization; a prerquisite for Flu-Mag (a combination of fluorescence and magnetic) SELEX (ongoing work) [259].

5.2.3 Fabrication of BSA-stabilized AuNCs

BSA (lyophilized powder, ≥ 96%) and tetrachloroauric (III) acid hydrate ($HAuCl_4 \cdot 3H_2O$, Au ≥ 99.9% trace metal basis) was acquired from Sigma-Aldrich. Sodium hydroxide (NaOH) and NaCl was purchased from Himedia Laboratories. All other chemicals used were of molecular biology grade.

All solutions were prepared using water obtained from a Millipore water purification system. All the buffer solutions were filtered using the 0.22 µM syringe filters stored for not more than 5 days. Glasswares for preparation of gold nanoclusters were washed with aqua regia before use. Instruments: Automated ultra-high vacuum (UHV) X-ray photoelectron spectroscopy, (Make: M/s Physical Electronics, USA; Model: PHI5000 versa probe III), field emission transmission electron microscope (Make: JEOL, Model: 2100F), field emission scanning electron microscope (Make: Zeiss, Model: Gemini 300)

BSA-AuNCs were synthesized by a previously reported approach with minor modifications [156]. Briefly, $HAuCl_4$ aqueous solution (10 mL, 10 mM) was added to an equal volume of freshly prepared BSA solution (50 mg/mL). The resultant solution was vigorously

stirred at 37 °C. Slowly, 1.5 mL NaOH (1 M) was added to the mixture and left for 24 hours under vigorous stirring. The colour change of the solution from pale yellow to dark brown indicated the formation of BSA templated AuNCs. The as prepared BSA-AuNCs were dialyzed against ultrapure water (nuclease free) for 12 hours using a 3 kDa MWCO dialyzer. The dialysate water was changed from time to time. This was done to efficiently remove all excess reagents and ions from the BSA-AuNCs. The solution was stored in dark. The concentration of BSA-AuNCs in the final retentate from the dialyzer was determined by the weighting method after freeze-drying.

5.3 Results and Discussion

5.3.1 Computational docking of aptamers to MPT64

The reported DNA aptamer sequences collected from literature is depicted in the following table with their calculated GC%. We evaluated the sequence for finding consensus motifs that were present in all three aptamers [260]. Consensus motifs often bear chemical relevance to determine binding site affinities in an aptamer/protein interaction. As showed in Table 5.1, we summarized the sequences and motifs (highlighted in blue italics) and calculated their GC richness.

Table 5.1 DNA Aptamer sequences reported against MPT64 biomarker.

Sl. No.	Aptamer name	Sequence (5′ → 3′)	Length	GC%	Reference
1	MPT-A1	GTACAAACGACGGCCAGTCCTTGGG*ATGATT*CAAG*CAAA*GCCTCACGCCTACGGCTAAGTCATAGCTGTCTCTCCTG	77	53.2	[120]
2	MPT-A2	TTCGGGA*ATGATT*AT*CAAA*TTTATGCCCT*CTGAT*	34	35.3	[255]
3	MPT-A3	TGGGAG*CTGAT*GTCGCATGGGTTTTGATCACATGA	35	48.6	[255]

Next, simulation of the interaction between aptamers and MPT64 were done by molecular docking of the aptamers with the deposited structure of MPT64 (RCSB PDB 2HHI) target on the HDOCK web server [256] using the tertiary structures obtained after Step 1 (v) as input. *In silico*

docking resorts to a bioinformatics approach to obtain all possible binding conformations of the aptamer to the target. Then, the assembled docking models are assigned a hierarchy based on a scoring function. In the case of HDOCK, the score classification follows the optimum shape complementarity as well as the algorithm that maps the plausible intermolecular interactions involved in the aptamer-target stabilization. Although several possible docking models were obtained, only the model with the best docking score for each aptamer was used for further analysis. The docking scores and the models obtained are represented in Table 5.2 and Fig. 5.2 respectively. We could visualize the positive interaction with aptatope I (colour code: cyan green region) and aptatope II (colour code: gray region) by all three MPT64 reported aptamers as highlighted in the MPT64 surface (MPT64 in blue) in Fig. 5.2.

Table 5.2 Docking scores rom HDOCK.

Aptamer	HDOCK Docking score			HDOCK Confidence score		
	Model 1	**Model 2**	**Model 3**	**Model 1**	**Model 2**	**Model 3**
MPT64_1	-329.74	-266.46	-266.01	0.9733	0.9113	0.9105
MPT64_2	-286.40	-267.20	-267.06	0.9387	0.9125	0.9122
MPT64_3	-331.10	-285.26	-267.48	0.9740	0.9373	0.9129

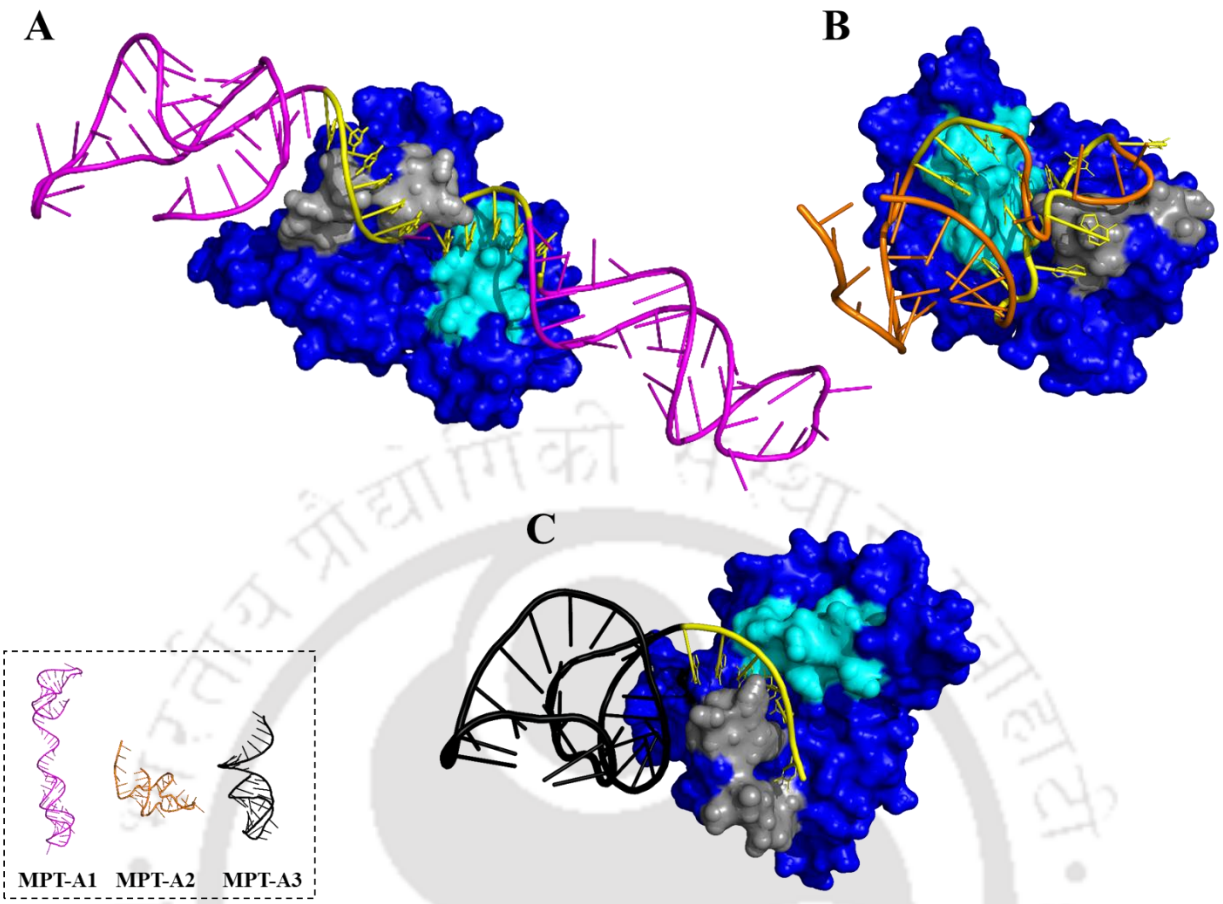

Fig. 5.2 Docking results of aptamer binding to MPT64 protein. (A) Docked structure of MPT64 and MPT-A1 (B) Docked structure of MPT64 and MPT-A2 (C) Docked structure of MPT-A3. Interacting nucleotide bases of aptamers are marked in yellow. INSET: tertiary structure of MPT-A1, MPT-A2 and MPT-A3. The peptide motifs that interacted positively with all three aptamers MPT-A1, MPT-A2 and MPT-A3 are coloured as cyan-green and grey on the surface of MPT64 protein (blue) The RCSB PDB structure of MPT64 protein (ID 2HHI; atom count 1,579) is shown in blue. The structure can be accessed at https://www.rcsb.org/structure/2HHI

Based on the best molecular docking model (model 1 from Table 5.2), the non-covalent interactions between the target molecules and aptamers were also determined using the PLIP web server [261]. This tool allowed identifying residues and the type of interactions between the aptamer and the target protein. The interaction report identifies the chemical group involved in the interaction, improving the knowledge on the mechanisms involved in stabilizing the aptamer-target interaction.

Next, the analysis of MPT64 protein sequence from all the deposited entries in Uniprot (https://www.uniprot.org/) pertaining to the organisms belonging to the MTBC were downloaded and multiple sequence alignment was done. The alignment results included approximately 156

sequences (sequences which had full length amino acid sequence length similar to that of MPT64 H37Rv with an average of 50 aa more or less were considered, 2 reviewed and rest unreviewed). We indicated identical amino acid residues with green highlight, conserved substitutions with yellow highlight and grey highlight indicated semi-conserved substitution as shown below (Fig 5.3).

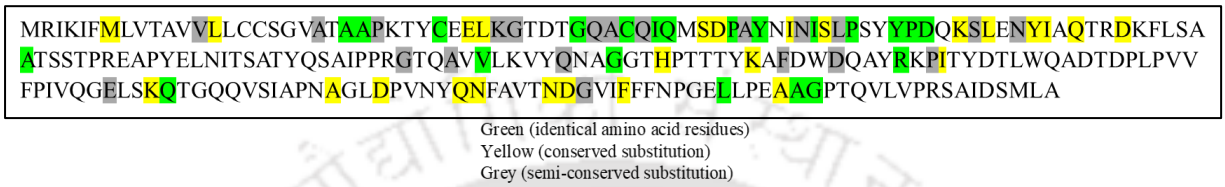

Fig. 5.3 MPT64 protein showing identical amino acid residues, conserved substitutions, semi-cnserved substitutions (seuqences obtained from Uniprot (https://www.uniprot.org/)

Based on the above idea of aa likely to get mutated in MPT64 and the ones that bore conservation, our approach was to select regions that had more number of conserved amino acid residues on surface epitopic regions.

Next, we braced the interaction results of PLIP tool with the information obtained on conserved aa for our next step. So our inclusion criteria during prediction of epitopes for the next set of studies were to keep at least three identical or conserved substitutions in the sequence of aa as shown in the following predicted epitopes (Table 5.3).

Table 5.3 Identification of aptamer-target contact residues and type of non-covalent interaction involved in the stabilization of the complexes from *in silico* docking.

Aptamer	Hydrogen bonds	Hydrophobic interactions	pi-Stacking	Salt Bridge	pi-cation Interactions
MPT-A1	43SER:38A 46ASN:35G 50GLN:36C 50GLN:35G 50GLN:36C 53ASP:1G 122TYR:37A 126TRP:42C 128ALA:43T 129ASP:45A 130THR:41C 206ALA:43T	49ALA:1G 126TRP:41C	126TRP:40G	None	None
MPT-A2	119PRO:8A 122TYR:20G 122TYR:11A 120ILE:10G 121THR:10G 50GLN:23A 53ASP:22T 46ASN:9T	47TYR:10G 121THR:8A	None	108LYS:12T	None
MPT-A3	43SER:3G 43SER:2G 46ASN:5A 47TYR:2G 108LYS:2G 119PRO:6G 121THR:5A 121THR:4G 122TYR:4G 126TRP:3G	None	None	40ASP:4G	47TYR:2G

Interestingly, the aptatopes showed positive interaction with some common overlapping nucleotide motifs present in all three aptamers. Colour coded in red, green and blue in Table 5.3.

The motifs $G^{35}C^{36}A^{37}A^{38}$ from MPT-A1, $A^{8}T^{9}G^{10}A^{11}$ from MPT-A2, $G^{2}G^{3}G^{4}A^{5}$ from MPT-A3 are unique motifs that showed positive interactions with either aptatope I or aptatope II or both on MPT64 (Table 5.4). Thus, the consensus motifs GAAC, GATA, GAGG were incorporated in the constant primer binding regions of the library designed for current study. It appeared to us that these motifs hold important binding site affinities that could initiate the formation of first few H-bonds with MPT64 peptide mimotopes during SELEX. Moreover, it is established in literature that pre-designing constant regions often improve the binding affinities of the final aptamer [262].

Table 5.4 Structural motif scanning. Motifs are colour coded, bold and kept underlined.

Sl. No.	Aptamer name	Sequence (5′ → 3′)	Length	GC %	Reference
1	MPT-A1	GTACAAACGACGGCCAGTCCTTGGGAT GATTCAA**GCAA**AGCCTCACGCCTACGG CTAAGTCATAGCTGTCTCTCCTG	77	53.2	[120];
2	MPT-A2	TTCGGGA**ATGA**TTATCAAATTTATGCCC TCTGAT	34	35.3	[255]
3	MPT-A3	T**GGGA**GCTGATGTCGCATGGGTTTTGA TCACATGA	35	48.6	[255]
Library designed for the current study		CT**GAGG**ATT**GATA**ATTCGNNNNNNNNN NNNNNNNNNNNNNNNGAATAT**GAAC**T GCTTAAC	60	-	-

Further, we validated the formation of any secondary structure in the primer-binding region of the library designed by Mfold (http://www.unafold.org/mfold/applications/dna-folding-form.php) as shown in Fig. 5.4. Both the secondary structures showed the formation of a small hairpin loop that would ideally play unique structural roles in assisting the random region during binding interactions with the target. From the analysis of various target-aptamer binding sites, it is also reported that the presence of a protruding hairpin structure is the easiest binding site for a target [262,263].

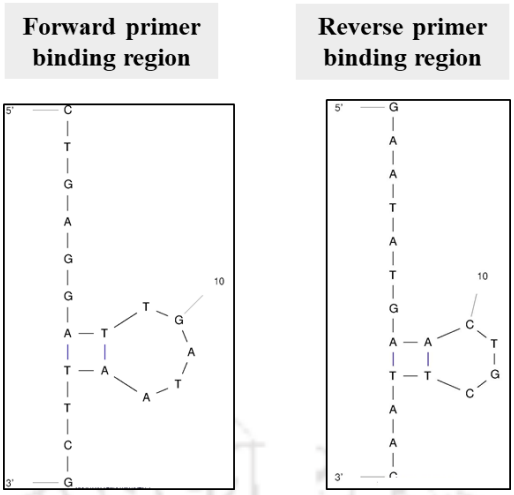

Fig. 5.4 Secondary structure of the primer binding regions of the library that are likely to play an assisting role in target recognition.

In summary, we could show that the aptamers interacted with the aptatopes I and II (predicted by HDOCK analysis). We merged this information with the epitopic sites (predicted by ABCpred and BCpred) to come up with four unique structurally relevant mimotopes for MPT64 that are less likely to show variation for designing an aptamer biorecognition molecule specific for MPT64. Previous *in silico* reports also claim that two aptamers having different potential secondary structures, can recognize the same peptide sequence in the protein [264,265]. This further helped in our analysis of picking all the four mimotopes for MPT64. All the four mimotopes are presented in Table 5.5 and Fig. 5.5**.** Each one was assigned a name and given for chemical synthesis.

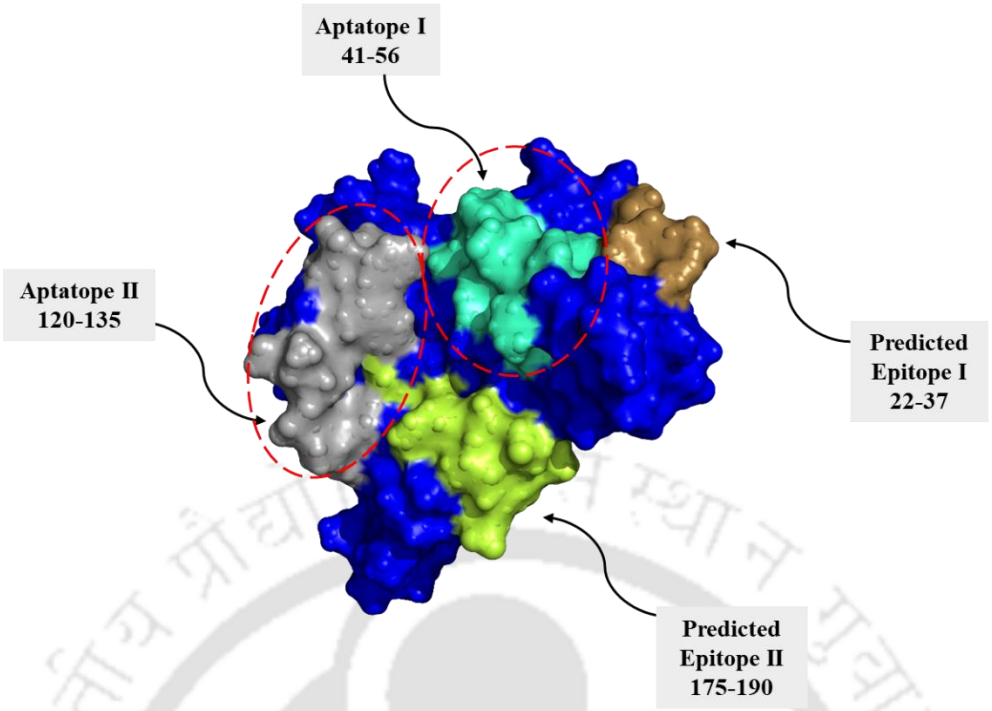

Fig. 5.5 MPT64 structure as visualized by PyMol. The exosite I (aa 41 to 56) and exosite II (aa 120-135) shows positive interaction with the reported aptamers MPT-A1, MPT-A2, MPT-A3. The predicted epitopic sites I and II in our study covers aa 22-37 and 175-190 respectively.

Table 5.5 Peptide mimotopes of MPT64.

Sl. No.	Amino acid stretch	Sequence	Length	Site on protein	Peptide Name Assigned
1	22-37	TAAPKTYCEELKGTDT	16	Predicted epitope I	MPT-E5
2	41-56	CQIQMSDPAYNINISL	16	Aptatope I	MPT-E9
3	120-135	AGGTHPTTTYKAFDWD	16	Aptatope II	MPT-E24
4	175-190	SIAPNAGLDPVNYQNF	16	Predicted epitope II	MPT-E35

5.3.2 Synthesis and characterization of MPT64 peptide mimotopes

There are various strategies for development of purified mimotopes. The experimental cost of obtaining the mimotopes from *E. coli* cloning vectors carrying the sequences and purification of good quality recombinant mimotopes is relatively higher. Computational methods to predict B-cell epitopes are much more efficient and cost effective. Moreover, peptide mimotopes hold well-defined structures useful for interaction with nucleic acids [266].

We procured the synthetic peptides (generated chemically) and verified their mass and purity by analytical methods. The HPLC spectrum confirmed the absence of any contaminating peaks (Fig 5.6). The molecular weight of all the peptide mimotopes were confirmed by electrospray ionization mass spectrometry (Fig 5.7).

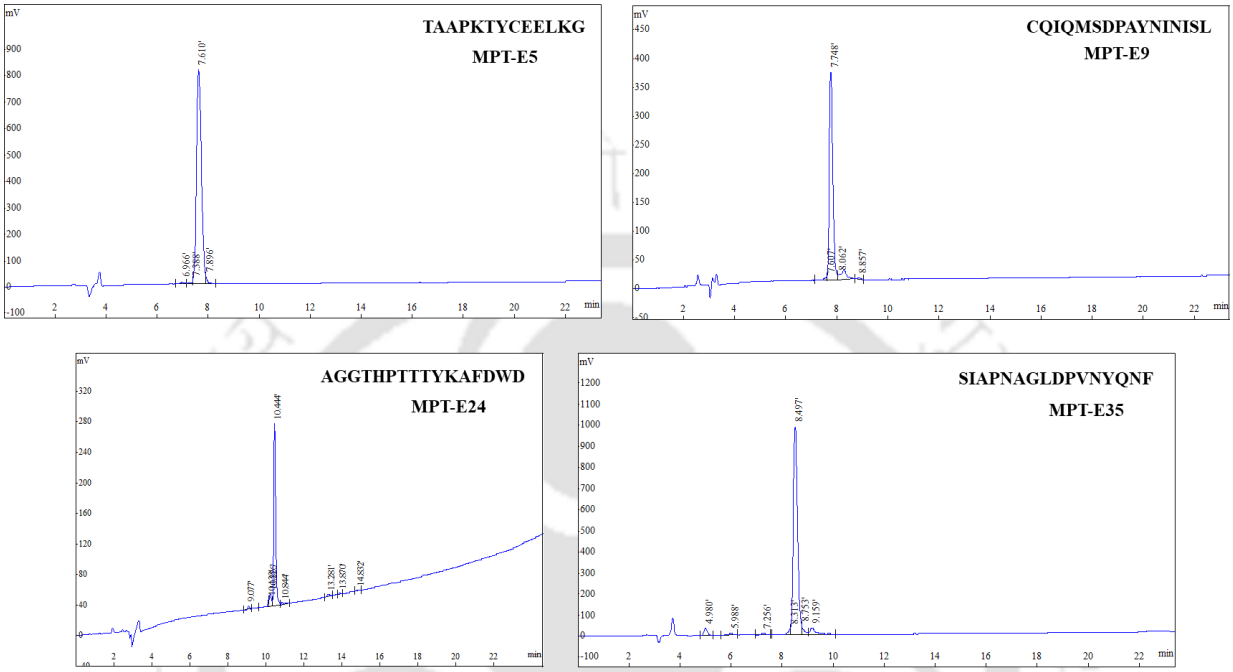

Fig. 5.6 HPLC analysis of MPT64 peptides. HPLC chromatograms we obtained from a 10 µL concentrated sample injection. Chromatogram was extracted from wavelength of 220 nm; peak corresponding to the purified MPT-E5, MPT-E9, MPT-E24, MPT-E35 peptides.

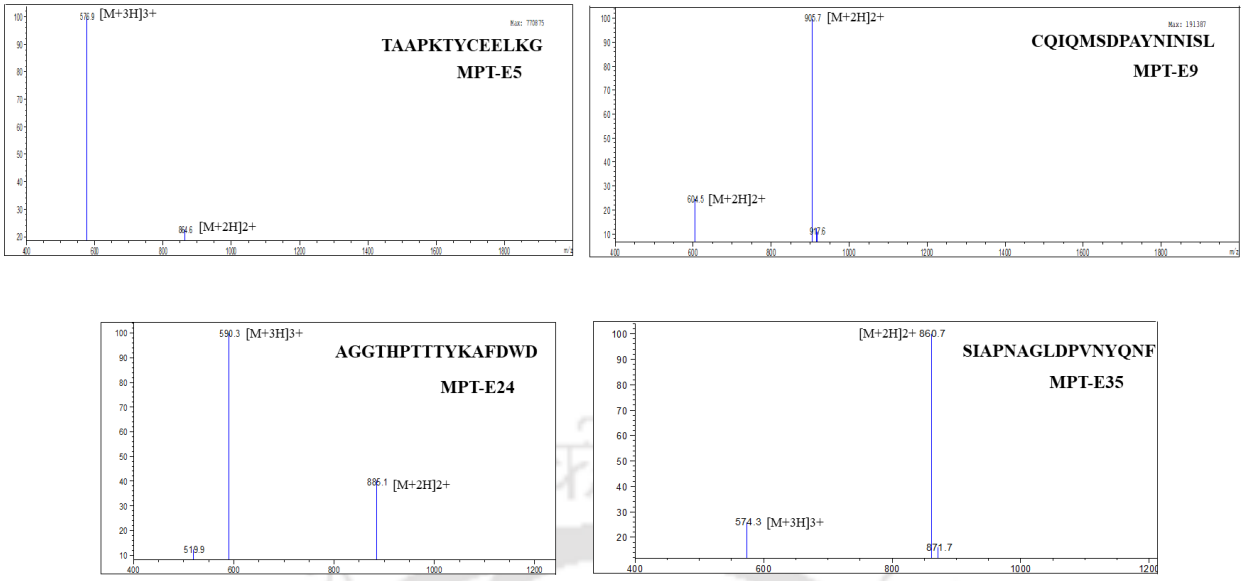

Fig. 5.7 Electrospray ionization mass spectrometry spectra for MPT64 peptides. ESI-MS (electrospray ionization mass spectrometry) spectrum of the purified MPT-E5, MPT-E9, MPT-E24, MPT-E35 showing their respective peaks.

Therefore, it can be concluded that the synthesized peptides were pure and ready to be used for SELEX screening with the prepared DNA aptamer library. Therefore, we characterized the solvent preferences and tabulated the results for future use in SELEX (Table 5.6).

Table 5.6 Mass, purity and solubility analysis of MPT64 peptides.

Sl. No.	Peptide	Calculated weight	Molecular weight from MS analysis	Purity from HPLC analysis	Solubility
1	MPT-E5	1727.9101	1728.12	~97.67	PBS: 2 mg/0.4 mL DMSO: --
2	MPT-E9	1810.0825	1810.18	~91.01	PBS: -- DMSO: 1 mg/0.2 mL
3	MPT-E24	1779.9268	1768.08	~87.74	PBS: 5 mg/mL DMSO: 5 mg/mL
4	MPT-E35	1704.9004	1719.99	~88.75	PBS: -- DMSO: 2 mg/0.2 mL

5.3.3 Characterization of BSA-AuNCs

BSA-AuNCs were prepared from $HAuCl_4$ in one step by employing BSA as the reducing and stabilizing agent. In this procedure, BSA and $HAuCl_4$ were mixed without the need for additional reducing agents in an aqueous solution. Water was chosen as the reaction medium due to its favourable dielectric constant. The color of the solution changed from yellow to golden

brown during this reaction, indicating that they were reduced from Au^{1+} to Au^{0} to form clusters. The addition of NaOH to the solution increases pH, which in turn improves the reducing power of the BSA. Moreover, all precursor molecules of gold from $HAuCl_4$ was depleted as the reaction progressed after NaOH addition. At supersaturating concentrations of gold atoms, the nucleation event started which led to the formation of large number of clusters protected by BSA acting as the template [267]. The cysteine aa forming disulphide bonds of the BSA at higher alkalinity (or, higher pH contributed by NaOH) become readily available to form stronger Au-S bonds, thereby attributing to the capping nature of BSA.

The simple approach outlining the major steps of BSA-AuNC synthesis is schematically represented in Fig. 5.8A. The aqueous solution of BSA-AuNCs was golden-brown under irradiation of natural light as shown in inset (i) of Fig. 5.8A. When irradiated with UV light at 365 nm, BSA-AuNCs solution emitted red fluorescence as shown in inset (ii) of Fig. 5.8A).

The optical properties of BSA-AuNCs were characterized by UV-vis spectrophotometry and fluorescence spectroscopy. The UV-vis absorption spectrum of BSA-AuNCs shows an absorption shoulder at about 280 nm (Fig. 5.8B). Interestingly, the absence of any surface plasmon resonance peak around the 510-520 nm region of the spectrum (potentially contributed by larger nanoparticles in the visible range wavelengths) clearly indicates exclusive formation of nanoclusters [268]. Additionally, the fluorescence emission properties were studied by recording emission spectra with different excitation wavelengths ranging from 420 to 500 nm. The BSA-AuNCs displayed a maximum emission at ~640 nm upon excitation at 450 nm which correlated well with existing literature (Fig. 5.8C).

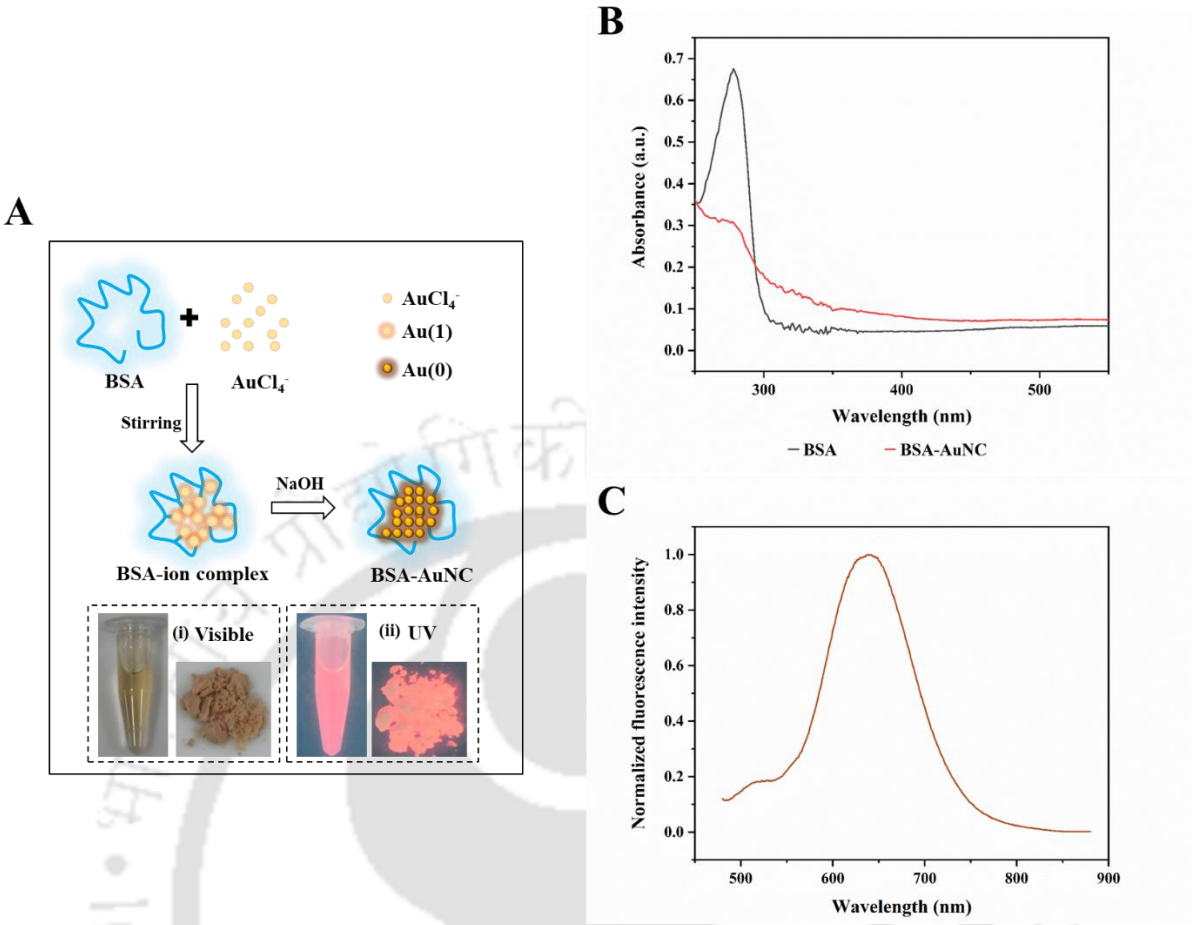

Fig. 5.8 Synthesis of BSA-AuNCs. (A) Schematic representation of synthesis scheme adopted for BSA-AUNCs in this study (inset: BSA-AuNCs photographed under visible and UV light in aqueous and free-dried forms). (B) UV-Vis absorption spectra of BSA and BSA-AuNCs. (C) Fluorescence emission spectra of BSA-AuNCs.

The particle size and morphology information of BSA-AuNCs were observed by FETEM and HRTEM analysis. FETEM image demonstrates that the clusters were well dispersed (Fig. 5.9A). The selected area diffraction (SAED) pattern confirmed the high crystallinity of the BSA-AuNCs as indicated by the presence of bright spots that corroborates with earlier reports (inset, Fig. 5.9A) [269,270]. It is well reported that metallic nanoclusters of gold have an average size of less than 3 nm. The TEM image recorded in our study indicates the size of the synthesized BSA-AuNCs as 2 ± 1 nm (Fig. 5.9B). Further, the high resolution TEM (HRTEM) image of a single BSA-AuNC shows one dimensional lattice fringes (Fig. 5.9C). The measured interfringe distance of ~0.247 nm is closer but not exactly consistent with lattice spacing of the face centered

cubic (Au_{111}) of gold (~.22 to .24 nm) [269].

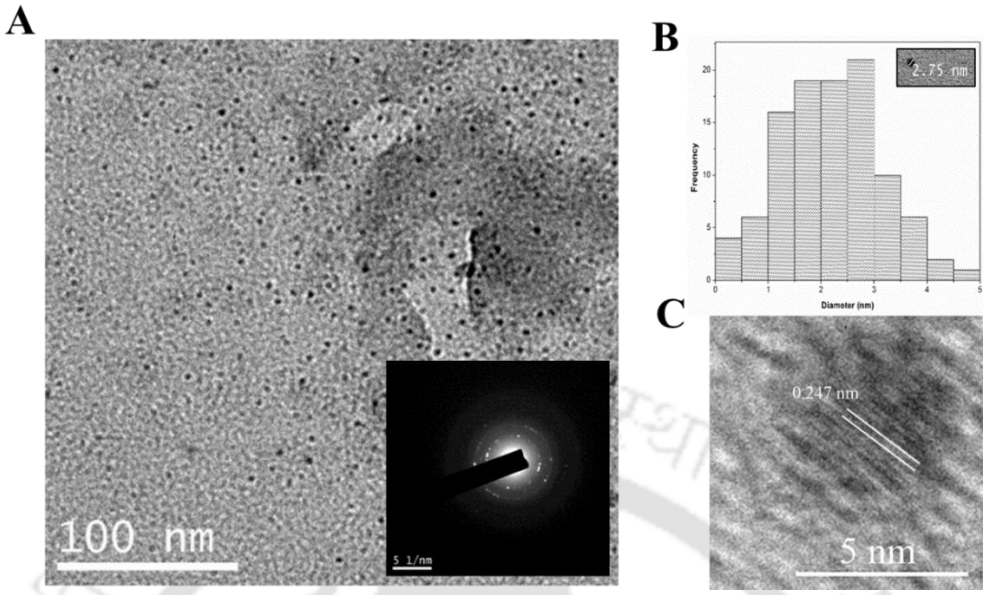

Fig. 5.9 TEM analysis of BSA-AuNCs. (A) FETEM image of BSA-AuNC (inset: SAED pattern of BSA-AuNCs). (B) Particle size distribution histogram of the BSA-AuNCs (inset: measurement of diameter from an individual nanocluster from the corresponding image in A). (C) HRTEM image the lattice fringe of an individual nanocluster showing the lattice planes separated by 0.247 nm.

The surface chemical composition of BSA-AuNCs were examined using XPS. As shown in the XPS full spectra (Fig. 5.10A), the signals of O, N, C, and Au elements are observed. We noted the strong signal of Au in the M (2.22 keV) emission peak corresponding to gold [271]. The presence of negligible amounts of Na element might be a result of incomplete dialysis of excess ions after synthesis of the clusters. The presence of aluminium foil in sample preparation contributed to the Al elemental peak. Furthermore, FTIR spectroscopy was used to probe the functional groups of BSA-AuNCs (Fig. 5.10B). The characteristic peaks at 1645 cm^{-1} and 1539 cm^{-1} are attributed to amide I (C-O stretching) and amide II (primary amine, C-N stretching coupled to the N-H bond) regions respectively. Another peak corresponding to the N-H stretching depicted at 3282 cm^{-1} was also observed. Towards this end, it can be inferred that the AuNCs have been successfully made on BSA and the observations correlate well with the previous reports [272,273].

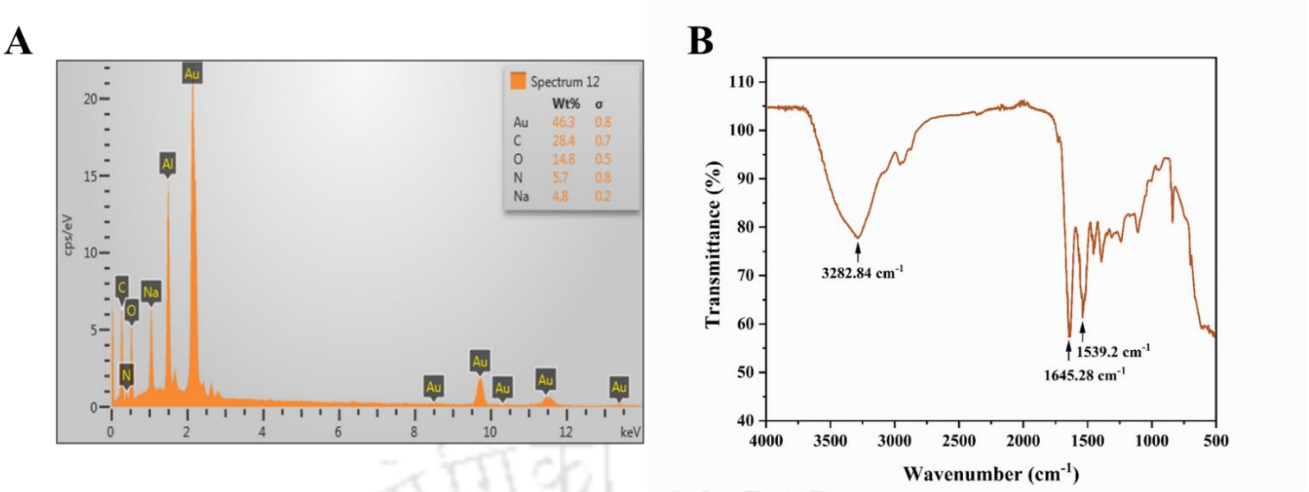

Fig. 5.10 EDX and FTIR spectrum of BSA-AuNCs. (A) EDX elemental analysis of BSA-AuNCs show presence of Au, N, O, and C (B) FTIR spectrum (operated in ATR mode) depicts characteristic bands of N-H, C-O stretching for the BSA-AuNCs.

Fig. 5.11A displays the XPS survey spectrum of the as prepared BSA-AuNCs. This survey spectrum showed that all five (Au, N, C, S and O) elements of BSA-AuNCs appeared, thereby confirming the composition of the BSA-AuNCs. The deconvoluted regions of Au 4f, N 1s, S 2p, C 1s are depicted in Fig. 5.11B. The Au 4f spectrum corroborates with the characteristic Au $4f_{5/2}$ and Au $4f_{7/2}$ peaks, respectively at ~87.5 and ~84.1 eV, with a spin-orbit coupling of 3 eV. This can be suggestive of the zero valency state of Au atoms which in turn confirms the successful synthesis of AuNCs. Likewise, the N 1s spectrum with the peak at ~400 eV indicates the presence of amine groups. Additionally, the C 1s spectrum of the BSA-AuNCs at ~288 eV and ~285 eV indicates the presence of carboxyl groups [273,274].

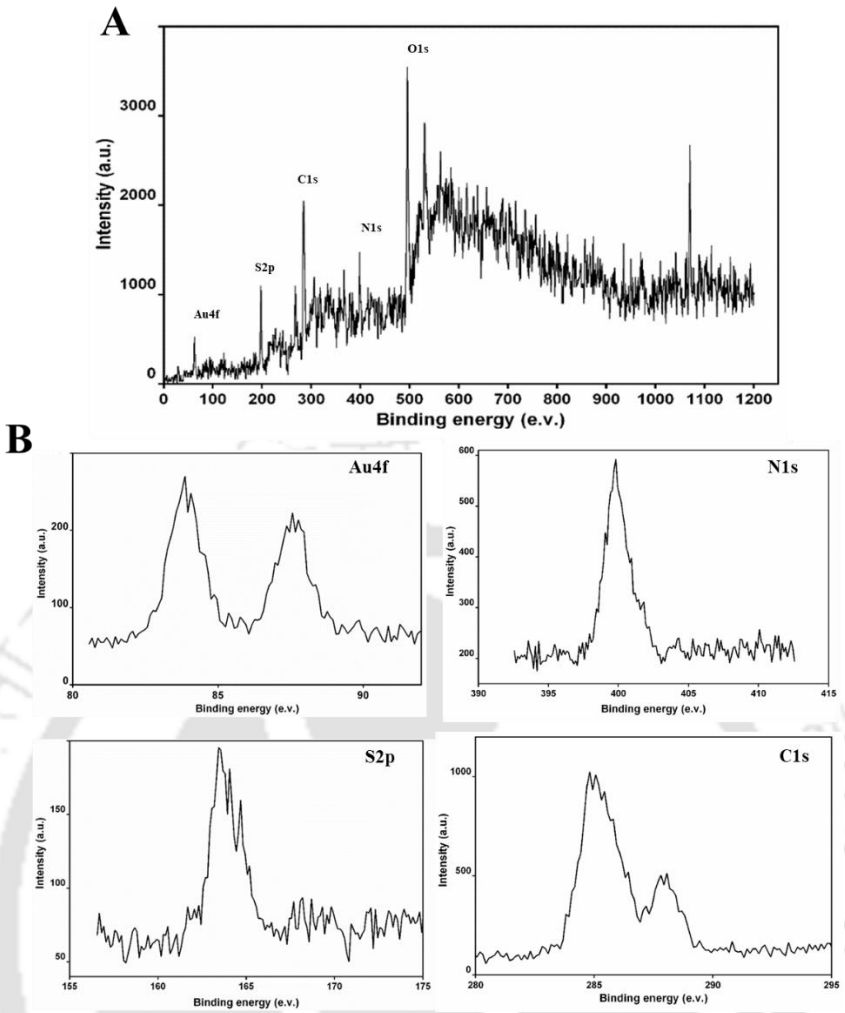

Fig. 5.11 XPS spectral analysis of BSA-AuNCs. (A) XPS survey spectrum (B) Au 4f, N 1s, S 2p, C 1s spectrum of BSA-AuNCs.

5.4 Conclusion

In conclusion, our study provided useful information about the conserved amino acid residues and structural aptatopes (chemical equivalent of epitopes) of the MPT64 protein. The selection of residues on MPT64 that are less likely to show sequence variations is also carried out at the backdrop of this study, that would in turn address the anomaly of Capilia-negative isolates in TB detection.

Thus, it can be put forward that we have designed a combination of manually curated and bioinformatics based approach for the development of a systematic workflow for designing better aptamers for target biomarker detection. We performed a comparative analysis of the interacting surfaces detected in aptamer complexes formed by MPT64. Our results indicated that signature

motifs of the aptamer sequence, rather than the exosite area, dictates the shape complementarity of an aptamer-target complex formation. In a parallel approach, we designed a library with nucleotide motifs that are screened from previously reported aptamers which showed positive interaction with the said MPT64 target. This will play a role in the target interaction with MPT64 peptide mimotopes in SELEX.

Intriguingly, our approach also sheds light on the design and development of peptide mimotopes of proteins for aptamer development. Peptide mimotopes can be a useful alternative to use of recombinant proteins for SELEX. In this scenario it can also be argued that, recombinant MPT64 produced from different batches may differ in properties. This anomaly is also one of the reasons behind our approach to design highly stable and structurally robust peptide mimotopes for selecting aptamers instead of using recombinant MPT64 during repeated cycles of SELEX screening. Also, proteins show several abnormalities during use in SELEX, such as spontaneous precipitation and or losing the 3D conformations upon encountering potential contaminants in buffers. Our process is also designed to care of such anomalies. Another intriguing aspect of this study.

In a nutshell, our methodology will encompass a three-step refinement before final selection of specific aptamers for MPT64: Step 1: *in vitro* screening of aptamers through Flu-Mag SELEX by contacting the designed library with peptide mimotopes of MPT64; Step 2: further validation of the selected aptamers by binding affinity analysis with the recombinant MPT64 to choose the best aptamer that binds to the native MPT64 protein and Step 3: using gold nanoclusters towards design and development of a sensitive MPT64 aptasensing platform. This will aid in efficient diagnosis of MPT64 irrespective of the subtle amino acid differences it might harbor in its sequence from clinical samples of varied geographical origin worldwide. By using the method described here, additional aptamers can be thoroughly characterized, and based on the specificity requirements, an aptamer with the required motifs can be chosen. To this end, this

will enable aptamers to realize their full potential as distinct molecular recognition elements in TB diagnostics.

Ongoing work

Characterization of peptide-immobilized magnetic nanoparticles (MNPs)

MNPs were prepared by using $NaBH_4$ method, as per previously reported protocol with slight modification to obtain naïve Fe_3O_4 particles [275]. Silanization with organofunctional alkoxysilane molecules (TEOS and APTES) was used to functionalize the surface of MNPs, following a modified procedure described in the literature [276]. The first step is to prepare an amine-functionalized MNP, denoted Fe_3O_4-NH_2, by stepwise addition of TEOS/ APTES onto the surface of Fe_3O_4 nanoparticles.[277]. After drying, the functionalized MNPs were resuspended in 0.02 M PBS (pH 7.4). It was washed and centrifuged 3 times with 1 ml of buffer following which 8% glutaraldehyde was added and mixed with the solution for 4-6 hours for activation. Thereafter, excess glutaraldehyde awas removed and the magnetic nanoparticles were resuspended in PBS [277]. Peptide solution (2 mg/mL) was added to the activated MNPs and mixed end-over-end overnight. Following magnetic separation, the supernatatnt was kept aside for protein estimation. MNPs coated with four different peptides in four different vials were separately processed. Next, the empty sites on the peptide-immobilized MNPs were blocked by resuspending the MNPs in 0.5 M glycine solution made in PBS and mixed for 30 minutes. Following the blocking step, magnetic separation was done and the supernatant was discared. The MNPs were then resuspended in appropriate buffer (containing glycerol) for storage and buffer without glycerol (for characterization). A schematic diagram is outlined in Fig. 5.12. Characterization is being carried out as a part of this ongoing work.

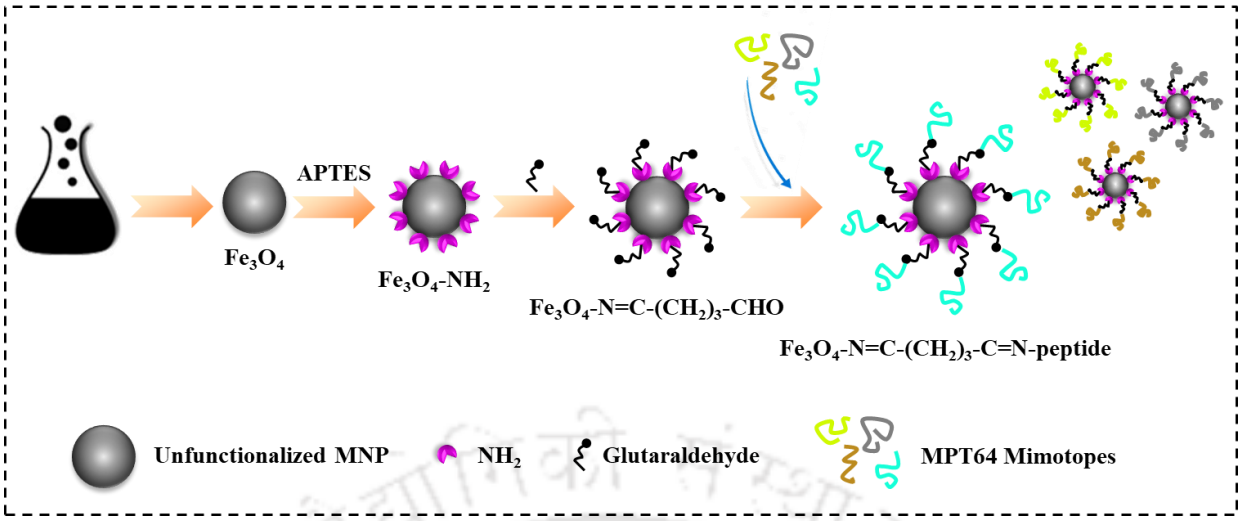

Fig. 5.12 Synthesis of magnetic nanoparticles for immobilization of MPT64 mimotopes. MNP: magnetic nanoparticle. MPT64 mimotopes correspond to peptides MPT-E5, MPT-E9, MPT-E24, MPT-E35)

6

Discussion & Future perspectives

6.1 Discussion

There are several challenges associated with the management of TB in the world. Fast and precise testing is a crucial step in the treatment of TB. Three important features of designing a platform to test for TB is to ensure that it is rapid, reproducible and robust. The "bacteriologically confirmed" cases of TB are those identified by rapid molecular testing as advised by the WHO [1]. But, rapid molecular tests are costly and unsuitable for large screening of high-risk populations. On the other hand, there are a number of drawbacks of the currently existing LFA (for testing urine lipoarabinomannan) that should be addressed for the benefit of users, including response times that vary depending on the size of the pores and holes that are blocked by matrix components. Likewise, sputum smear microscopy can only detect TB when the bacterial load is more than 10,000 cells/ml in a sputum sample. n the past couple of decades, various interdisciplinary fields such as biotechnology, nanotechnology, and biomedical engineering have been focused on developing alternative methods to traditional TB detection. This endeavor involves the utilization of biosensors, which represent futuristic tools in clinical research. We have witnessed a significant development in the field of immunosensors (devices utilizing antibodies as biorecognition elements), which have shown promising results. However, antibodies possess inherent limitations, as discussed earlier in our chapters. Therefore, to devise a simple and effective toolkit for TB detection, considering the shortcomings of existing methods, we have embarked on a journey to address these challenges through "aptasensing."

In the beginning, we cloned, expressed, purified and characterized three important secretory biomarkers from the MTB H37Rv as recombinant proteins for our study under native conditions (Fig. 2.4). Next, these recombinant proteins were used for the development of aptamers.

Our work primarily focussed on different screening approaches to develop high-affinity aptamers for the biomarkers of TB that has useful applications in diagnosis and therapeutics. We

proved that aptamers can be screened by molecular-weight cut-off filtration assemblies in a novel "COFA"-based SELEX screening approach that helped in circumventing the bottlenecks of traditional protein-based SELEX which use immobilized targets (Fig. 3.1). Especially, in terms of developing aptamers for infectious disease diagnosis, immobilized targets do not correctly represent all the exposed regions or potential binding sites on the surface to mimic the actual scenario in biological fluids. In conclusion, we developed a short (69 nucleotide) ssDNA aptamer having G-quadruplexes against the target protein antigen Ag85B and characterized it through various analytical techniques in our study. Through the COFA-SELEX method, we addressed the existing challenges of (i) determining the optimal amounts of template for each positive and control round of selection (Fig. 3.5) and (ii) minimizing the number of steps in the SELEX cycle (Fig. 3.6). Our findings suggest that optimization of binding buffer constituents, especially the divalent and monovalent ions K^+ and Mg^{2+}, as well as pH has significant effect on the conformational plasticity of this G-quadruplex Ag85B aptamer (Fig. 3.12). We concluded that understanding the structural peculiarities of an aptamer before employing it on a sensor platform can provide valuable insights on improving binding affinity and sensor performance of aptamers. Akin to earlier reports that indicate that the parameter of K_D is not the only indicator of the aptamer's exact biding affinity to its cognate target and there are variations in the K_D parameters depending on the technique used and models for curve-fitting in non-linear regression, our study also reported variations in the K_D values (Fig. 3.17). We report K_D values of ~ 800-900 nM determined by the ALISA method collectively for the serum samples. We also looked into the effect of matrices used for study, so we interpreted our K_D results in both binding buffer and serum. This was done to obtain a deeper understanding of the challenges that the aptamer might face when tested with clinical samples. The lower affinities of the aptamer for the non-target proteins (as shown by the higher K_D values) also exemplify the selective binding properties of the aptamer to the target (Fig. 4.8, 4.9, 4.10).

Nonetheless, the dissociation constants were found to lie in the nanomolar range indicating moderate to high affinity of the aptamer for the Ag85B studied by us, despite the relatively high SD observed. Additionally, we report for the first time a Ag85B aptasensor fabricated with a fluorescently labelled Ag85B aptamer and GO as quencher. The aptasensor showed good reproducibility and analytical precision when tested with spiked serum samples. The aptasensor was found suitable for real-world applications with LOD of 68-74 nM in serum (Fig. 4.16 and Fig. 4.18, Table 4.2). We have also compared our prepared aptasensor with the monoclonal antibody based detection of Ag85B protein reported by Saengdee et al. (Table 6.1) [180].

Table 6.1 Comparison of the designed Ag85B aptasensor with Ag85B immunosensor.

Target	Biorecognition molecule	Method	Sample	LOD	Reference
Ag85B	Aptamer	GO-based fluorescence assay	Ag85B spiked serum samples	1.485 μg/mL	**This work**
	Monoclonal antibody	Silicon-nitride ISFET biosensor	Ag85B from mycobacterial cultures	0.12 μg/mL	[180]

Furthermore, we have also presented a “SMART” approach with valuable insights on the choice of MPT64 as a TB biomarker and developing a systematic workflow to design new aptamers against this secretory protein that show amino acid variations across various clinical isolates of MTB (Fig. 5.1). Secondly, we envisioned this workflow with the aim to establish the idea of creating only one strong-affinity aptamer instead of contributing to the already existing repertoire of aptamers for a target (that often do not reach the clinical trials). We have reused the existing knowledge on nucleotide interactions with specific aa on the surface of MPT64 protein to develop this workflow towards improving the quality of future aptamers using multiple computational tools.

Until now, aptatope mapping has not received much attention, particularly when it comes to clinically significant disease biomarkers, where low specificity and cross-reactivity are major

obstacles to aptamer discovery. Aptatope mapping helped us identify unique sites on MPT64 and thereafter screen structurally relevant nucleotide motifs of already existing aptamers that play pivotal roles in recognizing them (Fig. 5.5). We also hypothesized that pre-structuring constant regions of aptamer libraries can have a profound impact on the final outcome of an aptamer. In a nutshell, the above approach provided us interesting cues to select the peptide mimotopes of MPT64. Our ongoing work involves the characterization of these synthetically obtained peptides which are immobilized on magnetic nanoparticles to be used in the Flu-Mag SELEX technique to screen aptamers from the as-designed DNA library.

Furthermore, our work provides a detailed characterization of gold nanoclusters successfully synthesized to serve as the MPT64 aptamer label. These gold nanoclusters will be integrated into fabricating a sensitive aptasensor for detecting the TB biomarker MPT64.

6.2 Future perspectives

- Testing of the developed aptasensor with presumptive TB, active TB (bacteriologically not confirmed) and latent TB clinical blood samples would further validate our findings.
- Dynamic light scattering and zeta potential studies to characterize nanoclusters before and after immobilization of peptide mimotopes of MPT64 will be done. Characterization by several other techniques such as FTIR, TEM, SEM etc. followed by development of an aptasensor for detection of MPT64 in clinical serum samples will be done.
- Use of multiple secretory biomarkers on a single aptasensing platform could be beneficial for TB. Firstly, combining multiple biomarkers increases the sensitivity and specificity of diagnostic assays, enhancing their accuracy in detecting an infection, especially in cases of low MTB burden or extrapulmonary TB where single biomarker based sensing platform may lack sensitivity. Indirectly, use of multiple antigens will help in better differentiation between different stages of infection and the identification of drug-resistant strains. Secondly, a multi-biomarker approach would enable the differentiation between an active TB and latent TB

infection, aiding clinicians to make prompt treatment decisions. Another significant outcome of using multiple antigens on a single platform is in reducing assay complexity and enhancing cost-effectiveness. As research continues to uncover novel secretory biomarkers associated with TB, the potential for aptasensors to incorporate these biomarkers into multiplexed assays will drive their future development in diagnostics, offering clinicians powerful tools for precise and timely TB diagnosis.

- Translation of the developed Ag85B aptasensor towards commercialization as a kit based diagnostic device with one-step "MIX and GO" reagents for fluorescence estimation.
- Interestingly, there are different mathematical models to fit the binding data (either absorbance, fluorescence, SPR, BLI, etc.) for K_D calculation. We did not find any published report to help us with the better understanding of non-linear curve fitting. A future outcome of this work is to also develop a unified learning application with inputs from three major data analysis softwares (GraphPad Prism, OriginPro and SigmaPlot) for binding affinity studies. In terms of K_D estimations, there are advantages and disadvantages to each approach and it is recommended to perform data analysis using at least two methods/instruments to compare the obtained K_D values. It is also recommended to collect data across the binding fraction range of 0.2 to 0.8. Our analysis can be extended with more number of samples and more methods for optimal determination of K_D.
- We could not find any comprehensive database to fetch the sequences of aptamers from one platform. The existing databases on aptamers are not sufficient to provide the aptamer details with up-to-date information. Thus, we are in the process of collecting information on the patented as well as published aptamer sequences to curate into the form of a database with inputs such as: (i) target, (ii) existing aptasensor platform for the disease, (iii) secondary structure prediction tools, (iv) K_D values etc.
- Use of MD simulations in future can be used for further refinement of the docking studies

in our work.

- Interestingly, some recent literature on aptamer trimming (truncating lengths) has showed promise. Hence, keeping in line with the existing reports we would also like to improve the affinity upon truncating the Ag85B-18C-20 aptamer for better performance. Among the different post-SELEX optimization strategies, truncation and chemical modification are the two most important aspects that has proved to be a very powerful and effective approach to reduce the selection time from library pools.
- The abundance of modified structural motifs in starting libraries has emerged as a better starting pool to give rise to highly functional complex aptamers with improved binding affinities. Random libraries are now being replaced by such pre-structured libraries. This also suggests, the need to revisit literature and incorporate useful motifs from already existing aptamer sequences during designing new libraries.
- Given the significance of aptamers, we believe what we have seen so far in this important domain of research; is only the tip of an enormous aptasensor iceberg. In the past few decades, there are many reported aptamers in literature which could not be translated into clinical practice. We envision that after bioinformatics analysis, more than one aptamer against a target having nanomolar affinities can be tailored together and joined via "linkers" to improve their performance (such as increased thermal stabilities, resistance to nuclease digestion, flexibility and lower K_D values). Effectively, the biorecognition involving more than one aptamer will be highly specific and sensitive based on stronger affinity covering multiple aptatope sites on the target. As a result, the cumulative recognition of two aptamers designed to target more than one region of the target can help in improving the detection on sensing platforms. It would eventually reduce false outcomes in clinical scenarios. Also, the concept of making a dimeric or multimeric concatenated aptamer by linker addition will be pivotal for fabricating a multi-pronged approach to capture a disease biomarker from patient samples [278]. An interesting illustration of the same

is represented here as a part of our ongoing work on MPT64 aptamers (Fig. 6.1).

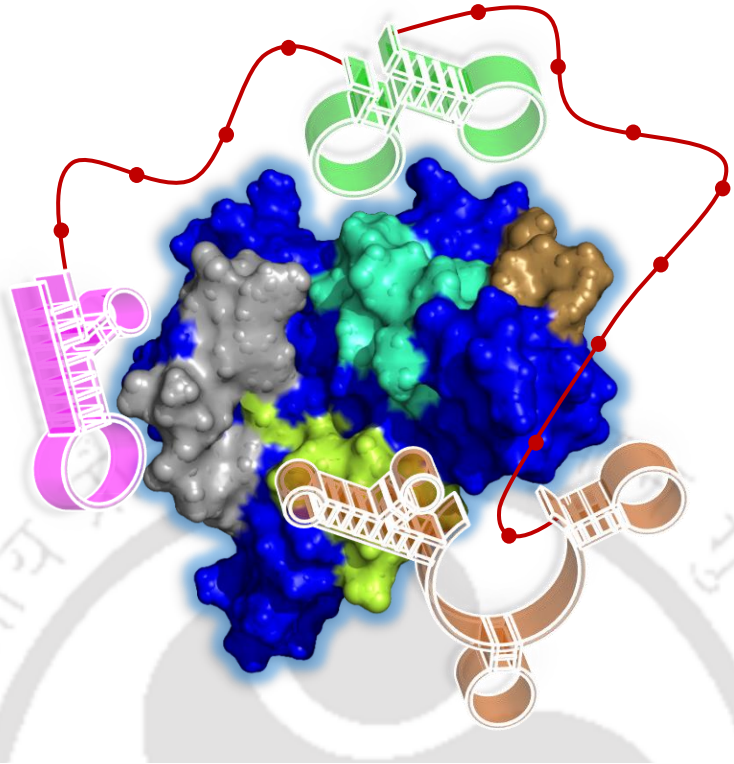

Fig. 6.1 Repurposing old aptamers for new diagnostic and therapeutic uses. Multiple aptamers are connected by poly dT or oligonucleotide linkers to assemble into a concatemer against a diseased biomarker (blue protein) whose aptatopes are highlighted in four different colours to show recognition sites of the three aptamers.

Outstanding questions

- Can aptamer Ag85B-18C-20 be truncated to provide better binding affinity?
- Can the process of COFA SELEX be standardized to give optimum performance for proteins having different molecular weights?
- Can old aptamers be repurposed for new uses?
- Can molecular dynamic simulations improve the docking outcomes of the MPT64 aptamer binding models?
- Can pre-fabricated primer-binding regions add to the diversity of the initial library for SELEX?
- Can SELEX outcomes be predicted computationally through bioinformatics tools to minimize chances of selection failure and false negative outcomes?
- Can novel aptatope (chemical equivalent of epitopes) prediction tools be designed?

Forget antibodies, use aptamers!

Appendix

Culture media

For this study, the molecular biology-grade components of bacterial culture media were procured from HiMedia (HiMedia Laboratories Pvt. Ltd., India) The growth media for cell culture were sterilized by autoclaving at 121 °C and 15 psi for 20 minutes, while heat-sensitive elements such as antibiotics were sterilized through filtration using a 0.22 µ membrane filter. The composition of different media used in the study are given below.

Luria Bertani (LB)

5 g/L Yeast extract, 10 g/L Tryptone and 10 g/L NaCl. For the preparation of LB agar plates, 20 g/L agar was added to the media before autoclaving. A stock solution of ampicillin at a concentration of 100 mg/mL was prepared in sterile distilled water, filter sterilized, and stored at -20 °C. The antibiotic was added to the autoclaved LB agar media which was moderately warm, just before pouring it into the plates.

Buffers for protein purification

Lysis buffer

50 mM Tris-HCl (pH 7.5), 200 mM Nacl, 10 mM imidazole, 0.1% Triton X-100, 20% glycerol (v/v), 1 mM PMSF, 1X protease inhibitor cocktail without EDTA. The protease inhibitor cocktail was added just before using the buffer.

Equilibration buffer

50 mM Tris-HCl (pH 7.5), 200 mM NaCl, 30 mM imidazole, 0.1% Triton X-100 and 20% glycerol.

Wash buffer

50 mM Tris-HCl (pH 7.5), 200 mM NaCl and imidazole at varying concentrations of 60 mM, 80 mM and 100 mM.

Elution buffer

50 mM Tris-HCl (pH 7.5), 200 mM NaCl and 250-500 mM imidazole.

Buffers and solutions for SDS-PAGE

30% Acrylamide solution

29 g acrylamide, 1 g bis-acrylamide dissolved in 100 mL water

10% Sodium Dodecyl Sulphate (SDS)

10 g SDS dissolved in 100 mL water

Resolving gel mix (10%, 10 mL)

4 mL Tris-Cl (1M, pH 8.8), 1 mL SDS (1%), 3.3 mL acrylamide: bis-acrylamide (29:1), 1.7 mL H_2O, 100 µl ammonium persulphate (APS) (10%), 10 µl TEMED.

Stacking gel mix (4%, 5 mL)

0.6 mL Tris-Cl (1M, pH 6.8), 0.5 mL SDS (1%), 0.7 mL acrylamide: bis-acrylamide (29:1), 3.2 mL H_2O, 50 µl ammonium persulphate (APS) (10%), 5 µl TEMED.

SDS sample buffer (SSB)

0.1 M Tris-Cl (pH 6.8), 20% Glycerol (v/v), 4% SDS (w/v), 0.0002% bromophenol blue, 10% β-mercaptoethanol. The SDS sample buffer was prepared as a 2X concentrate and used at 1X final concentration.

SDS-PAGE electrophoresis buffer

0.25 M Tris-Cl (pH 8.0), 1.92 M Glycine and 1% SDS. A 10X stock solution was prepared and used at 1X final concentration.

Gel fixing solution

40% (v/v) ethanol, 10% (v/v) glacial acetic acid and 50% water

Coomassie Brilliant Blue (CBB) staining solution

0.1% Coomassie Brilliant Blue R-250, 50% (v/v) Methanol and 10% (v/v) Glacial acetic acid

Destaining solution

40% (v/v) Methanol, 10% (v/v) Glacial acetic acid, and 50% water

Buffers for western blotting

Transfer buffer (10X stock solution)

0.25 M Tris-Cl (pH 8.0), 1.92 M Glycine and 1% SDS. A 10X stock solution was prepared and used at a final concentration of 1X containing 20% methanol.

Tris-Buffered Saline (TBS)

50 mM Tris and 150 mM NaCl, final pH was adjusted to 7.4 with HCl. TBS buffer was made as a 10X concentrate and used at a final concentration of 1X.

Wash buffer (TBS-T)

TBS (1X final concentration) with 0.1% Tween-20. The required volume was mixed with water.

Blocking buffer

TBST (1X final concentration), with 5% skim milk, 0.1% Tween-20

Ponceau S staining solution

0.25% (w/v) Ponceau S, 40% (v/v) Methanol and 15% (v/v) Acetic acid

Size exclusion chromatography (SEC) buffers

Column equilibration buffer

50 mM Tris-Cl pH 7.5, 200 mM NaCl, and 5% glycerol

Native polyacrylamide gel electrophoresis (Native PAGE) buffers (8%, 10 mL)

2.5 mL Tris-Cl (1.5 M, pH 8.8), 2 mL 40% acrylamide: bis-acrylamide, 5.5 mL deionized H_2O, 100 µl APS (10%), 10 µl TEMED.

Other buffers

Phosphate buffer for buffer exchange (20 mM, pH 8)

1000 mM phosphate buffer (pH 8) contains 93.2 mL 1000 mM of Na_2HPO_4 and 6.8 mL 1000 mM of NaH_2PO_4

Tris-acetic acid EDTA (TAE) buffer

40 mM Tris base, 0.5 M EDTA. Final pH was adjusted to 8 with glacial acetic acid. TAE buffer was prepared as a 10X concentrate and used at a final concentration of 1X.

Tris-borate EDTA (TBE) buffer

54 g of Tris base, 27.5 g of boric acid, 20 mL of 0.5 M EDTA (pH 8.0)

Microbiological techniques

Bacterial growth and storage conditions

Escherichia coli DH5α cells were used for cloning purposes. The cells were cultured at 37 °C in LB medium with the addition of ampicillin (100 µg/mL) and/or kanamycin (50 µg/mL) when required. The strains were preserved as stocks in glycerol (850 µl cell culture and 150 µl 87% glycerol) and stored at –80 °C. To revive the cells from glycerol stocks, they were streaked onto agar plates containing the appropriate antibiotic marker.

To isolate plasmids, bacterial cells that contain a selection marker, such as ampicillin, were grown overnight in LB medium with the appropriate antibiotic at 37 °C and 180 rpm. The overnight cultured cells were then harvested by centrifugation and subsequently used for plasmid extraction.

Molecular biology techniques

PCR for cloning of biomarker genes

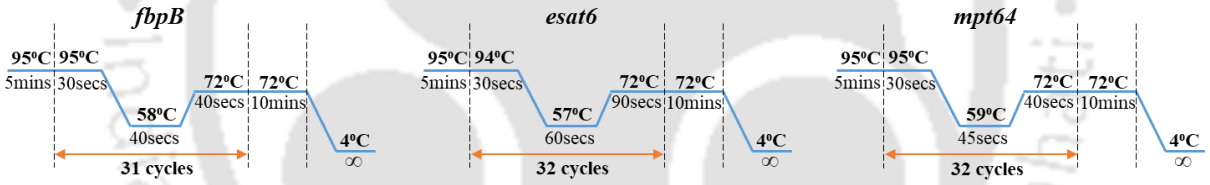

Western blotting for confirmation of biomarkers

After protein purification, protein concentration was determined using Lowry's protein estimation technique or Bradford protein estimation method. Subsequently, equal amount of protein was loaded in each lane of the gel. The gels were run at a constant voltage of 120 V and then transferred onto nitrocellulose membrane using Bio-Rad Trans-Blot®Turbo™. The membrane was treated with a blocking solution (either 5% skimmed milk or 5% bovine serum albumin) at room temperature for a duration of 2 hours. The blots were probed with antibodies. The blots were developed using the Bio-Rad ECL substrate and captured using the Bio-Rad ChemiDoc™ XRS+ system.

MS analysis of Ag85B

Ag85B peptides obtained after tryptic digest in MALDI-TOF-TOF are highlighted in green below:

MTDVSRKIRAWGRRLMIGTAAAVVLPGLVGLAGGAATAGAFSRPGLPVEYLQVPSPSMGR
DIKVQFQSGGNNSPAVYLLDGLRAQDDYNGWDINTPAFEWYYQSGLSIVMPVGGQSSFYS
DWYSPACGKAGCQTYKWETFLTSELPQWLSANRAVKPTGSAAIGLSMAGSSAMILAAYHP

QQFIYAGSLSALLDPSQGMGPSLIGLAMGDAGGYKAADMWGPSSDPAWERNDPTQQIPKL
VANNTRLWVYCGNGTPNELGGANIPAEFLENFVRSSNLKFQDAYNAAGGHNAVFNFPPNG
THSWEYWGAQLNAMKGDLQSSLGAG

Size exclusion chromatography (SEC) analysis

SEC was carried out using HiLoad™ 16/600 Superdex™ 200 pg column (GE Healthcare #28-9893- 35) connected to a AKTA-GO chromatography system. The column was equilibrated with a buffer comprising 50 mM phosphate buffer pH 8 and 300 mM NaCl. The column was calibrated at room temperature with β-amylase (200 kDa), alcohol dehydrogenase (158 kDa), albumin (66 kDa), carbonic anhydrase, (29 kDa) and cytochrome C (12.4 kDa) at a flow rate of 1 mL/min. The SEC of affinity-purified Ag85B and MPT64 was then carried out under the same operating conditions.

MS instrument details for analysis of MPT64 peptide epitopes:

Instrument: Agilent-6125B, Buffer: 50% H_2O / 50% ACN, Detector 1.5kv, Probe: ESI, Probe Bias:+ 4.5kv, Nebulizer Gas Flow: 1.5L/min.

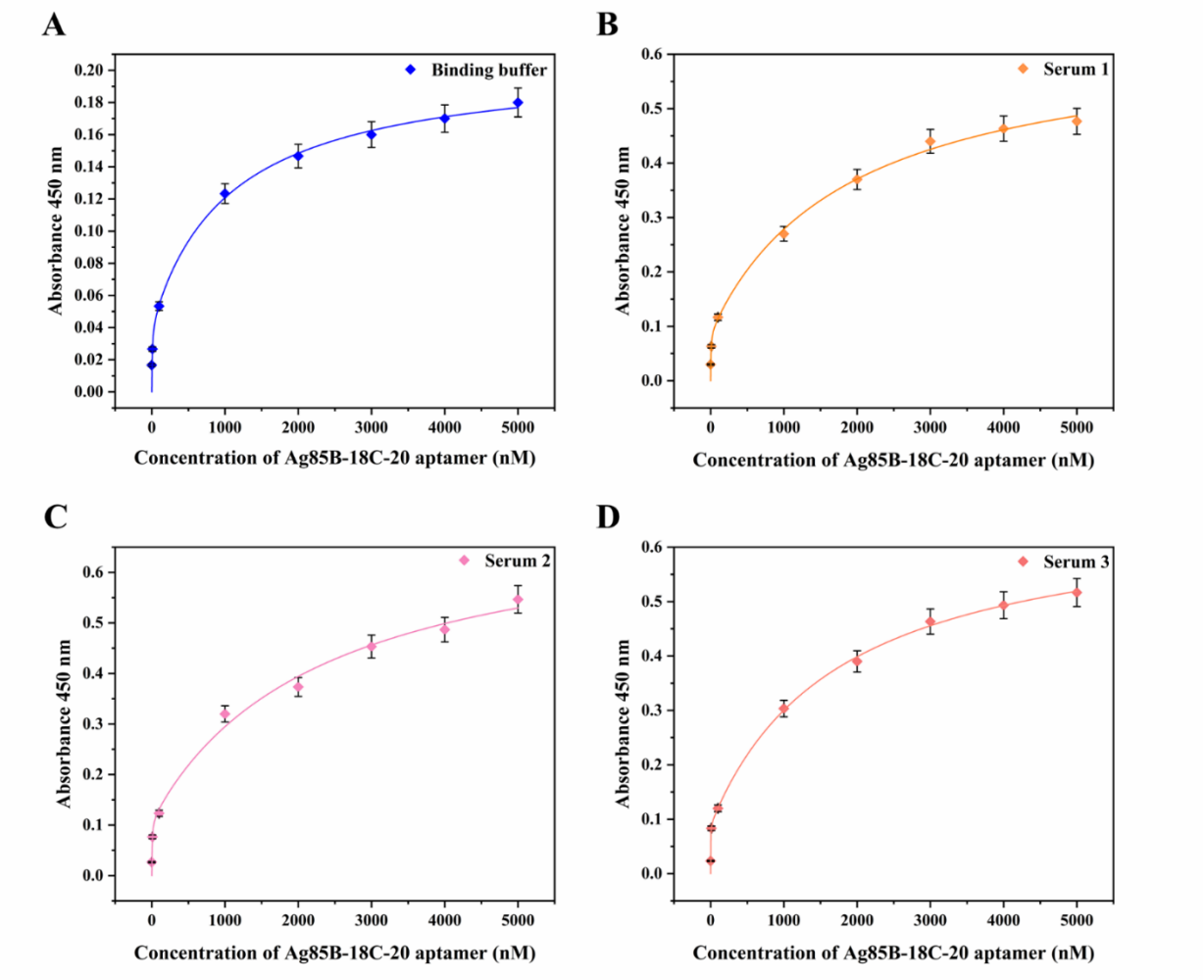

Figure: K_D estimation of Ag85B aptamer with two site binding model (A) binding buffer (B) Serum 1, (C) Serum 2, (D) Serum 3. K_D values have been represented in Table 4.1.

Primers used in this study

Primer	Sequence
Ag85B for	5′ -CCGCATATGTTCTCCCGGCCGGGGCTG- 3′
Ag85B rev	5′ -ATTGGATCCTCAGCCGGCGCCTAAC- 3′
ESAT6_frw	5′ -CGGCATATGATGACAGAGCAGGAGTG- 3′
ESAT6_rev	5′ -ATCCTCGAGTGCGAACATCCCAGTGA- 3′
MPT64_frw	5′ -GATGGATCCCGCGCCCAAGACCTACTG- 3′
MPT64_rev	5′ -ATACTCGAGGGCCAGCATCGAGTCGATC- 3′
Aptamer_rev	5′ -CTGTGCAGAGCGAATACCACG- 3′
Aptamer_forw	5′ -GGCAGTCTGGGCATACTTCACTC- 3′

Plasmids used in this study

Plasmid	Description	Source
pET28a	kan^R	Novagen
pQE30	amp^R	Qiagen
pGEMT Easy	amp^R	Promega

List of commercially used antibodies

Primary antibody				
Name	**Dilution used**	**Source**	**Clonality**	**Company**
α -His	1:5000	Rabbit	Polyclonal	Biobharti Life Science
Secondary antibody				
α -rabbit IgG (HRP-conjugated)	1:5000	Goat	Polyclonal	Biobharti Life Science

List of commercially used molecular biology reagents

Chemical	Name	Manufacturer
Enzymes	Taq DNA polymerase	New England Biolabs
	T4 DNA ligase	New England Biolabs
	Restriction enzymes	New England Biolabs
Kits	Plasmid isolation Miniprep kit	Macherey-Nagel
	PCR purification kit	Macherey-Nagel
	Gel extraction kit	Macherey-Nagel
	TA cloning kit	Promega
Other chemicals	ECL substrate	BioRad
	Resorufin butyrate	Cayman Chemicals
	Protease inhibitor cocktail without EDTA	SigmaAldrich
	Ponceau reagent	SRL Chemicals
MW Markers	Precision Plus Protein™ Dual Xtra Prestained Protein Standards #1610377	BioRad
	GeneRuler Low Range DNA Ladder #SM1191	Thermo Scientific
	High Range DNA Ruler #MBD29	Geneilabs

Optimization of asssay conditions for ALISA

Challenge	Solution			Final optimized parameter
	Reagent	**Protocol**	**Condition**	
Optimization of assay conditions to receive uniform coating and assay reproducibility	Normal 96 well plates	-	ON, 4 °C	Maxisorp 96 well plate + precoating, ON 4 °C
	Maxisorp 96 well plates	Pre-coating with 500ng/mL poly L- lysine	ON, 4 °C	
	Protein + coating buffer	500 ng per mL in 0.1 M carbonate-bicarbonate buffer	ON, 4 °C	1600 ng per mL 0.05 M carbonTe-bicarbonate buffer pH 9, ON, 4 °C
		1000 ng per mL + 0.21 M carbonate-bicarbonate buffer	ON, 4 °C	
		1600 ng per mL + 0.05 M carbonate-bicarbonate buffer	3 hour, 37 °C	
		1600 ng per mL + binding buffer	ON, 4 °C	
	Blocking buffer	5% BSA	1 hour, 4 °C	1% BSA + 0.05% Tween 20, 3 hours, 4 °C
		3% BSA	3 hours, 4 °C	
		1% BSA + 0.05% Tween 20	3 hours, 4 °C	
	No. of washes in wash buffer	6 washes	Interittent shaking for 1 minutes	3 washes
		3 washes		
	Streptavidin HRP	1:5000	-	1:10000
		1:10000		

HPLC instrument details for analysis of MPT64 peptide epitopes:

Column: 250*4.6mm, Boston Green 0DS-AQ, Solvent A: 0.1% TFA in 100% water, Solvent B :0.1% TFA in 100% ACN, Flow rate:1.0ml/min, Volume:10ul, Wavelength(nm):220.

Gradient :	A	B
0.1min	85	15
25min	60	40
25.01min	0	100
30min	0	100

MPT-E5

Rank	Time	Conc.	Area	Height
1	6.966	0.7836	82549	7004
2	7.388	0.5779	60878	9417
3	7.610	97.67	10290378	809295
4	7.896	0.9649	101652	25785
Total		100	10535457	851501

MPT-E9

Rank	Time	Conc.	Area	Height
1	7.607	0.9619	34063	4652
2	7.748	91.01	3222384	360268
3	8.062	7.57	268044	7749
4	8.857	0.4629	16393	2010
Total		100	3540884	374679

MPT-E24

Rank	Time	Conc.	Area	Height
1	9.077	1.152	20390	4157
2	10.133	2.189	38736	9313
3	10.226	5.819	102967	16912
4	10.444	87.74	1552738	237897
5	10.844	0.9924	17561	2244
6	13.281	1.129	19972	3072
7	13.870	0.5883	10411	2078
8	14.832	0.3866	6841	1145
Total		100	1769616	276818

MPT-E35

Rank	Time	Conc.	Area	Height
1	4.980	2.331	282876	32498
2	5.988	0.6813	82661	6698
3	7.256	0.5202	63120	5388
4	8.313	1.493	181101	28573
5	8.497	88.75	10769012	983268
6	8.753	2.179	264411	39631
7	9.159	4.042	490472	32347
Total		100	12133653	1128403

Sequence listing for the NGS results of aptamer clones in pGEMT vector

Group I

>1st_BASE_4899396_**SR_III_-_4C_-_12**_PLASMID_M13F-pUC_-40_
NNGNNCNNNNTTGTATACGACTCACTATAGGGCGAATTGGGCCCGACGTCGCATGCTCCCGGCCGCCATGGC
GGCCGCGGGAATTCGATT**GGCAGTCTGGGCATACTTCACTCCGTCAACTGGCCGCGGGGGGGCCGGCGTGGT**
ATTCGCTCTGCACAGAATCACTAGTGAATTCGCGGCCGCCTGCAGGTCGACCATATGGGAGAGCTCCCAACG
CGTTGGATGCATAGCTTGAGTATTCTATAGTGTCACCTAAATAGCTTGGCGTAATCATGGTCATAGCTGTTT
CCTGTGTGAAATTGTTATCCGCTCACAATTCCACACAACATACGAGCCGGAAGCATAAAGTGTAAAGCCTGG
GGTGCCTAATGAGTGAGCTAACTCACATTAATTGCGTTGCGCTCACTGCCCGCTTTCCAGTCGGGAAACCTG
TCGTGCCAGCTGCATTAATGAATCGGCCAACGCGCGGGGAGAGGCGGTTTGCGTATTGGGCGCTCTTCCGCT
TCCTCGCTCACTGACTCGCTGCGCTCGGTCGTTCGGCTGCGGCGAGCGGTATCAGCTCACTCAAAGGCGGTA
ATACGGTTATCCACAGAATCAGGGGATAACGCAGGAAAGAACATGTGAGCAAAAGGCCAGCAAAAGGCCAGG
AACCGTAAAAAGGCCGCGTTGCTGGCGTTTTTCCATAGGCTCCGCCCCCCTGACGAGCATCACAAAAATCGA
CGCTCAAGTCAGAGGTGGCGAAACCCGACAGGACTATAAAGATACCAGGCGTTTCCCCCTGGAAGCTCCCTC
GTGCGCTCTCCTGTTCCGACCCTGCCGCTTACCGGATACCTGTCCGCCTTTCTCCCTTCGGGAAGCGTGGCG
CTTTCTCATAGCTCACGCTGTAGGTATCTCAGTTCGGTGTAGGTCGTTCGCTCCAAGCTGGGCTGTGTGCAC
GAACCCCCCGTTCAGCCCGACCGCTGCGCCTTATCCGGTAACTATCGTCTTGAGTCCAACCCGGTAAGACAC
GACTTATCGCCACTGGCAGCAGCCACTGGTAACAGGATTAGCAAACCAAGGTATGTAGGCGGTGCTACAGAA
TTCTTGAAATGGTGGCCTAACTACGGCTACACTAGAAGAACAGTATTTGGTATCTGCGCTCTGCTGAACCCA
GTTACCTTCCGAAAAAGAATTGGTAACTTTTGATCGGCAAACAACCACGCTGGTACCGTGGTTTTTTTTTTG
CAACCACCAATTACCCCCAAAAAAAAGGATTCCAAAAAATCTTTTATTTTT

>1st_BASE_4899400_**SR_III_-_18C_-_20**_PLASMID_M13F-pUC_-40_
NNNNCNNNNTTGTATACGACTCACTATAGGGCGAATTGGGCCCGACGTCGCATGCTCCCGGCCGCCATGGCG
GCCGCGGGAATTCGATT**GGCAGTCTGGGCATACTTCACTCCCGGAGCTCTATACCGGGCCCGGGCCGTGGTA**
TTCGCTCTGCACAGAATCACTAGTGAATTCGCGGCCGCCTGCAGGTCGACCATATGGGAGAGCTCCCAACGC
GTTGGATGCATAGCTTGAGTATTCTATAGTGTCACCTAAATAGCTTGGCGTAATCATGGTCATAGCTGTTTC
CTGTGTGAAATTGTTATCCGCTCACAATTCCACACAACATACGAGCCGGAAGCATAAAGTGTAAAGCCTGGG
GTGCCTAATGAGTGAGCTAACTCACATTAATTGCGTTGCGCTCACTGCCCGCTTTCCAGTCGGGAAACCTGT
CGTGCCAGCTGCATTAATGAATCGGCCAACGCGCGGGGAGAGGCGGTTTGCGTATTGGGCGCTCTTCCGCTT
CCTCGCTCACTGACTCGCTGCGCTCGGTCGTTCGGCTGCGGCGAGCGGTATCAGCTCACTCAAAGGCGGTAA
TACGGTTATCCACAGAATCAGGGGATAACGCAGGAAAGAACATGTGAGCAAAAGGCCAGCAAAAGGCCAGGA
ACCGTAAAAAGGCCGCGTTGCTGGCGTTTTTCCATAGGCTCCGCCCCCCTGACGAGCATCACAAAAATCGAC
GCTCAAGTCAGAGGTGGCGAAACCCGACAGGACTATAAAGATACCAGGCGTTTCCCCCTGGAAGCTCCCTCG
TGCGCTCTCCTGTTCCGACCCTGCCGCTTACCGGATACCTGTCCGCCTTTCTCCCTTCGGGAAGCGTGGCGC
TTTCTCATAGCTCACGCTGTAGGTATCTCAGTTCGGTGTAGGTCGTTCGCTCCAAGCTGGGCTGTGTGCACG
AACCCCCCGTTCAGCCCGACCGCTGCGCCTTATCCGGTAACTATCGTCTTGAGTCCAACCCGGTAAGACACG
ACTTATCGCCACTGGCAGCAGCCACTGGTAACAGGATTAGCAGAGCGAGGTATGTAGGCGGTGCTACAGAGT
TCTTGAAATGGTGGCCTAACTACGGCTACCTAGAAAAACAGTATTTGGTATCTGCCCTCTGCTAAACCATTA
CCTTCGAAAAAGAATTGGTAACTTTTGATCCGCAAANAACCACCGCTGGTACCGTGGTTTTTTGTTTTNAAC
CACAAATTACCCCAAAAAAAAGGATTCAGAGAACCTTTATTTTTCTCAGGGGTTTAACCTCATGGGAAAGAA

>1st_BASE_4911311_**SR_III_-_18C_-_19**_PLASMID_M13F-pUC_-40_
NGNNCNGTGNTTGTATACGACTCACTATAGGGCGAATTGGGCCCGACGTCGCATGCTCCCGGCCGCCATGGC
GGCCGCGGGAATTCGATT**GGCAGTCTGGGCATACTTCACTCGGGGGGGGGGAGCTGGCTATAGGATTGCTGGT**
ATTCGCTCTGCACAGAATCACTAGTGAATTCGCGGCCGCCTGCAGGTCGACCATATGGGAGAGCTCCCAACG
CGTTGGATGCATAGCTTGAGTATTCTATAGTGTCACCTAAATAGCTTGGCGTAATCATGGTCATAGCTGTTT
CCTGTGTGAAATTGTTATCCGCTCACAATTCCACACAACATACGAGCCGGAAGCATAAAGTGTAAAGCCTGG
GGTGCCTAATGAGTGAGCTAACTCACATTAATTGCGTTGCGCTCACTGCCCGCTTTCCAGTCGGGAAACCTG
TCGTGCCAGCTGCATTAATGAATCGGCCAACGCGCGGGGAGAGGCGGTTTGCGTATTGGGCGCTCTTCCGCT
TCCTCGCTCACTGACTCGCTGCGCTCGGTCGTTCGGCTGCGGCGAGCGGTATCAGCTCACTCAAAGGCGGTA
ATACGGTTATCCACAGAATCAGGGGATAACGCAGGAAAGAACATGTGAGCAAAAGGCCAGCAAAAGGCCAGG
AACCGTAAAAAGGCCGCGTTGCTGGCGTTTTTCCATAGGCTCCGCCCCCCTGACGAGCATCACAAAAATCGA
CGCTCAAGTCAGAGGTGGCGAAACCCGACAGGACTATAAAGATACCAGGCGTTTCCCCCTGGAAGCTCCCTC
GTGCGCTCTCCTGTTCCGACCCTGCCGCTTACCGGATACCTGTCCGCCTTTCTCCCTTCGGGAAGCGTGGCG
CTTTCTCATAGCTCACGCTGTAGGTATCTCAGTTCGGTGTAGGTCGTTCGCTCCAAGCTGGGCTGTGTGCAC

GAACCCCCCGTTCAGCCCGACCGCTGCGCCTTATCCGGTAACTATCGTCTTGAGTCCAACCCGGTAAGACAC
GACTTATCGCCACTGGCAGCAGCCACTGGTAACAGGATTAGCAGAGCGAGGTATGTAGGCGGTGCTACAGAG
TTCTTGAAGTGGTGGCCTAACTACGGCTACACTAGAGGAACAGTATTTGGTATCTGCGCTCTGCTGAAGCCA
GTTACCTTCGGAAAAAGAATTGGTAGCTCTTGATCCGGCAAACAACCCCCGCTGGTACCGGTGGTTTTTTTG
TTGGCAACCCCCAGATTACCTCCAAAAAAAAGGATTCCAGANGAANTCT

>1st_BASE_4925920_**SR_III_-_18C_-_7**_Plasmid_M13F-pUC_-40_
NNNNNNNNNATGTATACGACTCACTATAGGGCGAATTGGGCCCGACGTCGCATGCTCCCGGCCGCCATGGCG
GCCGCGGGAATTCGATT**GGCAGTCTGGGCATACTTCACTCCCGGGGGCTGGGCGGCTGGCGGGGGCGTGGTA
TTCGCTCTGCACAGA**ATCACTAGTGAATTCGCGGCCGCCTGCAGGTCGACCATATGGGAGAGCTCCCAACGC
GTTGGATGCATAGCTTGAGTATTCTATAGTGTCACCTAAATAGCTTGGCGTAATCATGGTCATAGCTGTTTC
CTGTGTGAAATTGTTATCCGCTCACAATTCCACACAACATACGAGCCGGAAGCATAAAGTGTAAAGCCTGGG
GTGCCTAATGAGTGAGCTAACTCACATTAATTGCGTTGCGCTCACTGCCCGCTTTCCAGTCGGGAAACCTGT
CGTGCCAGCTGCATTAATGAATCGGCCAACGCGCGGGGAGAGGCGGTTTGCGTATTGGGCGCTCTTCCGCTT
CCTCGCTCACTGACTCGCTGCGCTCGGTCGTTCGGCTGCGGCGAGCGGTATCAGCTCACTCAAAGGCGGTAA
TACGGTTATCCACAGAATCAGGGGATAACGCAGGAAAGAACATGTGAGCAAAAGGCCAGCAAAAGGCCAGGA
ACCGTAAAAAGGCCGCGTTGCTGGCGTTTTTCCATAGGCTCCGCCCCCCTGACGAGCATCACAAAAATCGAC
GCTCAAGTCAGAGGTGGCGAAACCCGACAGGACTATAAAGATACCAGGCGTTTCCCCCTGGAAGCTCCCTCG
TGCGCTCTCCTGTTCCGACCCTGCCGCTTACCGGATACCTGTCCGCCTTTCTCCCTTCGGGAAGCGTGGCGC
TTTCTCATAGCTCACGCTGTAGGTATCTCAGTTCGGTGTAGGTCGTTCGCTCCAAGCTGGGCTGTGTGCACG
AACCCCCCGTTCAGCCCGACCGCTGCGCCTTATCCGGTAACTATCGTCTTGAGTCCAACCCGGTAAGACACG
ACTTATCGCCACTGGCAGCAGCCACTGGTAACAGGATTAGCAANGCAAGGTATGTAGGCGGTGCTACAGATT
TCTTGAAGTGGTGGCCTAACTACGGCTACCCTAGAAGAACAGTATTTGGTATCTGCCCTCTGCTGAAGCCAG
TTACTTTCGGAAAAAGAGTTGGTAGCTCTTGATCCGGCAAACAAACCACCGCTGGTACCGGGGTTTTTTTTT
TGCAACCGCAGATTACCCCCAAAAAAAGGATTCCAGAAGATCTTTGATTTTTTCACGGGGNTGAC

Group II

>1st_BASE_4899398_**SR_III_-_4C_-_18**_PLASMID_M13F-pUC_-40_
NNNGTTCNNNGNNGNATACGACTCACTATAGGGCGAATTGGGCCCGACGTCGCATGCTCCCGGCCGCCATGG
CGGCCGCGGGAATTCGATT**GGCAGTCTGGGCATACTTCACTCCTTTCCTATGGTTGGTGGTGCAGCCCGTGG
TATTCGCTCTGCACAGA**ATCACTAGTGAATTCGCGGCCGCCTGCAGGTCGACCATATGGGAGAGCTCCCAAC
GCGTTGGATGCATAGCTTGAGTATTCTATAGTGTCACCTAAATAGCTTGGCGTAATCATGGTCATAGCTGTT
TCCTGTGTGAAATTGTTATCCGCTCACAATTCCACACAACATACGAGCCGGAAGCATAAAGTGTAAAGCCTG
GGGTGCCTAATGAGTGAGCTAACTCACATTAATTGCGTTGCGCTCACTGCCCGCTTTCCAGTCGGGAAACCT
GTCGTGCCAGCTGCATTAATGAATCGGCCAACGCGCGGGGAGAGGCGGTTTGCGTATTGGGCGCTCTTCCGC
TTCCTCGCTCACTGACTCGCTGCGCTCGGTCGTTCGGCTGCGGCGAGCGGTATCAGCTCACTCAAAGGCGGT
AATACGGTTATCCACAGAATCAGGGGATAACGCAGGAAAGAACATGTGAGCAAAAGGCCAGCAAAAGGCCAG
GAACCGTAAAAAGGCCGCGTTGCTGGCGTTTTTCCATAGGCTCCGCCCCCCTGACGAGCATCACAAAAATCG
ACGCTCAAGTCAGAGGTGGCGAAACCCGACAGGACTATAAAGATACCAGGCGTTTCCCCCTGGAAGCTCCCT
CGTGCGCTCTCCTGTTCCGACCCTGCCGCTTACCGGATACCTGTCCGCCTTTCTCCCTTCGGGAAGCGTGGC
GCTTTCTCATAGCTCACGCTGTAGGTATCTCAGTTCGGTGTAGGTCGTTCGCTCCAAGCTGGGCTGTGTGCA
CGAACCCCCCGTTCAGCCCGACCGCTGCGCCTTATCCGGTAACTATCGTCTTGAGTCCAACCCGGTAAGACA
CGACTTATCGCCACTGGCAGCAGCCACTGGTAACAGGATTAGCAGAGCGAGGTATGTAGGCGGTGCTACAGA
GTTCTTGAAGTGGTGGCCTAACTACGGCTACCCTAAAAAAACAGTATTTGGTATTTGCCCTTTGCTGAACCC
NTTACCTTCGGAAAAAAATTGGTACCTNTTGATCCGGCAAAAAACCACGCTGGTAACGNTGGTTTTNTTGTT
NCAACCACCAAATACCCCCAAAAAAAAGGATCCCAGAAAAATCTTGTATTTTTTTTACGGGGTCTAA

>1st_BASE_4925918_**SR_III_-_4C_-_14**_Plasmid_M13F-pUC_-40_
NNNNNNNNGNNNTATACGACTCACTATAGGGCGAATTGGGCCCGACGTCGCATGCTCCCGGCCGCCATGGCG
GCCGCGGGAATTCGATT**GGCAGTCTGGGCATACTTCACTCATAAGGTGCCTTGGTCAGCGTGGTTCGTGGTA
TTCGCTCTGCACAGA**ATCACTAGTGAATTCGCGGCCGCCTGCAGGTCGACCATATGGGAGAGCTCCCAACGC
GTTGGATGCATAGCTTGAGTATTCTATAGTGTCACCTAAATAGCTTGGCGTAATCATGGTCATAGCTGTTTC
CTGTGTGAAATTGTTATCCGCTCACAATTCCACACAACATACGAGCCGGAAGCATAAAGTGTAAAGCCTGGG
GTGCCTAATGAGTGAGCTAACTCACATTAATTGCGTTGCGCTCACTGCCCGCTTTCCAGTCGGGAAACCTGT
CGTGCCAGCTGCATTAATGAATCGGCCAACGCGCGGGGAGAGGCGGTTTGCGTATTGGGCGCTCTTCCGCTT
CCTCGCTCACTGACTCGCTGCGCTCGGTCGTTCGGCTGCGGCGAGCGGTATCAGCTCACTCAAAGGCGGTAA
TACGGTTATCCACAGAATCAGGGGATAACGCAGGAAAGAACATGTGAGCAAAAGGCCAGCAAAAGGCCAGGA

ACCGTAAAAAGGCCGCGTTGCTGGCGTTTTTCCATAGGCTCCGCCCCCCTGACGAGCATCACAAAAATCGAC
GCTCAAGTCAGAGGTGGCGAAACCCGACAGGACTATAAAGATACCAGGCGTTTCCCCCTGGAAGCTCCCTCG
TGCGCTCTCCTGTTCCGACCCTGCCGCTTACCGGATACCTGTCCGCCTTTCTCCCTTCGGGAAGCGTGGCGC
TTTCTCATAGCTCACGCTGTAGGTATCTCAGTTCGGTGTAGGTCGTTCGCTCCAAGCTGGGCTGTGTGCACG
AACCCCCCGTTCAGCCCGACCGCTGCGCCTTATCCGGTAACTATCGTCTTGAGTCCAACCCGGTAAGACACG
ACTTATCGCCACTGGCAGCAGCCACTGGTAACAGGATTAGCAGAGCGAGGTATGTAGGCGGTGCTACAGAGT
TCTTGAAGTGGTGGCCTAACTACGGCTACACTAGAAGAACAGTATTTGGTATCTGCGCTCTGCTGAAGCCAG
TTACCTTCGGAAAAAGAATTGGTAGCTCTTGATCCGGCAAACAAACCACCGCTGGTACCGGTGGTTTTTTGT
TTGCAACCAACAAANTACCCCCAAAAAAAAGGATTTCAGAAAAATCTTNGATTTTTTTCCGGGNTT

>1st_BASE_4925922_**SR_III_-_18C_-_12**_Plasmid_M13F-pUC_-40_
NNNNCNNNANGNATACGACTCACTATAGGGCGAATTGGGCCCGACGTCGCATGCTCCCGGCCGCCATGGCGG
CCGCGGGAATTCGATT**GGCAGTCTGGGCATACTTCACTCGTAATGTCTCTGGTACACTTCGCGGCGTGGTAT**
TCGCTCTGCACAGAATCACTAGTGAATTCGCGGCCGCCTGCAGGTCGACCATATGGGAGAGCTCCCAACGCG
TTGGATGCATAGCTTGAGTATTCTATAGTGTCACCTAAATAGCTTGGCGTAATCATGGTCATAGCTGTTTCC
TGTGTGAAATTGTTATCCGCTCACAATTCCACACAACATACGAGCCGGAAGCATAAAGTGTAAAGCCTGGGG
TGCCTAATGAGTGAGCTAACTCACATTAATTGCGTTGCGCTCACTGCCCGCTTTCCAGTCGGGAAACCTGTC
GTGCCAGCTGCATTAATGAATCGGCCAACGCGCGGGGAGAGGCGGTTTGCGTATTGGGCGCTCTTCCGCTTC
CTCGCTCACTGACTCGCTGCGCTCGGTCGTTCGGCTGCGGCGAGCGGTATCAGCTCACTCAAAGGCGGTAAT
ACGGTTATCCACAGAATCAGGGGATAACGCAGGAAAGAACATGTGAGCAAAAGGCCAGCAAAAGGCCAGGAA
CCGTAAAAAGGCCGCGTTGCTGGCGTTTTTCCATAGGCTCCGCCCCCCTGACGAGCATCACAAAAATCGACG
CTCAAGTCAGAGGTGGCGAAACCCGACAGGACTATAAAGATACCAGGCGTTTCCCCCTGGAAGCTCCCTCGT
GCGCTCTCCTGTTCCGACCCTGCCGCTTACCGGATACCTGTCCGCCTTTCTCCCTTCGGGAAGCGTGGCGCT
TTCTCATAGCTCACGCTGTAGGTATCTCAGTTCGGTGTAGGTCGTTCGCTCCAAGCTGGGCTGTGTGCACGA
ACCCCCCGTTCAGCCCGACCGCTGCGCCTTATCCGGTAACTATCGTCTTGAGTCCAACCCGGTAAGACACGA
CTTATCGCCACTGGCAGCAGCCACTGGTAACAGGATTAGCAGAGCGAGGTATGTAGGCGGTGCTACAGAGTT
CTTGAAGTGGTGGCCTAACTACGGCTACACTAGAAGAACAGTATTTGGTATCTGCGCTCTGCTGAAGCCAGT
TACCTTCGGAAAAAGAGTTGGTAGCTCTTGATCCGGCAACAAACCACCGCTGGTACCGGGGGTTTTTTGTTN
GCAACCANCAANTTACCCCCAAAAAAAAAGGATTTCAGAAGAATCTTTGATTTTTTCACGGGG

>1st_BASE_4925924_**SR_III_-_18C_-_17**_Plasmid_M13F-pUC_-40_
NNNNNNNNNTTGTATACGACTCACTATAGGGCGAATTGGGCCCGACGTCGCATGCTCCCGGCCGCCATGGCG
GCCGCGGGAATTCGATT**GGCAGTCTGGGCATACTTCACTCTACAAATACCGCTTCTCAGGTGTCGCGTGGTA**
TTCGCTCTGCACAGAATCACTAGTGAATTCGCGGCCGCCTGCAGGTCGACCATATGGGAGAGCTCCCAACGC
GTTGGATGCATAGCTTGAGTATTCTATAGTGTCACCTAAATAGCTTGGCGTAATCATGGTCATAGCTGTTTC
CTGTGTGAAATTGTTATCCGCTCACAATTCCACACAACATACGAGCCGGAAGCATAAAGTGTAAAGCCTGGG
GTGCCTAATGAGTGAGCTAACTCACATTAATTGCGTTGCGCTCACTGCCCGCTTTCCAGTCGGGAAACCTGT
CGTGCCAGCTGCATTAATGAATCGGCCAACGCGCGGGGAGAGGCGGTTTGCGTATTGGGCGCTCTTCCGCTT
CCTCGCTCACTGACTCGCTGCGCTCGGTCGTTCGGCTGCGGCGAGCGGTATCAGCTCACTCAAAGGCGGTAA
TACGGTTATCCACAGAATCAGGGGATAACGCAGGAAAGAACATGTGAGCAAAAGGCCAGCAAAAGGCCAGGA
ACCGTAAAAAGGCCGCGTTGCTGGCGTTTTTCCATAGGCTCCGCCCCCCTGACGAGCATCACAAAAATCGAC
GCTCAAGTCAGAGGTGGCGAAACCCGACAGGACTATAAAGATACCAGGCGTTTCCCCCTGGAAGCTCCCTCG
TGCGCTCTCCTGTTCCGACCCTGCCGCTTACCGGATACCTGTCCGCCTTTCTCCCTTCGGGAAGCGTGGCGC
TTTCTCATAGCTCACGCTGTAGGTATCTCAGTTCGGTGTAGGTCGTTCGCTCCAAGCTGGGCTGTGTGCACG
AACCCCCCGTTCAGCCCGACCGCTGCGCCTTATCCGGTAACTATCGTCTTGAGTCCAACCCGGTAAGACACG
ACTTATCGCCACTGGCAGCAGCCACTGGTAACAGGATTAGCAGAGCGAGGTATGTAGGCGGTGCTACAGAGT
TCTTGAAGTGGTGGCCTAACTACGGCTACACTAGAAGAACAGTATTTGGTATCTGCGCTCTGCTGAAGCCAG
TTACCTTCGGAAAAAGAATTGGTAGCTCTTGATCCGGCAACCAACCACCGCTGGTACCGGTGGTTTTTTTGT
TGCAACCACCAATTACCCGCAAAAAAAAGGATTNNANAAAATCTTTGATTTTTCTACGGGGTCTGACCNCAN
TGGAACAAAATCCCCTTAAGGGATTTTGGTNN

Bibliography

[1] WHO, Global Tuberculosis Report 2023, (2024). https://www.who.int/teams/global-tuberculosis-programme/tb-reports/global-tuberculosis-report-2023 (accessed May 9, 2024).

[2] R.M.G.J. Houben, P.J. Dodd, The global burden of latent tuberculosis infection: a re-estimation using mathematical modelling, PLoS Med 13 (2016) e1002152.

[3] J. Hayman, Mycobacterium ulcerans: an infection from Jurassic time?, (1984).

[4] S. Gagneux, Ecology and evolution of Mycobacterium tuberculosis, Nat Rev Microbiol 16 (2018) 202–213.

[5] I. Barberis, N.L. Bragazzi, L. Galluzzo, M. Martini, The history of tuberculosis: from the first historical records to the isolation of Koch's bacillus, J Prev Med Hyg 58 (2017) E9. https://pmc.ncbi.nlm.nih.gov/articles/PMC5432783/ (accessed November 12, 2024).

[6] T.M. Daniel, The history of tuberculosis, Respir Med 100 (2006) 1862–1870.

[7] S. Luca, T. Mihaescu, History of BCG vaccine., Maedica (Bucur) 8 (2013) 53–58.

[8] P.D. Hart, Efficacy and applicability of mass BCG vaccination in tuberculosis control., Br Med J 1 (1967) 587.

[9] S.H. Kim, J.H. Shin, Identification of nontuberculous mycobacteria using multilocous sequence analysis of 16S rRNA, hsp65, and rpoB, J Clin Lab Anal 32 (2018) e22184.

[10] C. Arnold, Molecular evolution of Mycobacterium tuberculosis, Clinical Microbiology and Infection 13 (2007) 120–128.

[11] M.C. Gutierrez, N. Ahmed, E. Willery, S. Narayanan, S.E. Hasnain, D.S. Chauhan, V.M. Katoch, V. Vincent, C. Locht, P. Supply, Predominance of ancestral lineages of Mycobacterium tuberculosis in India, Emerg Infect Dis 12 (2006) 1367.

[12] W.F. Wells, Airborne contagion and air hygiene: an ecological study of droplet infection, Harvard University Press for the Commonwealth Fund, 1955.

[13] M. Coleman, L. Martinez, G. Theron, R. Wood, B. Marais, Mycobacterium tuberculosis transmission in high-incidence settings—New paradigms and insights, Pathogens 11 (2022) 1228.

[14] CDC, Tuberculosis Transmission and Pathogenesis of Tuberculosis, Atlanta, Geoorgia, 2019. https://www.cdc.gov/tb/education/ssmodules/pdfs/module1.pdf (accessed April 19, 2024).

[15] L. Ramakrishnan, Revisiting the role of the granuloma in tuberculosis, Nat Rev Immunol 12 (2012) 352–366.

[16] J.D. Ernst, The immunological life cycle of tuberculosis, Nat Rev Immunol 12 (2012) 581–591.

[17] R.L. Leistikow, R.A. Morton, I.L. Bartek, I. Frimpong, K. Wagner, M.I. Voskuil, The Mycobacterium tuberculosis DosR regulon assists in metabolic homeostasis and enables rapid recovery from nonrespiring dormancy, J Bacteriol 192 (2010) 1662–1670.

[18] B.D. Kana, B.G. Gordhan, K.J. Downing, N. Sung, G. Vostroktunova, E.E. Machowski, L. Tsenova, M. Young, A. Kaprelyants, G. Kaplan, others, The resuscitation-promoting factors of Mycobacterium tuberculosis are required for virulence and resuscitation from dormancy but are collectively dispensable for growth in vitro, Mol Microbiol 67 (2008) 672–684.

[19] F. Ahmad, M.I. Ansari, M. Ashfaque, M.H. Islam, M. Khubaib, others, Toxin-Antitoxin system of Mycobacterium tuberculosis: Roles beyond stress sensor and growth regulator, Tuberculosis (2023) 102395.

[20] M.E. Urbanowski, A.A. Ordonez, C.A. Ruiz-Bedoya, S.K. Jain, W.R. Bishai, Cavitary tuberculosis: the gateway of disease transmission, Lancet Infect Dis 20 (2020) e117–e128.

[21] I. Rodrigues, A. Aguiar, G.B. Migliori, R. Duarte, Impact of the COVID-19 pandemic on tuberculosis services, Pulmonology 28 (2022) 210–219.

[22] D. Visca, C.W.M. Ong, S. Tiberi, R. Centis, L. D'ambrosio, B. Chen, J. Mueller, P. Mueller, R. Duarte, M. Dalcolmo, others, Tuberculosis and COVID-19 interaction: a review of biological, clinical and public health effects, Pulmonology 27 (2021) 151–165.

[23] K. Siddiqi, M.-L. Lambert, J. Walley, Clinical diagnosis of smear-negative pulmonary tuberculosis in low-income countries: the current evidence, Lancet Infect Dis 3 (2003) 288–296.

[24] E. Girardi, M.S. Schepisi, D. Goletti, M. Bates, P. Mwaba, D. Yeboah-Manu, F. Ntoumi, F. Palmieri, M. Maeurer, A. Zumla, others, The global dynamics of diabetes and tuberculosis: the impact of migration and policy implications, International Journal of Infectious Diseases 56 (2017) 45–53.

[25] M. Purohit, T. Mustafa, Laboratory diagnosis of extra-pulmonary tuberculosis (EPTB) in resource-constrained setting: state of the art, challenges and the need, J Clin Diagn Res 9 (2015) EE01.

[26] D. Pedrazzoli, M. Lalli, D. Boccia, R. Houben, K. Kranzer, Can tuberculosis patients in resource-constrained settings afford chest radiography?, European Respiratory Journal 49 (2017).

[27] H. Walker, W. Hall, J. Hurst, Clinical methods: the history, physical, and laboratory examinations, (1990). https://pubmed.ncbi.nlm.nih.gov/21250045/ (accessed November 12, 2024).

[28] K.R. Steingart, M. Henry, V. Ng, P.C. Hopewell, A. Ramsay, J. Cunningham, R. Urbanczik, M. Perkins, M.A. Aziz, M. Pai, Fluorescence versus conventional sputum smear microscopy for tuberculosis: a systematic review, Lancet Infect Dis 6 (2006) 570–581.

[29] WHO, Biomarkers in risk assessment: validity and validation, (2001).

[30] M. Pai, C.M. Denkinger, S. V. Kik, M.X. Rangaka, A. Zwerling, O. Oxlade, J.Z. Metcalfe, A. Cattamanchi, D.W. Dowdy, K. Dheda, N. Banaei, Gamma interferon release assays for detection of Mycobacterium tuberculosis infection, Clin Microbiol Rev 27 (2014) 3–20. https://doi.org/10.1128/CMR.00034-13/ASSET/075F2933-2E4D-486D-BD65-6E945AE95C32/ASSETS/GRAPHIC/ZCM9990924460005.JPEG.

[31] K.M. Little, M. Pai, D.W. Dowdy, Costs and consequences of using interferon-γ release assays for the diagnosis of active tuberculosis in India, PLoS One 10 (2015) e0124525.

[32] T. Broger, R. Basu Roy, A. Filomena, C.H. Greef, S. Rimmele, J. Havumaki, D. Danks, N. Schneiderhan-Marra, C.M. Gray, M. Singh, others, Diagnostic performance of tuberculosis-specific IgG antibody profiles in patients with presumptive tuberculosis from two continents, Clinical Infectious Diseases 64 (2017) 947–955.

[33] M.M. Ninan, M. Gowri, D.J. Christopher, P. Rupali, J.S. Michael, The diagnostic utility of line probe assays for multidrug-resistant tuberculosis, Pathog Glob Health 110 (2016) 194–199.

[34] J.H. Soh, H.-M. Chan, J.Y. Ying, Strategies for developing sensitive and specific nanoparticle-based lateral flow assays as point-of-care diagnostic device, Nano Today 30 (2020) 100831.

[35] R.M. Califf, Biomarker definitions and their applications, Exp Biol Med 243 (2018) 213–221.

[36] B.M.F. Nogueira, S. Krishnan, B. Barreto-Duarte, M. Araújo-Pereira, A.T.L. Queiroz, J.J. Ellner, P. Salgame, T.J. Scriba, T.R. Sterling, A. Gupta, others, Diagnostic biomarkers for active tuberculosis: progress and challenges, EMBO Mol Med 14 (2022) e14088.

[37] R.S. Wallis, M. Pai, D. Menzies, T.M. Doherty, G. Walzl, M.D. Perkins, A. Zumla, Biomarkers and diagnostics for tuberculosis: progress, needs, and translation into practice, The Lancet 375 (2010) 1920–1937.

[38] R. McNerney, P. Daley, Towards a point-of-care test for active tuberculosis: obstacles and opportunities, Nat Rev Microbiol 9 (2011) 204–213.

[39] M.M. Thomas, T.S.C. Hinks, S. al Raghuraman, N. Ramalingam, M. Ernst, R. Nau, C. Lange, K. Kösters, C. Gnanamuthu, G.T. John, others, Rapid diagnosis of Mycobacterium tuberculosis meningitis by enumeration of cerebrospinal fluid antigen-specific T-cells, The International Journal of Tuberculosis and Lung Disease 12 (2008) 651–657.

[40] C. Jafari, S. Thijsen, G. Sotgiu, D. Goletti, J.A.D. Ben\'\itez, M. Losi, R. Eberhardt, D. Kirsten, B. Kalsdorf, A. Bossink, others, Bronchoalveolar lavage enzyme-linked immunospot for a rapid diagnosis of tuberculosis: a Tuberculosis Network European Trialsgroup study, Am J Respir Crit Care Med 180 (2009) 666–673.

[41] H. Albert, R.R. Nathavitharana, C. Isaacs, M. Pai, C.M. Denkinger, C.C. Boehme, Development, roll-out and impact of Xpert MTB/RIF for tuberculosis: what lessons have we learnt and how can we do better?, European Respiratory Journal 48 (2016) 516–525.

[42] S. Hazra, S. Patra, Alleviating the neglected tropical diseases: recent developments in diagnostics and detection, Curr Top Med Chem 18 (2018) 1559–1574.

[43] M.D. Perkins, D.R. Bell, Working without a blindfold: the critical role of diagnostics in malaria control, Malar J 7 (2008) 1–9.

[44] F. for Innovative New Diagnostics, S.P. for Research, T. in Tropical Diseases, W.H. Organization, Diagnostics for tuberculosis: global demand and market potential, World Health Organization, 2006.

[45] M. Vitoria, R. Granich, C.F. Gilks, C. Gunneberg, M. Hosseini, W. Were, M. Raviglione, K.M. De Cock, The global fight against HIV/AIDS, tuberculosis, and malaria: current status and future perspectives, Am J Clin Pathol 131 (2009) 844–848.

[46] St. Cole, R. Brosch, J. Parkhill, T. Garnier, C. Churcher, D. Harris, S. V Gordon, K. Eiglmeier, S. Gas, C.E. Barry Iii, others, Deciphering the biology of Mycobacterium tuberculosis from the complete genome sequence, Nature 396 (1998) 190.

[47] G. Delogu, M.J. Brennan, R. Manganelli, PE and PPE genes: a tale of conservation and diversity, Strain Variation in the Mycobacterium Tuberculosis Complex: Its Role in Biology, Epidemiology and Control (2017) 191–207.

[48] A. Bekmurzayeva, M. Sypabekova, D. Kanayeva, Tuberculosis diagnosis using immunodominant, secreted antigens of Mycobacterium tuberculosis, Tuberculosis 93 (2013) 381–388.

[49] C.-J. Kuo, C.P. Ptak, C.-L. Hsieh, B.L. Akey, Y.-F. Chang, Elastin, a novel extracellular matrix protein adhering to mycobacterial antigen 85 complex, Journal of Biological Chemistry 288 (2013) 3886–3896.

[50] G. Harth, B.-Y. Lee, J. Wang, D.L. Clemens, M.A. Horwitz, Novel insights into the genetics, biochemistry, and immunocytochemistry of the 30-kilodalton major extracellular protein of Mycobacterium tuberculosis, Infect Immun 64 (1996) 3038–3047.

[51] L. Kremer, W.N. Maughan, R.A. Wilson, L.G. Dover, G.S. Besra, The M. tuberculosis antigen 85 complex and mycolyltransferase activity, Lett Appl Microbiol 34 (2002) 233–237.

[52] J.T. Belisle, V.D. Vissa, T. Sievert, K. Takayama, P.J. Brennan, G.S. Besra, Role of the major antigen of Mycobacterium tuberculosis in cell wall biogenesis, Science (1979) 276 (1997) 1420–1422.

[53] S. Haldar, M. Bose, P. Chakrabarti, H.F. Daginawala, B.C. Harinath, R.S. Kashyap, S. Kulkarni, A. Majumdar, H.K. Prasad, C. Rodrigues, others, Improved laboratory diagnosis of tuberculosis–the Indian experience, Tuberculosis 91 (2011) 414–426.

[54] H.P. Godfrey, Z. Feng, S. Mandy, K. Mandy, K. Huygen, J. De Bruyn, C. Abou-Zeid, H.G. Wiker, S. Nagai, H. Tasaka, Modulation of expression of delayed hypersensitivity by mycobacterial antigen 85 fibronectin-binding proteins, Infect Immun 60 (1992) 2522–2528.

[55] G. Kumar, P.K. Dagur, M. Singh, V.S. Yadav, R. Dayal, H.B. Singh, V.M. Katoch, U. Sengupta, B. Joshi, Diagnostic potential of Ag85C in comparison to various secretory antigens for childhood tuberculosis, Scand J Immunol 68 (2008) 177–183.

[56] R. Dayal, A. Singh, V.M. Katoch, B. Joshi, D.S. Chauhan, P. Singh, G. Kumar, V.D. Sharma, Serological diagnosis of tuberculosis, The Indian Journal of Pediatrics 75 (2008) 1219–1221.

[57] R.S. Kashyap, S.D. Shekhawat, A.R. Nayak, H.J. Purohit, G.M. Taori, H.F. Daginawala, Diagnosis of tuberculosis infection based on synthetic peptides from Mycobacterium tuberculosis antigen 85 complex, Clin Neurol Neurosurg 115 (2013) 678–683.

[58] D.S. Chauhan, V.D. Sharma, D. Parashar, A. Chauhan, D. Singh, H.B. Singh, R. Das, B.M. Aggarwal, B. Malhotra, A. Jain, others, Molecular typing of Mycobacterium tuberculosis isolates from different parts of India based on IS6110 element polymorphism using RFLP analysis, Indian Journal of Medical Research 125 (2007) 577–581.

[59] A. Raj, N. Singh, K.B. Gupta, D. Chaudhary, A. Yadav, A. Chaudhary, K. Agarwal, M. Varma-Basil, R. Prasad, G.K. Khuller, others, Comparative evaluation of several gene targets for designing a multiplex-PCR for an early diagnosis of extrapulmonary tuberculosis, Yonsei Med J 57 (2016) 88.

[60] R.J. Wilkinson, L.E. DesJardin, N. Islam, B.M. Gibson, R.A. Kanost, K.A. Wilkinson, D. Poelman, K.D. Eisenach, Z. Toossi, An increase in expression of a Mycobacterium tuberculosis mycolyl transferase gene (fbpB) occurs early after infection of human monocytes, Mol Microbiol 39 (2001) 813–821.

[61] M. Fauville-Dufaux, B. Vanfleteren, L. De Wit, J.P. Vincke, J.-P. Van Vooren, M.D. Yates, E. Serruys, J. Content, Rapid detection of tuberculous and non-tuberculous mycobacteria by polymerase chain reaction amplification of a 162 bp DNA fragment from antigen 85, European Journal of Clinical Microbiology and Infectious Diseases 11 (1992) 797–803.

[62] Y. Xu, P. Wu, H. Zhang, J. Li, Rapid detection of Mycobacterium tuberculosis based on antigen 85B via real-time recombinase polymerase amplification, Lett Appl Microbiol 72 (2021) 106–112.

[63] R.S. Kashyap, K.M. Dobos, J.T. Belisle, H.J. Purohit, N.H. Chandak, G.M. Taori, H.F. Daginawala, Demonstration of components of antigen 85 complex in cerebrospinal fluid of tuberculous meningitis patients, Clinical and Vaccine Immunology 12 (2005) 752–758.

[64] H. Mukundan, S. Kumar, D.N. Price, S.M. Ray, Y.-J. Lee, S. Min, S. Eum, J. Kubicek-Sutherland, J.M. Resnick, W.K. Grace, others, Rapid detection of Mycobacterium tuberculosis biomarkers in a sandwich immunoassay format using a waveguide-based optical biosensor, Tuberculosis 92 (2012) 407–416.

[65] B. Murphy, E. Dempsey, Evaluation of an Ag85B immunosensor with potential for electrochemical Mycobacterium tuberculosis diagnostics, ECS Journal of Solid State Science and Technology 9 (2020) 115011.

[66] J. Ma, M. Du, C. Wang, X. Xie, H. Wang, T. Li, S. Chen, L. Zhang, S. Mao, X. Zhou, others, Rapid and sensitive detection of mycobacterium tuberculosis by an enhanced nanobiosensor, ACS Sens 6 (2021) 3367–3376.

[67] N. Singh, V. Sreenivas, K.B. Gupta, A. Chaudhary, A. Mittal, M. Varma-Basil, R. Prasad, S.K. Gakhar, G.K. Khuller, P.K. Mehta, Diagnosis of pulmonary and extrapulmonary tuberculosis based on detection of mycobacterial antigen 85B by immuno-PCR, Diagn Microbiol Infect Dis 83 (2015) 359–364.

[68] A. Khan, R. Singh, S. Sharma, V. Singh, A. Sheoran, A. Soni, V. Dhull, P.S. Gill, A. Yadav, D. Chaudhary, others, Diagnosis of osteoarticular tuberculosis by immuno-PCR assay based on mycobacterial antigen 85 complex detection, Lett Appl Microbiol 74 (2022) 17–26.

[69] K. Chuensirikulchai, W. Laopajon, P. Phunpae, N. Apiratmateekul, S. Surinkaew, C. Tayapiwatana, S. Pata, W. Kasinrerk, Sandwich antibody-based biosensor system for identification of Mycobacterium tuberculosis complex and nontuberculous mycobacteria, J Immunoassay Immunochem 40 (2019) 590–604.

[70] B. Acharya, A. Acharya, S. Gautam, S.P. Ghimire, G. Mishra, N. Parajuli, B. Sapkota, Advances in diagnosis of Tuberculosis: an update into molecular diagnosis of Mycobacterium tuberculosis, Mol Biol Rep 47 (2020) 4065–4075. https://doi.org/10.1007/S11033-020-05413-7/FIGURES/3.

[71] P. Andersen, M.E. Munk, J.M. Pollock, T.M. Doherty, Specific immune-based diagnosis of tuberculosis, The Lancet 356 (2000) 1099–1104.

[72] T. Notomi, H. Okayama, H. Masubuchi, T. Yonekawa, K. Watanabe, N. Amino, T. Hase, Loop-mediated isothermal amplification of DNA, Nucleic Acids Res 28 (2000) e63–e63.

[73] T. Iwamoto, T. Sonobe, K. Hayashi, Loop-mediated isothermal amplification for direct detection of Mycobacterium tuberculosis complex, M. avium, and M. intracellulare in sputum samples, J Clin Microbiol 41 (2003) 2616–2622.

[74] Z. Liu, C. Zhu, H. Yang, H. Hu, Y. Feng, L. Qin, Z. Cui, A. Bi, R. Zheng, R. Jin, others, Clinical value of ELISA-MPT64 for the diagnosis of tuberculous pleurisy, Curr Microbiol 65 (2012) 313–318.

[75] C. Zhu, J. Liu, Y. Ling, H. Yang, Z. Liu, R. Zheng, L. Qin, Z. Hu, Evaluation of the clinical value of ELISA based on MPT64 antibody aptamer for serological diagnosis of pulmonary tuberculosis, BMC Infect Dis 12 (2012) 1–8.

[76] Y. Xie, H. Ning, Y. Lu, J. Kang, L. Bai, T. Dai, J. Hu, Z. Xu, B. Liu, Y. Bai, Establishment and preliminary application of Mycobacterium tuberculosis MPT64 double-antibody sandwich ELISA., (2023).

[77] R. Qu, K. Wu, J. Wu, X. Fan, J. Lu, Prokaryotic expression of early secretory protein MPT64 from Mycobacterium tuberculosis and its application in serological diagnosis of tuberculosis., (2021).

[78] K. Sakashita, R. Takeuchi, K. Takeda, M. Takamori, K. Ito, Y. Igarashi, E. Hayashi, M. Iguchi, M. Ono, T. Kashiyama, others, Ultrasensitive enzyme-linked immunosorbent assay for the detection of MPT64 secretory antigen to evaluate Mycobacterium tuberculosis viability in sputum, International Journal of Infectious Diseases 96 (2020) 244–253.

[79] T. Takahashi, M. Tamura, T. Takasu, others, The PCR-based diagnosis of central nervous system tuberculosis: up to date, Tuberc Res Treat 2012 (2012).

[80] T. Takahashi, M. Tamura, Y. Asami, E. Kitamura, K. Saito, T. Suzuki, S.N. Takahashi, K. Matsumoto, S. Sawada, E. Yokoyama, others, Novel wide-range quantitative nested real-time PCR assay for Mycobacterium tuberculosis DNA: clinical application for diagnosis of tuberculous meningitis, J Clin Microbiol 46 (2008) 1698–1707.

[81] T. Takahashi, M. Tamura, Y. Asami, E. Kitamura, K. Saito, T. Suzuki, S.N. Takahashi, K. Matsumoto, S. Sawada, E. Yokoyama, others, Novel wide-range quantitative nested real-time PCR assay for Mycobacterium tuberculosis DNA: development and methodology, J Clin Microbiol 46 (2008) 1708–1715.

[82] B.W. Lee, J. Tan, S.C. Wong, C.B. Tan, H.K. Yap, P.S. Low, J.N. Chia, J.S.H. Tay, DNA amplification by the polymerase chain reaction for the rapid diagnosis of tuberculous meningitis. Comparison of protocols involving three mycobacterial DNA sequences, IS6110, 65 kDa antigen, and MPB64, J Neurol Sci 123 (1994) 173–179.

[83] P.Y.-F. Liu, Z.-Y. Shi, Y.-J. Lau, B.-S. Hu, Rapid diagnosis of tuberculous meningitis by a simplified nested amplification protocol, Neurology 44 (1994) 1161.

[84] D. Gou, G. Xie, Y. Li, X. Zhang, H. Chen, Voltammetric immunoassay for Mycobacterium tuberculosis secretory protein MPT64 based on a synergistic amplification strategy using rolling circle amplification and a gold electrode modified with graphene oxide, Fe 3 O 4 and Pt nanoparticles, Microchimica Acta 185 (2018) 1–9.

[85] G. Seo, G. Lee, W. Kim, I. An, M. Choi, S. Jang, Y.-J. Park, J.-O. Lee, D. Cho, E.C. Park, Ultrasensitive biosensing platform for Mycobacterium tuberculosis detection based on functionalized graphene devices, Front Bioeng Biotechnol 11 (2023) 1313494.

[86] S. Nzuza, S. Ombinda-Lemboumba, H. Abrahamse, P. Mthunzi-Kufa, S.H. Chauke, Improved sensitivity of tuberculosis antigen MPT64 detection using SPR phase difference, in: Optical Interactions with Tissue and Cells XXXV, 2024: pp. 126–132.

[87] B.D. Malhotra, A. Chaubey, Biosensors for clinical diagnostics industry, Sens Actuators B Chem 91 (2003) 117–127.

[88] E.E. Ferapontova, Hybridization Biosensors Relying on Electrical Properties of Nucleic Acids, Electroanalysis 29 (2017) 6–13. https://doi.org/10.1002/ELAN.201600593.

[89] B. Huo, Y. Hu, Z. Gao, G. Li, Recent advances on functional nucleic acid-based biosensors for detection of food contaminants, Talanta 222 (2021) 121565. https://doi.org/10.1016/J.TALANTA.2020.121565.

[90] X. Yu, S. Zhang, W. Guo, B. Li, Y. Yang, B. Xie, K. Li, L. Zhang, Recent Advances on Functional Nucleic-Acid Biosensors, Sensors 2021, Vol. 21, Page 7109 21 (2021) 7109. https://doi.org/10.3390/S21217109.

[91] X. Cao, C. Chen, Q. Zhu, Biosensors based on functional nucleic acids and isothermal amplification techniques, Talanta 253 (2023) 123977. https://doi.org/10.1016/J.TALANTA.2022.123977.

[92] Z. yue Wang, P. Li, L. Cui, J.G. Qiu, B.H. Jiang, C. yang Zhang, Integration of nanomaterials with nucleic acid amplification approaches for biosensing, TrAC Trends in Analytical Chemistry 129 (2020) 115959. https://doi.org/10.1016/J.TRAC.2020.115959.

[93] E. Rasouli, Z. Shahnavaz, W.J. Basirun, M. Rezayi, A. Avan, M. Ghayour-Mobarhan, R. Khandanlou, M.R. Johan, Advancements in electrochemical DNA sensor for detection of human papilloma virus - A review, Anal Biochem 556 (2018) 136–144. https://doi.org/10.1016/J.AB.2018.07.002.

[94] S. Campuzano, P. Yáñez-Sedeño, J. Manuel Pingarrón, Molecular Biosensors for Electrochemical Detection of Infectious Pathogens in Liquid Biopsies: Current Trends and Challenges, Sensors 2017, Vol. 17, Page 2533 17 (2017) 2533. https://doi.org/10.3390/S17112533.

[95] A.D. Ellington, J.W. Szostak, Selection in vitro of single-stranded DNA molecules that fold into specific ligand-binding structures, Nature 355 (1992) 850–852.

[96] J. Jeon, J. Lee, J. So, J. Lee, H. Lee, Y. Chang, S. Shin, J. Jo, C. Ban, Homogeneous fluorescent aptasensor for active tuberculosis diagnosis by direct quantification of circulating TB7. 7 based on aptamer beacon with graphene oxide, Sens Actuators B Chem 317 (2020) 128126.

[97] W. Zhao, J.C.F. Lam, W. Chiuman, M.A. Brook, Y. Li, Enzymatic cleavage of nucleic acids on gold nanoparticles: a generic platform for facile colorimetric biosensors, Small 4 (2008) 810–816.

[98] A.D. Ellington, J.W. Szostak, In vitro selection of RNA molecules that bind specific ligands, Nature 346 (1990) 818–822.

[99] L.F. Yang, M. Ling, N. Kacherovsky, S.H. Pun, Aptamers 101: aptamer discovery and in vitro applications in biosensors and separations, Chem Sci (2023).

[100] N. Hamaguchi, A. Ellington, M. Stanton, Aptamer beacons for the direct detection of proteins, Anal Biochem 294 (2001) 126–131.

[101] M. MacGregor-Fairlie, S. Wilkinson, G.S. Besra, P.G. Oppenheimer, Tuberculosis diagnostics: overcoming ancient challenges with modern solutions, Emerg Top Life Sci 4 (2020) 435–448. https://doi.org/10.1042/ETLS20200335.

[102] V. Cengiz Ozalp, M. Kavruk, O. Dilek, A. Tahir Bayrac, Aptamers: molecular tools for medical diagnosis, Curr Top Med Chem 15 (2015) 1125–1137.

[103] B. Golichenari, R. Nosrati, A. Farokhi-Fard, K. Abnous, F. Vaziri, J. Behravan, Nano-biosensing approaches on tuberculosis: Defy of aptamers, Biosens Bioelectron 117 (2018) 319–331.

[104] M. Yüce, N. Ullah, H. Budak, Trends in aptamer selection methods and applications, Analyst 140 (2015) 5379–5399.

[105] D. Mabey, R.W. Peeling, A. Ustianowski, M.D. Perkins, Diagnostics for the developing world, Nat Rev Microbiol 2 (2004) 231–240.

[106] F. He, Y. Xiong, J. Liu, F. Tong, D. Yan, Construction of Au-IDE/CFP10-ESAT6 aptamer/DNA-AuNPs MSPQC for rapid detection of Mycobacterium tuberculosis, Biosens Bioelectron 77 (2016) 799–804.

[107] L.S. Rotherham, C. Maserumule, K. Dheda, J. Theron, M. Khati, Selection and application of ssDNA aptamers to detect active TB from sputum samples, (2012).

[108] X.-L. Tang, Y.-X. Zhou, S.-M. Wu, Q. Pan, B. Xia, X.-L. Zhang, CFP10 and ESAT6 aptamers as effective Mycobacterial antigen diagnostic reagents, Journal of Infection 69 (2014) 569–580.

[109] E. Mozioglu, O. Gokmen, C. Tamerler, Z.T. Kocagoz, M. Akgoz, Selection of nucleic acid aptamers specific for Mycobacterium tuberculosis, Appl Biochem Biotechnol 178 (2016) 849–864.

[110] D.R. Martin, N.R. Sibuyi, P. Dube, A.O. Fadaka, R. Cloete, M. Onani, A.M. Madiehe, M. Meyer, Aptamer-Based Diagnostic Systems for the Rapid Screening of TB at the Point-of-Care, Diagnostics 2021, Vol. 11, Page 1352 11 (2021) 1352. https://doi.org/10.3390/DIAGNOSTICS11081352.

[111] S. Lavania, R. Das, A. Dhiman, V.P. Myneedu, A. Verma, N. Singh, T.K. Sharma, J.S. Tyagi, Aptamer-based TB antigen tests for the rapid diagnosis of pulmonary tuberculosis: potential utility in screening for tuberculosis, ACS Infect Dis 4 (2018) 1718–1726.

[112] M. Sypabekova, P. Jolly, P. Estrela, D. Kanayeva, Electrochemical aptasensor using optimized surface chemistry for the detection of Mycobacterium tuberculosis secreted protein MPT64 in human serum, Biosens Bioelectron 123 (2019) 141–151.

[113] P. Kumari, S. Lavania, S. Tyagi, A. Dhiman, D. Rath, D. Anthwal, R.K. Gupta, N. Sharma, A.K. Gadpayle, R.S. Taneja, others, A novel aptamer-based test for the rapid and accurate diagnosis of pleural tuberculosis, Anal Biochem 564 (2019) 80–87.

[114] M.H. Yunus, N.A. Yusof, N.H.A. Raston, S.S.M. Noor, Y. Sulaiman, J. Abdullah, A novel amperometric aptamer–antibody sandwich assay for the detection of tuberculosis with diazonium electrografted enhanced modified electrode, IEEE Sens J 21 (2021) 22442–22449.

[115] J. Li, K. Hu, Z. Zhang, X. Teng, X. Zhang, Click DNA cycling in combination with gold nanoparticles loaded with quadruplex DNA motifs enable sensitive electrochemical quantitation of the tuberculosis-associated biomarker CFP-10 in sputum, Microchimica Acta 186 (2019) 1–7.

[116] R. Das, A. Dhiman, S.K. Mishra, S. Haldar, N. Sharma, A. Bansal, Y. Ahmad, A. Kumar, J.S. Tyagi, T.K. Sharma, Structural switching electrochemical DNA aptasensor for the rapid diagnosis of tuberculous meningitis, Int J Nanomedicine (2019) 2103–2113.

[117] Y. Chen, X. Liu, S. Guo, J. Cao, J. Zhou, J. Zuo, L. Bai, A sandwich-type electrochemical aptasensor for Mycobacterium tuberculosis MPT64 antigen detection using C60NPs decorated N-CNTs/GO nanocomposite coupled with conductive PEI-functionalized metal-organic framework, Biomaterials 216 (2019) 119253.

[118] N. Li, X. Huang, D. Sun, W. Yu, W. Tan, Z. Luo, Z. Chen, Dual-aptamer-based voltammetric biosensor for the Mycobacterium tuberculosis antigen MPT64 by using a gold electrode modified with a peroxidase loaded composite consisting of gold nanoparticles and a Zr (IV)/terephthalate metal-organic framework, Microchimica Acta 185 (2018) 1–7.

[119] N. Li, X. Huang, D. Sun, Y. Zhong, Z. Chen, A sensitive and rapid electrochemical aptasensor based on au@ PB for selective detection of mycobacterium tuberculosis antigen MPT64, J Electrochem Soc 166 (2019) B604.

[120] H. Thakur, N. Kaur, P. Sabherwal, D. Sareen, N. Prabhakar, Aptamer based voltammetric biosensor for the detection of Mycobacterium tuberculosis antigen MPT64, Microchimica Acta 184 (2017) 1915–1922.

[121] P. Kumari, A. Dhiman, S. Lavania, P. Sharma, D. Rath, D. Anthwal, R.K. Gupta, A. Kochar, N. Sharma, A.K. Gadpayle, others, Assessment of DNA aptamers targeting GlcB and HspX antigens for application in the diagnosis of abdominal tuberculosis, Tuberculosis 134 (2022) 102206.

[122] Y. Li, D. Peng, S. Guo, B. Yang, J. Zhou, J. Zhou, Q. Zhang, L. Bai, Aptasensor for Mycobacterium tuberculosis antigen MPT64 detection using anthraquinone derivative confined in ordered mesoporous carbon as a new redox nanoprobe, Bioelectrochemistry 147 (2022) 108209.

[123] H. Huang, Y. Chen, J. Zuo, C. Deng, J. Fan, L. Bai, S. Guo, MXene-incorporated C60NPs and Au@ Pt with dual-electric signal outputs for accurate detection of Mycobacterium tuberculosis ESAT-6 antigen, Biosens Bioelectron 242 (2023) 115734.

[124] J. Zuo, Y. Yuan, M. Qing, Y. Chen, H. Huang, J. Zhou, L. Bai, H. Liang, Surface-Activated Ti3C2Tx Adsorption of Acetylene Black Coupled with Polyaniline as a Signal Tag for the Detection of the ESAT-6 Antigen of Mycobacterium tuberculosis, ACS Appl Mater Interfaces (2024).

[125] L. Bai, Y. Chen, Y. Bai, Y. Chen, J. Zhou, A. Huang, Fullerene-doped polyaniline as new redox nanoprobe and catalyst in electrochemical aptasensor for ultrasensitive detection of Mycobacterium tuberculosis MPT64 antigen in human serum, Biomaterials 133 (2017) 11–19.

[126] M. Sypabekova, K. Dukenbayev, A. Tsepke, A. Akisheva, N. Oralbayev, D. Kanayeva, An aptasensor for the detection of Mycobacterium tuberculosis secreted immunogenic protein MPT64 in clinical samples towards tuberculosis detection, Sci Rep 9 (2019) 16273.

[127] H. Thakur, N. Kaur, D. Sareen, N. Prabhakar, Electrochemical determination of M. tuberculosis antigen based on Poly (3, 4-ethylenedioxythiophene) and functionalized carbon nanotubes hybrid platform, Talanta 171 (2017) 115–123.

[128] J. Xie, Z. Mu, B. Yan, J. Wang, J. Zhou, L. Bai, An electrochemical aptasensor for Mycobacterium tuberculosis ESAT-6 antigen detection using bimetallic organic framework, Microchimica Acta 188 (2021) 1–10.

[129] U.Z.M. Azmi, N.A. Yusof, J. Abdullah, F. Mohammad, S.A.A. Ahmad, S. Suraiya, N.H.A. Raston, F.N.M. Faudzi, S.K. Khiste, H.A. Al-Lohedan, Aptasensor for the detection of Mycobacterium tuberculosis in sputum utilising CFP10-ESAT6 protein as a selective biomarker, Nanomaterials 11 (2021) 2446.

[130] F. He, Y. Xiong, J. Liu, F. Tong, D. Yan, Construction of Au-IDE/CFP10-ESAT6 aptamer/DNA-AuNPs MSPQC for rapid detection of Mycobacterium tuberculosis, Biosens Bioelectron 77 (2016) 799–804.

[131] N. Ansari, K. Ghazvini, M. Ramezani, M. Shahdordizadeh, R. Yazdian-Robati, K. Abnous, S.M. Taghdisi, Selection of DNA aptamers against Mycobacterium tuberculosis Ag85A, and its application in a graphene oxide-based fluorometric assay, Microchimica Acta 185 (2018) 1–8.

[132] R.A. Karaballi, A. Nel, S. Krishnan, J. Blackburn, C.L. Brosseau, Development of an electrochemical surface-enhanced Raman spectroscopy (EC-SERS) aptasensor for direct detection of DNA hybridization, Physical Chemistry Chemical Physics 17 (2015) 21356–21363.

[133] L. Li, Z. Liu, H. Zhang, W. Yue, C.-W. Li, C. Yi, A point-of-need enzyme linked aptamer assay for Mycobacterium tuberculosis detection using a smartphone, Sens Actuators B Chem 254 (2018) 337–346.

[134] K. Pobanz, A. Lupták, Improving the odds: Influence of starting pools on in vitro selection outcomes, Methods 106 (2016) 14–20. https://doi.org/10.1016/J.YMETH.2016.04.021.

[135] M. Legiewicz, C. Lozupone, R. Knight, M. Yarus, Size, constant sequences, and optimal selection, RNA 11 (2005) 1701–1709. https://doi.org/10.1261/RNA.2161305.

[136] N. Kacherovsky, L.F. Yang, H. V. Dang, E.L. Cheng, I.I. Cardle, A.C. Walls, M. McCallum, D.L. Sellers, F. DiMaio, S.J. Salipante, D. Corti, D. Veesler, S.H. Pun, Discovery and Characterization of Spike N-Terminal Domain-Binding Aptamers for Rapid SARS-CoV-2 Detection, Angewandte Chemie International Edition 60 (2021) 21211–21215. https://doi.org/10.1002/ANIE.202107730.

[137] C. Roxo, W. Kotkowiak, A. Pasternak, G-Quadruplex-Forming Aptamers—Characteristics, Applications, and Perspectives, Molecules 2019, Vol. 24, Page 3781 24 (2019) 3781. https://doi.org/10.3390/MOLECULES24203781.

[138] K.Y. Chan, A.B. Kinghorn, M. Hollenstein, J.A. Tanner, Chemical Modifications for a Next Generation of Nucleic Acid Aptamers, ChemBioChem 23 (2022) e202200006. https://doi.org/10.1002/CBIC.202200006.

[139] B. Majumdar, D. Sarma, Y. Yu, A. Lozoya-Colinas, J.C. Chaput, Increasing the functional density of threose nucleic acid, RSC Chem Biol (2023). https://doi.org/10.1039/D3CB00159H.

[140] C.M. McCloskey, Q. Li, E.J. Yik, N. Chim, A.K. Ngor, E. Medina, I. Grubisic, L. Co Ting Keh, R. Poplin, J.C. Chaput, Evolution of Functionally Enhanced α-l-Threofuranosyl Nucleic Acid Aptamers, ACS Synth Biol 10 (2021) 3190–3199. https://doi.org/10.1021/ACSSYNBIO.1C00481/ASSET/IMAGES/LARGE/SB1C00481_0005.JPEG.

[141] F. Pfeiffer, F. Tolle, M. Rosenthal, G.M. Brändle, J. Ewers, G. Mayer, Identification and characterization of nucleobase-modified aptamers by click-SELEX, Nature Protocols 2018 13:5 13 (2018) 1153–1180. https://doi.org/10.1038/nprot.2018.023.

[142] Z.J. Tolnai, J. András, Z. Szeitner, K. Percze, L.F. Simon, R.E. Gyurcsányi, T. Mészáros, Spiegelmer-Based Sandwich Assay for Cardiac Troponin I Detection, International Journal of Molecular Sciences 2020, Vol. 21, Page 4963 21 (2020) 4963. https://doi.org/10.3390/IJMS21144963.

[143] S. Rana, A. Kaur, A. Bharti, S. Singh, A. Bhatnagar, N. Prabhakar, Electrochemical detection of hepcidin based on spiegelmer and MoS2NF-GNR@AuNPs as sensing platform, Anal Chim Acta 1181 (2021) 338863. https://doi.org/10.1016/J.ACA.2021.338863.

[144] N.K. Singh, B. Chakma, P. Jain, P. Goswami, Protein-induced fluorescence enhancement based detection of Plasmodium falciparum glutamate dehydrogenase using carbon dot coupled specific aptamer, ACS Comb Sci 20 (2018) 350–357.

[145] C. Zhu, G. Yang, M. Ghulam, L. Li, F. Qu, Evolution of multi-functional capillary electrophoresis for high-efficiency selection of aptamers, Biotechnol Adv 37 (2019) 107432. https://doi.org/10.1016/J.BIOTECHADV.2019.107432.

[146] K. Morihiro, O. Hasegawa, Y. Kasahara, S. Mori, T. Kasai, M. Kuwahara, S. Obika, Azobenzene-modified DNA aptamers evolved by capillary electrophoresis (CE)-SELEX method, Bioorg Med Chem Lett 31 (2021) 127607. https://doi.org/10.1016/J.BMCL.2020.127607.

[147] F. Yu, H. Li, W. Sun, Y. Zhao, D. Xu, F. He, Selection of aptamers against Lactoferrin based on silver enhanced and fluorescence-activated cell sorting, Talanta 193 (2019) 110–117. https://doi.org/10.1016/J.TALANTA.2018.09.063.

[148] N. Xu, X. Ma, Y. Cao, H. Wang, H. Wu, H. Zheng, C. Yang, R. Zou, J. Liu, C. Sun, Y. Yuan, A novel fluorescent structure-switching aptasensor for the sensitive detection of acrylamide based

on AuNPs-assisted separation of ssDNA, Advanced Agrochem 2 (2023) 276–283. https://doi.org/10.1016/J.AAC.2023.07.001.

[149] H.R. Kim, B.C. Kim, Development of multi-reactive aptamers for Cronobacter spp. using the sequential partitioning method to detect them in powdered infant formula, Anal Chim Acta 1249 (2023) 340935. https://doi.org/10.1016/J.ACA.2023.340935.

[150] V. Bachu, M. Mili, A. Dutta, P.D. Thungon, P. Goswami, Electrochemiluminescence-Based Lateral Flow Assay for Detection of Cardiac Troponin T Using Aptamers Developed through a Modified SELEX Technique, ACS Applied Optical Materials (2024). https://doi.org/10.1021/ACSAOM.4C00258/ASSET/IMAGES/LARGE/OT4C00258_0011.JPEG.

[151] F. Tolle, J. Wilke, J. Wengel, G. Mayer, By-Product Formation in Repetitive PCR Amplification of DNA Libraries during SELEX, PLoS One 9 (2014) e114693. https://doi.org/10.1371/JOURNAL.PONE.0114693.

[152] K. Shao, X. Shi, X. Zhu, L. Cui, Q. Shao, D. Ma, Construction and optimization of an efficient amplification method of a random ssDNA library by asymmetric emulsion PCR, Biotechnol Appl Biochem 64 (2017) 239–243. https://doi.org/10.1002/BAB.1467.

[153] M. Ramesh, R. Janani, C. Deepa, L. Rajeshkumar, Nanotechnology-enabled biosensors: A review of fundamentals, design principles, materials, and applications, Biosensors (Basel) 13 (2022) 40.

[154] M. Miernicki, T. Hofmann, I. Eisenberger, F. von der Kammer, A. Praetorius, Legal and practical challenges in classifying nanomaterials according to regulatory definitions, Nat Nanotechnol 14 (2019) 208–216.

[155] N. Mohseni, M. Moodi, A. Kefayat, F. Shokati, F. Molaabasi, Challenges and Opportunities of Using Fluorescent Metal Nanocluster-Based Colorimetric Assays in Medicine, ACS Omega 9 (2024) 3143–3163.

[156] Q. Chen, R. Gao, L. Jia, Enhancement of the peroxidase-like activity of aptamers modified gold nanoclusters by bacteria for colorimetric detection of Salmonella typhimurium, Talanta 221 (2021) 121476.

[157] L. Li, Y. Yuan, Y. Chen, P. Zhang, Y. Bai, L. Bai, Aptamer based voltammetric biosensor for Mycobacterium tuberculosis antigen ESAT-6 using a nanohybrid material composed of reduced graphene oxide and a metal-organic framework, Microchimica Acta 185 (2018) 1–9.

[158] P. Andersen, D. Askgaard, L. Ljungqvist, J. Bennedsen, I. Heron, Proteins released from Mycobacterium tuberculosis during growth, Infect Immun 59 (1991) 1905–1910.

[159] A.L. Sørensen, S. Nagai, G. Houen, P. Andersen, A.B. Andersen, Purification and characterization of a low-molecular-mass T-cell antigen secreted by Mycobacterium tuberculosis, Infect Immun 63 (1995) 1710–1717.

[160] H.G. Wiker, K. Sletten, S. Nagai, M. Harboe, Evidence for three separate genes encoding the proteins of the mycobacterial antigen 85 complex, Infect Immun 58 (1990) 272–274.

[161] A.S. Świerzko, M.A. Bartłomiejczyk, A. Brzostek, J. Łukasiewicz, M. Michalski, J. Dziadek, M. Cedzyński, Mycobacterial antigen 85 complex (Ag85) as a target for ficolins and mannose-binding lectin, International Journal of Medical Microbiology 306 (2016) 212–221.

[162] G. Ramalingam, S. Jayaraman, J.M. Khan, M.Z. Ahmed, A. Ahmad, E. Manickan, P. Rajagopal, Exploring recombinant secretory proteins from Mycobacterium tuberculosis to develop a serological platform for tuberculosis diagnosis, Int J Biol Macromol 249 (2023) 126769.

[163] L. Favrot, A.E. Grzegorzewicz, D.H. Lajiness, R.K. Marvin, J. Boucau, D. Isailovic, M. Jackson, D.R. Ronning, Mechanism of inhibition of Mycobacterium tuberculosis antigen 85 by ebselen, Nat Commun 4 (2013) 2748.

[164] A.A. Wahid, A. Doekhie, A. Sartbaeva, J.M.H. van den Elsen, Ensilication Improves the Thermal Stability of the Tuberculosis Antigen Ag85b and an Sbi-Ag85b Vaccine Conjugate, Scientific Reports 2019 9:1 9 (2019) 1–15. https://doi.org/10.1038/s41598-019-47657-9.

[165] T.-P.J. Chu, J.-M.P. Yuann, Expression, purification, and characterization of protective MPT64 antigen protein and identification of its multimers isolated from nontoxic Mycobacterium tuberculosis H37Ra, Biotechnol Appl Biochem 58 (2011) 185–189.

[166] M. Hemmati, A. Seghatoleslam, M. Rasti, S. Ebadat, N. Mosavari, M. Habibagahi, M. Taheri, A.R. Sardarian, Z. Mostafavi-Pour, Expression and purification of recombinant Mycobacterium tuberculosis (TB) antigens, ESAT-6, CFP-10 and ESAT-6/CFP-10 and their diagnosis potential for detection of TB patients, Iran Red Crescent Med J 13 (2011) 556.

[167] D.R. Ronning, V. Vissa, G.S. Besra, J.T. Belisle, J.C. Sacchettini, Mycobacterium tuberculosis antigen 85A and 85C structures confirm binding orientation and conserved substrate specificity, Journal of Biological Chemistry 279 (2004) 36771–36777.

[168] D.R. Ronning, T. Klabunde, G.S. Besra, V.D. Vissa, J.T. Belisle, J.C. Sacchettini, Crystal structure of the secreted form of antigen 85C reveals potential targets for mycobacterial drugs and vaccines, Nat Struct Biol 7 (2000) 141–146.

[169] C.M. Goins, S. Dajnowicz, M.D. Smith, J.M. Parks, D.R. Ronning, Mycolyltransferase from Mycobacterium tuberculosis in covalent complex with tetrahydrolipstatin provides insights into antigen 85 catalysis, Journal of Biological Chemistry 293 (2018) 3651–3662.

[170] N. Assal, M. Lin, PCR procedures to amplify GC-rich DNA sequences of Mycobacterium bovis, J Microbiol Methods 181 (2021) 106121.

[171] M.A. Jensen, M. Fukushima, R.W. Davis, DMSO and betaine greatly improve amplification of GC-rich constructs in de novo synthesis, PLoS One 5 (2010) e11024.

[172] A. Kumar, J. Kaur, Primer based approach for PCR amplification of high GC content gene: Mycobacterium gene as a model, Mol Biol Int 2014 (2014).

[173] Z.R. Newman, J.M. Young, N.T. Ingolia, G.M. Barton, Differences in codon bias and GC content contribute to the balanced expression of TLR7 and TLR9, Proceedings of the National Academy of Sciences 113 (2016) E1362–E1371.

[174] Z. Fang, W.-D. Schubert, N.C.G. Van Pittius, Expression and production of soluble Mycobacterium tuberculosis H37Rv mycosin-3, Biochem Biophys Rep 5 (2016) 448–452.

[175] G.R.M. Kleiner-Grote, J.M. Risse, K. Friehs, Secretion of recombinant proteins from E. coli, Eng Life Sci 18 (2018) 532–550.

[176] J. James, B. Yarnall, A. Koranteng, J. Gibson, T. Rahman, D.A. Doyle, Protein over-expression in Escherichia coli triggers adaptation analogous to antimicrobial resistance, Microb Cell Fact 20 (2021) 1–11.

[177] P.J. Shilling, K. Mirzadeh, A.J. Cumming, M. Widesheim, Z. Köck, D.O. Daley, Improved designs for pET expression plasmids increase protein production yield in Escherichia coli, Commun Biol 3 (2020) 214.

[178] C. Platella, C. Riccardi, D. Montesarchio, G.N. Roviello, D. Musumeci, G-quadruplex-based aptamers against protein targets in therapy and diagnostics, Biochimica et Biophysica Acta (BBA)-General Subjects 1861 (2017) 1429–1447.

[179] A.J. Stevens, L. de Jong, M.A. Kennedy, The dynamic regulation of G-quadruplex DNA structures by cytosine methylation, Int J Mol Sci 23 (2022) 2407.

[180] P. Saengdee, W. Chaisriratanakul, W. Bunjongpru, W. Sripumkhai, A. Srisuwan, C. Hruanun, A. Poyai, P. Phunpae, S. Pata, W. Jeamsaksiri, others, A silicon nitride ISFET based immunosensor for Ag85B detection of tuberculosis, Analyst 141 (2016) 5767–5775.

[181] P. Phunpae, S. Chanwong, C. Tayapiwatana, N. Apiratmateekul, A. Makeudom, W. Kasinrerk, Rapid diagnosis of tuberculosis by identification of Antigen 85 in mycobacterial culture system, Diagn Microbiol Infect Dis 78 (2014) 242–248. https://doi.org/10.1016/J.DIAGMICROBIO.2013.11.028.

[182] E.J. Kim, E.B. Kim, S.W. Lee, S.A. Cheon, H.J. Kim, J. Lee, M.K. Lee, S. Ko, T.J. Park, An easy and sensitive sandwich assay for detection of Mycobacterium tuberculosis Ag85B antigen using quantum dots and gold nanorods, Biosens Bioelectron 87 (2017) 150–156. https://doi.org/10.1016/J.BIOS.2016.08.034.

[183] L.M.T. Phan, E.B. Kim, S.A. Cheon, T.S. Shim, H.J. Kim, T.J. Park, Reliable naked-eye detection of Mycobacterium tuberculosis antigen 85B using gold and copper nanoshell-enhanced immunoblotting techniques, Sens Actuators B Chem 317 (2020) 128220. https://doi.org/10.1016/J.SNB.2020.128220.

[184] R. Lorenzo-Gómez, R. Miranda-Castro, J.R. de Los Toyos, N. de-Los-Santos-Álvarez, M.J. Lobo-Castañón, Aptamers targeting a tumor-associated extracellular matrix component: The human mature collagen XIα1, Anal Chim Acta 1189 (2022) 339206.

[185] M.F. Adasme, K.L. Linnemann, S.N. Bolz, F. Kaiser, S. Salentin, V.J. Haupt, M. Schroeder, PLIP 2021: Expanding the scope of the protein–ligand interaction profiler to DNA and RNA, Nucleic Acids Res 49 (2021) W530–W534.

[186] P. Kalra, S.K. Mishra, S. Kaur, A. Kumar, H.K. Prasad, T.K. Sharma, J.S. Tyagi, G-quadruplex-forming DNA aptamers inhibit the DNA-binding function of HupB and Mycobacterium tuberculosis entry into host cells, Molecular Therapy-Nucleic Acids 13 (2018) 99–109.

[187] T.S. Yeoh, A. Anna, T.-H. Tang, M. Citartan, Development of an optimization pipeline of asymmetric PCR towards the generation of DNA aptamers: a guide for beginners, World J Microbiol Biotechnol 38 (2022) 31.

[188] M. Heiat, R. Ranjbar, A.M. Latifi, M.J. Rasaee, G. Farnoosh, Essential strategies to optimize asymmetric PCR conditions as a reliable method to generate large amount of ssDNA aptamers, Biotechnol Appl Biochem 64 (2017) 541–548.

[189] A.I. Karsisiotis, N.M. Hessari, E. Novellino, G.P. Spada, A. Randazzo, M.W. da Silva, Topological characterization of nucleic acid G-quadruplexes by UV absorption and circular dichroism, Angewandte Chemie 45 (2011) 10833–10836.

[190] A. V Pavlova, M. V Monakhova, A.M. Ogloblina, N.A. Andreeva, G.Y. Laptev, V.I. Polshakov, E.S. Gromova, M.I. Zvereva, M.G. Yakubovskaya, T.S. Oretskaya, others, Responses of DNA

mismatch repair proteins to a stable G-quadruplex embedded into a DNA duplex structure, Int J Mol Sci 21 (2020) 8773.

[191] L. Olejko, A. Dutta, K. Shahsavar, I. Bald, Influence of different salts on the G-quadruplex structure formed from the reversed human telomeric DNA sequence, Int J Mol Sci 23 (2022) 12206.

[192] T. Yoshitomi, M. Hayashi, T. Oguro, K. Kimura, F. Wayama, H. Furusho, K. Yoshimoto, Binding and structural properties of DNA aptamers with VEGF-A-mimic activity, Molecular Therapy-Nucleic Acids 19 (2020) 1145–1152.

[193] H. Gattuso, A. Spinello, A. Terenzi, X. Assfeld, G. Barone, A. Monari, Circular dichroism of DNA G-quadruplexes: combining modeling and spectroscopy to unravel complex structures, J Phys Chem B 120 (2016) 3113–3121.

[194] T. Hianik, V. Ostatná, M. Sonlajtnerova, I. Grman, Influence of ionic strength, pH and aptamer configuration for binding affinity to thrombin, Bioelectrochemistry 70 (2007) 127–133.

[195] K. Jakab, N. Melios, G. Tsekenis, A. Shaban, V. Horváth, Z. Keresztes, Comparative Analysis of pH and Target-Induced Conformational Changes of an Oxytetracycline Aptamer in Solution Phase and Surface-Immobilized Form, Biomolecules 13 (2023) 1363.

[196] T.K. Sharma, J.G. Bruno, A. Dhiman, ABCs of DNA aptamer and related assay development, Biotechnol Adv 35 (2017) 275–301.

[197] Y.-M. Chang, C.K.-M. Chen, M.-H. Hou, Conformational changes in DNA upon ligand binding monitored by circular dichroism, Int J Mol Sci 13 (2012) 3394–3413.

[198] A. Geldert, X. Zhang, H. Zhang, C.T. Lim, others, Enhancing the sensing specificity of a MoS 2 nanosheet-based FRET aptasensor using a surface blocking strategy, Analyst 142 (2017) 2570–2577.

[199] L. Li, S. Xu, X. Peng, Y. Ji, H. Yan, C. Cui, X. Li, X. Pan, L. Yang, L. Qiu, others, Engineering G-quadruplex aptamer to modulate its binding specificity, Natl Sci Rev 8 (2021) nwaa202.

[200] A.T. Catherine, S.N. Shishido, G.A. Robbins-Welty, A. Diegelman-Parente, Rational design of a structure-switching DNA aptamer for potassium ions, FEBS Open Bio 4 (2014) 788–795.

[201] D. Bhattacharyya, G. Mirihana Arachchilage, S. Basu, Metal cations in G-quadruplex folding and stability, Front Chem 4 (2016) 38.

[202] L.M. Hellman, M.G. Fried, Electrophoretic mobility shift assay (EMSA) for detecting protein–nucleic acid interactions, Nat Protoc 2 (2007) 1849–1861.

[203] J. Vivekananda, J.L. Kiel, Anti-Francisella tularensis DNA aptamers detect tularemia antigen from different subspecies by Aptamer-Linked Immobilized Sorbent Assay, Laboratory Investigation 86 (2006) 610–618.

[204] S.Y. Toh, M. Citartan, S.C.B. Gopinath, T.-H. Tang, Aptamers as a replacement for antibodies in enzyme-linked immunosorbent assay, Biosens Bioelectron 64 (2015) 392–403.

[205] M. Citartan, S.C.B. Gopinath, J. Tominaga, S.-C. Tan, T.-H. Tang, Assays for aptamer-based platforms, Biosens Bioelectron 34 (2012) 1–11.

[206] Å. Larsson, Regression analysis of simulated radio-ligand equilibrium experiments using seven different mathematical models, J Immunol Methods 206 (1997) 135–142.

[207] D.A. Deranleau, Theory of the measurement of weak molecular complexes. I. General considerations, J Am Chem Soc 91 (1969) 4044–4049.

[208] G. Weber, S.R. Anderson, Multiplicity of binding. Range of validity and practical test of Adair's equation, Biochemistry 4 (1965) 1942–1947.

[209] H. Joshi, D. Kandari, S.S. Maitra, R. Bhatnagar, Biosensors for the detection of Mycobacterium tuberculosis: a comprehensive overview, Crit Rev Microbiol 48 (2022) 784–812.

[210] P. Damborsk\`y, J. Švitel, J. Katrl\'\ik, Optical biosensors, Essays Biochem 60 (2016) 91–100.

[211] L. Lecarme, E. Prado, A. De Rache, M.-L. Nicolau-Travers, R. Bonnet, A. van Der Heyden, C. Philouze, D. Gomez, J.-L. Mergny, H. Jamet, others, Interaction of polycationic Ni (II)-salophen complexes with G-quadruplex DNA, Inorg Chem 53 (2014) 12519–12531.

[212] R.S. Kasai, A. Kusumi, Single-molecule imaging revealed dynamic GPCR dimerization, Curr Opin Cell Biol 27 (2014) 78–86.

[213] N. Tuleuova, C.N. Jones, J. Yan, E. Ramanculov, Y. Yokobayashi, A. Revzin, Development of an aptamer beacon for detection of interferon-gamma, Anal Chem 82 (2010) 1851–1857.

[214] K. Ma, F. Zhang, N. Sayyadi, W. Chen, A.G. Anwer, A. Care, B. Xu, W. Tian, E.M. Goldys, G. Liu, "Turn-on" fluorescent aptasensor based on AIEgen labeling for the localization of IFN-γ in live cells, ACS Sens 3 (2018) 320–326.

[215] A. Tsuchiya, S.N. Hashim, S. Ise, T. Furuhata, K. Kawai, R. Wakabayashi, M. Goto, N. Kamiya, S. Sando, Bodipy-labeled fluorescent aptamer sensors for turn-on sensing of interferon-gamma and adenine compounds on cells, Analytical Sciences 32 (2016) 543–547.

[216] G. Liu, K. Zhang, K. Ma, A. Care, M.R. Hutchinson, E.M. Goldys, Graphene quantum dot based "switch-on" nanosensors for intracellular cytokine monitoring, Nanoscale 9 (2017) 4934–4943.

[217] K. Hu, J. Liu, J. Chen, Y. Huang, S. Zhao, J. Tian, G. Zhang, An amplified graphene oxide-based fluorescence aptasensor based on target-triggered aptamer hairpin switch and strand-displacement polymerization recycling forbioassays, Biosens Bioelectron 42 (2013) 598–602.

[218] N. Dhenadhayalan, M.I. Sriram, K.-C. Lin, Aptamer-based fluorogenic sensing of interferon-gamma probed with ReS2 and TiS2 nanosheets, Sens Actuators B Chem 258 (2018) 929–936.

[219] L. Qiu, F. Wimmers, J. Weiden, H.A. Heus, J. Tel, C.G. Figdor, A membrane-anchored aptamer sensor for probing IFNγ secretion by single cells, Chemical Communications 53 (2017) 8066–8069.

[220] O.V. Uhuo, T.T. Waryo, S.F. Douman, K.C. Januarie, K.C. Nwambaekwe, M.M. Ndipingwi, P. Ekwere, E.I. Iwuoha, Bioanalytical methods encompassing label-free and labeled tuberculosis aptasensors: A review, Anal Chim Acta 1234 (2022) 340326.

[221] L.S. Liu, F. Wang, Y. Ge, P.K. Lo, Recent developments in aptasensors for diagnostic applications, ACS Appl Mater Interfaces 13 (2020) 9329–9358.

[222] G.M. Ziarani, R. Moradi, N. Lashgari, H.G. Kruger, Metal-free synthetic organic dyes, Elsevier, 2018.

[223] P. Zheng, N. Wu, Fluorescence and sensing applications of graphene oxide and graphene quantum dots: a review, Chemistry–An Asian Journal 12 (2017) 2343–2353.

[224] D.P. Singh, C.E. Herrera, B. Singh, S. Singh, R.K. Singh, R. Kumar, Graphene oxide: An efficient material and recent approach for biotechnological and biomedical applications, Materials Science and Engineering: C 86 (2018) 173–197.

[225] M. Sypabekova, A. Bekmurzayeva, R. Wang, Y. Li, C. Nogues, D. Kanayeva, Selection, characterization, and application of DNA aptamers for detection of Mycobacterium tuberculosis secreted protein MPT64, Tuberculosis 104 (2017) 70–78.

[226] I. Jarmoskaite, I. AlSadhan, P.P. Vaidyanathan, D. Herschlag, How to measure and evaluate binding affinities, Elife 9 (2020) e57264.

[227] Y. Lyu, I.-T. Teng, L. Zhang, Y. Guo, R. Cai, X. Zhang, L. Qiu, W. Tan, Comprehensive regression model for dissociation equilibria of cell-specific aptamers, Anal Chem 90 (2018) 10487–10493.

[228] M. Jing, M.T. Bowser, Methods for measuring aptamer-protein equilibria: a review, Anal Chim Acta 686 (2011) 9–18.

[229] F. Rahimi, H. Roshanfekr, H. Peyman, Ultra-sensitive electrochemical aptasensor for label-free detection of Aflatoxin B1 in wheat flour sample using factorial design experiments, Food Chem 343 (2021) 128436.

[230] Y. Zhang, L. Huang, Y. Wang, J. Tang, Y. Wang, M. Cheng, Y. Du, K. Yang, M.J. Kipper, M. Hedayati, The preparation and study of ethylene glycol-modified graphene oxide membranes for water purification, Polymers (Basel) 11 (2019) 188.

[231] N. Pan, D. Guan, T. He, R. Wang, I. Wyman, Y. Jin, C. Xia, Removal of Th 4+ ions from aqueous solutions by graphene oxide, J Radioanal Nucl Chem 298 (2013) 1999–2008.

[232] M. Tavassoli, A. Khezerlou, H. Hamishehkar, A. Ehsani, B. Khalilzadeh, An ultrasensitive aptamer-based fluorescent on/off system for trace amount evaluation of Yersinia enterocolitica in food samples, Microchimica Acta 190 (2023) 253.

[233] Z. Liu, B. Liu, J. Ding, J. Liu, Fluorescent sensors using DNA-functionalized graphene oxide, Anal Bioanal Chem 406 (2014) 6885–6902.

[234] W.P. Carey, B.R. Kowalski, Chemical piezoelectric sensor and sensor array characterization, Anal Chem 58 (1986) 3077–3084.

[235] D. Thakur, N.P. Dubey, R. Singh, A review on spike and recovery method in analytical method development and validation, Crit Rev Anal Chem (2022) 1–19.

[236] C.A. Royer, S.F. Scarlata, Fluorescence approaches to quantifying biomolecular interactions, Methods Enzymol 450 (2008) 79–106.

[237] S. Deshayes, G. Divita, Fluorescence technologies for monitoring interactions between biological molecules in vitro, Prog Mol Biol Transl Sci 113 (2013) 109–143.

[238] M. Al-Tamimi, M. El-Sallaq, S. Altarawneh, A. Qaqish, M. Ayoub, Development of Novel Paper-Based Assay for Direct Serum Separation, ACS Omega 8 (2023) 20370–20378.

[239] N. Muhammad, M.T. Khan, S. Ali, T.A. Khan, A.S. Khan, N. Ullah, H. Higazi, S. Ali, S. Mohamed, M. Qasim, Novel mutations in MPT64 secretory protein of Mycobacterium tuberculosis complex, Int J Environ Res Public Health 20 (2023) 2530.

[240] A. Ramos, T. Carvalho, M. Ribeiro, J.T. Guimarães, Capilia™ TB-Neo assay: a new tool for rapid distinction between tuberculous and non-tuberculous mycobacteria, The International Journal of Tuberculosis and Lung Disease 20 (2016) 753–756.

[241] H. Yang, Z.-H. Liu, L.-T. Zhang, J. Wang, H.-S. Yang, L.-H. Qin, R.-L. Jin, Y.-H. Feng, Z.-L. Cui, R.-J. Zheng, others, Selection and application of peptide mimotopes of MPT64 protein in Mycobacterium tuberculosis, J Med Microbiol 60 (2011) 69–74.

[242] Y. Jiang, H. Liu, H. Wang, X. Dou, X. Zhao, Y. Bai, L. Wan, G. Li, W. Zhang, C. Chen, others, Polymorphism of antigen MPT64 in Mycobacterium tuberculosis strains, J Clin Microbiol 51 (2013) 1558–1562.

[243] J. Advani, R. Verma, O. Chatterjee, P.K. Pachouri, P. Upadhyay, R. Singh, J. Yadav, F. Naaz, R. Ravikumar, S. Buggi, others, Whole genome sequencing of Mycobacterium tuberculosis clinical isolates from India reveals genetic heterogeneity and region-specific variations that might affect drug susceptibility, Front Microbiol 10 (2019) 309.

[244] Z. Song, W. He, S. Pei, B. Zhao, X. Cao, Y. Wang, P. He, D. Liu, A. Ma, X. Ou, others, Association of lineage 4.2. 2 of Mycobacterium tuberculosis with the 63-bp deletion variant of the mpt64 gene, Microbiol Spectr 11 (2023) e01842–23.

[245] A.B. Kinghorn, L.A. Fraser, S. Liang, S.C.-C. Shiu, J.A. Tanner, Aptamer bioinformatics, Int J Mol Sci 18 (2017) 2516.

[246] R. Troisi, N. Balasco, I. Autiero, L. Vitagliano, F. Sica, Structural Insights into Protein–Aptamer Recognitions Emerged from Experimental and Computational Studies, Int J Mol Sci 24 (2023) 16318.

[247] A. Barenholz, A.-H. Hovav, Y. Fishman, G. Rahav, J.M. Gershoni, H. Bercovier, A peptide mimetic of the mycobacterial mannosylated lipoarabinomannan: characterization and potential applications, J Med Microbiol 56 (2007) 579–586.

[248] S. Niazi, I.M. Khan, W. Akhtar, F. ul Haq, I. Pasha, M.K.I. Khan, A. Mohsin, S. Ahmad, Y. Zhang, Z. Wang, Aptamer functionalized gold nanoclusters as an emerging nanoprobe in biosensing, diagnostic, catalysis and bioimaging, Talanta (2023) 125270.

[249] K. Tan, H. Ma, X. Mu, Z. Wang, Q. Wang, H. Wang, X.-D. Zhang, Application of gold nanoclusters in fluorescence sensing and biological detection, Anal Bioanal Chem (2024) 1–21.

[250] Y. Zheng, J. Wu, H. Jiang, X. Wang, Gold nanoclusters for theranostic applications, Coord Chem Rev 431 (2021) 213689.

[251] C.N. Loynachan, A.P. Soleimany, J.S. Dudani, Y. Lin, A. Najer, A. Bekdemir, Q. Chen, S.N. Bhatia, M.M. Stevens, Renal clearable catalytic gold nanoclusters for in vivo disease monitoring, Nat Nanotechnol 14 (2019) 883–890.

[252] Q. Yao, X. Yuan, V. Fung, Y. Yu, D.T. Leong, D. Jiang, J. Xie, Understanding seed-mediated growth of gold nanoclusters at molecular level, Nat Commun 8 (2017) 927.

[253] R. Jin, Quantum sized, thiolate-protected gold nanoclusters, Nanoscale 2 (2010) 343–362.

[254] X. Qu, Y. Li, L. Li, Y. Wang, J. Liang, J. Liang, Fluorescent gold nanoclusters: synthesis and recent biological application, J Nanomater 2015 (2015) 4.

[255] L. Qin, R. Zheng, Z. Ma, Y. Feng, Z. Liu, H. Yang, J. Wang, R. Jin, J. Lu, Y. Ding, others, The selection and application of ssDNA aptamers against MPT64 protein in Mycobacterium tuberculosis, Clin Chem Lab Med 47 (2009) 405–411.

[256] Y. Yan, D. Zhang, P. Zhou, B. Li, S.-Y. Huang, HDOCK: a web server for protein–protein and protein–DNA/RNA docking based on a hybrid strategy, Nucleic Acids Res 45 (2017) W365–W373.

[257] S. Saha, G.P.S. Raghava, Prediction of continuous B-cell epitopes in an antigen using recurrent neural network, Proteins: Structure, Function, and Bioinformatics 65 (2006) 40–48.

[258] S. Saha, G.P.S. Raghava, BcePred: prediction of continuous B-cell epitopes in antigenic sequences using physico-chemical properties, in: International Conference on Artificial Immune Systems, 2004: pp. 197–204.

[259] R. Stoltenburg, C. Reinemann, B. Strehlitz, FluMag-SELEX as an advantageous method for DNA aptamer selection, Anal Bioanal Chem 383 (2005) 83–91.

[260] J. Caroli, C. Taccioli, A. De La Fuente, P. Serafini, S. Bicciato, APTANI: a computational tool to select aptamers through sequence-structure motif analysis of HT-SELEX data, Bioinformatics 32 (2016) 161–164.

[261] S. Salentin, S. Schreiber, V.J. Haupt, M.F. Adasme, M. Schroeder, PLIP: fully automated protein–ligand interaction profiler, Nucleic Acids Res 43 (2015) W443–W447.

[262] C. Yang, Y. Jiang, S.H. Hao, X.Y. Yan, H. Naranmandura, others, Aptamers: an emerging navigation tool of therapeutic agents for targeted cancer therapy, J Mater Chem B 10 (2022) 20–33.

[263] T. Streckerová, J. Kurfürst, E.A. Curtis, Single-round deoxyribozyme discovery, Nucleic Acids Res 49 (2021) 6971–6981.

[264] V. Frezza, C. Pinto-D\'\iez, G. Fernández, M. Soto, M.E. Mart\'\in, A. Garc\'\ia-Sacristán, V.M. González, DNA aptamers targeting Leishmania infantum H3 protein as potential diagnostic tools, Anal Chim Acta 1107 (2020) 155–163.

[265] M. Mili, V. Bachu, P.R. Kuri, N.K. Singh, P. Goswami, Improving synthesis and binding affinities of nucleic acid aptamers and their therapeutics and diagnostic applications, Biophys Chem (2024) 107218.

[266] R.H. Meloen, W.C. Puijk, J.W. Slootstra, Mimotopes: realization of an unlikely concept, Journal of Molecular Recognition 13 (2000) 352–359.

[267] S. Govindaraju, S.R. Ankireddy, B. Viswanath, J. Kim, K. Yun, Fluorescent gold nanoclusters for selective detection of dopamine in cerebrospinal fluid, Sci Rep 7 (2017) 40298.

[268] C.R. Lillo, M.N. Calienni, B.R. Aiello, M.J. Prieto, D.R. Sartori, J. Tuninetti, P. Toledo, S. del Valle Alonso, S. Moya, M.C. Gonzalez, others, BSA-capped gold nanoclusters as potential theragnostic for skin diseases: Photoactivation, skin penetration, in vitro, and in vivo toxicity, Materials Science and Engineering: C 112 (2020) 110891.

[269] A.M. Alkilany, S. Alsotari, M.Y. Alkawareek, S.R. Abulateefeh, facile Hydrophobication of Glutathione-protected Gold nanoclusters and encapsulation into poly (lactide-co-glycolide) nanocarriers, Sci Rep 9 (2019) 11098.

[270] S.M. Anju, K.A. Merin, S. Varghese, A.I. Shkhair, G. Rajeevan, G. Indongo, S. George, Antibody-functionalized gold nanoclusters/gold nanoparticle platform for the fluorescence turn-on detection of cardiac troponin I, Microchimica Acta 191 (2024) 1–12.

[271] D.N. Castillo-López, U. Pal, Green synthesis of Au nanoparticles using potato extract: stability and growth mechanism, Journal of Nanoparticle Research 16 (2014) 1–15.

[272] J.G. Croissant, D. Zhang, S. Alsaiari, J. Lu, L. Deng, F. Tamanoi, A.M. AlMalik, J.I. Zink, N.M. Khashab, Protein-gold clusters-capped mesoporous silica nanoparticles for high drug loading, autonomous gemcitabine/doxorubicin co-delivery, and in-vivo tumor imaging, Journal of Controlled Release 229 (2016) 183–191.

[273] S. Shankar, N.S.K. Gowthaman, P. Arul, F. Chen, H.N. Lim, F.-X. Qin, Ultra-sensitive and selective determination of a phenolic food additive using protein capped gold nanoclusters: a dual in-line fluorometric and colorimetric sensing probe, New Journal of Chemistry 45 (2021) 1278–1285.

[274] H.S. Al-Mashriqi, M. Cai, S. Qi, H. Zhai, BSA capped gold nanoclusters modulated by copper ion for sensitive and selective detection of histidine in biological fluid, J Fluoresc 33 (2023) 697–706.

[275] R. Yuvakkumar, V. Elango, V. Rajendran, N. Kannan, Preparation and characterization of zero valent iron nanoparticles, Dig J Nanomater Biostruct 6 (2011) 1771–1776.

[276] A.H.A. Al-Dhrub, S. Sahin, I. Ozmen, E. Tunca, M. Bulbul, Immobilization and characterization of human carbonic anhydrase I on amine functionalized magnetic nanoparticles, Process Biochemistry 57 (2017) 95–104.

[277] C.I. Olariu, H.H.P. Yiu, L. Bouffier, T. Nedjadi, E. Costello, S.R. Williams, C.M. Halloran, M.J. Rosseinsky, Multifunctional Fe 3 O 4 nanoparticles for targeted bi-modal imaging of pancreatic cancer, J Mater Chem 21 (2011) 12650–12659.

[278] H. Hasegawa, K.I. Taira, K. Sode, K. Ikebukuro, Improvement of Aptamer Affinity by Dimerization, Sensors 2008, Vol. 8, Pages 1090-1098 8 (2008) 1090–1098. https://doi.org/10.3390/S8021090.

List of Publications, Conferences & Workshops attended

Journal publications from thesis:

- **Hazra S**, Patra S. Alleviating the neglected tropical diseases: recent developments in diagnostics and detection. **Current Topics in Medicinal Chemistry**. **2018** Jul 1;18(18):1559-74. DOI: https://doi.org/10.2174/1568026618666181106124015
- **Hazra S**, Hazarika R, Patra S. Multitargeting: An Alternative Approach to Tackle Multidrug Resistance in Tuberculosis. **Current Drug Targets. 2023.** volume- 24, issue number- 9, pp. 75-775, 2023. DOI: https://doi.org/10.2174/1389450124666230505145335
- **Hazra S**, Patra S. Development of DNA aptamers towards detection of tuberculosis biomarker Ag85B in a fluorescence-based sensing platform **(Manuscript under revision, Analytica Chimica Acta, Elsevier)**

Journal publications from collaborative work:

- Sarkar S, **Hazra S**, Patra S, Gogoi M. Biosensors for cancer detection: A review. **TrAC Trends in Analytical Chemistry. 2024** Sep 19:117978. DOI: https://doi.org/10.1016/j.trac.2024.117978

Patent

- **NUCLEIC ACID APTAMER BINDING TO AG85B (**Indian Patent Application no. 202431029861**)**

Book Chapters

- **Hazra S**, Thakur MS, Patra S. Enzymatic Biosensor Platforms for Infectious Disease Diagnosis: Focus on Tuberculosis and Neglected Tropical Diseases. *In* **Enzyme-based Biosensors: Recent Advances and Applications in Healthcare 2024** Jan 23 (pp. 237-254). Singapore: Springer Nature Singapore. DOI: https://doi.org/10.1007/978-981-15-6982-1_10
- **Hazra S**, Patra S. Carbon Nanomaterials in Biosensor Applications for Infectious Disease Diagnostics. *In* **Carbon Nanostructures in Biomedical Applications 2023** May 5 (pp. 257-283). Cham: Springer International Publishing. DOI: https://doi.org/10.1007/978-3-031-28263-8_10
- **Hazra S**, Patra S. Importance of protein structure and function in pathogenesis: Highlights on the multifaceted organism Mycobacterium tuberculosis. *In* **Microbial and Natural**

Macromolecules 2021 Jan 1 (pp. 775-809). Academic Press. DOI: https://doi.org/10.1016/B978-0-12-820084-1.00030-2

- Das B, Gogoi M, **Hazra S**, Patra S. Nanocarrier-Assisted Drug Delivery for Neglected Tropical Diseases. *For* **Drug Delivery**: 447. DOI: https://doi.org/10.1201/9781351171045
- **Hazra S**, Sarkar S, Gogoi M, Patra S; Nucleic acids used in biosensor applications for biomarker detection, In: Vol 2, Materials & Components of Biosensors in Healthcare, Biosensors for Healthcare, Elsevier. (In review)
- **Hazra S**, Senthamizh R, Chakraborty T, Patra S; Current challenges and future prospects for biosensor applications in healthcare, In: Vol 3, Applications of Biosensors in Healthcare, Elsevier. (In review)
- **Hazra S**, Nofal G, Bhat S, Senthamizh R, Chakraborty T, Patra S; Enzymatic biosensors, In: Vol 1, Fundamentals of Biosensors in Healthcare, Elsevier. (In review)

Conferences and workshops attended

- **Hazra S** and Patra S, Pharmacoproteomics of multitargeting in antimycobacterial drug-target discovery**.** 9th Annual Meeting of Proteomics Society, India (PSI), **International Conference on Proteomics in Health and Disease. November 30-December 02, 2017**. Institute of Life Sciences (ILS), Bhubaneswar, India (Poster Presentation)
- **Image J and Excel Advanced workshop,** Research Conclave, IIT Guwahati, 2018.
- **Quick Look of Technologies workshop**, 5th International Conference on Advanced Nanomaterials and Nanotechnology (ICANN), IIT Guwahati, **18th December, 2017**.
- **Hazra S** and Patra S, Aptamers in TB research. **International Conference on Biotechnology for Sustainable Agriculture, Environment and Health**. **4th-8th April, 2021**, Jaipur, Rajasthan, INDIA (BSAEH-2021) (Poster presentation)
- **Hazra S** and Patra S, Aptamers for smart diagnostics: towards improved sensing of tuberculosis. **Applied Biology Research & Innovation Conference (ABRICON)-2021.** A Virtual Event. **December 18-20, 2021.** Indian Consortium for Research & Innovation in Biology (Poster presentation)
- **Hazra S** and Patra S, Investigating the potential of aptamers for multiple biomarker based detection of tuberculosis. **3rd National Biomedical Research Competition (NBRCOM) 2021.** Online Competition. **December 6-10, 2021** (Oral presentation)

- **Hazra S** and Patra S, Exploring the potential of aptamers for detection of tuberculosis. **Research & Industrial Conclave 2022. January 20-22, 2022**. IIT Guwahati, India (Poster presentation)
- **Hazra S** and Patra S, Aptamers as a healthcare tool for point-of-care diagnosis of tuberculosis. **North-East Research Conclave (NERC) 2022**, Sustainable Science and Technology. May 20-22, 2022. Indian Institute of Technology Guwahati, India (Oral presentation)
- **Hazra S** and Patra S, Aptamer based nanobiosensing platform for detection of tuberculosis biomarkers. "Indo-USA International Conference on Applications of Nanotechnology in Biology, Biotechnology and Biopharmaceuticals (ICNB3)" organized by School of Life Sciences, B.S. Abdur Rahman Crescent Institute of Science & Technology in association with University of Missouri, USA, **The Biotech Research Society, India, Microbiologist Society, India, Nano & Biomaterials Association, BSACIST. August 11-12, 2022** (Oral presentation)
- **Hazra S** and Patra S, Aptasensing platform for multiple biomarker based detection of tuberculosis. **44th all India Cell Biology Conference & International Symposium on Molecular And Cellular Insights Of Human Diseases**, Organized by the Department of Biochemistry, University of Kashmir. **September 2-3, 2022** -Srinagar, J&K, India (Poster presentation)
- **Hazra S** and Patra S, Detection of secretory biomarkers of tuberculosis using DNA aptamer based sensing platform. **62nd Annual International Conference of the Association of Microbiologists of India (AMI)** conducted by University of Mysore. **September 21-23, 2022 (Best oral presentation award)**
- National workshop on intellectual property right (IPR) "**Implementation of MSME Innovative Scheme -Intellectual Property Right (IPR) component**" Organized by MSME-Development & Facilitation Office, Guwahati Ministry of MSME, Govt. of India In association with IIT Guwahati, held on **February 22, 2023**.
- National workshop on **"Hands-on training workshop on Piezoelectric Sensor development"** Organized by Department of Mechanical Engineering, IIT Guwahati, Assam, India.